

Proceedings of the Workshop on Geochemical Modeling

HYDROLOGY DOCUMENT NUMBER 626

September 14-17, 1986
Fallen Leaf Lake,
California

Sponsored by the Office of
Civilian Radioactive Waste
Management Program and
the Institute of Geophysics
and Planetary Physics at
the Lawrence Livermore
National Laboratory

Technical Organizers:

Kenneth J. Jackson
William L. Bourcier

CONF-8609134



DISCLAIMER

This document was prepared as an account of work sponsored by an agency of the United States Government. Neither the United States Government nor the University of California nor any of their employees, makes any warranty, express or implied, or assumes any legal liability or responsibility for the accuracy, completeness, or usefulness of any information, apparatus, product, or process disclosed, or represents that its use would not infringe privately owned rights. Reference herein to any specific commercial products, process, or service by trade name, trademark, manufacturer, or otherwise, does not necessarily constitute or imply its endorsement, recommendation, or favoring by the United States Government or the University of California. The views and opinions of authors expressed herein do not necessarily state or reflect those of the United States Government or the University of California, and shall not be used for advertising or product endorsement purposes.

**Proceedings of the
Workshop on Geochemical Modeling**

**Kenneth J. Jackson
and
William L. Bourcier**

Technical Organizers

Fallen Leaf Lake, California

September 14-17, 1986

**Lawrence Livermore National Laboratory
Livermore, California**

INTRODUCTION

The following collection of papers was presented at a workshop on geochemical modeling held in September, 1986 that was sponsored by the Office of Civilian Radioactive Waste Management Program at the Lawrence Livermore National Laboratory (LLNL). The LLNL Waste Management Program sponsored this conference based on their belief that geochemical modeling is particularly important to the radioactive waste disposal project because of the need to predict the consequences of long-term water-rock interactions at the proposed repository site.

The workshop consisted of three days of talks and poster sessions presented at the Fallen Leaf Lake conference facility run by Stanford University. The purpose of the workshop was to bring together a variety of workers in the field, including those who develop the geochemical modeling codes and those who actively use them. It was hoped that the results of the symposium would include an assessment of the current status of geochemical modeling programs and would assist in directing future work in the area.

The papers included in this volume represent a subset of the papers presented at the Fallen Leaf Lake Conference and cover a broad spectrum of detail and breadth in a subject that reflects the diverse research interests of the conference participants. These papers provide an insightful look into the current status of geochemical modeling and illustrate how various geochemical modeling codes have been applied to problems of geochemical interest. The emphasis of these papers includes traditional geochemical modeling studies of individual geochemical systems, the mathematical and theoretical development and refinement of new modeling capabilities, and enhancements of data bases on which the computations are based. The papers in this proceedings volume have been organized into the following four areas: Geochemical Model Development, Hydrothermal and Geothermal Systems, Sedimentary and Low Temperature Environments, and Data Base Development. The participants of this symposium and a complete list of the talks presented are listed in the appendices.

We are particularly indebted to Linda Hansen and Debbie Kiraly for taking care of the planning and organization of the workshop. It was largely a result of their efforts, and the staff of the Fallen Leaf Lake Lodge, that this conference was possible. We are also grateful for the generous financial support afforded this conference by the Waste Management Project at LLNL, funded chiefly through the Nevada Nuclear Waste Storage Investigations (NNWSI) and Salt Repository Project (SRPO) offices of the U.S. Department of Energy. Finally, we would like to thank all the conference participants who helped make this a successful and productive symposium.

Kenneth J. Jackson and William L. Bourcier

Technical Organizers



UNITED STATES
NUCLEAR REGULATORY COMMISSION
WASHINGTON, D. C. 20555

Don

Reply to:
1050 East Flamingo Road
Suite 319
Las Vegas, Nevada 89119
Tel: (702) 388-6125
FTS: 598-6125

TO: King Stablein, HLPD, Division of High-Level Waste
Management, M/S 4-H-3

FROM: Paul T. Prestholt, Sr. On-Site Licensing Representative

DATE: June 1, 1989

SUBJECT: PROCEEDINGS OF THE WORKSHOP ON GEOCHEMICAL MODELING

Please find the above-referenced publication that we
received in this office recently.

PTP:nan
cc: John J. Linehan, M/S 4-H-3

Contents

Geochemical Model Development

Multiple Reaction Path Model Describing Mass Transfer in Geochemical Systems <i>Peter C. Lichtner</i>	3
EQ3/6 - Status and Future Development <i>Thomas J. Wolery</i>	10
A Theoretical Basis for the Coupling of Chemical Reactions to Open System Processes <i>E. H. Perkins</i>	20
Calculations of Geochemical Mass Transfer as a Function of Temperature and Time <i>William M. Murphy</i>	27
Development and Application of Stable Isotope Mass Transfer Reaction Path Models <i>Teresa Suter Bowers</i>	34
Improvements in the Solid Solution Modeling Capabilities of EQ3/6 <i>William L. Bourcier</i>	41

Hydrothermal and Geothermal Systems

Preliminary Chemical Modeling of Epithermal Processes at Creede, Colorado: The Role of Fluid Mixing as an Ore Deposition Mechanism <i>Geoffrey S. Plumlee and Daniel O. Hayba</i>	51
Boiling of Geothermal Waters: Precipitation of Base and Precious Metals, Speciation of Arsenic and Antimony, and the Role of Gas Phase Metal Transport <i>Nicolas F. Spycher and Mark H. Reed</i>	58
Progressive Mineral Alteration and Coupled ¹⁸O Depletions in the Lake City Hydrothermal System (23 Ma), Colorado <i>Peter B. Larson</i>	66
Application of EQ3/6 to Modeling the Chemical Evolution in Hydrothermal Systems: An Example at the Valles Caldera, N.M. <i>Art F. White and Nancy J. Chuma</i>	72
Serpentinization Reaction Pathways: Implications for Modeling Approach <i>D. R. Janecky</i>	80
Predicted Reaction Paths During the Hydrothermal Alteration of Columbia River Basalt: A Sensitivity Analysis of Variability in the Composition of the Mesostasis <i>R. C. Arthur</i>	86

Sedimentary and Low Temperature Environments

Chemical Equilibrium in Mineral Formation and Diagenesis in the Carbonate Evaporite System: An Assessment of Chemical Model Application to Site Performance <i>John H. Weare, Nancy Moller, Jerry Greenberg, and Andrew Felmy</i>	97
Modelling Mass Transfer Reaction Rates: Calcite Precipitation and CO₂ Outgassing in a Karst Stream <i>Janet S. Herman and Michelle M. Lorah</i>	103
Predicting Mineral Dissolution and Precipitation During Burial: Synthetic Diagenetic Sequences <i>Carol J. Bruton</i>	111

Modelling Interaction of Deep Groundwaters with Bentonite	
<i>Hans Wanner</i>	120
Evaluation of an Equilibrium Speciation Model for the Acid Aqueous Iron Sulfate System at 25°C	
<i>Susan L. Stipp</i>	130
Thermodynamic and Kinetic Modeling of Glass Leaching in a Waste Package Environment	
<i>B. Grambow</i>	138
Computer Modeling of the Aqueous Geochemistry of the Archean Hydrosphere and the Formation of Banded Iron Formations	
<i>William E. Glassley, Kenneth J. Jackson, and William L. Bourcier</i>	146

Database Development

The NEA Thermochemical Data Base	
<i>Hans Wanner</i>	157
EQ3/6 Data Base - Ongoing Development at Lawrence Livermore National Laboratory	
<i>Joan M. Delany</i>	162
A Consistent Set of Thermodynamic Constants for Americium (III) Species with Hydroxyl and Carbonate	
<i>Jerry F. Kerrisk and Robert J. Silva</i>	167
Software for the Computation and Graphical Display of Intensive Variable Phase Diagrams	
<i>E. H. Perkins, R. Berman, and T. H. Brown</i>	176
Chlorite Solubility Between 200°C and 350°C: An Experimental and Theoretical Modeling Study	
<i>Edward C. Thornton, William E. Seyfried, Jr., and Jeffrey Seewald</i>	184

Appendices

A. Agenda	191
B. List of Attendees	195

Geochemical Model Development

MULTIPLE REACTION PATH MODEL DESCRIBING MASS TRANSFER IN GEOCHEMICAL SYSTEMS

Peter C. Lichtner
Department of Geology and Geophysics
University of California
Berkeley, California 94720

Abstract

Geochemical reaction path models for open systems approximate interacting continua models describing flowing systems for sufficiently large Peclet numbers and surface controlled mineral dissolution rates. Two distinct time scales characterize mass transfer for such systems, related to fluid transport and mineral reaction rates along the flow path. The reaction path formulation is valid when the time required for a packet of fluid to traverse a characteristic distance along the flow path is much shorter than the time characterizing changes in mineral volume fraction, porosity, permeability and mineral surface area. The open system reaction path model results in a steady state regime in which the fluid composition and mineral reaction rates are constant in time, but may vary with distance. Mineral alteration zones are stationary throughout the steady state regime despite a constant fluid flow rate. Whenever a mineral in an alteration zone completely dissolves, or significant changes occur in reacting surface area, porosity or permeability, a new reaction path is formed. By considering a consecutive series of such paths, the time evolution of a geochemical system can be predicted over geologic time spans. It is suggested that a multiple reaction path approach may be applicable to the description of metasomatic processes and weathering phenomena including the formation of bauxite deposits. The issue of model verification and validation in light of this new interpretation of reaction path models is briefly discussed.

Introduction

Computationally, geochemical reaction path models have advanced considerably since the pioneering work of Helgeson and co-workers (Helgeson *et al.*, 1966; Helgeson, 1968; Helgeson *et al.*, 1969). However, the development of a conceptual and quantitative framework which incorporates a spatial representation of mineral alteration products and fluid composition in response to fluid flow within the reaction path approach has received relatively little attention. Previous applications of the open system reaction path formulation to geochemical systems have been limited to a description of the change in mineral and fluid composition with time or reaction progress, but not as a function of distance along the flow path. The rapid approach to equilibrium exhibited by both open and closed reaction path calculations involving the dissolution of feldspar has been interpreted as implying that quasi-equilibrium conditions are established instantaneously on a geologic time scale (Helgeson and Murphy, 1983). However, as demonstrated below, when interpreted spatially these results imply that conditions far from equilibrium may persist in flowing systems over geologic time.

Although an open system option for product mineral assemblages is incorporated in the computer code EQ3/6 (Wolery, 1987), Wolery dismissed its applicability to circulating hydrothermal systems in favor of the closed system path model (Wolery, 1980). Bowers and Taylor (1985) combined both open and closed variations of the reaction path approach in an attempt to describe isotopic changes in the midocean ridge hydrothermal system resulting from seawater-basalt interaction and fluid flow in the presence of a thermal gradient. The present contribution proposes that the open rather than the closed system reaction path model is the appropriate description for flowing systems, regardless of whether fluids are circulating or not, or whether the system contains variations in

temperature.

Recent calculations by Lichtner *et al.* (1987) have compared the open system reaction path model with a transient, time-space continuum model. Following a brief transient period, excellent agreement between the two models was found throughout a spatial region in which a steady state formed. These results apply to systems characterized by large Péclet numbers and surface controlled mineral dissolution rates. It thus appears that the open system reaction path model has greater generality than previously acknowledged. This contribution outlines the basis for a conceptual framework that combines fluid flow with chemical reactions by generalizing the open system reaction path model to incorporate multiple reaction paths based on a mixed Lagrangian-Eulerian description of fluid flow in porous media. Further details of this approach and numerical examples can be found in Lichtner (1987).

Reinterpretation of the Open System Reaction Path Model for Flowing Systems

The open system reaction path model applied to a flowing system determines the change in composition of a single packet of fluid as it traverses the flow path and reacts with minerals with which it comes in contact. The packet is presumed closed with respect to transfer of matter within the aqueous phase, but open with respect to minerals. Mineral products precipitated from the packet are left behind as the packet advances along the flow path and do not back react with the fluid in the packet. One difficulty in interpreting the results of reaction path calculations in terms of a space coordinate is relating the amount of reacted rock to distance along the flow path. The incorporation of reaction kinetics into these models (Helgeson and Aagaard, 1979; Helgeson and Murphy, 1983), has been of primary significance for merging fluid flow with geochemical reaction path calculations by providing an absolute scale of time with which to correlate fluid flow rates with mineral reaction rates.

Incorporating kinetics into the reaction path model allows the chemical composition of the fluid in the packet to be parameterized by a single parameter t , equal to the time the packet is in contact with the rock along the flow path. Conservation of mass requires that the composition of the fluid packet satisfy equations of the form developed by Helgeson and Murphy (1983) and, for example, solved by more recent versions of the computer code EQ3/6 which incorporate dissolution and precipitation kinetics of the reacting host rock (Wolery, 1987). A solution to these equations yields the concentration and mineral reaction rates as a function of elapsed time of the packet along the flow path. Also obtained are the times of appearance and disappearance of product minerals. Equivalently, for fluid flow in a one-dimensional porous medium with constant porosity and permeability, time can be related to the distance x along the flow path by multiplying by the average pore velocity according to

$$x = \frac{vt}{\phi}, \quad (1)$$

where v denotes the Darcy velocity and ϕ designates the porosity. This formulation is equivalent to the Lagrangian representation of fluid flow (Bear, 1972). Transforming the time-dependent functions $C_j(t)$, $I_\pi(t)$ representing the concentration of the j th species and reaction rate of the π th mineral, respectively, according to Eqn.(1), yields an equivalent spatial representation in terms of functions $C'_j(x)$ and $I'_\pi(x)$. These functions have the form

$$C'_j(x) = \begin{cases} C_j\left(\frac{x\phi}{v}\right) & x \leq l(t) \\ C_j^\infty & x > l(t) \end{cases}, \quad (2)$$

and

$$I'_\pi(x) = \begin{cases} I_\pi\left(\frac{x\phi}{v}\right) & x \leq l(t) \\ 0 & x > l(t) \end{cases}, \quad (3)$$

where $l(t) = vt/\phi$ designates the travel distance of the infiltrating fluid at time t , and C_j^∞ denotes the initial solute concentration which is assumed to be in equilibrium with the host rock.

This interpretation of the open system reaction path model implies that at any given point along the flow path within a distance $l(t)$ of the inlet, the concentration and reaction rates are constant in time, but may vary with position. Accordingly, a steady state spatial regime is established extending from the inlet to $l(t)$. Furthermore, zones of secondary mineralization within the steady state regime are stationary in time despite a continuous fluid flow rate. The width of a particular reaction zone Δl_π can be determined by noting the times of appearance and disappearance of the corresponding mineral, denoted by τ_1^π and τ_2^π respectively, and multiplying the difference in these times by the flow rate to give

$$\Delta l_\pi = \frac{v}{\phi}(\tau_2^\pi - \tau_1^\pi). \quad (4)$$

Although not immediately apparent from Eqn.(4), Δl_π is independent of the porosity for $\phi \ll 1$. This is because the time τ_1^π is directly proportional to the porosity as can be seen by noting that the surface area in contact with the fluid packet and hence the reaction rate are inversely proportional to the porosity. The leading boundary of the reaction zone farthest downstream advances linearly with time, its position coinciding with the front of infiltrating fluid according to Eqns.(2) and (3).

The first packet of fluid determines the sequence of mineral reaction zones and their widths. During the duration of the steady state subsequent packets repeat the behavior of the first packet and merely alter the amounts of reacting minerals precipitated or dissolved. It is this first reaction path that is computed by computer codes such as EQ6. Before considering how long such a steady state may last and how the first reaction path may become modified with time, it is necessary to first ascertain whether the formation of a steady state is a reasonable assumption in the first place.

Comparison with Time-Space Continuum Models

The formation of a steady state requires that the characteristic time for complete dissolution of minerals in the reacting host rock, or for significant changes to occur in reacting surface area, porosity and permeability of the porous medium, be much larger than the time required to attain steady state. An immediate question which arises is whether a steady state condition is consistent with an exact, transient description of fluid flow coupled to fluid/rock interactions. One means of answering this question is from calculations using so-called interacting continua models based on the Eulerian representation of fluid flow in porous media. In the Eulerian description, mass conservation equations are formulated relative to a fixed reference volume of rock referred to as a representative elemental volume (REV). The resulting set of nonlinear, partial differential equations must generally be solved numerically using finite difference techniques. Calculations performed for the reaction of microcline and quartz at 100°C in a porous medium of porosity 0.2 demonstrated that a steady state regime was achieved after only approximately 5×10^5 sec had elapsed (Lichtner *et al.*, 1987). A flow rate of 1 m/yr and a diffusion coefficient of 10^{-6} cm²/sec were used in the calculation. After a brief transient period during which reaction zones of secondary minerals phyrophyllite, gibbsite, kaolinite and muscovite were formed, a steady state was reached consisting of the mineral zones gibbsite and muscovite. The gibbsite-muscovite boundary remained stationary while the leading muscovite boundary advanced at a slightly retarded rate. Within the steady state regime the position of the gibbsite-muscovite boundary, as well as solute concentration and mineral reaction rates agreed with that obtained from the open system reaction path model. Lichtner *et al.* (1987) further demonstrated that for systems with large Peclet numbers, the open system reaction path model and the Eulerian formulation of the transport equations are identical in the steady state limit.

Time Scales for Mineral Reaction and Fluid Flow

The condition of steady state cannot last indefinitely. A measure of the duration of steady state is given by the time required for a mineral grain in the host rock to completely dissolve. The characteristic time τ_r^D for the r th mineral to dissolve can be estimated for conditions of far from equilibrium surface controlled reaction using the rate law of Helgeson *et al.* (1984). The following expression is obtained:

$$\tau_r^D = \frac{a \phi_r^0}{\bar{V}_r k_r s_r^0}, \quad (5)$$

where ϕ_r^0 denotes the initial mineral volume fraction, \bar{V}_r denotes the corresponding molar volume, k_r denotes the rate constant, and s_r^0 denotes the initial surface area per unit volume of bulk porous medium. The coefficient a has the value one for constant surface area, and three for variable surface area, taken to be proportional to the mineral volume fraction raised to the two-thirds power. The results for 1mm sized grains of microcline in a porous medium with a porosity of 0.1 are shown in the accompanying figure as a function of temperature. Both pH-dependent and pH-independent forms of the rate law, the former for pH 4, are illustrated. Solid lines correspond to variable surface area and crosses to constant surface area. The dissolution time ranges from approximately 10^5 years at 25°C to 10^{-4} years or 3×10^3 sec at 600°C .

The mineral dissolution time τ_r^D can be compared with the time τ_d required for a packet of fluid to travel a characteristic distance d given by

$$\tau_d = \frac{\phi d}{v}. \quad (6)$$

When

$$\tau_r^D \gg \tau_d, \quad (7)$$

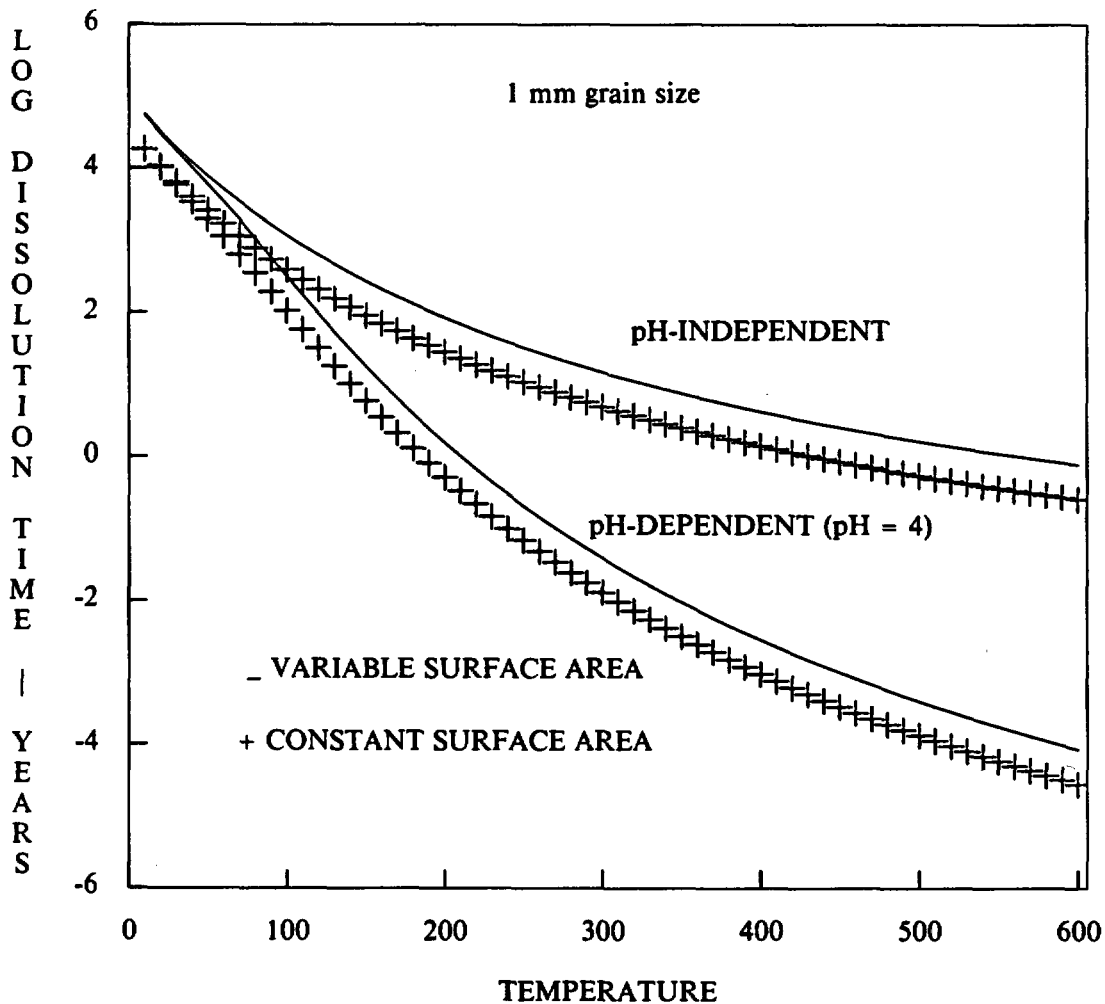
then many fluid packets traverse the flow path before significant changes occur in porosity, permeability and surface area. For example, according to the figure with a Darcy flow rate of 1 m year^{-1} and a distance d of 1 m, $\tau_d = 10^{-1}$ years, and condition (7) is satisfied for temperatures up to 600°C for the pH-independent rate law and for temperatures less than approximately 200°C for the pH-dependent form of the rate law. For temperatures higher than these local equilibrium conditions are approached and a chromatographic description applies.

Multiple Reaction Path Model

As time progresses and additional packets of fluid traverse the flow path, several feedback mechanisms operate to alter the steady state pattern. At first, only the amounts of minerals present along the flow path change while the positions of the reaction zones remained fixed. Eventually, however, after sufficient time has elapsed, the mineral volume fractions become altered enough to effect the porosity and permeability of the porous medium and surface area of the reacting minerals, thereby perturbing the steady state reaction path. As the surface area and hence dissolution rate of the dissolving minerals decrease, where previously a secondary mineral was precipitating, for the new path it may be dissolving. A new steady state path is formed which persists until the surface area, permeability or porosity is again sufficiently altered to disturb the path. When one of the minerals in the host rock completely dissolves in some region of space, the various secondary minerals in the region and those downstream must readjust their zone boundaries to accommodate the new situation.

The multiple reaction path model consists of accounting for changes in the reaction path with time, while keeping track of the amount of each mineral precipitated or dissolved along the flow path. In this model subsequent packets of fluid react not only with the initial host rock, but also with secondary minerals deposited by preceding fluid packets. The change in mineral volume fraction with

MICROCLINE



Logarithm of the dissolution time in years for 1 mm sized grains of microcline in a porous medium of porosity 0.1 plotted as a function of temperature. Rate laws for pH-dependent and pH-independent dissolution of microcline were taken from Helgeson *et al.* (1984).

time at a fixed position along the flow path can be computed by noting that for each path the reaction rates are constant in time. Thus the transport process consists of a series of steady state reaction paths. For the multiple reaction path model to be valid, each steady state path must be separated in time by an interval which is long compared to the time required to reach steady state, but short compared to the time for a mineral to completely dissolve.

Preliminary calculations for the dissolution of microcline at 25°C in response to infiltrating rainwater, indicate that the first reaction path lasts for several thousand years (Lichtner, 1987). During this time, according to the model calculations, secondary minerals gibbsite and kaolinite precipitate within stationary reaction zones. The second path results in gibbsite dissolving at the inlet end of the initial gibbsite zone and precipitating further downstream. Succeeding reaction paths generally exist for periods of time on the order of tens to hundreds of years as the mineral alteration zones slowly migrate downstream. Such a model may account for the formation of bauxite deposits by chemical weathering, a process probably requiring on the order of hundreds of thousands of years

(Butty and Chapallaz, 1984).

Model Verification and Validation

A complete and rigorous formulation of reaction path models for flowing systems also has important consequences for model verification and validation. Model verification here refers to establishing that the model in question solves equations which are believed to represent physical reality as well as ensuring that the model was correctly programmed, while model validation refers to demonstrating that the model agrees with physical reality. Clearly model validation represents a much more difficult task.

Models can be divided into two categories: those which are complete and those which are incomplete. Completeness of a model signifies whether or not the model provides a complete description within its range of applicability of the processes it attempts to explain. In principle an incomplete model is cannot be validated. The open system reaction path model represents an incomplete model since it only accounts for the first of many reaction paths that are necessary to describe coupled fluid flow and fluid/rock interaction. Hence in principle this model cannot be validated for situations in which more than one reaction path is important. The reaction path model may be *partially* validated however, if it can be demonstrated that the first reaction path correctly predicts the observed mineral assemblages, and that subsequent paths do not alter the mineralogy but only the amounts and location of minerals deposited along the flow path.

Concluding Remarks

There appears to be little fundamental basis for applying the closed system reaction path model or some combination of closed and open systems to flowing systems. This is true for circulating hydrothermal systems as well as flow in the presence of a temperature gradient. The physical basis for the validity of the multiple reaction path model is the existence of two distinct characteristic time scales related to fluid transport and mineral reaction rates. The multiple reaction path model applicable to systems characterized by large Peclet numbers at a much reduced computational effort compared to time-space continuum models based on an Eulerian formulation. Finally the model may lead to a qualitatively new understanding of the formation of mineral reaction zones and their propagation in time.

Acknowledgements

I am greatly indebted to Hal Helgeson, Bill Murphy, Eric Oelkers, Barbara Ransom, Everett Shock, J. K. Bohlke and Charlie Alpers for helpful discussions during the course of this work. In addition I want to thank Ken Jackson for reviewing the manuscript. Financial support was provided by a grant to Professor H. C. Helgeson by the Department of Energy (DOE Grant DE-AT03-83ER-13100).

References

- Bear J. (1972) *Dynamics of Fluids in Porous Media*, Elsevier. 764 pp.
- Butty D. L. and Chapallaz C. A. (1984) Bauxite genesis. In, *Bauxite, Proceedings of the 1984 Bauxite Symposium*, Ed. Leonard Jacob, Jr., Los Angeles, California.
- Bowers T. S. and Taylor H. P. Jr. (1985) An integrated chemical and stable-isotope model of the origin of midocean ridge hot spring systems. *Jour. Geophys. Res.* **90**, 12583-12606.
- Helgeson H. C., Garrels R. M. and MacKenzie F. T. (1966) Evaluation of irreversible reactions involving minerals and aqueous solutions (abstract): 1966 Annual Meeting, Geological Society of

America, *GSA Special Paper #101*, 92.

- Helgeson H. C. (1968) Evaluation of irreversible reactions in geochemical processes involving minerals and aqueous solutions I. Thermodynamic relations. *Geochim. Cosmochim. Acta* **33**, 853-877.
- Helgeson H. C., Garrels R. M. and MacKenzie F. T. (1969) Evaluation of irreversible reactions in geochemical processes involving minerals and aqueous solutions II. Applications. *Geochim. Cosmochim. Acta* **33**, 455-481.
- Helgeson H. C. and Aagaard P. (1979) A retroactive clock for geochemical processes, *Geological Society of America Abstracts with Programs*, **11**, 442.
- Helgeson H. C. and Murphy W. M. (1983) Calculation of mass transfer among minerals and aqueous solutions as a function of time and surface area in geochemical processes. I. Computational Approach. *Math. Geol.* **15**, 109-130.
- Helgeson H. C., Murphy W. M. and Aagaard P. (1984) Thermodynamic and kinetic constraints on reaction rates among minerals and aqueous solutions. II. Rate constants, effective surface area, and the hydrolysis of feldspar. *Geochim. Cosmochim. Acta* **48**, 2405-2432.
- Lichtner P. C. (1985) Continuum model for simultaneous chemical reactions and mass transport in hydrothermal systems. *Geochim. Cosmochim. Acta* **49**, 779-800.
- Lichtner P. C., Helgeson H. C. and Murphy W. M. (1987) Lagrangian and Eulerian descriptions of metasomatic alteration processes. In, *Proceedings of the Nato Conference on Metamorphic Reactions and Metasomatism*, Ed. H. C. Helgeson. In Press.
- Lichtner P. C. (1987) A mixed Lagrangian-Eulerian formulation of fluid-rock interaction coupled to fluid flow. In preparation.
- Wolery T. J. (1979) Calculation of chemical equilibrium between aqueous solutions and minerals: The EQ3/EQ6 software package. UCRL-52658.
- Wolery T. J. (1980) Chemical modeling of geologic disposal of nuclear waste: progress report and a perspective. Lawrence Livermore National Laboratory, Livermore, CA, UCRL-52748.
- Wolery T. J. (1987) EQ6, a computer code for reaction-path modeling of aqueous geochemical systems: user's guide and documentation. Lawrence Livermore National Laboratory, Livermore, CA, UCRL report in preparation.

EQ3/6 - STATUS AND FUTURE DEVELOPMENT

Thomas J. Wolery
Earth Sciences Department and
Nuclear Waste Management Program
Lawrence Livermore National Laboratory
Livermore, CA 94550

Abstract

EQ3/6 is a software package for geochemical modeling of aqueous systems, focused on speciation-solubility and reaction-path modeling. It includes a large thermodynamic data base and a collection of data base handling programs. EQ3/6 is being developed primarily for applications related to the disposal of high level nuclear waste, but the software is much more widely applicable in aqueous geochemistry. Recent work has focused on growth and improvement in the data base, creation of data base management software, the introduction of precipitation growth kinetics into reaction-path modeling, an option to compute reaction paths at fixed gas fugacities, improvements in the treatment of solid solutions, and inclusion of equations to represent activity coefficients in concentrated aqueous salt solutions. In addition, the coding has changed from FORTRAN 66 to FORTRAN 77, and a set of coding standards has been developed in order to assist code portability and future development.

Introduction

EQ3/6 is a software package for geochemical modeling of aqueous geochemical systems, first developed to allow reaction-path modeling of seawater and basalt under hydrothermal conditions (WOLERY, 1978). It consists of the following elements:

- o EQ3NR - speciation-solubility code (WOLERY, 1983)
- o EQ6 - reaction-path code (WOLERY, 1978; WOLERY, 1987a)
- o MCRT - thermodynamic data processing code (WOLERY et al., 1987)
- o EQLIB - supporting code library
- o DATA0 - the EQ3/6 main data file
- o MDAS - the MCRT master data file (see DELANY, 1986, this volume)
- o Special data bases to support the use of Pitzer's equations (WOLERY, 1987b)
- o Various data base manipulation codes and preprocessors (see DELANY, 1986, this volume)

There have been five previous major public releases of EQ3/6: version 2020, Feb. 1979; version 2055, Nov. 1979; version 3015, Dec. 1980; version 3175, Dec., 1981; and version 3230, Aug. 1983. Since the release of the latter, the code package has been self-contained (older versions required math routines from the IMSL library, a proprietary software package). Recent work has focused on the preparation of version 3245 (estimated release in Jan. or Feb., 1987).

Current EQ3/6 development is funded by the three major DOE projects for the geologic disposal of high level nuclear waste, each of which is

investigating a candidate site for the nation's first high-level waste repository. The Nevada Nuclear Waste Storage Investigations (NNWSI) is investigating a site in tuff at Yucca Mountain, Nevada; the Salt Repository Project (SRP), a site in bedded salt in Deaf Smith County, Texas; and the Basalt Waste Isolation Project (BWIP), the Hanford site in the Columbia basalt near Richland, Washington. The proposed repository at the Nevada site would be situated in a thick hydrologically unsaturated zone (in which water is present in the pores with a gas phase that is very similar to air), whereas the proposed repositories at the other two sites would be located below the groundwater table.

Performance requirements for a high-level waste repository have been mandated by the Nuclear Regulatory Commission (10CFR60) and the Environmental Protection Agency (40CFR191). The NRC requirements apply to both near-field and far-field behavior (the near-field comprises the immediate zone of the repository itself); the EPA requirements limit the eventual exposure of human beings to radiation released from the repository. Release and transport of radionuclides is expected to be effected principally by groundwater. The relevant geochemical processes include rock-water interactions and processes analogous to rock-water interactions (e.g., container corrosion and deposition of insoluble phases of waste form elements).

Most software products developed for the high-level waste disposal projects appear to have a single well-defined function that falls into a single project niche. In contrast, EQ3/6 can be used to make several kinds of related but dissimilar geochemical calculations, and can be applied in more than one of the traditional lines of waste project organization. In the remainder of this paper, I review the various kinds of geochemical calculations that can be made, how EQ3/6 usage fits into the waste projects, some examples of usage outside the waste projects, the current status of the code package, and plans for future development.

Types of EQ3/6 Calculations

Aqueous speciation (distribution of dissolved components among free ions, ion pairs, and complexes) and saturation indices ($\log Q/K$) for minerals and other solids can be calculated from analytical data using the EQ3NR code (WOLERY, 1983). This provides a useful means of screening analytical data by means of rigorous charge balance calculations, and has already been useful in detecting problems in NNWSI work in at least two instances (see KERRISK, 1983, and DELANY, 1984). This code has also been used to calculate temperature corrections to the pH of standard buffer solutions used in dissolution rate experiments (KNAUSS and WOLERY, 1986). More recently, it has been used design custom pH buffer compositions for solubility and dissolution rate experiments at desired temperatures.

It is also possible to use EQ3NR to compute the solubilities of various solids from thermodynamic data, if a sufficient set of solution parameters is constrained; otherwise, the EQ6 code must be used. Solubility is generally affected by solution composition, either directly through mass action effects, or indirectly by ion pairing or complexing or by effects on the activity coefficients. All of these effects are taken into account in both codes. Which code must be used depends upon exactly how the problem is posed, because solubility problems come in different forms. If the form of the question is, "how much of a mineral will dissolve in a water of known initial composition,"

then EQ6 is usually called for. In such a situation, dissolution of the mineral might change, for example, the pH. If the solubility depends directly or indirectly on the pH, it is necessary to calculate not only the solubility, but also the pH of the equilibrated solution, because one knows in advance only the initial pH.

The function of the EQ6 code (WOLERY, 1987a) is generally to answer the question, "what happens when an aqueous solution of known composition reacts with specified materials." As such materials react, many phenomena of interest may occur: reaction rates may speed up or slow down; new phases may begin to form; with further reaction, some newly formed phases may disappear; and the solution composition changes. The goal of reaction path modeling is to predict such effects. Originally, the process modeled by EQ6 had no kinetic framework, but followed a non-kinetic formalism laid down by HELGESON (1968); in essence, the water was "titrated" with reactant solids according to specified "relative reaction rates." Overall progress was measured not in terms of time, but of a "reaction progress variable." More recently, the development of increased understanding of controls on the rates of mineral growth and dissolution have permitted an expansion of reaction-path modeling to include a time framework (see HELGESON and MURPHY, 1983, and DELANY et al., 1987). This was included in the EQ6 code, for the case of mineral dissolution only, in version 3230. The case of mineral growth has since been added to version 3245 (DELANY et al., 1987).

EQ6 treats chemical processes in considerable detail, using a variety of coupled submodels for such things as rate laws and activity coefficients. Some of these are the targets of ongoing research in the field of aqueous geochemistry. In some cases, a large number of specific submodels already exist, with others under current development. Our response to this situation has been to offer within EQ6 a menu of the most adequate or useful specific submodels. This has been done partly with a viewpoint on doing comparative analysis of such submodels, and partly with an eye on providing a computational superstructure for the testing of new specific submodels. The basic type of system the code models is a closed one with a homogeneous aqueous fluid phase. The code does not offer a general model combining the processes of chemistry and fluid transport, a topic of much current interest. It does allow modeling of a flow-through system which is focused on the evolution of a packet of fluid flowing through a reactive medium (which can be visualized as a pipe, fracture, or porous medium). However, this model does not solve any transport equations, and it only follows what happens to what may be thought of as the first of possibly many packets of water. It has been described as "pseudo-one dimensional."

Usages of EQ3/6 on the High Level Waste Projects

In order to obtain a license for a repository from the NRC, the U.S. Department of Energy must present a strong case that the NRC and EPA performance requirements will be satisfied at the proposed site. The job of making this case is unusual in that it focuses on the behavior of a large underground engineered structure, and unprecedented in terms of the time scale involved (thousands of years).

One major strategy for dealing with geochemical effects, which actually precedes the current requirements by many years, has been to conduct various

kinds of "applications level" experiments and to pipe the results, which may reflect the lumped effects of many detailed processes, directly into a computer code containing a model for fluid transport. Such coupling is generally at the level of dimensional analysis, and the applicability of the experimental results to behavior of an actual repository in the field at even short times, let alone long time periods, is merely assumed without any proof or check. In general, this approach ignores any theoretical framework for treating geochemical interactions, and makes little or no attempt to relate any of the results to known fundamental data, such as thermodynamic data.

There has actually been at least one attempt to claim credit for the results of thermodynamic modeling calculations, made with an unchecked data base. Such calculations can be wholly off the mark because of bad and/or incomplete supporting data and/or lack of provision for important detailed processes. Premature efforts in this direction tended to give "geochemical modeling" a bad name, and emphasis was again placed upon "applications level" experiments.

The present strategy for applying EQ3/6 and other geochemical modeling tools on the waste projects is to provide the critical link between the results of "applications level" experiments on the one hand and concepts from detailed modeling and known fundamental data on the other (McKENZIE et al., 1986). This creates a focus on modeling the experiments before any serious attempt is made to model the repository. It becomes possible to demonstrate consistency (or inconsistency) between the results of "application" experiments and fundamental data. It also provides a means to identify and isolate any artifactual effects in the experiments (e.g., interactions with vessel walls, effects of finely ground materials and other artificially prepared surfaces, presence or absence of air) that would not apply to behavior in an actual repository and may also point out critical errors or omissions in the measurements. Finally, detailed modeling should point to a better methodology for including chemical effects in a larger model of repository performance, providing a conceptual basis for the degree of extrapolation that will of necessity be required in this process.

In order to realistically apply this strategy, it is necessary to address the current limitations of geochemical models and geochemical modeling codes, and the scope and quality of existing fundamental data. The current plan for developing EQ3/6 is discussed in detail by McKENZIE et al. (1986) and will be touched upon later in this paper. It focuses on three types of inadequacies which must be addressed before EQ3/6 can be fully utilized for all of the intended purposes. The code package presently lacks consideration of certain processes and phenomena, such as sorption on mineral surfaces. This requires code development. Some of the specific submodels, such as sets of equations for describing activity coefficients, are not adequate under all anticipated conditions. This requires submodel development. The data base is inadequate for some key intended purposes. This requires data base development.

Development of new specific submodels and of the supporting base of fundamental data can only partially be addressed by culling the existing literature. It is possible in only rare instances to extract fundamental data from "applications level" experiments. In general, a new category of experiments is required. Although experimental activity of this kind is called for in the EQ3/6 development plan (McKENZIE et al., 1986), adequate funding is developing slowly.

The present and anticipated usages of EQ3/6 on the waste projects overlap the traditional waste project organizational lines of site evaluation, waste package design, and performance assessment. This has probably caused more problems in gaining acceptance of the code package by the waste projects than it has helped.

Site evaluation requires, or at least is aided, by speciation-solubility calculations of the groundwaters present at a candidate site. This allows an assessment of the degree of equilibration between a groundwater and coexisting minerals. The use of charge balance calculations to screen analytical data has been mentioned earlier, but is particularly useful in site work. Reaction-path modeling may also be useful in elucidating patterns of groundwater evolution along a flow path (e.g., see KERRISK, 1983). Such modeling has also been used to infer the direction of groundwater flow in an area of the Hanford site in which the hydraulic head is too small for this to be determined by conventional hydrologic testing (SOLOMON, 1986, this volume).

Waste package design requires a detailed understanding of the geochemical interactions that will occur in the so-called near-field environment. While several exact definitions of this have been proposed, the operative concept is based on the fact that young radioactive waste produces a lot of heat, and rock (of all the types of interest here) is a poor heat conductor. Within about the first 600 years, significantly elevated temperatures will prevail about the immediate vicinity of the waste canisters, producing a localized hydrothermal environment. At the NNWSI site, this scenario is expected to be a bit different than it would at the other two sites. Here high temperatures in the hydrologically unsaturated zone are expected at first to drive off water. As the waste eventually cools, however, a hydrothermal environment will eventually be established.

Important near-field chemical processes therefore include both hydrothermal rock/water interactions and also reactions between water, rock, and materials introduced in the construction of the repository, in both the hydrothermal and post-hydrothermal phases. For the most part, such processes must be investigated by means of laboratory "applications level" experiments. The connections with geochemical modeling are several. First, speciation-solubility modeling of fluid samples are essential to determine the degree of thermodynamic stability (or instability) during these experiments. This process normally begins with EQ3NR calculations on analyses of quenched fluid samples. Screening of the analytical data by means of a charge balance calculation is as useful here as in site evaluation. The pH value available generally pertains to the quenched sample and is generally not identical to the value at elevated temperatures. The "in situ" pH can be calculated by feeding the EQ3NR output into the EQ6 code. This then also yields the pertinent calculation of the "in situ" species distribution and saturation indices.

The methodology given above describes how EQ3/6 can be used to analyze the results of a hydrothermal experiment. However, using appropriate assumptions concerning rate laws, it is possible to use the EQ6 code to compute a reaction-path model that is an attempt to predict the experimental results. DELANY (1984) has used this approach to model Dickson gold-bag hydrothermal experiments in which devitrified tuff from the Nevada site has been reacted with J-13 well water (a proxy for Yucca Mountain groundwater) at various

temperatures. The initial attempt used rate law formulations and rate constant values taken from single-mineral dissolution rate experiments reported in the literature, though some runs were made with slightly altered rate constant values in order to see if better fits were obtainable.

It was found that reasonably good matches to the experimental data could be obtained in the case of experiments at 150°C, if the formation of a significant number of possible product minerals was suppressed in the face of supersaturation in the fluid. Such suppressed phases were not found in the reaction vessel after the completion of the experiments. It is very clear that the fluids were highly supersaturated with respect to a number of potential product phases, which simply did not form on the time scale of the experiments (about three months). At present, there is no way to include such information into reaction-path models without doing the experiments, though as more work of this kind is done, useful rules of thumb may emerge.

To the extent that such "applications level" experiments can be successfully modeled, the results can be extrapolated to conditions more like those expected to occur in an actual repository. For example, it is possible to run kinetic reaction path models out to times exceeding the length of the experiments, although this requires choosing some assumptions from among various possibilities. It is also possible to extrapolate an experiment to different physicochemical conditions, such as lower temperatures likely to be of greater significance in the hydrothermal period, or a system in which the gas phase of the unsaturated zone at Yucca Mountain is present (the experimental system modeled by DELANY, 1984, did not include provision for the presence of such a phase).

On the other hand, DELANY (1984) found that modeling of experiments at 250°C was generally unsatisfactory, because of the formation in the experiments of significant amounts of dachiardite, a zeolite mineral which was not represented in the EQ3/6 data base. This, and similar problems in geochemical modeling, require new experiments designed to extract fundamental data which is presently unavailable.

There is presently increasing interest in applying geochemical modeling techniques to systems including the artificial components of the repository, such as the waste radionuclide elements, the original waste form itself, and the canister metal. Attempts are underway to extend the kinetic rock/water modeling described above to include leaching of waste forms. It may be possible to extend it as well to canister corrosion. However, there is now an increased emphasis in the waste projects to call upon solubility limitations in order to demonstrate compliance with the NRC near-field release requirements. The feasibility of developing geochemical modeling tools such as EQ3/6 to deal with this subject is currently more obvious. However, actually doing the work will require a number of new "fundamental data" experiments to complement "applications level" experiments.

Both site evaluation and waste package design activities feed into performance assessment, as it is defined in the broad sense. However, one of the special needs of performance assessment is to integrate detailed modeling into a grand model that shows that the repository will or will not meet the performance requirements. Such integration inevitably requires simplification of these detailed models. One way EQ3/6 can assist in this is to identify the essential features in geochemical models for specific reaction scenarios. In

addition to simplifying the detailed models, EQ3/6 may be used, in scaled down form, to run the simplified models directly for a grand model code. There are no specific plans for this yet, however.

Improvements to the 3245 Version of EQ3/6

A number of major improvements have been made to the EQ3/6 package since the release of the 3230 version. Some of these affect both EQ3NR and EQ6. An option was created to allow the use of Pitzer's equations (PITZER, 1973, 1975) for the activity coefficients of aqueous species (WOLERY, 1987b; see also JACKSON and WOLERY, 1986, this volume). A special data file of virial coefficients is required. This allows calculations to be made in highly concentrated solutions, but is currently applicable to only a limited set of components, mostly strong electrolytes and "sea salts." A simplex algorithm was implemented to calculate the "maximum" hypothetical saturation index of solid solutions (BOURCIER, 1985). The previous algorithm for treating this was unreliable.

Other code improvements pertained to the EQ6 code. Its capability to model dissolution kinetics was extended to include precipitation growth kinetics (DELANY et al., 1986), and some new rate law forms were added for both dissolution and precipitation. An option was created to allow the fugacities of selected gases to be fixed at chosen values during reaction path runs, simulating the effect of the presence of a large gas reservoir (DELANY and WOLERY, 1984). This was done primarily in order to make such calculations, taking into account the gas phase in the unsaturated zone at Yucca Mountain; however, it is also useful in treating many other settings, including some experimental configurations. Sample calculations have shown that fixed fugacities of CO₂ can introduce major changes in reaction paths. Two faster calculational modes ("economy" and "super-economy") were developed in the EQ6 code. These allow greater step sizes in reaction-path runs which do not involve kinetics.

Substantial changes have been made to the thermodynamic data base which supports EQ3/6 calculations (see DELANY, 1986, this volume). A two-tier structure has been adopted, with DATAO, the EQ3/6 operational data base being supported by MDAS, the "MCRT data base." MCRT (WOLERY et al., 1987) for processing thermodynamic data, including making temperature extrapolations. It produces data blocks that can be inserted into DATAO. Nearly all of the data in DATAO is now documented as to the source, and the size of this data base has increased significantly. New data base management software has also been written.

The entire EQ3/6 package was adapted to run on 32-bit UNIX-based computers (Ridge 32C and 32S; the code package was originally written on CDC 6600 and 7600 computers, with some work also being done on Cray-1 machines by the time of the 3230 release). The EQ3/6 codes were originally written in FORTRAN 66; much it has since been rewritten in FORTRAN 77. A set of coding standards has been developed to increase portability and ease of future development. Much of this has been implemented.

Improvements to Appear in the 3270 Version

Plans for the 3270 version, which will succeed the 3245 version, include adding additional activity coefficient models (see JACKSON and WOLERY, 1986, this volume): the model of HELGESON et al. (1981) as modified by WOLERY and JACKSON (1987), and a model based upon hydration theory, under development at LLNL. Plans also call for adding pressure corrections to the thermodynamic data, increasing the temperature range of the data base from 0-300°C to 0-500°C, some algorithmic improvements designed to increase computational speed, and a partial code rewrite to more implement FORTRAN 77 structures and our own recently adopted coding standards. The 3270 version may also see some extension of the solid solution modeling capabilities. The data base is expected to be larger and still further improved.

Other Future Improvements

A number of other future improvements are planned (McKENZIE et al., 1986). These include the development of site-mixing models for solid solutions, EQ6 options for dealing with redox disequilibrium, inclusion of some sorption models to allow treatment of chemical processes on mineral surfaces, the addition of a gas phase, and the development of a "leaching cell" flow-through model. This model would be centered at a fixed location as opposed to following a particular packet of water. The data base will continue to be maintained, and it will continue to be expanded as necessary to meet the needs of the waste projects. Other improvements and enhancements are also possible as project needs arise.

Availability of EQ3/6 Outside the Waste Projects

LLNL's Nuclear Waste Management Program desires to enhance the credibility and usefulness of EQ3/6, and is willing to provide the code package to "informal collaborators" for non-commercial applications, in return for useful feedback. In addition, changes in LLNL regulations regarding software distribution now make possible direct transfers to industry.

Acknowledgments

Prepared by Nevada Nuclear Waste Storage Investigations (NNWSI) Project participants as part of the Civilian Radioactive Waste Management Program. The NNWSI Project is managed by the Waste Management Project Office of the U.S. Department of Energy, Nevada Operations Office. NNWSI Project work is sponsored by the Office of Geologic Repositories of the DOE Office of Civilian Radioactive Waste Management.

References

- BOURCIER, W.L. (1985) Improvements in the Solid Solution Modeling Capabilities of the EQ3/6 Geochemical Code. UCID-20587, Lawrence Livermore National Laboratory, Livermore, California.
- DELANY, J.M. (1985) Reaction of Topopah Spring Tuff with J-13 Water: A Geochemical Modeling Approach Using the EQ3/6 Reaction Path Code. UCRL-53631, Lawrence Livermore National Laboratory, Livermore, California.

- DELANY, J.M. (1986) EQ3/6 data base - ongoing development at Lawrence Livermore National Laboratory. Pp.162-166, this volume.
- DELANY, J.M., PUIGDOMENECH, I., and WOLERY, T.J. (1987) Precipitation Kinetics Option for the EQ6 Geochemical Reaction Path Code, Report in preparation, Lawrence Livermore National Laboratory, Livermore, California.
- DELANY, J.M., and WOLERY, T.J. (1984) Fixed-Fugacity Option for the EQ6 Geochemical Reaction Path Code. UCRL-53598, Lawrence Livermore National Laboratory, Livermore, California.
- HELGESON, H.C. (1968) Evaluation of irreversible reactions in geochemical processes involving minerals and aqueous solutions - I. Thermodynamic relations. *Geochim. Cosmochim. Acta* 32, 853-877.
- HELGESON, H.C., and MURPHY, W.M. (1983) Calculation of mass transfer among minerals and aqueous solutions as a function of time and surface area in geochemical processes. I. Computational approach. *Math. Geol.* 15, 109-130.
- HELGESON, H.C., KIRKHAM, D.H., and FLOWERS, G.C. (1981) Theoretical prediction of the thermodynamic behavior of aqueous electrolytes at high pressures and temperatures: IV. Calculation of activity coefficients, osmotic coefficients, and apparent molal and standard and relative partial molal properties to 600°C and 5 Kb. *Amer. Jour. Sci.* 281, 1249-1516.
- JACKSON, K.J., and WOLERY, T.J., 1986, this volume.
- KERRISK, J.F. (1983) Reaction-Path Calculations of Groundwater Chemistry and Mineral Formation at Rainier Mesa, Nevada. LA-9912-MS, Los Alamos National Laboratory, Los Alamos, New Mexico.
- KNAUSS, K.G., and WOLERY, T.J. (1986) Dependence of albite dissolution kinetics on pH and time at 25°C and 70°C. *Geochim. Cosmochim. Acta* 50, 2481-2497.
- McKENZIE, W.F., WOLERY, T.J., DELANY, J.M., SILVA, R.J., JACKSON, K.J., BOURCIER, W.L., and EMERSON, D.O. (1986) Geochemical Modeling (EQ3/6) Plan - Office of Civilian Radioactive Waste Management Program. UCID-20864, Lawrence Livermore National Laboratory, Livermore, California.
- PITZER, K.S. (1973) Thermodynamics of electrolytes I: Theoretical basis and general equations. *J. Phys. Chem.* 77, 268-277.
- PITZER, K.S. (1975) Thermodynamics of electrolytes V: Effects of higher order electrostatic terms. *J. Solution Chem.* 4, 249-265.
- SOLOMON, C. (1986) this volume
- WOLERY T.J. (1983) EQ3NR, A Computer Program for Geochemical Aqueous Speciation-Solubility Calculations: User's Guide and Documentation. UCRL-53414, Lawrence Livermore National Laboratory, Livermore, California.

WOLERY, T.J., ISHERWOOD, D.J., JACKSON, K.J., DELANY, J.M., and PUIGDOMENECH, I. (1984) EQ3/6: Status and Applications. Pp. 54-65 in JACOBS, G.K., and WHATLEY, S.K., eds., Proceedings of the Conference on the Application of Geochemical Models to High-Level Nuclear Waste Repository Assessment, NUREG/CP-0062, U.S. Nuclear Regulatory Commission, Washington, D.C., and ORNL/TM-9585, Oak Ridge National Laboratory, Oak Ridge, Tennessee.

WOLERY T.J. (1987a) EO6. A Computer Program for Reaction-Path Modeling of Aqueous Geochemical Systems: User's Guide and Documentation. Report in preparation, Lawrence Livermore National Laboratory, Livermore, California.

WOLERY T.J. (1987b) EO3/6 Modifications for Geochemical Modeling of Brines. I. Pitzer's Equations. Report in preparation, Lawrence Livermore National Laboratory, Livermore, California.

WOLERY T.J., BOURCIER, W.L., AND MOORE, R.M., (1987) MCRT. A Data Base Building Code for the EQ3/6 Geochemical Modeling Software Package: User's Guide and Documentation. Report in preparation, Lawrence Livermore National Laboratory, Livermore, California.

WOLERY, T.J., and JACKSON, K.J. (1987) Activity coefficients in aqueous salt solutions. I. The ion size problem. Ms. in preparation.

A Theoretical Basis for the Coupling of Chemical Reactions to Open System Processes

E.H. Perkins

Alberta Research Council, Oil Sands Research Department,
PO Box 8330, Postal Station F,
Edmonton, Alberta, Canada. T6H 5X2

Abstract

In order to understand the processes involved in natural and industrial geological phenomenon involving an aqueous fluid and solid phases, the chemical interactions between the fluid and surrounding minerals must be known as functions of pressure, temperature, composition, and time. In addition to the boundary conditions, these processes are also dependent upon external sources of work, energy and mass (for example, injection wells).

Equations have been derived which allow the chemical reactions between a fluid and solid phases to be evaluated in any open system. They are based on derivatives of the mass action and mass balance equations taken with respect to time and can be used to predict the distribution of mass at future times. These equations are coupled to modified version of the flow, heat transport and solute transport equations through the derivatives of the volume and number of moles of each of the solid phase, through derivatives of the molalities and partial molal volumes of the aqueous species, through the derivative of the total number of moles of water and through the amount of heat generated/consumed by the process. Using these equations, a computer program has been written and used to model various systems.

Introduction

In any regional or local flow system, the fluid can react with the surrounding media. These reactions are manifested by the spatial and temporal distribution of phases and by the spatial and temporal variation in the composition of the phases and the fluid. Geological examples are abundant: weathering, hydrothermal alteration, diagenesis, metasomatism and ore deposition are familiar results of these processes. Industrial examples include in-situ mining, waste disposal and secondary/enhanced oil recovery.

Beginning in the late sixties, a number of authors began to mathematically model chemical reactions as functions of temperature, pressure and composition in closed systems in order to place constraints on natural analogies. Some of the natural systems and calculated models includes: *weathering*- Helgeson, Garrels and Mackenzie (1969);

ore deposition—Villas and Norton(1977); reaction of a vault fluid with different rock types—Wolery (1980); supergene alteration—Kwong, Brown and Greenwood (1982); geothermal areas—Capuano and Cole (1982). The success of these models has show that many processes can be modelled using a mathematical/geochemical approach, leading to a better understanding of rock-water interaction.

Because of the increasing problem of chemical and nuclear waste disposal and the potential problem of contaminating existing flow systems, considerable attention has been paid to the migration of dissolved material in ground water. In general, authors modelling the transport of dissolved material in a fluid have generally restricted themselves to near-surface conditions where the aqueous species and the solid phases are inert or where a retardation factor can be used to approximate the chemical reactions between the aqueous species and the surrounding matrix. A notable exception is Lichtner (1985), whose model is completely coupled.

The coupling of chemical reactions to open system process can be most clearly illustrated by first examining the partial differential equations constraining fluid flow, heat transport and solute transport. Using implicit summation, commonly accepted forms of these equations can be written as:

$$-\frac{\partial \rho q}{\partial x_i} = \rho Q + \frac{\partial \rho \theta}{\partial \tau} \quad (1)$$

$$\frac{\partial}{\partial x_i} \left(\left(\theta k_{i,j}^f + (1-\theta)k_{i,j}^m \right) \frac{\partial T}{\partial x_j} \right) + \rho^f C v^f q_i \frac{\partial T}{\partial x_i} = \left(\theta \rho^f C v^f + (1-\theta)\rho^m C v^m \right) \frac{\partial T}{\partial \tau} + Q \quad (2)$$

$$\frac{\partial}{\partial x_i} \left(D_{i,j} \theta \frac{\partial C}{\partial x_j} \right) - \frac{\partial}{\partial x_i} q_i \theta C = \frac{\partial \theta C}{\partial \tau} + Q \quad (3)$$

ρ , θ , Q , k , T , q , Cv , D and C are the density, porosity, source/sink term, thermal conductivity, temperature, velocity, heat capacity at constant volume, coefficient of dispersion and concentration of a component in the fluid, respectively. ∂x_i and $\partial \tau$ are the spatial and temporal partial derivatives. Subscripts f and m refer to fluid and matrix (minerals), respectively. Most of these terms are directly related to the chemical reactions through the number of moles of the solid phases and water, or through the molality of the aqueous species. Consider for example, the porosity which can be written:

$$\theta = \frac{V^{rev} - \sum_i V_i^o n_i}{V^{rev}} \quad (4)$$

n_i is the number of moles of the i 'th solid phase, V_i° and V^{rev} are the volume of the i 'th phases and of the REV, respectively. Taking the complete derivative with respect to time yields:

$$\begin{aligned} \frac{\partial \theta}{\partial \tau} = & \frac{\sum_i V_i^\circ n_i}{(V^{rev})^2} \left(\frac{\partial V^{rev}}{\partial P} \frac{\partial P}{\partial \tau} + \frac{\partial V^{rev}}{\partial T} \frac{\partial T}{\partial \tau} + \dots \right) \\ & - \sum_i \frac{n_i}{V^{rev}} \left(\frac{\partial V_i^\circ}{\partial P} \frac{\partial P}{\partial \tau} + \frac{\partial V_i^\circ}{\partial T} \frac{\partial T}{\partial \tau} + \dots \right) \\ & - \sum_i \frac{V_i^\circ}{V^{rev}} \frac{\partial n_i}{\partial \tau} \end{aligned} \quad (5)$$

The first terms on the right hand side describe the effects of the process on the REV itself, the second on the molar volume of the phases, and the last is the result of the changing number of moles of minerals. If enough is known or assumed about the process, this equation can often be simplified down to the last term. Similiar expansion can be made for almost all of the other parameters, including the source/sink terms.

At any point in time, the distribution of mass in any chemical system is completely specified and can be solved using the mass action (one for each non-component species and phase) and mass balance equations (one for each component). Any set of components which completely span the compositional space of all of the minerals, aqueous species and gases can be used. However, if the components are chosen such that np components have the same compositional vector and thermodynamic properties as the np equilibrium phases in the system, one has the same compositional vector and thermodynamic properties as water, and the remaining $nc - np - 1$ components have the same compositional vector and thermodynamic properties as the most abundant independent aqueous species, numerical accuracy is improved, speed of solution is increased, and the form of the equations is clearer. The component basis should be dynamic as it changes when new phases precipitate from solution or existing phases completely dissolve into solution. The component basis can be changed by simple matrix techniques.

The mass balance equation for the c 'th component in a system composed of equilibrium phases, aqueous species and reactant phases can be written as:

$$N_c^{Total} = \sum_s \nu_{c,s} n_w m_s / 55.51 + \sum_i \sum_k \nu_{c,i,k} n_{i,k} + \sum_r \nu_{c,r} n_r \quad (6)$$

$n_{k,i}$ is the number of moles of the k 'th endmember of the i 'th phase. n_r is the number of moles of the r 'th reactant phase while m_s is the molality of the s 'th aqueous species. $\nu_{c,i}$ is the number of moles of the c 'th component in the phases or species (as indicated by the other subscripts).

The mass action equation for the s 'th non-component aqueous species, expanded in terms of a component basis as described above, with the activity of each aqueous species replaced by the molality and the activity coefficient (γ_s), and the activity of each of the endmembers of the solid solution phases replaced by the number of moles and activity coefficient ($\lambda_{k,i}$) of the endmembers, can be written:

$$\ln K_s = \ln \gamma_s + \ln m_s + \nu_{s,w} \ln a_w + \sum_c^{nc-np-1} (\nu_{s,c} \ln \gamma_c + \nu_{s,c} \ln m_c) + \sum_i^{np} \sum_k \nu_{s,i,k} \left(\ln \lambda_{i,k} + \ln n_{i,k} - \ln \left(\sum_j n_{i,j} \right) \right) \quad (7)$$

The subscript "w" indicates water. The derivative of both the mass balance and mass action equations can now be taken with respect to time. Through the relationship, $\partial \ln X = X^{-1} \partial X$, all derivatives of the number of moles of each of the solid phases and of the molality of each of the aqueous species in the mass action equation can be written as normal derivatives. The derivative of the activity coefficient of the k 'th endmember of a solid phase can be expanded in terms of the derivative of number of moles of all of the endmembers of that solid solution phase. In a similar fashion, the derivative of the activity coefficient of each of the aqueous species could be reduced to the derivative of the molalities of all of the aqueous species. However, by leaving this derivative in terms of ionic strength, a faster numerical method of solution can be employed. For the identical reason, the derivative of the activity of water has not been expanded. Therefore, two new equations must be introduced. These are the derivative of the ionic strength equation and of the Gibbs-Duhem equation (which constrains the activity of water).

In order, the derivative of the mass balance equation (one for each component), the derivative of the ionic strength equation, the derivative of the Gibbs-Duhem equation and the derivative of the mass action equation (one for each non-component species in the system) are shown in figure 1. The coefficients $A \dots Z$ are constants and depend on the specific models used for the activity coefficients of aqueous species and of solid solution phases, and used for the gibbs free energy of solid phases and of aqueous species. D is the only term which contains the change in the total number of each component due to mass flux while K and Z are the only terms which contain derivatives with respect to temperature and pressure.

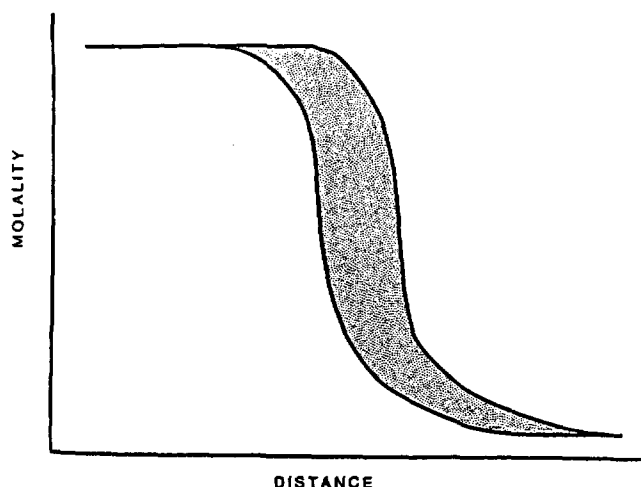
One significant feature of this matrix of equations is that all are linear with respect to the derivatives of molality of the aqueous species, the derivatives of number of moles of each of the endmembers of the solid phases, the derivative of the ionic strength and the derivative of the activity of water, thus they can be easily and quickly solved by linear matrix techniques. Another is that the last term on the left hand side of the last equation (the derivative of the mass action equation) has a coefficient of one. As this

Figure 1 - Tabular Forms of the Constraining Chemical Equations

$$\begin{array}{l}
 \sum_{i=2}^{N_{i,p}} A \frac{\partial \ln m_i}{\partial \tau} + \sum_{i=1}^{N_{i,c}} C \frac{\partial n_{i,1}}{\partial \tau} + \frac{\partial n_{sw}}{\partial \tau} + \sum_{i=1}^{N_{i,p}} \frac{\partial i}{\partial \tau} + \sum_{i=1}^{N_{i,p}} \frac{\partial i}{\partial \tau} + \left\{ \begin{array}{l} \sum_{i=1}^{N_{i,k}} S \frac{\partial n_{i,1}}{\partial \tau} \\ \sum_{i=1}^{N_{i,p}} \sum_{k=1}^{N_{i,k}} T \frac{\partial n_{i,k}}{\partial \tau} \\ \sum_{i=1}^{N_{i,p}} \sum_{k=1}^{N_{i,k}} \sum_{j=1}^{N_{i,k}} \frac{\partial n_{i,k}}{\partial \tau} \\ (\nu + \gamma) \sum_{k=1}^{N_{i,k}} \frac{\partial n_{i,k}}{\partial \tau} \\ (\mu + \psi) \frac{\partial n_{i,k}}{\partial \tau} \end{array} \right\} + \sum_{i=2}^{N_{i,p}} p \frac{\partial \ln m_i}{\partial \tau} + \sum_{i=2}^{N_{i,p}} \frac{\partial \ln m_i}{\partial \tau} = D \\
 - \sum_{i=2}^{N_{i,p}} f \frac{\partial \ln m_i}{\partial \tau} + \frac{\partial i}{\partial \tau} - \sum_{i=2}^{N_{i,p}} f \frac{\partial \ln m_i}{\partial \tau} = 0 \\
 \sum_{i=2}^{N_{i,p}} m_i \frac{\partial \ln m_i}{\partial \tau} + \frac{\partial \ln a_{sw}}{\partial \tau} + \sum_{i=1}^{N_{i,p}} j \frac{\partial i}{\partial \tau} + \frac{\partial \ln a_{sw}}{\partial \tau} - \left\{ \begin{array}{l} R \frac{\partial i}{\partial \tau} \\ N_{i,p} \frac{\partial i}{\partial \tau} \\ \sum_{c=2} Q \frac{\partial i}{\partial \tau} \end{array} \right\} + \sum_{i=2}^{N_{i,p}} m_i \frac{\partial \ln m_i}{\partial \tau} = K \\
 \sum_{i=2}^{N_{i,p}} \frac{\partial \ln m_i}{\partial \tau} + \frac{\partial \ln a_{sw}}{\partial \tau} - \left\{ \begin{array}{l} R \frac{\partial i}{\partial \tau} \\ N_{i,p} \frac{\partial i}{\partial \tau} \\ \sum_{c=2} Q \frac{\partial i}{\partial \tau} \end{array} \right\} + \frac{\partial \ln a_{sw}}{\partial \tau} = Z
 \end{array}$$

Although it was not done in the text, the first three equations have had the sums of the log molalities of the species separated into component and non-component terms.

Figure two



equation is repeated for every non-component species/phase in the system, an identity matrix is developed. This allows very efficient numerical techniques to be used.

This set of equations is repeated for every REV in the system. To keep the size of the program small, it is usually easiest to solve these equations separately from the flow, heat transport and solute transport equations, and iterate between them.

Although suitable for inclusion in the flow, heat transport and mass transport equations, the first derivative is rarely sufficient to calculate the number of moles of solid phases or molality of aqueous species at a future time. Successive derivatives of the mass action and mass balance equations can be taken, and the higher order derivatives solved for. All of these derivatives can then be used in a series expansion such as a Taylor's expansion. It is worth noting that the left hand side of the equations in figure one do not change, only the constant terms on the left hand side must be modified. Thus once the first derivative is obtained, it takes only minor computational effort to obtain any number of higher order derivatives.

Model Results

A large number of simulations have been made in the silica-water system. The initial conditions were of the form: *for time zero, for all x_i , isothermal and isobaric, solution in equilibrium with the matrix.* Boundary conditions were of the form: *for times greater than zero, the temperature and pressure were elevated at the first node.*

All of the modelling results indicate that the maximum rate of precipitation and dissolution will occur at the steepest temporal and spatial gradient in temperature. In

an isothermal system, the rates are much smaller and the maximum rate will occur at the steepest temporal and spatial gradient in pressure. This is shown schematically in figure two. The curve on the left is the molality of silica in equilibrium with quartz at the temperature and pressure of the matrix. The second is the the molality which would be expected if no silica precipitated during the time step. The shaded area is the potential amount of silica that could precipitate. Any process which remains close to equilibrium will precipitate this silica, decreasing porosity and permeability until advection is slower than conduction. These results are consistent with the rapid dissolution and subsequent precipitation of silica in the vicinity of a injection well during a steam flood into a heavy oil field.

If the flow system is to remain open, there must be sufficient mechanical energy available to hydraulically re-fracture the formation or other compensating reactions must be occurring to create new void space.

References

- Capuano, R.M. and Cole, D.R. 1982. Fluid-mineral Equilibria in a Hydrothermal System, Roosevelt Hot Springs, Utah. *Geochimica et Cosmochimica Acta*, 46, pp. 1353-1364.
- Helgeson, H.C., Garrels, R.M. and Mackenzie, F. 1969. Evaluation of irreversible reactions in geochemical processes involving minerals and aqueous solutions-II. Applications. *Geochimica et Cosmochimica Acta*, 33, pp. 455-481.
- Kwong, Y.T.J., Brown, T.H. and Greenwood, J.H. 1982. A thermodynamic approach to the understanding of the supergene alteration at the Afton copper mine, south-central British Columbia. *Canadian Journal of Earth Sciences*, 19, pp. 2378-2386.
- Lichtner, P.C. 1985. Continuum model for simultaneous chemical reactions and mass transport in hydrothermal systems. *Geochimica et Cosmochimica Acta*, 49, pp. 779-800.
- Villas, R.N. and Norton, D. 1977. Irreversible Mass Transfer Between Circulating Hydrothermal Fluids and the Mayflower Stock. *Economic Geology*, 72, pp. 1471-1504.
- Wolery, T.J. 1980. Chemical modelling of geological disposal of nuclear waste: progress report and a perspective. UCRL-52748, University of California, Lawrence Livermore Laboratory, Livermore, California. 66 pages.

CALCULATIONS OF GEOCHEMICAL MASS TRANSFER AS A FUNCTION OF TEMPERATURE AND TIME

William M. Murphy¹
University of California, Berkeley
Berkeley, CA 94720 USA

Abstract

Consideration of the temperature dependence of the rates of mineral dissolution permits kinetic calculations of geochemical mass transfer and transport in nonisothermal systems. Computations performed using a modified version of EQ6 show that differences in the variation of temperature with time significantly affect reaction paths. Nonisothermal kinetic reaction path models may be particularly useful in the understanding of the geochemical consequences of aqueous solutions flowing in thermal gradients.

Introduction

Irreversible mass transfer in geochemical systems results from perturbations to quasistatic states such as those accompanying variations in temperature. The rates of chemical reactions occurring in response to these perturbations exert a control on the temporal and, in dynamic systems, spatial distribution and composition of reactants and products, including aqueous solutions. Prediction of these phenomena for many geochemical systems is permitted by recent experimental and theoretical advances in the field of mineral dissolution kinetics and the generation of a data base of rate parameters for silicate mineral dissolution. The object of the present communication is to illustrate a means of computing time-temperature-reaction path relations for water-rock systems using a modified version of computer programs in the EQ3/6 software package.

A Nonisothermal Kinetic Reaction Path Model

The rapid rates of most homogeneous reactions in the aqueous phase and of precipitation of secondary minerals relative to the rates of irreversible dissolution of primary minerals permits many water-rock systems to be considered in partial equilibrium (e.g., Helgeson, 1979). Under such circumstances the rate of mass transfer and the direction of the reaction path can be calculated by taking explicit account of the rates of dissolution of the primary minerals. In contrast, for systems of more than one mineral reactant, partial equilibrium models calculated using arbitrary kinetics generally provide inaccurate predictions of the reaction path because variations in the relative rates of reaction of the dissolving minerals are neglected. This underscores the advantage of kinetic calculations even if the time of reaction is not of primary interest.

Transition state theory and irreversible thermodynamics have been used to interpret the rates of mineral dissolution in numerous recent publications (e.g., Aagaard and Helgeson, 1982; Lasaga, 1984). An operational rate equation consistent with transition state theory is (Aagaard and Helgeson, 1982)

$$d\xi_j / dt = k_j s_j a_{\pm}^{-n_j} (1 - \exp(-A_j / \sigma_j R T)) \quad (1)$$

¹Present address: Rockwell Hanford Operations, P.O. Box 800, Richland, WA 99352 USA

where ξ_j denotes the reaction progress variable for the i th dissolution reaction, t stands for time, k_j refers to the operational rate constant corresponding to the i th dissolution reaction, s_j signifies the total surface area of the dissolving mineral, a_{H^+} represents the activity of the aqueous hydrogen ion, $-n_j$ corresponds to the order of the i th dissolution reaction with respect to the aqueous hydrogen ion, A_i denotes the chemical affinity for the i th dissolution reaction, σ_i is a coefficient relating the stoichiometry of the activated complex to that of the dissolving mineral ($\sigma_i = 1$ for all applications in this paper), R refers to the gas constant, and T signifies the temperature in K. The variation of the operational rate constant with temperature is given by (Helgeson, Murphy and Aagaard, 1984)

$$\left[\frac{\partial \ln(k_j/T)}{\partial(1/T)} \right]_P = \frac{-\Delta H_i^\ddagger}{R} \quad (2)$$

where ΔH_i^\ddagger denotes the operational standard state activation enthalpy and P refers to pressure. For constant pressure, or for rate constants that are pressure independent, eq 2 can be integrated from T° to T to give

$$k_j = (T k_j^\circ / T^\circ) \exp((-\Delta H_i^\ddagger / R)(1/T - 1/T^\circ)) \quad (3)$$

where $k_j^\circ = k_j$ at T° , and ΔH_i^\ddagger has been taken to be temperature independent, which is warranted by the experimental data for silicate mineral dissolution. A tabulation of kinetic parameters for silicate mineral dissolution consistent with eqs 1-3 is given in Murphy (1985) (see also Murphy and Helgeson, 1986a,b).

For nonisothermal reaction path modeling the manner in which T varies must be specified. This may be accomplished by establishing a relation between temperature and reaction progress or between temperature and time. The former relation may be relevant, for instance, to certain adiabatic systems. The latter relation, which probably has greater geochemical applicability, could be used, for instance, to model a static closed system subjected to a thermal event or a fluid centered open system in which the fluid flows in a thermal gradient. In the second case, the rate of temperature change with time is given by the product of the thermal gradient and the rate of fluid flow (given in units of distance per time). The specific time-temperature (t - T) or reaction progress-temperature (ξ - T) relation will depend on the physical characteristics of the system being modeled, and in principle it may vary as the system evolves as a result of changes in permeability, porosity, heat capacity, etc.

Computational Strategy

In the reaction path computation using a modified version of EQ6, temperature is calculated at each step of reaction progress using a given t - T or ξ - T relation. Parameters in rate expressions for the rate limiting steps are then calculated as a function of T . Calculation of the k_j array requires a supporting data base of activation enthalpies and rate constants at the reference temperature (i.e. ΔH_i^\ddagger and k_j° in eq 3). Rates of individual irreversible dissolution reactions are then calculated with eq 1. The rate of dissolution, $d\xi_m/dt$, of each primary mineral m is given by the sum of the rates of parallel dissolution reactions for that mineral. Fractional rates of reaction for each primary reactant are then calculated by dividing each $d\xi_m/dt$ by the overall rate of reaction which is given by $d\xi/dt = \sum_m (d\xi_m/dt)$ where ξ is the overall reaction progress variable. Following Wolery (1979, 1984) and the coding in EQ6, prediction of the fractional rates of reaction over a succeeding reaction progress step is made by extrapolating a truncated Taylor's series approximation for the fractional rates as a function of the overall reaction progress. Integration of this expression yields the masses of each reactant to be added to the system in the succeeding step. In a similar manner, integration of a truncated Taylor's series approximation to the inverse of

the overall rate of reaction over the same step gives the time interval for that step. This enables calculation of the total time at the succeeding step and, from the time-temperature relation (if applicable), the estimated temperature at that time. After calculation of the new state of the system, and verification that the estimated fractional rates, time and temperature were sufficiently accurate, the sequence of calculations is repeated for the following step (see Wolery, 1984).

Example

Some results of a simple time-temperature-reaction path computation are shown in figures 1 and 2. Primary mineral reactants are albite, microcline, and quartz. Rate parameters for these minerals taken from Helgeson, Murphy and Aagaard (1984) and Murphy (1985) are presented in table 1. For albite and microcline rate parameters are given for parallel pH-dependent and pH-independent rate mechanisms. The rate of quartz dissolution was assumed to be pH-independent. Total surface areas per kilogram of H₂O for each reactant given in table 1 were taken to be independent of time. The sum of the total surface areas corresponds approximately to the surface area of a fractured medium with a fracture width of 2 mm.

A 10⁻² molal NaCl solution with pH 6 in equilibrium with muscovite and quartz and approximately saturated with respect to kaolinite was chosen as the starting fluid. The initial temperature was taken to be 50° C (323 K), and a linear time-temperature relation was imposed on the system according to the equation

$$T = 323 K + at \quad (4)$$

in which *a* is a constant which was taken to be 1°/year.

A fluid centered open system model was calculated in which precipitated minerals were not permitted to redissolve in the solution. One possible application of the linear t-T relation (eq 4) in the open system is to a fluid flowing at a constant velocity *v* (in units of meters/year) along a constant thermal gradient given by *av*⁻¹.

In fig 1 the logarithm of the rate of dissolution of the primary minerals is plotted versus the logarithm of time. Because of the linear t-T relation, temperature is also given on the abscissa on a log scale. Microcline is seen to dissolve at the outset of the path, then it precipitates at equilibrium from about 10^{-1.7} to 10^{0.7} years, then it dissolves again. (The horizontal line labeled PPT in fig 1 denotes precipitation at equilibrium.) Quartz follows a roughly complementary pattern; initially at equilibrium and precipitating, it dissolves through an intermediate period, then precipitates again, and then dissolves at the end of the reaction path. Albite dissolves throughout the reaction path except that it comes to equilibrium at the end of the simulation. Muscovite was predicted to

TABLE 1: Rate parameters for primary mineral reactants.

Reactant	25°C Rate Constant $\frac{\text{mole}}{\text{cm}^2 \text{ sec}}$	Hydrogen Ion Exponent (-n ₁)	ΔH_1^\ddagger $\frac{\text{kcal}}{\text{mole}}$	Surface Area $\frac{\text{cm}^2}{\text{kg H}_2\text{O}}$
ALBITE	1.9E-13 3.0E-16	1 0	20.6 8.5	8000
MICRO- CLINE	2.2E-13 3.0E-16	1 0	19.0 8.5	16000
QUARTZ	1.6E-18	0	18.0	16000

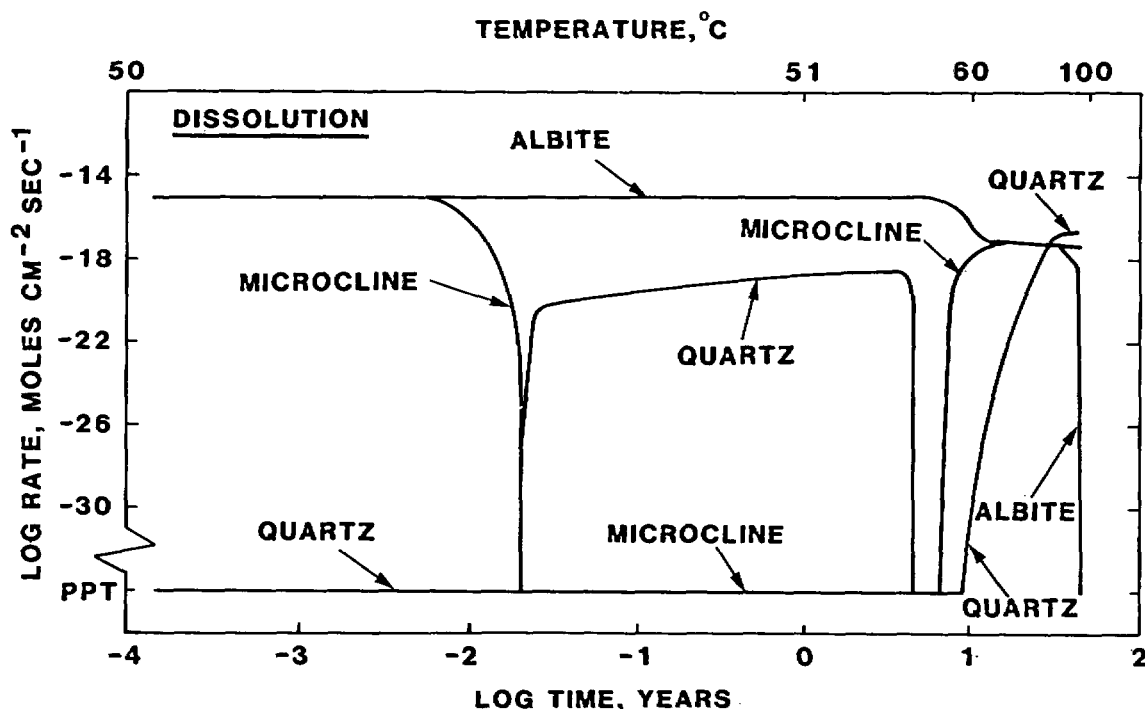


Figure 1. The logarithm of mineral dissolution rates as a function of the logarithm of time. Temperature is given at the top on the abscissa. (See text for discussion.)

precipitate at equilibrium throughout the reaction path and no other secondary phases (including gibbsite, kaolinite, and the EQ6 phyllosilicates) were predicted to come to equilibrium with the aqueous solution. It can be seen clearly in fig 1 that in this simple model the absolute and relative rates of reaction varied widely and affected significantly the sequence and timing of mass transfer events.

If we interpret the linear t-T relation as the consequence of the movement of a fluid at a constant rate in a constant thermal gradient, then the abscissa in fig 1 also corresponds to log distance, as well as to log time and log temperature. One can thus read from this figure the spatial regions over which each mineral dissolves or precipitates. Note also that the integral of the rate of dissolution over time gives the quantity of material dissolved. Therefore, imagining fig 1 to be transformed to a linear coordinate system, the areas under the curves would give the numbers of moles of minerals dissolved as a function of time, temperature, or distance.

A diagram analogous to fig 1 could be generated for the precipitated phases showing rates of precipitation as a function of time, temperature or distance. In this model the rates of precipitation are controlled by the overall rate of mass transfer and equilibrium constraints among the aqueous solution and the precipitating minerals.

Figure 2 is an illustration of the variation of solution composition for the same reaction path. Aqueous silica can be seen to follow closely quartz solubility. Na^+ increases as albite dissolves. Initially pH and $\text{Al}(\text{OH})_4^-$ increase as the two feldspars dissolve, then level off as microcline precipitates. Then, where microcline, muscovite and quartz are all in equilibrium with the aqueous phase, pH and $\text{Al}(\text{OH})_4^-$ increase dramatically, and this is accompanied by a large decrease in K^+ . Finally, as temperature increases from 60° to 100°C during a period of relatively little dissolution, the pH declines.

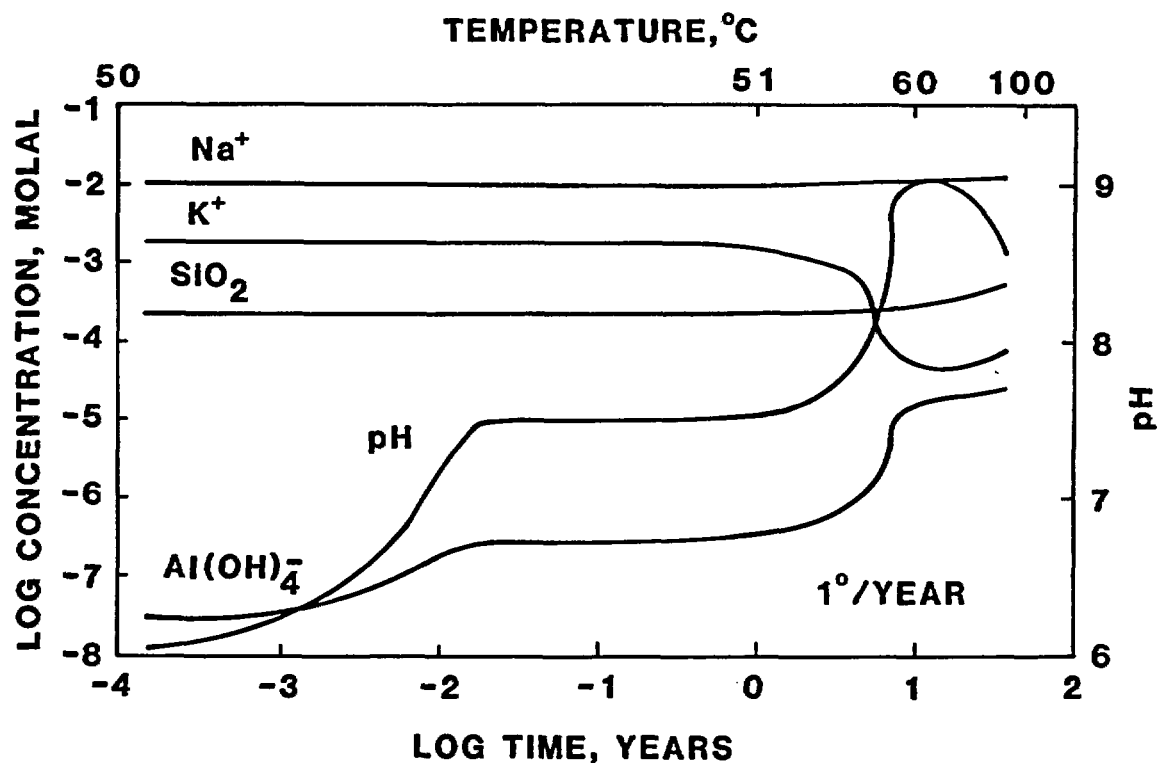


Figure 2. The logarithm of the molal concentration of principal aqueous species and pH (right scale) as a function of the logarithm of time. Temperature is given at the top on the abscissa. (See text for discussion.)

The computations used to generate figs 1 and 2 have all been made for a unique t-T relation, $1^\circ/\text{year}$. From these results it is difficult to appreciate which effects are a consequence of the variation in temperature and which are simply a result of the irreversible dissolution. This can be clarified by performing calculations for other t-T relations as illustrated in fig 3. In this figure the logarithm of the change of temperature, $\log \Delta T = \log (T - T^\circ)$, is plotted against log time. Time in years is given on a log scale at the top of the figure, and temperature in $^\circ\text{C}$ on a log scale is shown at the right. The dotted lines in this figure represent different linear t-T relations of 2° , 1° , 0.5° , and $0.25^\circ/\text{year}$ as indicated, with the initial temperature in each case being 50°C . Reaction paths with the same set of initial conditions as those described above have been calculated for each of these rates of temperature change. In fig 3 the fields in time-temperature space delineated by solid and dashed curves are labelled with symbols representing the primary mineral reactants that are out of equilibrium with the aqueous solution and dissolving in that space. The remaining primary minerals together with muscovite are predicted to be precipitating at equilibrium with the aqueous phase along reaction paths traversing the fields.

It can be seen in fig 3 that differences in the time-temperature relations significantly affect the reaction paths. If temperature variation was not important, the lines separating fields in this diagram would be vertical such as that separating the AB+MI disequilibrium field from the AB+Q disequilibrium field. Furthermore, the difference between t-T relations is not simply that events always occur sooner at higher temperatures and later at lower temperatures. This relation is observed for the transition from the AB+MI+Q disequilibrium field to the MI+Q disequilibrium field. However, the transition from the AB+Q disequilibrium field to the AB disequilibrium field occurs sooner at lower temperatures and later at higher temperatures. In fact, for the lowest rate of temperature increase shown here, $0.25^\circ/\text{year}$, this transition does not occur at all. In this case there is a direct transition from the AB+MI disequilibrium field to the AB disequilibrium field, and there is no intermediate period or zone of quartz dissolution.

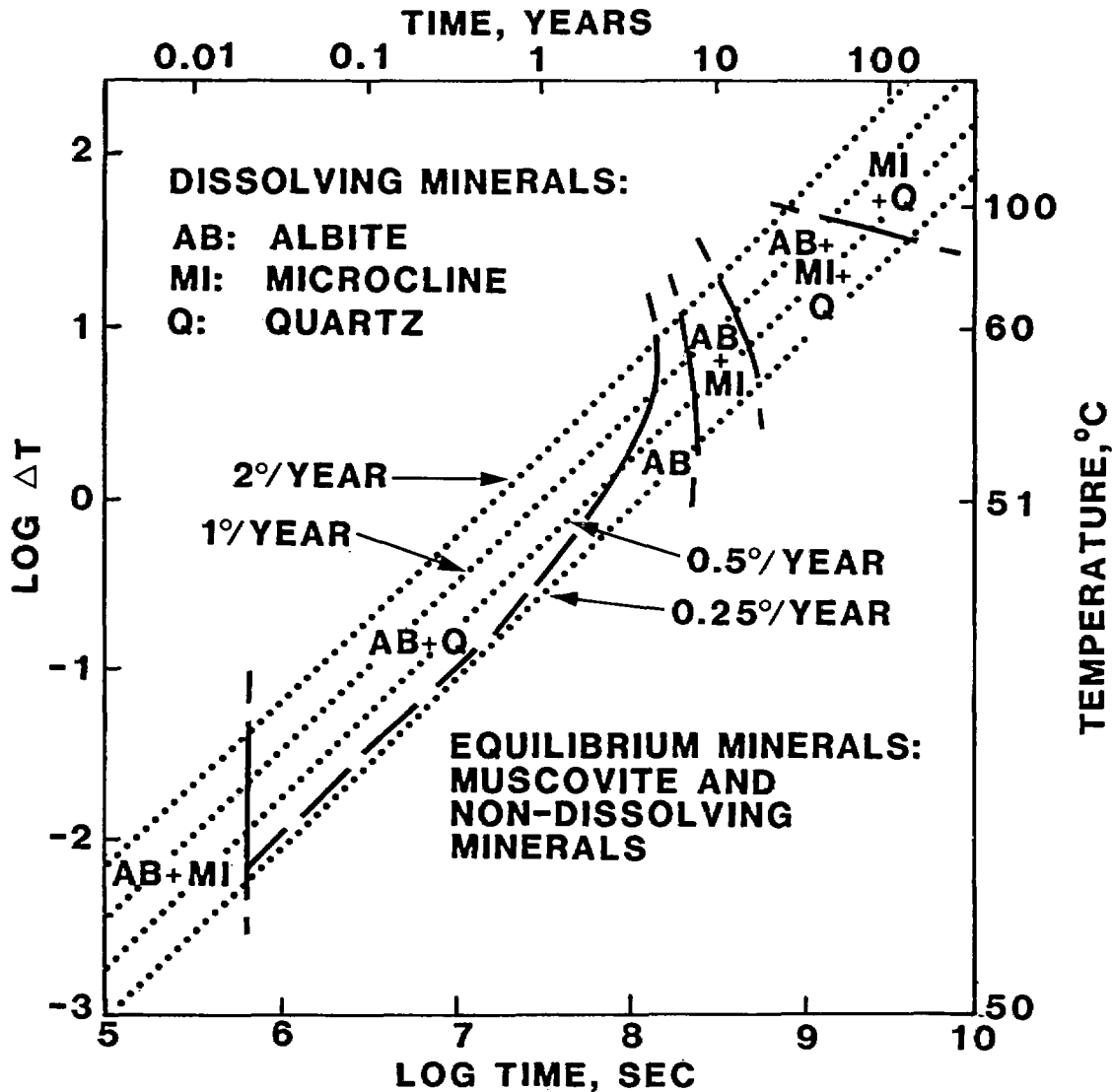


Figure 3. Time-temperature-reaction path diagram for the dissolution of albite, microcline and quartz in aqueous solutions initially at 50° C with temperature increasing as a function of time at rates from 0.25° to 2.0° / year. (See text for discussion.)

In summary, figure 3 is a time-temperature-transformation diagram for a class of irreversible water-rock interaction paths each with the same set of initial conditions but with different regimes of time-temperature evolution. The generation of this diagram requires a kinetic model for water-rock reactions as a function of temperature.

Concluding Remarks

Under far from equilibrium conditions rates of water-rock interactions are generally fast on a geologic time scale. Hence, most hydrothermal systems remain relatively close to equilibrium in quasistatic states (Helgeson and Murphy, 1983). Mass transfer will be induced in such systems by physical perturbations, among which variations in temperature are particularly important. It follows that kinetic modeling of nonisothermal water-rock systems provides a valuable means of predicting geochemical mass transfer. Calculations such as those summarized above and their representation in time-temperature-reaction path diagrams such as fig 3 should prove to be useful

in understanding the evolution of nonisothermal systems, and should be particularly relevant for predictions of the geochemical consequences of aqueous solutions flowing in thermal gradients.

References

- AAGAARD P. and HELGESON H. C. (1982) Thermodynamic and kinetic constraints on reaction rates among minerals and aqueous solutions. I. Theoretical considerations. *Am. J. Sci.* **282**, 237-285.
- HELGESON H. C. (1979) Mass transfer among minerals and hydrothermal solutions. In *Geochemistry of Hydrothermal Ore Deposits* (ed. H. L. BARNES) Wiley.
- HELGESON H. C. and MURPHY W. M. (1983) Calculation of mass transfer among minerals and aqueous solutions as a function of time and surface area in geochemical processes. I. Computational approach. *Math. Geo.* **15**, 109-130.
- HELGESON H. C., MURPHY W. M. and AAGAARD P. (1984) Thermodynamic and kinetic constraints on reaction rates among minerals and aqueous solutions. II. Rate constants, effective surface area, and the hydrolysis of feldspar. *Geochim. Cosmochim. Acta* **48**, 2405-2432.
- LASAGA A. C. (1984) Chemical kinetics of water-rock interactions. *J. Geophys. Res.* **89**, 4009-4025.
- MURPHY W. M. (1985) Thermodynamic and Kinetic Constraints on Reaction Rates Among Minerals and Aqueous Solutions. Ph.D. Dissertation, Univ. California, Berkeley.
- MURPHY W. M. and HELGESON H. C. (1986a) Thermodynamic and kinetic constraints on reaction rates among minerals and aqueous solutions. III. Activated complexes and the pH-dependence of the rates of feldspar, pyroxene, wollastonite, and olivine hydrolysis. *Geochim. Cosmochim. Acta* (in review).
- MURPHY W. M. and HELGESON H. C. (1986b) Thermodynamic and kinetic constraints on reaction rates among minerals and aqueous solutions. IV. Retrieval of rate constants and activation parameters for the hydrolysis of pyroxene, wollastonite, olivine, andalusite, and quartz. *Am. J. Sci.* (in review).
- WOLERY T. J. (1979) Calculation of chemical equilibrium between aqueous solutions and minerals: The EQ3/6 software package. LLNL doc. UCRL-52748.
- WOLERY T. J. (1984) EQ6, A computer program for reaction-path modeling of aqueous geochemical systems: User's guide and documentation. LLNL doc. UCRL-51__ (draft).

DEVELOPMENT AND APPLICATION OF STABLE ISOTOPE
MASS TRANSFER REACTION PATH MODELS

Teresa Suter Bowers
Department of Earth, Atmospheric and Planetary Sciences
Massachusetts Institute of Technology
Cambridge, MA 02139

Abstract

Modifications to EQ3/6 for the inclusion of oxygen, hydrogen and sulfur isotopes allow simultaneous calculation of the chemical and stable isotopic consequences of mass transfer in geologic systems. Addition of isotopes to the computer programs provides further constraints that can be used to evaluate water-rock interaction models. An application to mid-ocean ridge hydrothermal systems is included where chemical and isotopic changes attending seawater-basalt interaction are calculated for an evolutionary path of seawater to hydrothermal endmember such as that exiting from mid-ocean ridge hot springs.

Introduction

The use of stable isotopes to demonstrate the presence of hydrothermal activity has become widespread in recent years (Taylor, 1983, 1974 and references therein). Isotopic ratios have been used to indicate mineral alteration, type or source of infiltrating fluids and water-rock ratios. In fact, at times they give evidence of water-rock interaction when mineralogical or chemical evidence is scant (Gregory and Taylor, 1981). As a result, it seemed desirable to incorporate stable isotope systematics into existing geochemical mass transfer computer codes in order to develop integrated chemical and isotopic models describing hydrothermal systems. Computer models of this sort are important for (at least) two reasons: 1) they allow explicit accounting of the effect that formation of secondary mineral phases may have on isotopic ratios of the fluid, and 2) each element for which stable isotopes are included provides an additional constraint that must be met when attempting to model a geologic problem. One of the criticisms of geochemical models is that they often cannot be shown to provide a unique path. However, additional constraints, such as isotopes, that result in the rejection of some paths will further the utility of such models.

Computer Programs

An integrated chemical and oxygen and hydrogen isotope computer model based on EQ3/6 (Wolery, 1978, 1979, 1983) was developed by Bowers and Taylor (1985) to address hydrothermal circulation of seawater through basalt at mid-ocean ridges. A summary of the calculational scheme used by EQ3/6 for isotopes is presented here, however, details of the procedure are given in Bowers and Taylor (1985). The equations are presented here in terms of oxygen, but hold for other elements as well. Masses of each isotope can be conserved in a similar manner as are the

elements in EQ6. A $\delta^{18}\text{O}$ for the system ($\delta^{18}\text{O}_s$) at a reaction progress of (ξ) can be defined by

$$\delta^{18}\text{O}_s(\xi) = \frac{n_{\text{O}}^{\text{H}_2\text{O}}}{n_{\text{O}}^{\text{b}}} \delta^{18}\text{O}_{\text{H}_2\text{O}}(\xi) + \frac{1}{n_{\text{O}}^{\text{b}}} \sum_r n_{\text{O}}^r \delta^{18}\text{O}_r \quad (1)$$

where

$$n_{\text{O}}^{\text{b}} = n_{\text{O}}^{\text{H}_2\text{O}} + \sum_r n_{\text{O}}^r \quad (2)$$

where $n_{\text{O}}^{\text{H}_2\text{O}}$ represents the moles of oxygen in the fluid phase, n_{O}^r is the moles of oxygen in reactant phase r , and n_{O}^s denotes moles of oxygen in the system. ξ^* represents one ξ -step before the present value of ξ ; at the first step this is the initial state of the system prior to any dissolution of reactants. When products begin to form $\delta^{18}\text{O}_s$ must be redistributed between the fluid and these product phases according to

$$\delta^{18}\text{O}_s(\xi) = \frac{n_{\text{O}}^{\text{H}_2\text{O}}}{n_{\text{O}}^{\text{b}}} \delta^{18}\text{O}_{\text{H}_2\text{O}}(\xi) + \frac{1}{n_{\text{O}}^{\text{b}}} \sum_p n_{\text{O}}^p \delta^{18}\text{O}_p(\xi) \quad (3)$$

where n_{O}^r has the same value as in (1) but $n_{\text{O}}^{\text{H}_2\text{O}}$ has been modified by the precipitation of products, and $\delta^{18}\text{O}_{\text{H}_2\text{O}}$ and $\delta^{18}\text{O}_p$ at ξ must be calculated from equilibrium fractionation curves for the product minerals and H_2O , expressed by

$$\alpha_{p-\text{H}_2\text{O}} = \frac{1000 + \delta^{18}\text{O}_p}{1000 + \delta^{18}\text{O}_{\text{H}_2\text{O}}} \quad (4)$$

This procedure is followed for each ξ -step.

The distribution of sulfur isotopes between fluid and rock present a more complex situation because equilibrium between sulfate and sulfide in solution cannot always be assumed, for example, below approximately 250°C (Shanks et al., 1981). In this case, separate accounting must be taken of the sulfur assigned to either sulfate or sulfide and the interchange of isotopes between oxidation states not allowed.

The fractionation factors (α) for O, H, and S isotopes are included in additional databases attached to EQ6. The fractionation curves have either been determined experimentally or are known empirically for a large number of geologically important systems and are summarized elsewhere (Bowers and Taylor, 1985; Barnes, 1979; and Taylor, 1974).

Applications

Chemical and isotopic changes accompanying seawater-basalt interaction in axial mid-ocean ridge hydrothermal systems can now be assessed through the use of the above-described computer code. The illustrations here are meant to serve merely as an example of use of the modified computer codes and for details of the development of the geologic model the reader should refer to Bowers and Taylor (1985). The model is constrained by the chemical and stable-isotope compositions of both the starting solution (seawater) and the final hydrothermal endmember (21°N) (Von Damm et al., 1985; Craig et al., 1980), as well as petrologic observations of the alteration mineralogy of the basalt (Humphris and Thompson, 1978, Stakes and O'Neil, 1982).

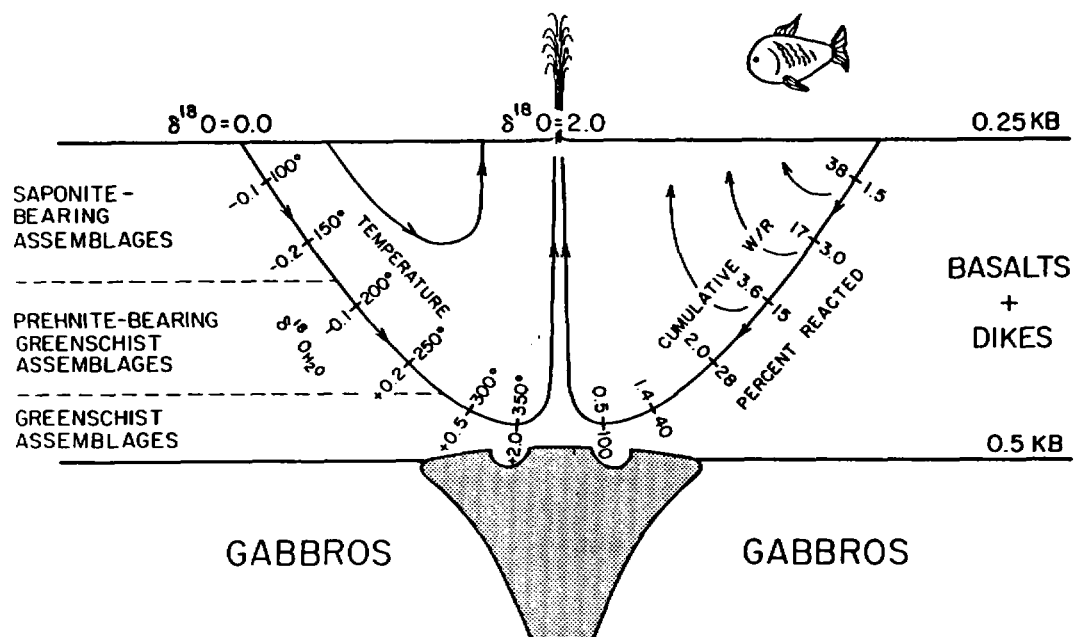


Fig. 1. Schematic illustration of seawater-basalt interaction at mid-ocean ridges

Fig. 1 is a schematic illustration of the model, where a hypothetical path shows the penetration of seawater through seafloor basalts at low temperature, circulation of the evolving fluid downward to the magma-chamber contact, and eventual exit of the hydrothermal endmember at 350°C from mid-ocean ridge hot springs. Cumulative water-rock ratio, percent reaction progress and $\delta^{18}O$ H₂O are shown along the two symmetrical path-lines at 50°C intervals. The increasing temperatures and decreasing water-rock ratio with depth provide a sharply increasing grade of hydrothermal metamorphism downward. The mineral assemblages listed at the left of the figure correspond to those found in nature and are essentially reproduced by the computer model.

Examples of the isotopic alteration of the system during development of secondary mineral phases as a function of reaction progress at 250°C and 350°C are shown in Fig. 2.

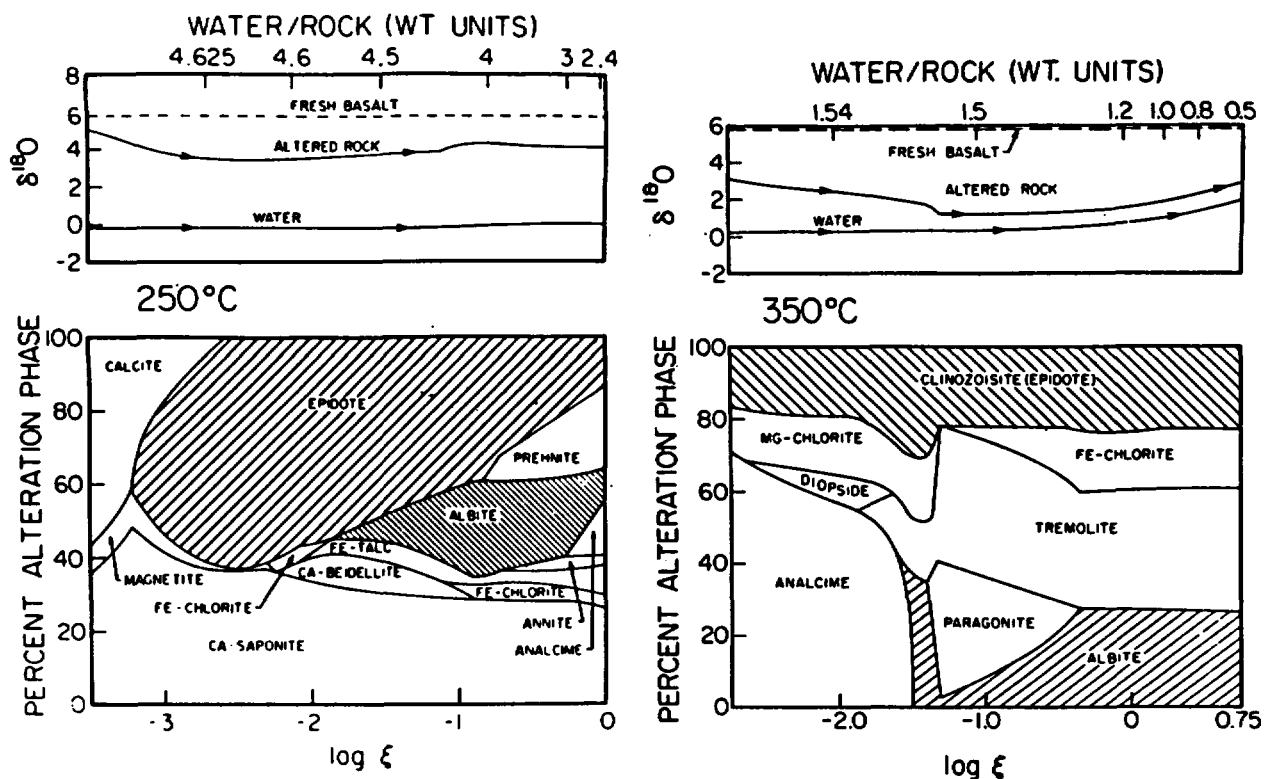


Fig. 2. Summary of predicted alteration phases and $\delta^{18}\text{O}$ values as a function of reaction progress at 250° and 350°

The reactant is fresh basalt, with $\delta^{18}\text{O} = +5.8$ o/oo. At 250°C the water-rock ratio is sufficiently high such that changes to $\delta^{18}\text{O}_{\text{H}_2\text{O}}$ are slight and the major controls on $\delta^{18}\text{O}$ of the altered rock are temperature and the identity of the alteration phases being produced. At 350°C the system has evolved to sufficiently low water-rock ratios so that $\delta^{18}\text{O}$ of both the altered rock and the fluid vary as a function of reaction progress, or the quantity of fresh basalt that has been altered (right side of diagram).

Hydrogen and sulfur isotopes can be followed in a similar manner and yield more information concerning potential paths of the evolving fluid.

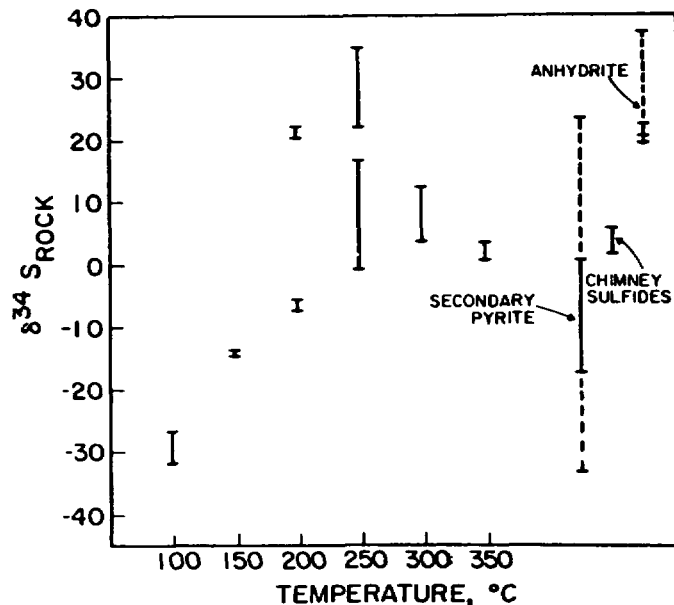


Fig. 3. Calculated $\delta^{34}\text{S}$ of predicted sulfides and anhydrite at discrete temperature steps together with ranges observed in natural samples

Fig. 3 illustrates some preliminary results of sulfur isotope modeling where equilibrium between sulfate and sulfide were assumed at all temperatures. The vertical bars at each temperature represent the range of $\delta^{34}\text{S}$ values of secondary sulfides (upper bars at 200° and 250°C are for anhydrite) calculated to form during alteration of basalt. Also shown in Fig. 3 for comparison are ranges typical of samples taken from DSDP cores, dredged basalts and chimney pieces (Alt et al., 1985; Styr et al., 1981; Andrews, 1979). The solid portion of the bars are where most samples fall; the dashed portions are extensions to include observations outside the normal range. The agreement between the low temperature calculated sulfide $\delta^{34}\text{S}$ values and the low observed $\delta^{34}\text{S}$ values for pyrite is coincidental and is not indicative of sulfate-sulfide equilibrium at 100°C. However, at intermediate temperatures calculated sulfide and anhydrite $\delta^{34}\text{S}$ values agree reasonably well with observation and at 350°C there is good agreement between the calculations and chimney sulfide values.

Tracking of the stable isotopes of oxygen, hydrogen and sulfur (or carbon) as a function of reaction progress in mass transfer computer codes such as EQ3/6 can yield additional information about water-rock interaction processes that may be of considerable use in determining relative closeness of fit of diverse models. This can lead to rejection of potential paths that fit the chemical data adequately, but not the isotopic.

References

- ALT J.C., SALTZMAN E.S. and PRICE D.A. (1985) Anhydrite in hydrothermally altered basalts: Deep sea drilling project hole 504B Leg 83. Init. Repts. DSDP, 83 Washington, U. S. Govt. Printing Office, 283-288.
- ANDREWS A.J. (1979) On the effect of low-temperature seawater-basalt interaction on the distribution of sulfur in oceanic crust, layer 2. *Earth Planet. Sci. Lett.* 46, 68-80.
- BARNES H.L. (1979) Geochemistry of Hydrothermal Ore Deposits. Wiley.
- BOWERS T.S. and TAYLOR H.P., Jr. (1985) An integrated chemical and stable-isotope model of the origin of mid-ocean ridge hot spring systems. *J. Geophys. Res.* 90, 12, 583-12,606.
- CRAIG H., WELHAN J.A., KIM K., POREDA R. and LUPTON J.E. (1980) Geochemical studies of the 21°N EPR hydrothermal fluids. *EOS, Trans. Amer. Geophys. Union* 61, abstract, 992.
- GREGORY R.T. and TAYLOR H.P., Jr. (1981) An oxygen isotope profile in a section of Cretaceous oceanic crust, Samail ophiolite, Oman: Evidence for $\delta^{18}\text{O}$ buffering of the oceans by deep (>5km) seawater-hydrothermal circulation at mid-ocean ridges. *J. Geophys. Res.* 86, 2737-2755.
- HUMPHRIS S.E. and THOMPSON G. (1978) Hydrothermal alteration of oceanic basalts by seawater. *Geochim. Cosmochim. Acta.* 42, 107-125.
- SHANKS W.C., III, BISCHOFF J.L. and ROSENBAUER R.J. (1981) Seawater sulfate reduction and sulfur isotope fractionation in basaltic systems: Interaction of seawater with fayalite and magnetite at 200-300°C. *Geochim. Cosmochim. Acta* 45, 1977-1995.
- STAKES D.S. and O'NEIL J.R. (1982) Mineralogy and stable isotope geochemistry of hydrothermally altered oceanic rocks. *Earth Planet. Sci. Lett.* 57, 285-304.
- STYRT M.M., BRACKMAN A.J., HOLLAND H.D., CLARK B.C., PISUTHA-ARNOLD V., ELDRIDGE C.S. and OHMOTO H. (1981) The mineralogy and the isotopic composition of sulfur in hydrothermal sulfide/sulfate deposits on the East Pacific Rise, 21°N latitude. *Earth Planet. Sci. Lett.* 53, 382-390.
- TAYLOR H.P., Jr. (1983) Oxygen and hydrogen isotope studies of hydrothermal interactions at submarine and subaerial spreading centers. NATO Symposium Vol. on Hydrothermal Processes at Seafloor Spreading Centers, P.A. Rona, K. Bostrom, L. Laubier, and K.L. Smith, eds. Plenum Press, New York, 83-139.

- TAYLOR H.P., Jr. (1974) The application of oxygen and hydrogen isotope studies to problems of hydrothermal alteration and ore deposition. *Econ. Geol.* 69, 843-883.
- VON DAMM K.L., EDMOND J.M., GRANT B., MEASURES C.I., WALDEN B. and WEISS R. (1985) Chemistry of submarine hydrothermal solutions at 21°N East Pacific Rise. *Geochim. Cosmochim. Acta.* 49, 2197-2220.
- WOLERY T.J. (1982) EQ3NR, A computer program for geochemical aqueous speciation-solubility calculations. UCRL-5, Distribution Category UC-70, Lawrence Livermore National Laboratory.
- WOLERY T.J. (1979) Calculation of chemical equilibrium between aqueous solution and minerals: the EQ3/6 software package. Lawrence Livermore Laboratory Report UCRL-52658, 41p.
- WOLERY T.J. (1978) Some chemical aspects of hydrothermal processes at mid-oceanic ridges - a theoretical study. I. Basalt-seawater reaction and chemical cycling between the ocean crust and the oceans. II. Calculation of chemical equilibrium between aqueous solutions and minerals. Ph.D. Dissertation, Northwestern University.

IMPROVEMENTS IN THE SOLID SOLUTION MODELING CAPABILITIES OF EQ3/6

*William L. Bourcier
Lawrence Livermore National Laboratory
Livermore, California 94550*

ABSTRACT

The EQ3/6 geochemical modeling codes have been expanded to include provision for the precipitation and dissolution of solid solution mineral phases in the calculation of water-rock reactions for both ideal and non-ideal solid solution models. The solid solution option can be used in both closed and open system modeling. In closed systems, the solid solution precipitates are assumed to completely re-equilibrate with the system at each step during the reaction. In open systems, a finite amount of solid solution which is precipitated at each step of reaction progress is removed from the system and not allowed to back-react with the fluid. The open system treatment can be used to model the zoning of solid solutions, which is commonly observed in nature.

Sample calculations using the solid solution option in the simulation of the diagenetic changes in an arkosic sandstone show that including solid solutions as product phases results in increased stability of clays and carbonates during burial.

INTRODUCTION

The EQ3/6 geochemical modeling codes (Wolery, 1988) have been expanded to take into account compositional variability of solid solution phases. In simulations of water-rock interactions, product phases can now continually change in composition in response to the evolving solution composition. This capability enables more accurate simulation of real systems in which solid solution phases are common and whose changing compositions record the progress of water-rock interaction.

This paper describes how solid solutions are handled in the EQ3/6 code package, describes the current database, provides instructions on how a user can add additional solid solution models to the database, and discusses some limitations of the current approach along with recommendations for future improvements.

THE SOLID SOLUTION PROBLEM

One aspect of the geochemical modeling of water-rock interactions is the prediction of the precipitation of secondary phases during the reactions. Water-rock interactions involving solid phases of fixed stoichiometry are modeled by forcing mineral phases to precipitate when their saturation indices are exceeded. The saturation index (SI) for the

phase i is defined as:

$$SI_i = \log \left(\frac{Q_i}{K_i} \right) \quad (1)$$

where Q is the activity product for phase i and K is the solubility product for phase i . The phase is supersaturated with respect to a given solution composition when SI_i is greater than zero.

For solid solution phases which have variable composition, the treatment is more complicated because the saturation index of the solid is a function of both the solution composition and the solid composition. The problem of treating solid solutions then becomes that of determining the least soluble solid solution composition for a given fluid composition, and then determining the saturation index for that phase.

The least soluble solid solution composition for a given fluid composition is calculated by finding the maximum of the saturation index of the solid solution. The saturation index for a solid solution (ss) is defined in an analogous way to equation (1) for a fixed composition phase (BOURCIER, 1985):

$$SI_{ss} = \sum_{i=1}^n X_i \cdot \log \left(\frac{Q_i}{K_i \cdot a_i} \right) \quad (2)$$

where X_i is the mole fraction of component i in the solid solution, a_i is the activity of component i in the solid solution, and n is the number of components in the solid solution.

Ideal solid solutions for which $X_i = a_i$, a simple analytical solution for the maximum value of equation (2) is:

$$X_i = \left(\frac{Q_i/K_i}{\sum_n Q_n/K_n} \right) \quad (3)$$

where the sum is over all the components of the solid solution. Equation 3 is used to calculate the mole fraction of each component in the solid solution from the saturation indices of each endmember component of the solid solution and the given solution composition. This equation is programmed into the subroutine HPSAT of the EQ3/6 package.

For non-ideal solid solutions, the relationship $X_i = a_i$ does not hold and a simple analytical solution for the maximum of equation (2) does not exist. In this case, a numerical method must be used to find the maximum of the affinity function. In EQ3/6 the Simplex method was chosen for this task. The Simplex method is a well known algorithm for solving linear programming problems (ANTON et al., 1974). It is also used for ideal site-mixing solid solution models where again the relationship $X_i = a_i$ does not hold.

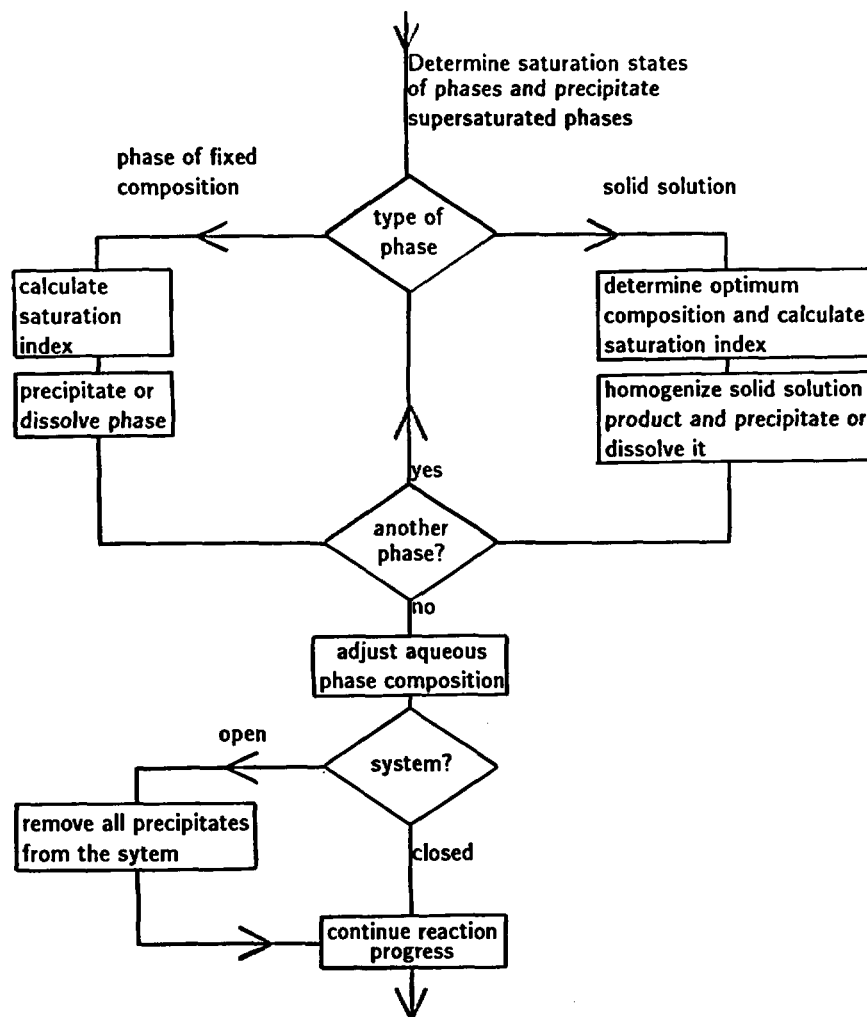


Figure 1. Flow chart showing how EQ6 treats solid solutions and fixed composition minerals during a reaction progress calculation.

SOLID SOLUTIONS IN GEOCHEMICAL MODELING

Solid solutions pose a special problem in calculations of water-rock reactions because of their variable composition. The composition of the precipitating solid solution phase changes steadily as the solution composition changes. In modeling this process, it can be assumed either that the previously precipitated solid mass continually re-equilibrates with the solution (closed system behavior) or that the solid mass is immediately isolated from the system so that it cannot back-react (open system behavior). Both open and closed system options are available in EQ6 and include provision for solid solution reactants and precipitates. Figure 1 is a flowchart illustrating the manner in which solid solutions are handled by EQ6. The NMODL1 option is used to specify either open or closed system behavior. In addition, the variable DLZIDP can be set in the input file to allow any arbitrary value of the dump interval for open systems. The dump interval refers to how much reaction progress is allowed before the product phases are isolated from the system. It allows any intermediate behavior between pure open and pure closed system behavior

to be modeled. If this interval is zero, the system behaves as a true open system. If DLZIDP is 0.1, the product phases are continually back-reacted with the system for each one tenth of the reaction progress, at which point the product phases are isolated from the system. Varying the size of the DLZIDP parameter controls the extent of back-reaction of the system and is therefore useful for modeling zoning of solid solutions.

The solid solution option is invoked in the EQ3NR and EQ6 input files by setting the IOPT4 parameter equal to 1. No other changes are needed. For EQ3NR runs where a fixed composition solid solution is assumed to be in equilibrium with a fluid phase (i.e. JFLAG=20 option), IOPT4 should be set equal to 2.

SOLID SOLUTION DATABASE

Most solid solutions present in the EQ3/6 database are assumed to follow ideal molecular mixing relations (see Table 1). By definition, ideal molecular mixing models hold that the enthalpy of mixing is zero, and that the endmembers mix as complete molecular entities. This is in contrast to site mixing models where ions are allowed to mix randomly on sites, independent of the populations on other sites. For the case where only one site is populated by more than one ion (such as the calcite-structured carbonate solid solution), molecular mixing and site mixing are identical. For solid solutions that have multiple sites, molecular mixing models therefore neglect the small favorable entropy of independent mixing over several sites and enthalpy changes associated with non-ideal mixing.

Ideal mixing is assumed for most minerals because experimental data on non-ideal mixing is generally not available for the relatively low temperature range (less than 300°C) of the EQ3/6 database. The equilibration rates of minerals are usually too slow at these temperatures, and metastability too common to allow useful thermodynamic data to be obtained from experiments. However, in nature, metastable low temperature phases are common, and it may be that for some systems, the assumption of ideal mixing is a better approximation for what precipitates in a real system than the thermodynamically most stable composition predicted from a rigorous non-ideal solid solution model derived from high-temperature data.

Additional solid solutions can easily be added to the EQ3/6 database. First add the appropriate block to the solid solution section of the file DATA0. A sample block for the orthopyroxene solid solution is given in Figure 2 below.

The data block contains the following information: the name of the solid solution (which must be distinct from any other solid), the number of endmember components, the type of solid solution model, and the names and maximum mole fractions of endmembers. The types of solid solution models available are listed in subroutine LAMDA and include ideal, third-order binary, Maclaurin binary, cubic binary with P,T dependence, Guggenheim

Table 1. Solid Solutions in the EQ3/6 Database

NAME	ENDMEMBERS		SOLUTION MODEL
(Na,K)-sanidine	sanidine high	albite high	ideal
biotite	phlogopite pd-oxyannite	annite	ideal
saponite-tri (trioctahedral)	saponite-Ca saponite-K saponite-Na	saponite-H saponite-Mg	ideal
smectite-di (dioctahedral)	beidellit-Ca beidellit-Mg nontronit-Ca nontronit-Mg montmor-Ca montmor-Mg	beidellite-K beidellit-Na nontronit-K nontronit-Na montmor-K montmor-Na	ideal
olivine	fayalite	forsterite	regular
orthopyroxene	ferrosilite	enstatite	ideal
plagioclase	albite high	anorthite	ideal
carbonate-calcite	calcite rhodochrosite smithsonite	magnesite siderite SrCO ₃ -cal	ideal
epidote-ss	epidote	clinozoisite	ideal
mordenite-ss	mordenite-Na mordenite-Ca	mordenite-K	ideal
phillipsite-ss	phillipsite-K phillipsite-Na	phillipsite-Ca	ideal
stilbite-ss	stilbite-Ca stilbite-Na	stilbite-K	ideal
garnet-ss	andradite	grossular	ideal site-mixing
chlorite-ss	clinochl-14a	daphnite-14a	ideal
dachiardite-ss	dachiardite-K dachiardite-Na	dachiardite-Ca	ideal

+					
orthopyroxene	2 0				
1.000 ferrosilite	1.000 enstatite				
0.0000	0.0000	0.0000	0.0000	0.0000	0.0000
0.0000	0.0000	0.0000	0.0000	0.0000	0.0000
+					

Figure 2. Solid solution data block for orthopyroxene.

binary, and regular ternary. The last twelve numbers in the pyroxene block (zeros in this

binary, and regular ternary. The last twelve numbers in the pyroxene block (zeros in this case) are non-ideal mixing parameters used in subroutine LAMDA. The thermodynamic data blocks for the endmembers must be present in DATA0.

Thermodynamic data for solid solution endmembers, which are often hypothetical, are usually different than data for real phases having the same composition. In this case, an entry for the endmember should be placed into the DATA0 file and given a different name than the real phase. For example, the calcite-structured carbonate solid solution has the component rhombohedral SrCO_3 , a solid phase that does not occur in nature. SrCO_3 is distinct from strontianite which has the aragonite structure. Both solids have been placed into DATA0 and given distinct names.

EXAMPLE - MODELING DIAGENESIS USING THE SOLID SOLUTION OPTION OF EQ6

This example of using the solid solution option of EQ3/6 simulates the reaction between minerals and pore fluids in a closed system during burial. The simulation yields the sequence and types of mineral dissolution and precipitation events that occur as the rock and fluid attempt to equilibrate with each other as temperature increases during burial (BRUTON, 1986). The initial pore fluid composition is that of a dilute river water of neutral pH. The rock composition is that of an arkosic sandstone. The predicted sequence of mineral deposition and dissolution events is shown in Figure 3a for the case where no solid solution is considered, and with solid solutions of dioctahedral smectite, trioctahedral saponite, and calcite-structured carbonate in Figure 3b.

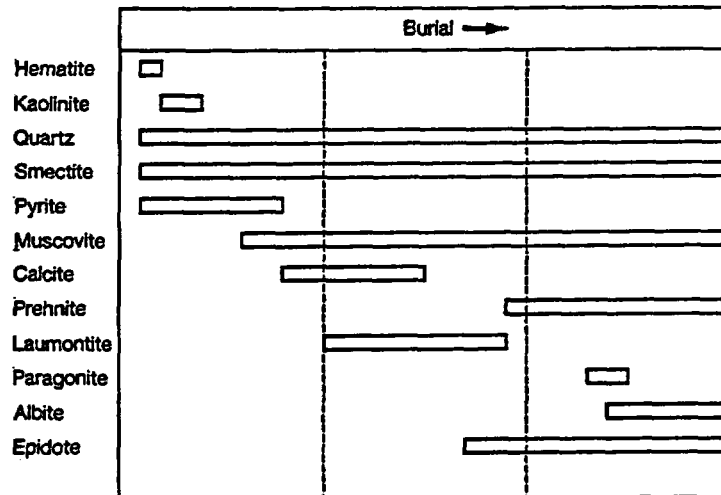
The diagenetic trends are similar in both cases. However, the stability fields of the clay and carbonate phases are expanded by treating them as solid solutions, and some minor phases such as hematite and paragonite are eliminated from the set of predicted secondary phases when solid solutions are considered.

Figure 4 shows the compositional variation of the 12-component dioctahedral smectite solid solution product phase during the diagenesis simulation described above. The solid solution model is an ideal mixing of molecular components with free energy values calculated using the method of TARDY and GARRELS (1974). The composition of the smectite phase changes abruptly at points coincident with the appearance or disappearance of other phases containing elements in common with the smectite. These changes do not correspond to significant changes in the fluid phase composition. An abrupt compositional change found in a natural smectite therefore may not necessarily be accompanied by a significant change in the fluid composition.

FUTURE WORK

Future work on solid solutions in the EQ3/6 code package will concentrate on putting in site mixing models for clays and zeolites. These models can be incorporated within

a) Diagenetic sequence—without solid solution option



b) Diagenetic sequence—with solid solution option

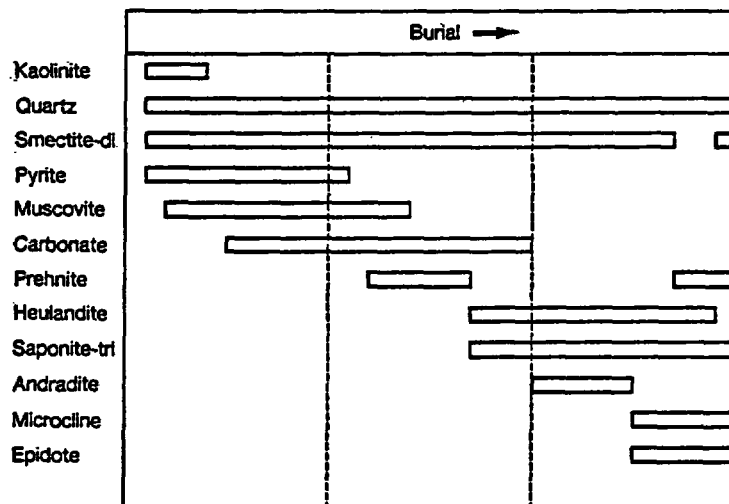


Figure 3. Predicted sequence of mineral precipitates for reaction of arkosic sandstone with river water. (a) no solid solution considered; (b) solid solutions of smectite, saponite, and calcite structured carbonate considered.

the existing Simplex algorithm by adding suitable site mixing models into the subroutine LAMDA.

The incorporation of trace components into solid solution phases is not yet considered in EQ3/6. Some trace elements can be handled using the existing framework by adding the appropriate endmembers to the solid solution models already present. Additional coding will be necessary for incorporating data on the solubility of minor elements in mineral phases described by Henry's Law-type behavior.

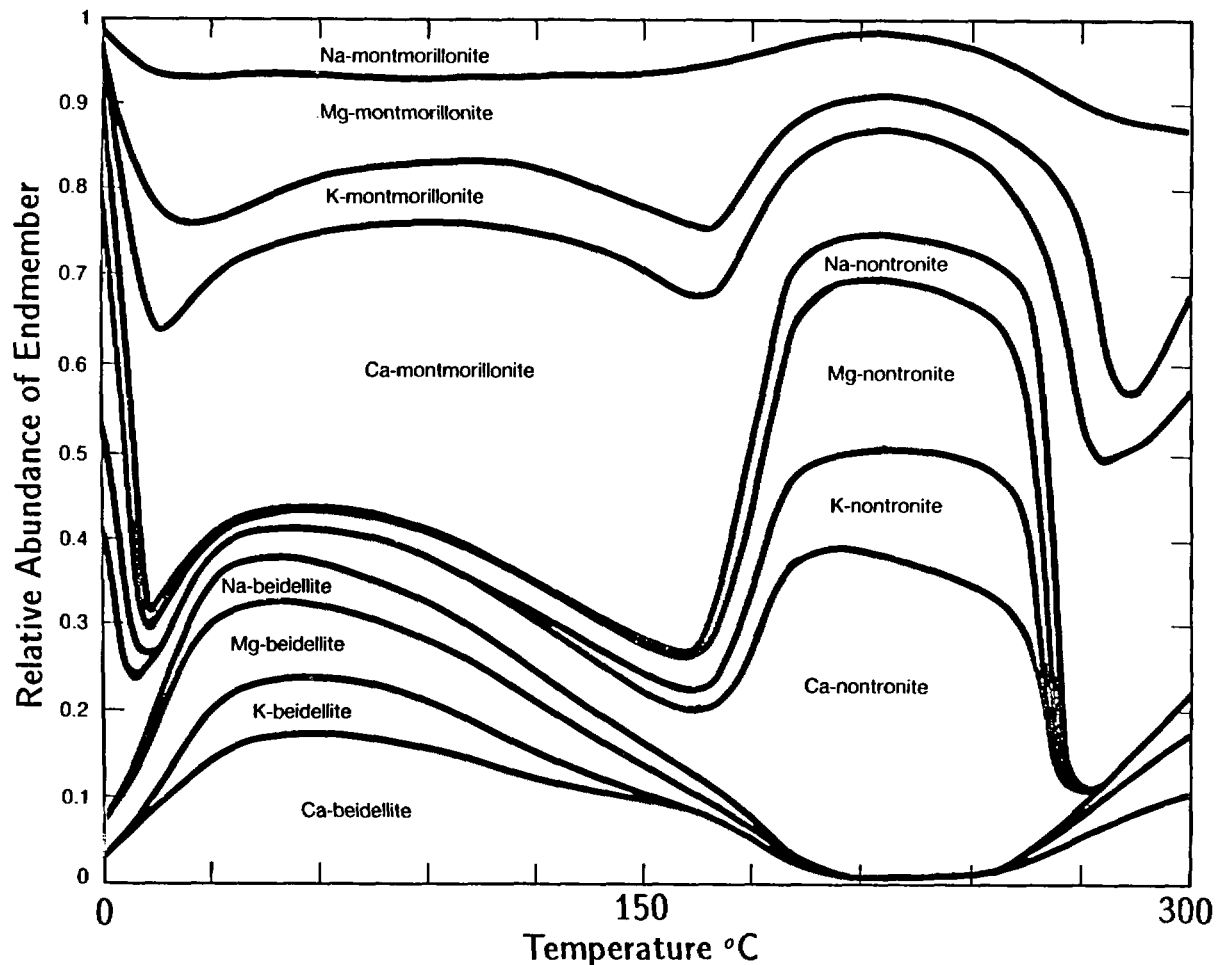


Figure 4. Compositional variation of smectite solid solution during diagenetic reaction of river water with arkosic sandstone.

REFERENCES

- ANTON, HOWARD, and BERNARD KOLMAN (1974) *Applied Finite Mathematics*. Academic Press, New York, 475 p.
- BOURCIER, W. L. (1985) *Improvements in the solid solution modeling capability of the EQ3/6 geochemical code*. Lawrence Livermore National Laboratory, UCID 20587.
- BRUTON, C. J. (1986) *Predicting mineral dissolution and precipitation during burial: Synthetic diagenetic sequences*. *Proceedings of the Workshop on Geochemical Modeling*, Fallen Leaf Lake, California, September, 1986.
- TARDY Y. and R. M. GARRELS (1974) *A method of estimating the Gibbs energies of formation of the layer silicates*. *Geochimica et Cosmochimica Acta*, 38:1101-1116.
- WOLERY, T. J. (1988) *EQ3/6 - Status and future development*. *Proceedings of the Workshop on Geochemical Modeling*, Fallen Leaf Lake, California, September 1986.

Hydrothermal and Geothermal Systems

Preliminary Chemical Modeling of Epithermal Processes at Creede, Colorado: The Role of Fluid Mixing as an Ore Deposition Mechanism

Geoffrey. S. Plumlee¹ and Daniel O. Hayba²
U. S. Geological Survey
¹MS 963, Federal Center, Denver, CO 80228
²959 National Center, Reston, VA 22092

Abstract

Continuing studies of epithermal ores from the Creede district, Colorado, have provided an extensive geological and geochemical basis for guiding quantitative chemical modeling of ore deposition processes in the Creede hydrothermal system. Preliminary modeling efforts to date suggest that the mixing of hot, metal-bearing brines with cooler, dilute, oxidizing groundwaters could have produced observed district-wide mineral zoning patterns. Initial boiling of the brines in the deeper parts of the Creede vein systems prior to mixing could also have contributed to the zoning patterns, however.

Introduction

During the past 30 years, extensive studies of Miocene epithermal Ag-Pb-Zn-Cu ores from Creede, Colorado, have provided a detailed geological and geochemical understanding of the Creede mineralizing system. Numerical modeling can be used to evaluate the chemical validity of ore deposition mechanisms suggested by fluid inclusion, stable isotope and ore petrology studies. This report discusses the geological and geochemical evidence used to constrain chemical modeling of ore deposition processes at Creede, and presents preliminary calculations assessing the role of fluid mixing as an ore deposition mechanism.

General Geologic and Hydrologic Setting

The Creede mining district is located in the mid-Tertiary San Juan volcanic field of southwestern Colorado, in a complex of nested calderas. The 25 Ma Creede ore deposits occur primarily as veins filling fractures of a graben extending to the north-northwest from the 26 Ma Creede caldera (Figure 1). The bulk of the production has come from the Amethyst, OH, P and Bulldog Mountain vein systems. The Creede ores are thought to have been deposited in response to boiling and fluid mixing at the top of a convectively-circulating, saline hydrothermal system (Hayba et al., 1986).

Mineralogy and Mineral Zoning The same general sequence of mineralization stages can be correlated throughout the Creede district (Heald-Wetlaufer and Plumlee, 1984; Hayba et al., 1986). However, one of two main sulfide stages at Creede, the so-called "B" stage, is strongly zoned mineralogically from north to south in the district. Sphalerite-galena-chalcopyrite-chlorite-pyrite-hematite ores in the northern veins (OH, P, northern Amethyst and northern Bulldog Mountain systems) grade laterally into southern silver-rich, barite-sulfide-native silver ores (southern Amethyst and southern Bulldog Mountain systems). Detailed mineralogical studies document that these northern and southern mineral

assemblages are correlateable facies reflecting the progressive north-to-south evolution of the ore-forming fluids as they traveled through the district vein systems (Barton, et al., 1977; Heald-Wetlaufer and Plumlee, 1984).

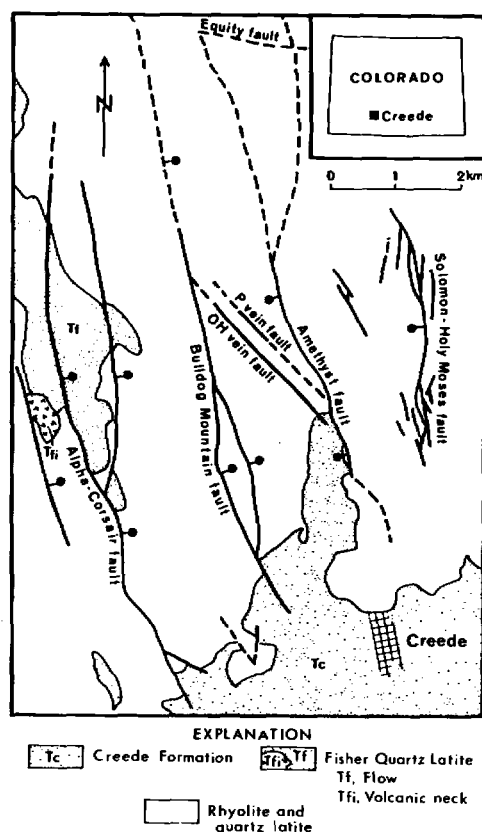


Figure 1. Geologic map of the Creede mining district showing locations of major vein systems.

The Role of Fluid Mixing as an Ore Deposition Mechanism

Extensive fluid inclusion and stable isotope studies indicate that the progressive north-to-south mixing of hydrothermal brines with overlying cooler, dilute ground water was an important mechanism controlling ore deposition and mineral zoning patterns during the two main sulfide stages at Creede. In a detailed study of the D stage "orange-brown" sphalerite growth zone, Hayba (1984) documented a progressive decrease in fluid inclusion temperatures and salinities from deep northern localities in the OH vein to higher southern localities. When plotted on an enthalpy-salinity diagram, these data document a mixing trend between a hot brine (~285°C, 11.5 wt% NaCl eq.) and a heated ground water (~160°C, ~0 wt% salinity) analogous to steam-heated waters observed in the upper levels of active geothermal systems (Hayba, et al., 1986).

B Stage Fluid Mixing and Mineral Zoning Robinson and Norman (1984) also documented decreasing fluid inclusion temperatures and salinities with increasing elevation in B stage quartz from the southern Amethyst vein system. Robinson and Norman's fluid inclusion data from the southern Amethyst are plotted in Figure 2, along with B stage sphalerite data (Woods et al., 1982) from the OH vein to the north. These B stage data also reflect the progressive mixing between saline brines and a cooler, dilute overlying ground water.

The strong north-south variations in B stage mineralogies discussed earlier correspond closely to the north-south trend of decreasing temperatures and salinities depicted in Figure 2. Deep vein ores deposited by the hottest, most saline fluids are sulfide-rich with hematite, chlorite, and pyrite gangue. With progressive mixing along the upper and southern OH and Amethyst veins, the fluids deposited increasingly barite- and silver-rich ores with rare chlorite, hematite, and pyrite. Similar north-to-south mineral zoning patterns and corresponding temperature-salinity trends are evident in the B-stage ores along the Bulldog Mountain vein system.

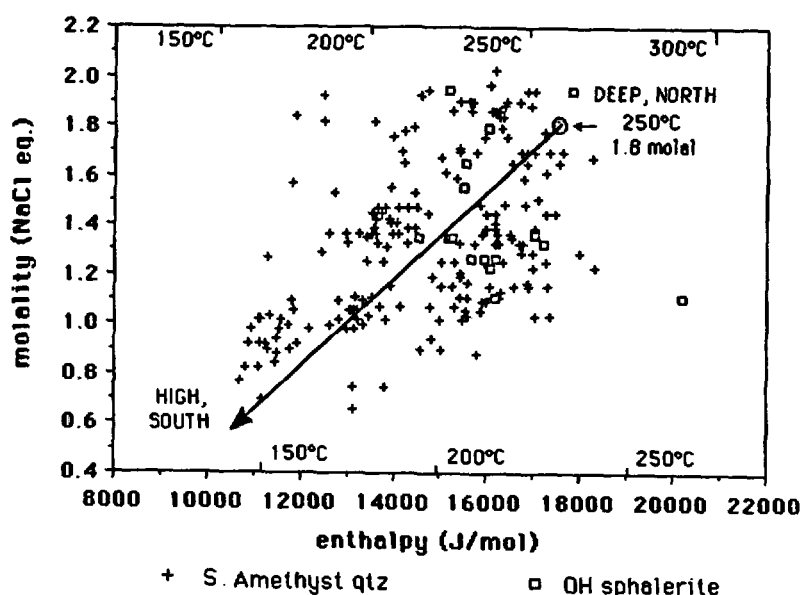
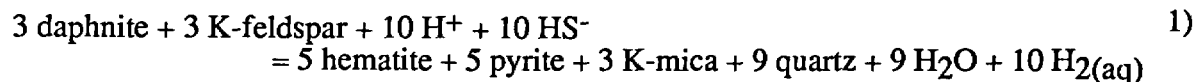


Figure 2. Enthalpy-salinity plot of B stage fluid inclusion data from the OH vein (squares) and southern Amethyst vein systems (crosses). Temperature contours cut diagonally across graph, from lower right to upper left. Arrow marks the mixing trend used in the calculations.

Chemical Constraints on Mineralization

Through detailed fluid inclusion, stable isotope, and thermochemical analyses of the northern Creede ores (Barton, et al., 1977; Hayba et al., 1986; Rye et al., in prep), the chemical composition of the B stage hydrothermal brines as they first entered the ore zone can be estimated. The fluid composition so established is used as a starting composition in numerical modeling calculations of B stage ore deposition processes. The parameters used to estimate the initial brine composition for the modeling are listed in Table 1. Initial temperature and total salinity values used for the deep brine were 250°C and 1.8 molal NaCl eq. (Figure 2).

Mineralogical and thermochemical constraints Barton et al. (1977) proposed that the OH vein's chlorite-pyrite-hematite mineral assemblage likely served to buffer the redox state and sulfur content of the B stage ore-forming fluids. By assuming that the pH and aluminum content of the fluids entering the ore zone were fixed through equilibrium reactions with wallrock K-feldspar and K-mica, the chlorite-pyrite hematite buffer can be used to calculate the activities of several important species in solution through the following reaction (modified from Hayba, et al., 1986):



Daphnite ($\text{Fe}_5\text{Al}_2\text{Si}_3\text{O}_{10}(\text{OH})_8$), an idealized iron endmember, is used to approximate the Creede iron-rich chlorite. The stability field for daphnite relative to those for other iron-bearing hydrothermal minerals is shown in Figure 3. If equilibrium did hold for reaction 1), then the activities and total amounts of $\text{H}_2(\text{aq})$, H^+ , Al^{+++} , H_2S , and Fe^{++} in a solution of known temperature and salinity can be calculated (Table 1). If saturation with sphalerite and galena is also assumed (sphalerite and galena were co-deposited with this assemblage in the OH vein B stage mineralization), then the total lead and zinc in solution can also be calculated. The absence of silver sulfides in the OH vein places a maximum limit on the total silver in solution. Similar mineral saturation arguments can be used to place bounds on other constituents in solution (ie, Ba^{++} , $\text{SO}_4^{=}$, F^-).

TABLE 1. Chemical parameters used to constrain initial brine composition.

Parameter	Fixed at:	Fixed by:
1. Temperature	250°C	Fluid inclusion studies
2. Total Cl	~1.8 molal	" " "
3. K/Na	0.1	" " "
Ca/Na	0.1-0.2	" " "
4. pH	5.5 *	Kspar-mica equilibrium
5. Al^{+++}	1.29×10^{-16} *	" "
6. Fe^{++}	1.41×10^{-16} *	Chlorite-pyrite-hematite buffer
$\text{H}_2(\text{aq})$	1.59×10^{-6} *	
$\text{H}_2\text{S}(\text{aq})$	7.94×10^{-5} *	
7. Pb^{++}	1.41×10^{-9} *	Sphalerite, galena, saturation
Zn^{++}	3.12×10^{-10} *	
8. $\text{SO}_4^{=}$	*	Maximum at anhydrite saturation.
9. Ba^{++}	*	Maximum at barite saturation.

* calculated activities - values vary depending on the thermodynamic data used in the calculations.

Implications of sulfide-sulfate disequilibrium Detailed isotope studies of B stage sulfides and barites have demonstrated conclusively that equilibrium between reduced and oxidized sulfur species in solution was not attained (Bethke et al., 1973; Rye et al., in prep.). In modeling of the B stage ores, therefore, sulfate and sulfide in solution have been treated as independent variables, with no redox interaction between the two. Instead, redox equilibrium (other than

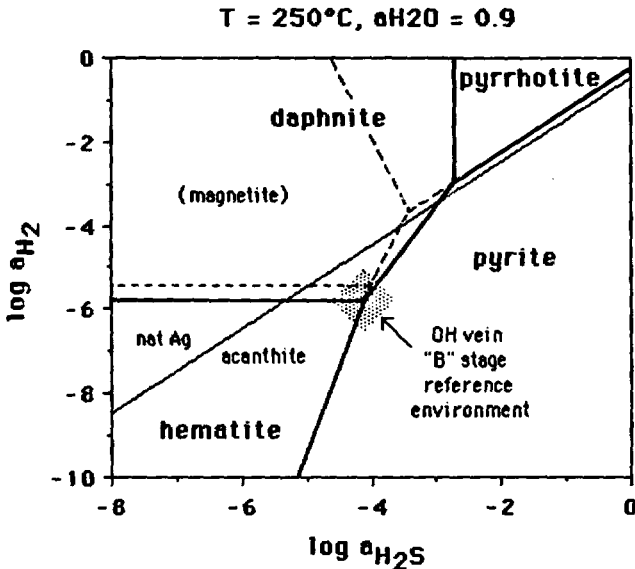


Figure 3. H₂-H₂S diagram showing stability fields of iron minerals and silver minerals. Daphnite field preempts magnetite field. Assumes saturation with K-feldspar, K-mica, and quartz. Stippled area marks reference environment for OH vein B stage fluid chemistry.

sulfate-sulfide) is assumed to be controlled by dissolved hydrogen and its reactions with reduced sulfur species (Figure 3). Although the validity of this assumption is questionable at lower temperatures, evidence from active geothermal systems suggests that measured H₂/H₂S ratios in solution reflect equilibrium with iron mineral assemblages at temperatures well below 200°C (Giggenbach, 1980).

Uncertainties in the thermochemical data Uncertainties in thermodynamic data can greatly affect both the starting fluid compositions calculated by the mineral equilibria discussed above, and the results of subsequent path calculations. For example, the calculated hydrogen, iron, and reduced sulfur contents in solution at the chlorite-pyrite-hematite triple point can vary by several orders of magnitude, depending on the free energy values used for daphnite in the calculations¹. The calculated effects of cooling and dilution on the stability of iron minerals are also highly variable, depending upon the thermodynamic data used for iron-chloride complexes.

Uncertainties in the chemistry of the overlying ground water The chemistry of the overlying ground water with which the hydrothermal brines mixed during the B stage mineralization is not well-constrained. The ground water was most likely dilute (~ 0 wt% NaCl eq.) and had temperatures of ~100-130°C (Figure 2). By drawing analogies with steam-heated waters seen in active geothermal systems, the overlying waters at Creede most likely contained bicarbonate, some sulfate, and had slightly acid pH values. In the mixing calculations, a range of compositions and temperatures for the overlying ground water is evaluated, to see which could produce the observed mineral zoning patterns.

¹Published thermodynamic data for Fe-chlorites are highly variable. These calculations use free energy values for idealized Creede "daphnite" empirically fixed by assuming equilibrium at 250°C with hematite, pyrite, and sphalerite of known iron content (Hayba et al., 1986).

Numerical Modeling of Fluid Mixing Processes

After calculating starting chemical compositions using the constraints outlined above, the chemical effects accompanying the progressive cooling and dilution of B stage ore fluids can be modeled numerically. Preliminary chemical modeling is currently being conducted with an Apple Macintosh Plus personal computer, using a BASIC program patterned after the mainframe modeling program SOLVEQ (Reed, 1982). The program calculates concentrations of all component species and complexes present in solution, and the amounts of minerals precipitated in a given temperature, boiling or mixing increment. Mixing and boiling increments are calculated isoenthalpically.

Calculated fluid mixing paths In order to fully assess the effects of all chemical and thermodynamic uncertainties discussed above, many different mixing paths with different input parameters must be calculated. Results of calculations modeling the progressive mixing of a Creede "B stage" brine with a 100°C, 0 wt% salinity ground water (chosen as representing one extreme of possible ground water compositions) are shown in Figure 4. Even with the extreme (and probably unrealistic) ground water composition used, the calculated sequence of ore minerals deposited agrees relatively well with the district ore mineral zoning: a sphalerite-galena assemblage is produced with low degrees of mixing, and a native silver-acanthite-sphalerite-galena assemblage is produced at lower temperatures and extreme degrees of mixing².

The only gangue mineral deposited in the calculations, however, is quartz, an uncommon mineral in the higher-temperature B stage ores. Hematite, pyrite and barite all become undersaturated with the first mixing increment, and remain undersaturated throughout the rest of the mixing calculation. In order to precipitate hematite, pyrite, and barite by mixing, the calculations show that the overlying ground water must have had a significant sulfate content, and also must have been able to oxidize the deep brine. Such an oxidizing chemistry would be similar to that of steam-heated waters seen in active geothermal systems, and so may be realistic for the Creede ground water. Boiling is also an oxidizing process, however, and could also have triggered deposition of the deeper, northern chlorite-pyrite-hematite-sulfide ores; after boiling, the same fluids could then have mixed to produce the barite- and silver-rich southern ores. Further calculations are underway to assess the role of boiling as a deposition mechanism in the deep, northern veins.

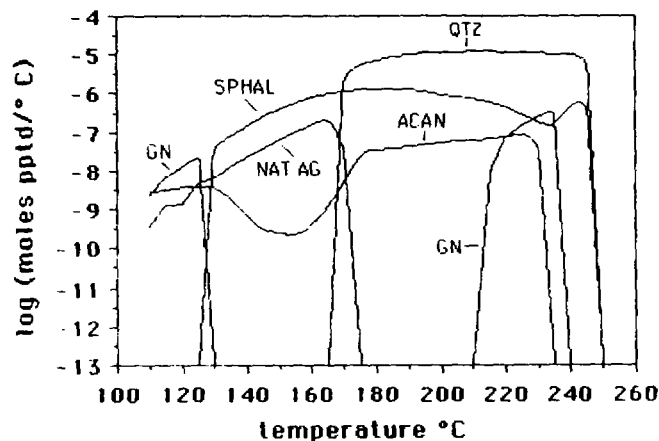


Figure 4. Calculated moles of minerals precipitated per degree temperature drop during the progressive mixing of a 250°C, 1.8 molal NaCl eq. brine with dilute, 100°C ground water.

²The gap in galena deposition between 210 - 130°C is probably an artifact of the way the program evaluates multiple mineral supersaturations, and therefore is not realistic. No equivalent gap in galena occurrence is observed in the Creede zoning patterns.

Conclusions

Preliminary chemical modeling of ore deposition processes at Creede suggest that the progressive cooling and dilution of a 250°C, 1.8 molal NaCl eq. brine by a cooler, dilute, oxidizing ground water is a valid mechanism to produce the mineral assemblages and mineral zoning patterns observed in the B sulfide stage; boiling in the deep, northern veins may also have occurred. Many more modeling runs are needed, however, to assess how the numerous geological, geochemical, and thermodynamic uncertainties will affect the calculations.

Future long-term U.S.G.S. modeling efforts at Creede will examine the chemistry and hydrology of the deeper and input parts of the hydrothermal system, as further geological and geochemical constraints become available.

References

- BARTON P. B. JR., BETHKE P. M., and ROEDDER E. (1977) Environment of ore deposition in the Creede mining district, San Juan Mountains, Colorado: Part III: Progress toward interpretation of the chemistry of the ore-forming fluid for the OH vein. *Econ. Geol.*, V 72, 1-24.
- BETHKE P.M., BARTON P.B. JR., and RYE R.O. (1973) Hydrogen, oxygen and sulfur isotopic compositions of ore fluids in the Creede district, Mineral County, Colorado (abs.). *Econ. Geol.*, V 68, 1205.
- GIGGENBACH W.F. (1980) Geothermal gas equilibria. *Geochim. Cosmochim. Acta*, V 44, 2021-2032.
- HAYBA D.O. (1984) Documentation of thermal and salinity gradients and interpretation of the hydrologic conditions in the OH vein, Creede, Colorado (abs.). *Geol. Soc. Am., Abs. wi. Progs.*, V 16, no. 6, 534.
- HAYBA D.O., BETHKE P.M., HEALD P. and FOLEY N.K. (1986) Geologic, mineralogic, and geochemical characteristics of volcanic-hosted epithermal precious metal deposits. in Berger, B.R., and Bethke, P. M. , eds., Geology and Geochemistry of Epithermal Systems: Society of Economic Geologists, *Reviews in Economic Geology*, V 2, 129-167.
- HEALD-WETLAUFER P. and PLUMLEE G.S. (1984) Significance of mineral variations in time and space along the Bulldog Mountain vein system with respect to the district-wide hydrology, Creede district, Colorado (abs.): *Geol. Soc. Am., Abs. wi. Progs.*, V 16, no. 6, 535.
- REED M.H. (1982) Calculation of multicomponent chemical equilibria and reaction processes in systems involving minerals, gases, and an aqueous phase. *Geochim. Cosmochim. Acta.*, V 46, 513-528.
- ROBINSON R.W. and NORMAN D.I. (1984) Mineralogy and fluid inclusion study of the southern Amethyst vein system, Creede mining district, Colorado. *Econ. Geol.*, V 79, 439-447.
- WOODS T.L., BETHKE P.M., and ROEDDER E. (1982) Fluid inclusion data at Creede, Colorado in relation to mineral paragenesis. U. S. Geological Survey, Open-File Report 82-813, 61 p.

BOILING OF GEOTHERMAL WATERS: PRECIPITATION OF BASE AND
PRECIOUS METALS, SPECIATION OF ARSENIC AND ANTIMONY,
AND THE ROLE OF GAS PHASE METAL TRANSPORT.

Nicolas F. Spycher and Mark H. Reed
Dept. of Geology, University of Oregon
Eugene, OR 97403

Abstract

Multicomponent heterogeneous equilibrium calculations are used to model the boiling of a Broadlands-type water, mixing of the boiled water with an acid sulfate water and condensation of the gas phase separated from the boiled water. Minerals, gases and aqueous species containing arsenic, antimony and mercury are included in the calculations. Upon boiling, silicate and sulfide minerals precipitate due to temperature drop and pH increase, respectively, and mercury partitions into the gas phase. Gas transport of arsenic and antimony is insignificant. Boiling of a sulfide-deficient water leads to native gold and silver deposition, at temperatures depending of the extent of sulfide deficiency of the solution. Mixing with acid sulfate water results in gold and enargite precipitation, together with stibnite and orpiment if the temperature is below 100 C. Condensation of the gas phase results in precipitation of cinnabar from reaction between Hg gas and H₂S gas.

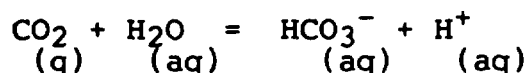
Introduction

Computer program CHILLER of Reed (1982) computes multicomponent heterogeneous chemical equilibria and is designed to model cooling, fluid-fluid mixing, fluid-solid-gas reactions, boiling of aqueous solutions and condensation of gases. This program was used here to simulate ore deposition in an epithermal system. Results of such calculations have previously been presented by Reed and Spycher (1985). A similar approach is used here, except that provisions have been included to take into account non-ideality of the gases (Spycher and Reed, in prep.) and to include an internal enthalpy constraint in the boiling calculations. In this study, special attention is given to the effect of aqueous sulfide concentration on gold precipitation, and to the the speciation of arsenic and antimony in the aqueous and gas phase. Mercury deposition from the gas phase is also investigated.

Boiling: Methods of Calculation

When simulating boiling, for any given bulk composition, temperature, and total enthalpy of a system, program CHILLER is used to solve for the amount and composition of the aqueous, solid and gas phases at equilibrium, and for the pressure at which gas and liquid are in such proportion that the sum of their respective heat contents equals the total enthalpy of the

initially homogeneous aqueous phase, plus an optional heat gain or loss for the system. This is accomplished by solving simultaneously a set of mass balance and mass action equations (Reed, 1982) and an enthalpy equation. The approach used here is different from that of Drummond and Ohmoto, (1985) in that true heterogeneous equilibrium is computed. The amount of each gas species in equilibrium with the aqueous phase is dictated by mass balance/mass action equations that are similar in form to the equations used for mineral solid solutions (Reed, 1982). Mass action equations for gases make use of true equilibrium constants, which are different from Henry's law constants, K_h , in being independent of salinity and defined for a given specific chemical reaction. For example, for CO_2 , we can write the following reaction:



for which the mass action equation is:

$$K = \frac{a_{\text{HCO}_3^-} a_{\text{H}^+}}{a_{\text{H}_2\text{O}} f_{\text{CO}_2}} = \frac{\gamma_{\text{HCO}_3^-} \gamma_{\text{H}^+}}{\gamma_{\text{H}_2\text{O}} \phi P (n_{\text{CO}_2} / (n_{\text{CO}_2} + n_{\text{H}_2\text{O}} + n_{\text{H}_2\text{S}} + \dots))}$$

The associated mass balance equation for carbonates is:

$$M_{\text{HCO}_3^-} = n_w (m_{\text{HCO}_3^-} + m_{\text{H}_2\text{CO}_3} + m_{\text{CO}_3^{2-}} + \dots) + n_{\text{CO}_2} + n_{\text{Calcite}} + \dots$$

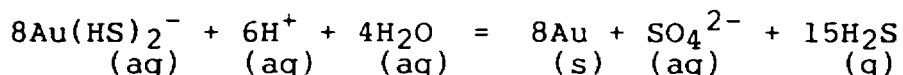
In these equations, a stands for activity, f is fugacity, m is molality, n is number of moles, n_w number of kilograms of solvent water in the aqueous phase, M_t is the total moles of a component species in the system, and γ and ϕ are activity and fugacity coefficients, respectively. Similar equations are written for each gas species and each component species. From such equations, we can solve simultaneously for the amount of CO_2 , for example, in the gas phase (n_{CO_2}) and in the aqueous phase ($m_{\text{HCO}_3^-} + m_{\text{H}_2\text{CO}_3} + \dots$). One of the advantages of this approach is that the amount and composition of both the aqueous and gas phases are simultaneously determined. Gases can be boiled off as well as recondensed, in the same way that minerals can be either precipitated or dissolved. Also, because we do not use Henry's law constants, speciation as a function of pH of a gas dissolved in the aqueous phase (e.g. HCO_3^- , H_2CO_3 , CO_3^{2-}) can be taken into account. Henry's law constants are commonly determined for systems of gas-H₂O-salt, where the pH is fixed by the concentration of dissolved gas and its pK. If pH is changed (e.g., by adding NaOH), the concentration of the aqueous gas species changes and the normal Henry's law treatment may not apply in the usual way. For example, in the CO_2 -H₂O system with CO_2 gas, the dominant aqueous carbonate species is H_2CO_3 . If pH is increased so that HCO_3^- dominates, the Henry's law constant must be used with the remaining H_2CO_3 , not total aqueous carbonate. In our approach, the "salting out" of gases is directly taken into account because activity coefficients, which are function of salinity, are part

of the mass action equations. Also, inclusion of fugacity coefficients in the mass action equations for the gases is a simple way to account for non-ideality and non ideal mixing of gases.

Boiling of Geothermal Waters

Many of the detailed effects of boiling on ore deposition have already been discussed by Reed and Spycher (1985) and Drummond and Ohmoto (1985). The calculations presented here apply to the Broadlands-like water composition used by Reed and Spycher (1985) with new metal concentrations of Brown (1986). As a hydrothermal solution rises from depth to the surface, the hydrostatic pressure decreases until saturation pressure of the solution is reached. Further pressure drop leads to boiling. If no heat is transferred to or from the host rock (isoenthalpic boiling), the temperature of the solution decreases because heat is used to vaporize the water. Calculated boiling results are shown in figures 1, 2 and 3 for such isoenthalpic boiling from 280 C, 80 bars to 101 C, 1 bar (0 to 36 wt.percent degassing). Degassing of CO₂ causes the pH to increase in accordance with the reaction: H⁺ + HCO₃⁻ --> CO₂ + H₂O. In sharp contrast, the same solution cooled without boiling experiences a pH drop (figure 1b) because the weak acids dissociate as temperature decreases. H₂S loss to the gas phase depletes aqueous sulfide, and boiling out of reduced gases such as CH₄ and H₂ partly oxidizes sulfide so that aqueous sulfate concentration increases. Upon boiling, silicates precipitate because of temperature drop, and deposition of sulfide minerals (figure 2) results from the increase of pH (Reed and Spycher, 1985). Quartz was not allowed to form below 200 C because its precipitation is kinetically retarded at T < 200 C. All minerals were fractionated as they formed, precluding their back-reaction with the solution. Gases were not fractionated.

To examine the effects of boiling on gold precipitation, we can write the following reaction:



According to this reaction, the pH increase accompanying boiling would stabilize gold in solution. However, according to the same reaction, losing H₂S to the gas phase by boiling could lead to gold precipitation. The effect of such sulfide loss on gold precipitation is more pronounced in sulfide-deficient waters. The water used in our calculation contained 340 ppm total sulfide. Gold barely saturates in this water at 100 C, and it is absent at higher temperatures. Numerical boiling of the same water, but with slightly smaller sulfide concentrations of 255 and 204 ppm causes gold to precipitate, as shown in figures 2b and 2c. It is thus evident that boiling causes gold to precipitate from sulfide-deficient waters but not from sulfide-excess waters that are otherwise the same. It is also apparent from figure 2 that the smaller the concentration of aqueous sulfide, the higher temperature of precipitation of gold and base metal sulfides and the

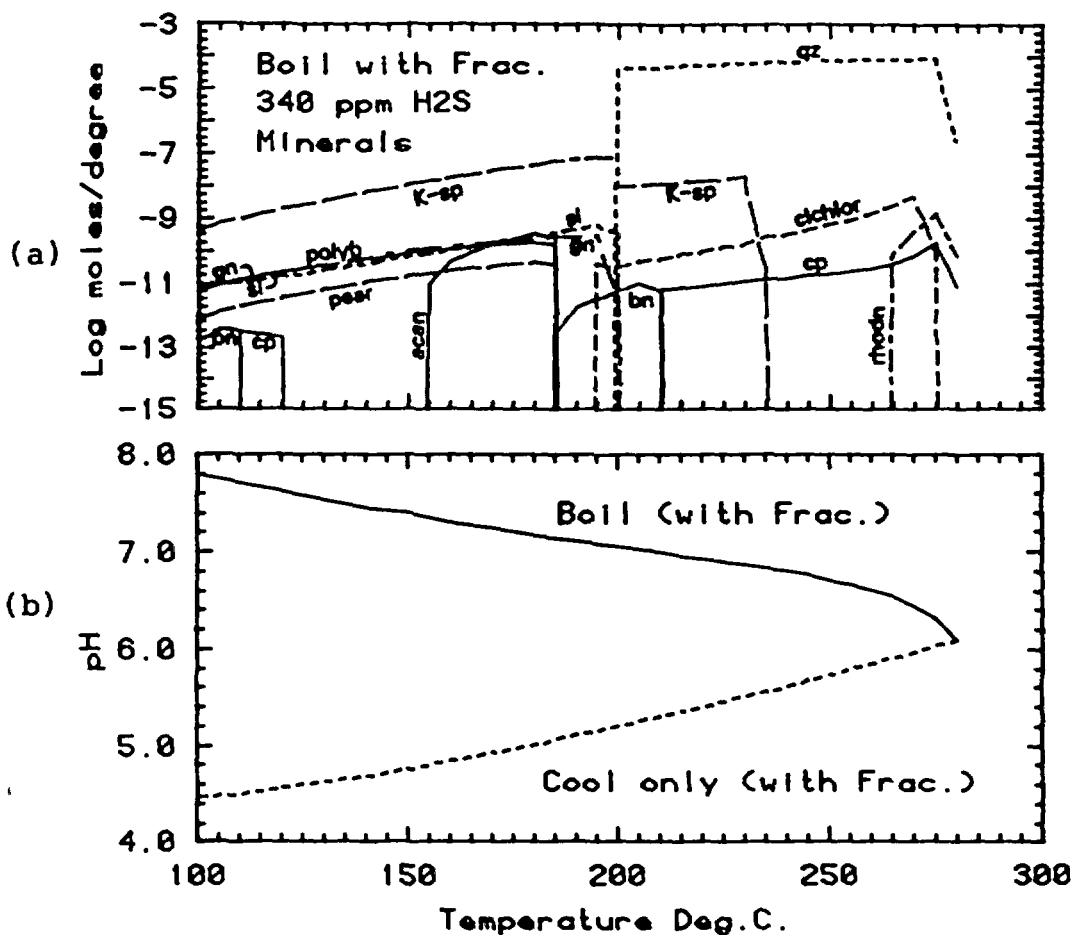


Figure 1 (See text)

more native silver forms in place of acanthite. Furthermore, it is likely that sulfide loss through precipitation of sulfide minerals from high chloride-low sulfide waters would lead to gold precipitation (see discussion by Reed and Spycher, 1985).

Arsenic and antimony aqueous species were included in the calculations. Data for arsenic oxyacids and antimony hydroxides were taken, and slightly modified, from Sergeyeva and Khodakovskiy (1969), and Popova et al. (1975). Data for thiosulfides were derived from least square fits and multicomponent equilibrium calculations with published solubility data (Spycher and Reed, in prep.). At high temperature and pH, H_3AsO_3 and $Sb(OH)_3$ are quite stable relative to the thiosulfides $HAs_2S_4^-$, $As_2S_4^{2-}$ and $HSb_2S_4^-$, and dominate over the whole temperature range when boiling. (After a very recent revision of our study on arsenic thiosulfides, we conclude that the arsenic species are $H_2As_3S_6^-$ and $HAs_3S_6^{2-}$ instead. This does not affect the results presented here). When the solution is cooled without boiling, thiosulfides become dominant below 150 C because of the lower pH and larger sulfide concentration owing to the lack of H₂S degassing. The

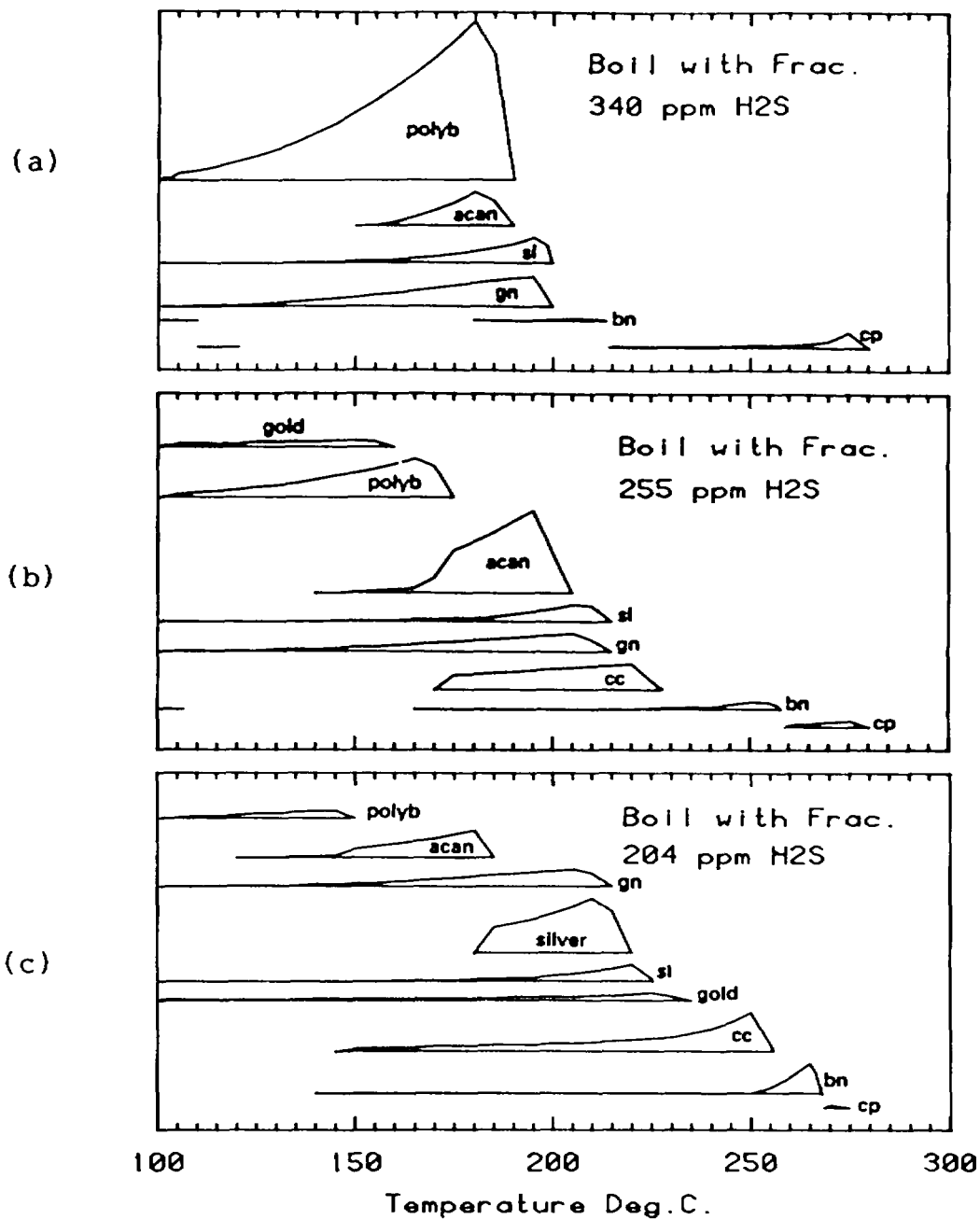
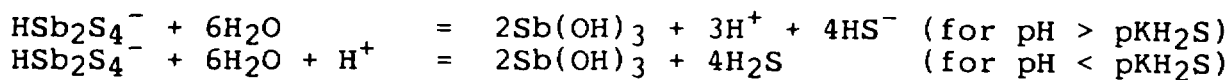


Figure 2 (See text)

equilibrium between As and Sb hydroxides (oxyacids) and thiosulfides as a function of pH can be described by the following equilibria:



Depending on whether the pH is smaller or larger than the pK for

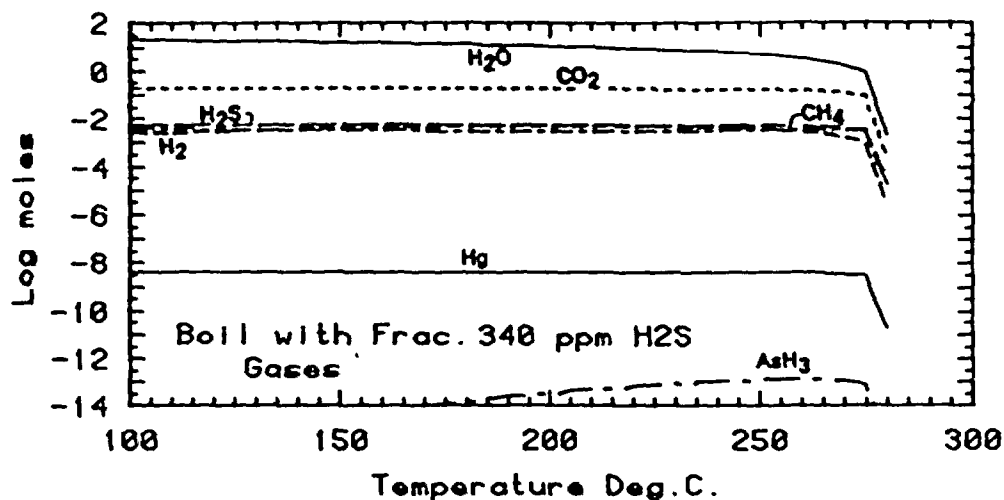


Figure 3 (See text)

T C. pH	BOIL WITH FRAC. log fugacities		
	280 6.10	200 7.05	101 7.80
Hg	-6.24	-8.24	-9.68
HgO	-22.29	-28.00	-36.48
HgCl	-22.43	-29.15	-37.44
HgH	-28.19	-35.23	-45.57
HgP	-31.39	-38.63	-49.59
AsH ₃	-10.78	-13.30	-17.06
As ₂	-12.21	-15.50	-20.72
As ₄ S ₄	-12.22	-16.03	-15.36
AsS	-12.75	-17.28	-23.49
As ₄	-12.89	-15.17	-17.92
As ₃	-19.47	-23.68	-30.23
As ₄ O ₆	-19.47	-19.98	-22.11
As	-21.77	-27.11	-36.32
AsF ₃	-22.27	-26.57	-34.28
AsCl ₃	-23.59	-31.13	-39.60
AsF ₅	-50.93	-58.96	-73.70
SbS	-14.35	-19.17	-25.73
Sb ₂ S ₃	-16.57	-22.47	-27.41
SbH ₃	-18.04	-22.91	-30.60
Sb ₂ S ₄	-18.05	-24.55	-29.04
Sb ₂	-19.87	-24.51	-31.81

Table 1

the first dissociation of H₂S, acidification will either stabilize or destabilize hydroxides relative to thiosulfides. Because pK(H₂S) is near pH neutral, in low-sulfide waters, thiosulfides are more abundant at pH's around neutral.

We investigated the importance of gas phase transport of metals by including thirty mercury, arsenic and antimony gases in our calculations. Almost all the mercury partitioned into the gas phase as Hg gas over the entire boiling interval. The concentrations of arsenic and antimony in the gas phase were insignificant. The calculated gas composition, and calculated gas fugacities of Hg, As and some Sb species are shown as functions of temperature in figure 3 and table 1. Arsine (AsH₃) is the dominant arsenic gas species, but its fugacity is too low to be geologically significant for As transport. Arsenic has been

reported in gas condensates from few geothermal areas and we wonder what other gas species, if any, could play an important role in transporting arsenic in the gas phase.

Fluid-Fluid Mixing

In order to model mineral deposition in hot spring environments, we numerically mixed the boiled water at 1 bar with an acid sulfate water. The acid sulfate water was previously generated by numerically oxidizing the gas phase separated from the boiled water at 100 C, 1 bar, with atmospheric oxygen (Reed and Spycher, 1985). The mixing calculations were carried out at 100 C and 90 C. The sequences of mineral precipitation resulting from these calculations are shown in figures 4a and 4b as a function of the mass of acid sulfate water added to the boiled

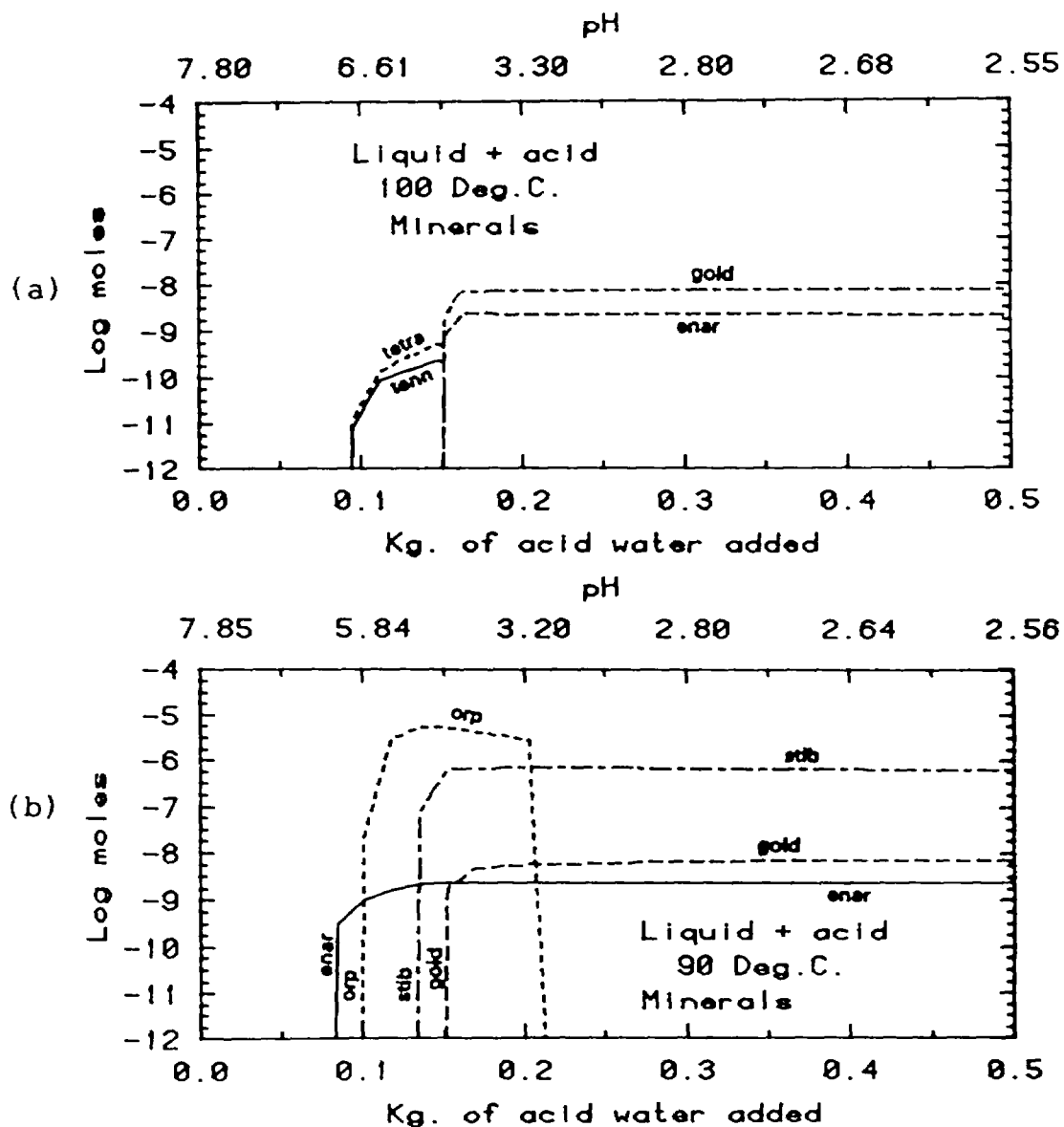


Figure 4 (See text)

water. The pH, originally fixed by bicarbonate, decreases following a titration-like curve after which it becomes fixed by sulfuric acid. At 100 C, such acidification results in precipitation of tennantite-tetrahedrite (solid solution), which is replaced by enargite and gold as pH further decreases (figure 4a). At 100 C, after few mixing increments, gases exsolve because of the acidification effect on CO₂ (Reed and Spycher, 1985). This degassing maintains the pH at higher values in the early stages of mixing. The same calculation carried out at 90 C does not show this secondary degassing because gas partial pressures are too small at lower temperature. The result is that, at 90 C, stibnite and orpiment precipitate together with enargite and gold (figure 4b), precluding precipitation of sulfosalts. This suggests that cooling is required, together with acidification, in order to precipitate stibnite and orpiment. Our calculation showed that although orpiment precipitated, a lot of arsenic (10 times more) was still in solution, whereas almost all antimony was precipitated as stibnite.

Gas Condensation

In our boiling calculations, most of the mercury partitioned into the gas phase. We wondered whether cinnabar could be deposited by condensing the gas phase. We separated the gas from the boiled water at 101 C and 1 bar, and numerically cooled it to 25 C at the constant pressure of 1 bar. Most of the mercury stays in the gas phase down to about 80 C. Below this temperature, cinnabar starts to precipitate as Hg gas reacts with H₂S gas. As expected, after condensation, the remaining gas is mainly CO₂.

References

- BROWN K.L. (1986) Gold deposition from geothermal discharges in New Zealand. *Economic Geology*, v.81, 979-983.
- DRUMMOND S.E. and OHMOTO H. (1985) Chemical evolution and mineral deposition in boiling hydrothermal systems. *Economic geology*, v.80, 126-147.
- POPOVA et al. (1975) Experimental determination of the thermodynamical properties of hydroxo- and hydroxofluoride complexes of antimony at temperatures up to 200 C (in Russian). *Geokhimiia*, no.6, 835-843.
- REED M.H. (1982) Calculation of multicomponent chemical equilibria and reaction processes in systems involving minerals, gases and aqueous phase. *Geochemica et Cosmochemica Acta*, v.46, 513-528.
- REED M.H. and SPYCHER N.F. (1985) Boiling, cooling and oxidation in epithermal systems: a numerical approach. In *Geology and Geochemistry of Epithermal Systems: Society of Economic Geologists, Reviews in Economic Geology*, v.2, ch.11, 249-272, Berger B.R. and Bethke P.M., editors.
- SERGEYEVA E.I. and KHODAKOVSKIY I.L. (1969) Physicochemical conditions of formation of native arsenic in hydrothermal deposits. *Geochemistry International*, v.6, 681-694.

PROGRESSIVE MINERAL ALTERATION AND COUPLED ^{18}O DEPLETIONS IN THE LAKE CITY HYDROTHERMAL SYSTEM (23 Ma), COLORADO

Peter B. Larson
Department of Geology
Washington State University
Pullman, WA 99164-2812 USA

Abstract

Water/rock interaction in hydrothermal systems typically results in the development of alteration product phases and mass transfer of oxygen isotopes among minerals and aqueous solutions. The hydrothermal system that was established in the Lake City caldera, San Juan Mountains, Colorado, shortly after collapse about 23 Ma is well-documented, and the quantity of mineral alteration products in the hydrothermally altered rocks correlates with the amount of oxygen isotope depletion measured in the rocks. Two units, the caldera-fill Sunshine Peak Tuff and the Precambrian Granite of Cataract Gulch outside the southwest margin of the caldera ring fault, are both mineralogically uniform. The proportion of sanidine phenocrysts in tuff samples that has been altered to product phases was estimated and the whole-rock oxygen isotope composition of each sample was measured. Trajectories that mimic oxygen isotope water/rock ratio trajectories, calculated using the water/rock equations of Taylor (1977), were generated when the volume of sanidine alteration was plotted against the whole-rock oxygen isotope composition measured for each sample. A similar correlation was found for the Precambrian granite when the amount of primary biotite altered to chlorite and sericite was used. These results show that both the quantity of mineral products and the amount of oxygen isotope depletion developed in a hydrothermal system are coupled functions of the progress of water/rock interaction. These relationships have been used to interpret the geometry of the Lake City hydrothermal system. The excellent documentation of mineral alteration and isotope depletion in this system provides a unique opportunity to test geochemical modeling codes in a natural hydrothermal system.

Introduction

Water/rock reactions in natural hydrothermal systems are recorded by several types of chemical changes in the altered rocks: (1) reactions between minerals and the fluid can produce new "alteration" minerals in the rock, and (2) some minerals can exchange structurally-bound oxygen with the fluid such that their initial oxygen isotope compositions also become altered. Geochemical models of water/rock interaction that utilize the reaction progress variable have shown that the amount of alteration minerals produced in a rock is a function of the extent to which a reaction has proceeded (e.g. Helgeson et al., 1970). However, water/rock reactions in natural hydrothermal systems occur in a dynamic environment where the fluid flows through the rock with which it is reacting (Ilorton, 1984). In order to apply reaction path models to a naturally altered sample, it is therefore necessary to know the amount of hydrothermal fluid that has reacted with the sample, and to know the extent of water/rock reaction that the fluid has

experienced prior to reaction with the sample. One convenient method of measuring these parameters is oxygen isotope analyses of the altered rocks.

Numerous studies have demonstrated that water/rock interaction in meteoric-hydrothermal systems typically produces oxygen isotope depletions in the altered rocks (e.g. Criss and Taylor, 1983). Taylor (1977) has used mass balance to develop equations that calculate water/rock ratios using oxygen isotope analyses of whole-rock samples. These equations are used to calculate the volume of fluid that has reacted with a rock when the whole-rock oxygen isotope composition has been measured. These techniques have recently been applied to the hydrothermal system associated with the Lake City caldera (23 Ma), Colorado (Larson and Taylor, 1986a,b). These studies show that the amount of alteration minerals produced in two units, the caldera-fill Sunshine Peak Tuff and the Precambrian granite of Cataract Gulch southwest of the caldera, correlate with the amount of measured oxygen isotope depletion. Thus, the oxygen isotope depletion that accompanies mineral alteration provides an independent gauge of the amount of fluid involved in the reaction and also a measure of the previous history of that fluid in the hydrothermal system.

Geology of the Lake City Caldera

The Lake City caldera (11 by 14 km) collapsed in response to eruption of the Sunshine Peak Tuff 23 Ma (Lipman, 1976; Steven and Lipman, 1976). The tuff comprises three members with an overall thickness greater than 1.3 km (Hon et al., 1973). Sanidine, quartz, and biotite occur as phenocrysts in all three members, and plagioclase is found as phenocrysts in the upper member. The tuff ranges from an alkali rhyolite (lower member 76 percent SiO₂) to a quartz trachyte (upper member 63 percent SiO₂). Quartz latites were subsequently erupted as ring domes on the eastern caldera ring fracture. A flat-topped quartz syenite intrusion then accompanied resurgence in the north central part of the caldera. A hydrothermal system developed in the caldera shortly after it collapsed, and nearly all the rocks in the caldera are now hydrothermally altered. K-Ar age determinations for biotite, sanidine, and alunite have shown that the tuff, ring domes, resurgent intrusion, and alteration in the caldera are all concordant at 23 Ma (Hon et al., 1983; Mehnert et al., 1980). Differential erosion has now exposed the altered rocks from near-surface solfataric alteration down through about 2 km into the resurgent intrusion, which served as a heat engine to convectively drive the meteoric-hydrothermal fluid.

The caldera was emplaced in older intermediate Tertiary volcanic rocks of the San Juan volcanic province, and these rocks now form most of the outer wall of the caldera ring fault except along the west and south margins of the caldera. Here, the Precambrian granite of Cataract Gulch forms the wall. The volcanic rocks unconformably overlie the granite. The granite consists of nearly equal proportions of quartz, orthoclase, and plagioclase, with 5 percent biotite and 1 percent muscovite. The west edge of the ring fault also truncates the older Eureka graben which has extensively faulted the granite and the older volcanic rocks in that area.

Alteration in the Tuff and Granite

The Lake City hydrothermal system has altered nearly all the rocks in the caldera, and has also affected all of the exposed granite. Quartz veins were deposited by the hydrothermal fluids in fractures and faults. The type and quantity of alteration products in the tuff change gradationally away from the quartz veins, and five facies (zones) have been identified in the shallow part of the caldera. Zone I, developed within about a meter of the veins, consists of total silicification of the tuff. Zone II, developed within tens of meters of zone I, consists of total replacement of sanidine and biotite by quartz and kaolinite/illite. Zone III grades outward from zone II. It comprises partial replacement of sanidine by kaolinite/illite and minor quartz and total replacement of biotite by sericite. Zone IV, the most extensively developed of the facies, consists of partial replacement of sanidine by kaolinite/illite and partial sericitization of biotite. Locally, chlorite accompanies the sericite. In zone V, sanidine exhibits only minor alteration, and more commonly only shows turbidity. Biotite in zone V is fresh. Zones I through III are controlled by proximity to the quartz-filled fractures and these zones are collectively called the fracture regime. Shallow solfataric alteration in the ring domes is also part of this regime.

Alteration in and adjacent to the resurgent intrusions is distinct from the fracture regime alteration, and is called the intrusive regime. This regime contains two facies. (1) Hornfelsed tuff, developed within several hundred meters of the intrusive contact, is characterized by recrystallization of the glassy groundmass to an even-grained mixture of quartz and sanidine. Sanidine phenocrysts in the hornfelsed tuff are typically unmixed to perthite. Hydrothermal alteration in this tuff is similar to zone IV alteration. (2) Alteration in the resurgent intrusive rocks is similar to that in the tuff, except chlorite commonly accompanies the sericite as an alteration product of biotite.

A third alteration regime, called the stratigraphic regime, includes the zone IV and V facies and an additional chlorite/calcite facies. This facies is best exposed in deeply eroded parts of the caldera away from the resurgent intrusion. It is typified by calcite and a green clay that partially replaces sanidine, and by biotite that is partially altered to chlorite without sericite. Quartz veins that cut this facies usually contain sulfide minerals and have narrow sericitic selvages.

Hydrothermal alteration in the Precambrian granite is less complex than in the tuff. Biotite in the granite has been altered to variable proportions of chlorite and sericite. Except for turbidity in the orthoclase, other mineralogic alteration in the granite is not common. The granite can be subdivided into three geographic groups based on their proximity to the Eureka graben, which transects the granite's western exposure. (1) Granite within the graben comprises the Eureka graben group, in which biotite is almost completely altered to product phases. (2) A 5.5 to 9.0 km group is exposed within those distances of the graben axis. Biotite in this group is altered to variable amounts of product phases, but is usually not completely altered. (3) Granite in the >9.0 km group contains biotite that is only slightly altered.

Relationships Between Mineral Alteration and ^{18}O Depletions

Whole-rock oxygen isotope analyses of 37 Precambrian granite samples and 153 caldera-fill samples were conducted (Larson and Taylor, 1986a,b). Petrographic examination of thin sections was used to estimate the volume of granite biotite that has been altered to product phases. Also estimated was the volume of sanidine that has been altered to product phases in the tuff and resurgent intrusive samples. Oxygen isotope analyses of outflow facies tuff show this unit had an initial oxygen isotope value of +7.2 per mil. The initial isotope value for the granite was +9.2. Nearly all of the analyzed samples have isotope values lower than the initial values, indicating that they have exchanged oxygen with a meteoric-hydrothermal fluid. Mid-Tertiary western San Juan meteoric water had an oxygen isotope value of about -15 per mil. These initial values were used to construct model water/rock ratio plots for the Precambrian granite, the tuff, and resurgent intrusions using the water/rock equations of Taylor (1977). Figure 1 shows these plots for the Precambrian granite. Both open and closed system plots for temperatures of 200° and 300°C are shown for initial water isotope values of -15 and -5 per mil. A value of -5 is typical of an ^{18}O -shifted meteoric-hydrothermal fluid. A similar plot has been generated for the Sunshine Peak Tuff (Larson and Taylor, 1986b).

Figure 2 shows measured whole-rock oxygen isotope values for the Precambrian granite plotted against the volume percent of the biotite that has been altered. The three groups of granite samples are delineated on Figure 2, and the 5.5 to 9.0 km group of the granite has been subdivided into high-elevation and low-elevation subgroups. Comparisons between Figures 1 and 2 suggest the following relationships between water/rock ratios, temperature, and elevation in the granite. (1) The >9.0 km group experienced the lowest temperature alteration and, locally, the smallest water/rock ratios. (2) The graben group experienced high temperature and high water/rock ratio alteration. (3) Vertical variations of isotope values exist in both the 5.5 to

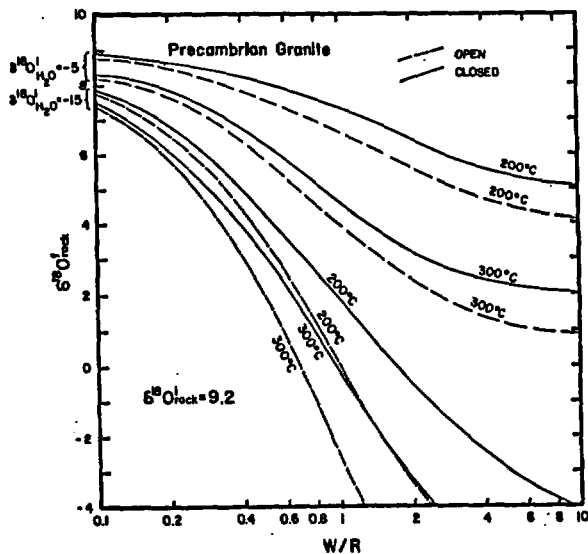


Figure 1. Model water/rock ratio trajectories for the Precambrian granite.

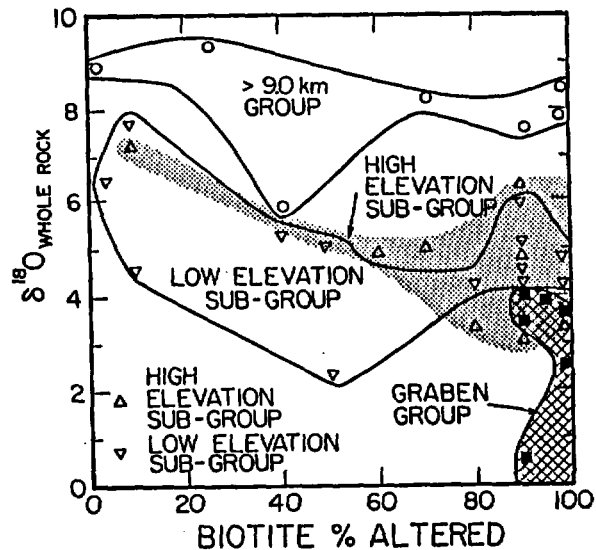


Figure 2. Measured oxygen isotope values vs. volume percent altered biotite for the granite.

9.0 km group and the >9.0 km group, with lower values at lower elevations. This suggests that a vertical thermal gradient existed throughout the granite away from the graben. However, in the middle group the lowest (deepest) samples exhibit the smallest amount of biotite alteration and are also the most ^{18}O depleted samples in the group. (4) A lateral gradient also probably existed with cooler temperatures away from the graben.

Figures 3 and 4 show oxygen isotope values for the tuff and resurgent intrusion samples plotted against the volume percent of sanidine that has been altered. Model water/rock ratio plots for these rocks are nearly identical to those for the granite (Fig. 1). Comparisons among Figures 1, 3, and 4 suggest that each of the three regimes of alteration was produced in distinct, but gradational, environments. (1) The fracture regime was altered under high water/rock ratios but relatively moderate temperature conditions. This alteration was produced adjacent to fractures that served as major flow channels for the hydrothermal fluids. (2) The intrusive regime was a higher-temperature regime, but one with very strong lateral and vertical gradients. Although these rocks have lower isotope values than the fracture regime tuff, they are much less mineralogically altered. (3) The chlorite/calcite altered samples plot at intermediate positions between the other two regimes. This alteration occurs deep in the stratigraphic sequence, beneath the argillized tuff, and peripheral to the intrusive regime. The low-grade alteration types (zones IV and V) that occupy most of the area of the caldera must be considered to include low-grade, low water/rock ratio end members of all three alteration regimes.

The volume of mineral alteration products in altered samples correlates with the amount of oxygen isotope exchange between the rocks and the hydro-

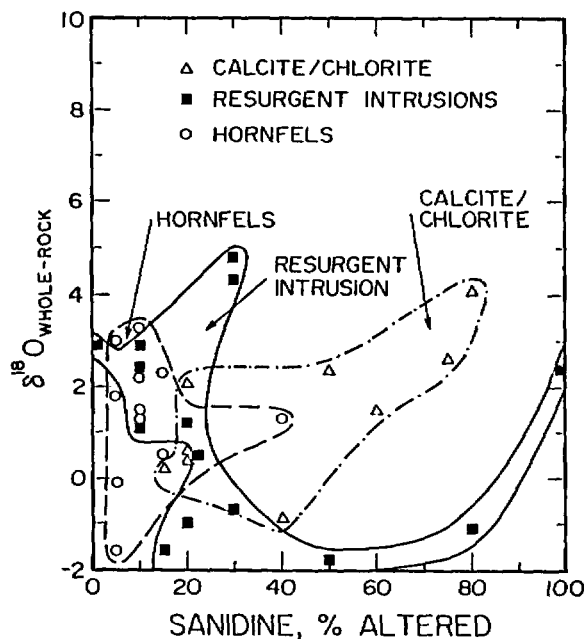


Figure 3. Measured oxygen isotope values vs. volume percent altered sanidine in the non-fracture regime tuff.

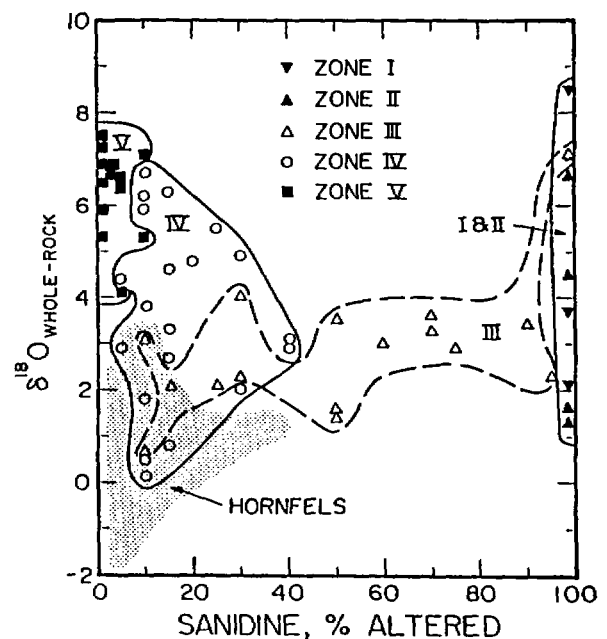


Figure 4. Measured oxygen isotope values vs. volume percent altered sanidine in the fracture regime tuff.

thermal fluid. However, the degree of mineralogic alteration in the samples is only a rough estimate of water/rock ratio. In the Precambrian granite 5.5 to 9.0 group, the lowest oxygen isotope values were recorded for the samples that displayed the least amount of biotite alteration. Also, in the caldera the most isotopically depleted samples, those from the intrusive regime, do not exhibit as great a degree of mineralogical alteration as the fracture regime samples. The production of alteration products is strongly dependent on fluid chemistry, as well as on temperature and water/rock ratio. But oxygen exchange between the fluid and rock is not known to be a function of fluid chemistry.

Summary

Mineralogic alteration and oxygen isotope exchange between meteoric-hydrothermal fluids and rocks have occurred in the 23 Ma Lake City hydrothermal system. In the Sunshine Peak Tuff and the Precambrian granite of Cataract Gulch the volume of mineral alteration products in the samples correlates with the amount of oxygen isotope depletion. These results show that fractured and faulted rocks adjacent to and above the resurgent intrusion experienced the highest ratios of water/rock interaction in the caldera. The temperature of alteration was higher, but water/rock ratios were lower, in and around the resurgent intrusion. In the granite, the highly-faulted Eureka graben experienced high water/rock ratios. The graben structures probably were a major recharge channel for the caldera hydrothermal system. Water/rock ratios and the temperature of alteration in the granite decrease gradationally away from the graben.

References

- CRISS R.E. and TAYLOR H.P. (1983) An $^{18}O/^{16}O$ and D/H study of Tertiary hydrothermal systems in the southern half of the Idaho batholith. *Geol. Soc. Amer. Bull.* 94, 640-663.
- HELGESON H.C., BROWN T.H., NIGRINI A and JONES T.A. (1970) Calculation of mass transfer in geochemical processes involving aqueous solutions. *Geochim. Cosmochim. Acta* 34, 569-592.
- HON K, LIPMAN P.W. and MEHNERT H.H. (1983) The Lake City caldera, western San Juan Mountains, Colorado (abs.). *Geol. Soc. Amer., Abs. with Prog.* 15, 339.
- LARSON P.B. and TAYLOR H.P. JR. (1986a) An oxygen-isotope study of water/rock interaction in the granite of Cataract Gulch, western San Juan Mountains, Colorado. *Geol. Soc. Amer. Bull.* 97, 505-515.
- LARSON P.B. and TAYLOR H.P. JR. (1986b) $^{18}O/^{16}O$ relationships in hydrothermally altered rocks from the Lake City caldera, San Juan Mountains, Colorado. *Jour. Volcan. Geotherm. Res.*, in press.
- LIPMAN P.W. (1976) Geologic map of the Lake City caldera area, western San Juan Mountains, southwestern Colorado. U.S. Geol. Surv. Map I-962.
- MEHNERT H.H., SLACK J.F. and CEBULA G.T. (1980) K-Ar age of alunite alteration at Red Mountain, Lake City area, western San Juan Mountains, Colorado. *Isotopes* 28, 9-11.
- NORTON D. (1984) Theory of hydrothermal systems. *Ann. Rev. Earth Planet. Sci.* 12, 155-177.
- STEVEN T.A. and LIPMAN P.W. (1976) Calderas of the San Juan volcanic field, southwestern Colorado: U.S. Geol. Surv. Prof. Paper 958, 35 p.
- TAYLOR H.P. JR. (1977) Water/rock interactions and the origin of H_2O in granitic batholiths. *Geol. Soc. London* 133, 509-558.

APPLICATION OF EQ3/6 TO MODELING THE CHEMICAL EVOLUTION IN HYDROTHERMAL SYSTEMS: AN EXAMPLE AT THE VALLES CALDERA, N.M.

Art F. White and Nancy J. Chuma
Lawrence Berkeley Laboratory
University of California
Berkeley, California 94720

Abstract

A kinetic-equilibrium reaction path model, utilizing the EQ3NR/EQ6 computer code, is produced for the central 300°C hydrothermal reservoir and the associated hot spring system in the Valles Caldera, New Mexico, U.S.A. A average rock-water ratio of 0.7 kg.kg⁻¹, a total reaction time of 2.9×10⁵ years, and a fluid residence time of 1.9 × 10³ years are calculated for the system based on ¹⁸O and Li mass balances and fluxes. A low reactive surface area of 6.15 × 10²cm².kg⁻¹, derived with a hydrothermal kinetic rate expression, implies a fracture dominated system controlled in part by diffusion. The reservoir fluid chemistry and secondary mineral assemblage are successfully reproduced by the model using only one fitting parameter, the mass of carbon derived from underlying Paleozoic rocks. The fluid-mineral chemistry is fixed based on phase rule constraints and is controlled by chloride sources in the primary glass phase and by temperature.

Introduction

The number and complexity of geochemical mass action computer codes have increased markedly in recent years. In addition to mathematical and computational sophistication, such simulators have come to rely on recent developments in estimating thermodynamic properties at high temperatures, pressures, and salinities, in describing kinetic reaction rates using transition state theory, and on analytical and numerical methods of coupling geothermal reactions with fluid and heat flow. As pointed out by Giggenbach (1984), the complexity and intractability of such codes will soon rival those of the natural geochemical systems which they are designed to describe. Few studies have successfully validated such simulations against well-defined natural geochemical systems.

The Valles hydrothermal system, located in the Jemez Mountains, northern New Mexico, is in many ways ideal for applying such a geochemical mass action model as EQ3NR/EQ6 (Wolery, 1979; Wolery, 1984) because the Valles area (Figure 1) contains a relatively simple lithology, has geographically defined recharge and discharge systems and contains adequately characterized fluids and secondary mineralogy.

The topographic and structural features of the Valles Caldera were formed during and after the eruption of the 1.1 MYP rhyolitic Bandelier Tuff. A central high temperature geothermal reservoir termed the Baca field, contained principally in the Bandelier Tuff, is located on the western flank of Redondo Peak, a resurgent dome structure within the caldera. The area has been extensively explored for potential geothermal development with chemical data from the wells being the most complete for any caldera system in North America. Published data on the Baca fluid chemistry include work by White (1986) and Truesdell and Janik (1986).

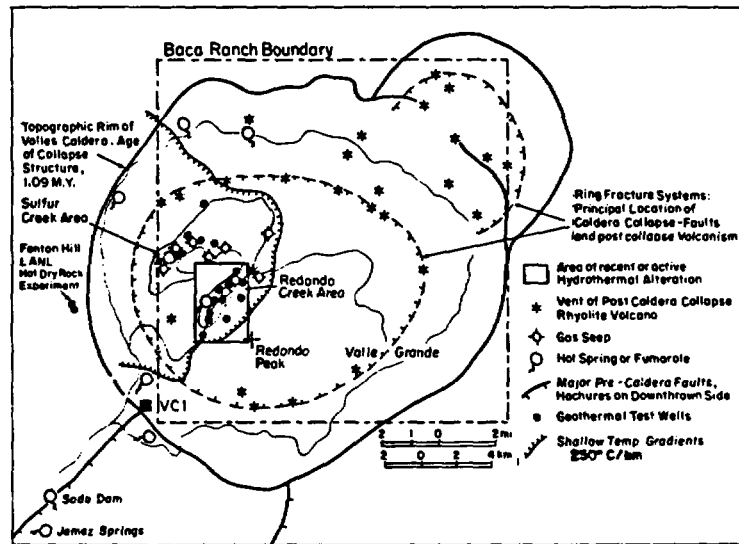


Figure 1. Map of the Valles Caldera area including location of Baca well field at Redondo Creek and major fluid discharge points at Soda Dam and Jemez Springs.

A phylitic mineral alteration sequence in the tuff is closely associated with documented major thermal fluid entries in the Baca wells (Hulen and Nielson, 1986). Phylitic alteration is characterized by partial to complete destruction of all original rock-forming minerals except quartz and the formation of micaceous illite with variable amounts of secondary quartz, pyrite, calcite, chlorite, epidote, and K feldspar. The thermodynamic relationships between the Baca reservoir fluids and secondary mineral assemblages were calculated using the EQ3NR program by White (1986). Cation activity ratios involving Na, K, Ca, Mg, and H indicated that the reservoir fluids were in general equilibrium with respect to albite, K-mica, epidote, and chlorite. Solubility calculations involving non-aluminum phases indicated that the fluids were saturated with quartz, calcite, anhydrite, dolomite, and siderite.

The EQ3NR/EQ6 software package was used to perform the numerical simulations of the hydrothermal reservoir system. An explicit pH, an input requirement for EQ3NR, is not available directly from flashed wellhead water and gas analyses. This problem was overcome by coupling the EQ3NR code with the PH code (Henley et. al, 1984) which interactively calculates reservoir pH based on concentrations of proton-ionizable aqueous species and total gas content including CO_2 , H_2S and NH_3 . Oxygen fugacities were calculated in the EQ3NR code based on the $\text{H}_2/\text{H}_2\text{O}$ couple. A fixed fugacity subroutine (Delany and Wolery, 1984) is employed in modeling CO_2 degassing. The EQ6 program was originally designed to compute reaction paths under either closed or flow-through conditions. The difference in the options relate to whether or not the mineral phases remain in contact with solutions as temperatures and compositions change. In the available computer package only the closed system option was operational. The EQ6 program was modified in the present study to include the kinetic rate expression of Wood and Walther (1983). The mass balance parameters in the program were determined by numerically integrating the rate expression using Simpsons Formula (Ake and Anderson, 1974). A number of additions and modifications to the thermodynamic data base were made to more closely approximate the mineral assemblages observed in the Valles system.

A quantitative estimate of the mass of rock reacted, a requirement in the model calculations, is based in part on the partitioning of the ^{18}O isotope between hydrothermal fluids and rocks. For a completely closed system, the ratio of mole atoms of oxygen in the fluid (W) to oxygen in the rock (R) can be calculated by the relationship (Taylor, 1977),

$$W/R = \left(\delta_f^{18}\text{O}_{\text{rock}} - \delta_i^{18}\text{O}_{\text{rock}} \right) / \left(\delta_i^{18}\text{O}_{\text{H}_2\text{O}} - \delta_f^{18}\text{O}_{\text{H}_2\text{O}} \right), \quad (1)$$

where ^{18}O is calculated in parts per mil., and i is the initial value and f is the final value after exchange. For a completely open system in which each increment of water makes only a single pass through the hydrothermal system, the extent of reaction can be calculated by the relationship;

$$W/R = \log_e \left(\delta_i^{18}\text{O}_{\text{H}_2\text{O}} - \delta_f\text{OH}_{\text{e}_2\text{O}} + \delta_f\text{O}_{\text{rock}} - \delta_i^{18}\text{O}_{\text{rock}} \right) / \left(\delta_i^{18}\text{O}_{\text{H}_2\text{O}} - \delta_f^{18}\text{O}_{\text{H}_2\text{O}} \right). \quad (2)$$

Extensive $\delta^{18}\text{O}$ data (Figure 2) exist for regional meteoric water as well as hydrothermal fluids within the caldera (Vuataz and Goff, 1986; and White, 1986), and indicate an approximate 2.1‰ enrichment in the latter case. Much more limited data for the Bandelier Tuff (Lambert and Epstein, 1980) indicate that the reservoir rocks are depleted in ^{18}O by approximately 6.9‰.

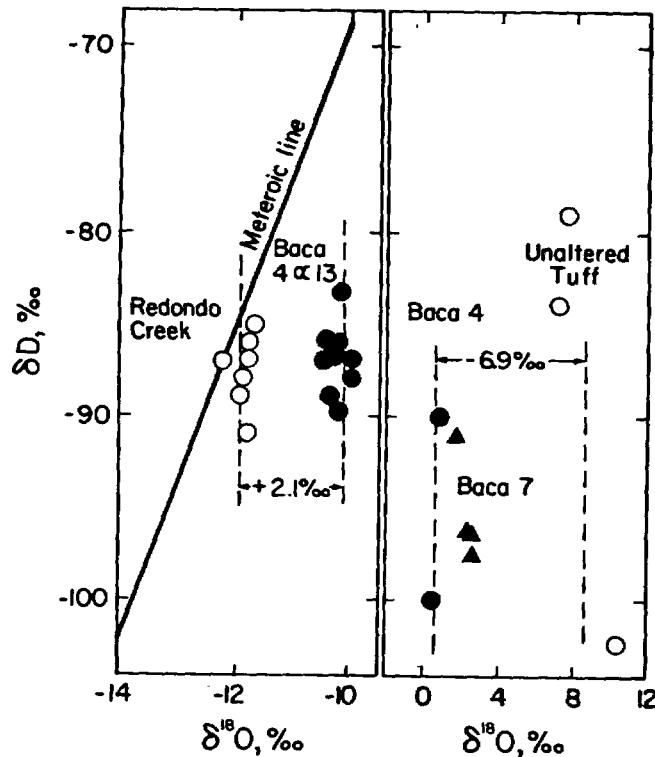


Figure 2. Extent of oxygen-18 increase in fluids and decrease in Bandelier Tuff as a function of hydrothermal alteration. Open and closed circles are respective deuterium-oxygen-18 data for surface meteoric water and Baca wells. Open and closed triangles are respective data for unaltered Bandelier Tuff and altered tuff.

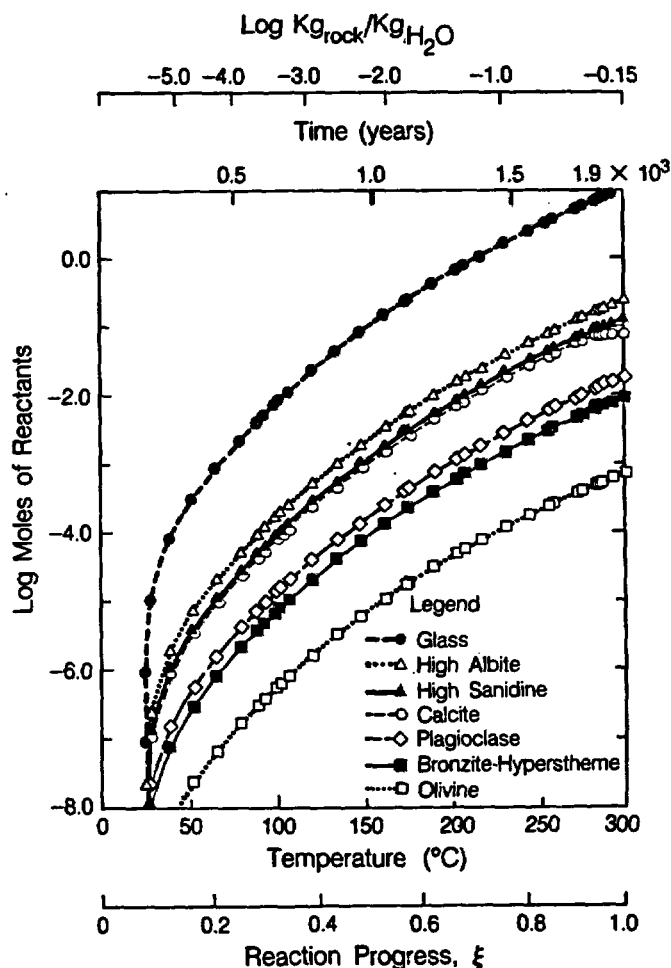


Figure 3. Moles of primary glass and minerals reacted as a function of the kinetic rate expression and plotted as functions of the reaction increment (ξ), time, temperature, and total rock mass.

Equation 1 thereby results in a calculated rock mass of 0.4 kg per kg of water for the closed system condition. Equation 2 produces a reacted rock mass of 0.9 kg of fluid assuming a flow-through scenerio. An average value of 0.7 kg.kg^{-1} employed in the model is comparable to ratios calculated for the Salton Sea and Warakei geothermal systems.

The EQNR3/EQ6 model considers reaction rates of the individual primarily mineral phases (Figure 3). Composition data and relative amounts of minerals are from estimates provided by Roy Bailey, U.S. Geological Survey and Jamie Gardner, Los Alamos National Laboratory. Ample hydrothermal sources of all elements, except chloride and carbon, occur in the primary mineral assemblage. Chloride is the principal anion in the Valles hydrothermal fluids and controls the overall chemistry by electrical charge balance and by the fact that it is not constrained by fluid-rock equilibria. An average of $2100 \text{ mg.kg}^{-1} \text{ Cl}$ has been reported for pumaceous layers in the Bandelier Tuff (Gardner et. al., 1986). Based on this analysis, a reacted rock-water ratio of 0.7 kg.kg^{-1} would release $1,470 \text{ mg.kg}^{-1} \text{ Cl}$ to the fluid compared to a average measured composition of $1960 \text{ mg.kg}^{-1} \text{ Cl}$, indicating that host rocks are the principal Cl source. This conclusion is in agreement with observed secular ^{36}Cl equilibrium between water and rock in the Valles system (Phillips et. al., 1984).

The high concentrations of CO₂ in the hydrothermal fluids (7x10³ to 3.4x10⁴ mg.kg⁻¹; White, 1986) require an additional source of carbon not contained in the meteoric recharge water nor in the primary volcanic rocks. Similarities in the ranges in δ¹³C of the Valles hydrothermal fluids (-3.8 to - 4.8 ‰) and of the underlying Madera limestone (-3.1 - 5.6 ‰) suggests that the carbon originated from thermal metamorphism of limestone (Truesdell and Janik, 1986). Thermal metamorphism is supported by the presence of minor amounts of calcium silicates including diopside and actinolite in the underlying Madera formation (Hulen and Nielson, 1986). Calcite is assumed to be the principal carbon source although it occurs as a primary mineral only in the spatially separated Madera Formation. Likewise, Ca-Mg silicates are allowed to precipitate in the secondary mineral assemblage, even though they are observed within the limestone and not in the overlying volcanic sequence.

The lithium fluxes in hot spring discharge from the reservoir can be linked with the mass ratio to estimate reaction times in the reservoir. The calculations are based on evidence from the Na-Li geothermometer (White et. al., 1984) that Li does reequilibrate in the hydrothermal system. The reaction time (t, sec) is expressed as the ratio between the total Li loss in the reservoir and the rate of Li loss in the discharging water,

$$t = \frac{V\rho(C_i - C_f)}{F}, \quad (3)$$

where V and ρ are the respective volume (m³) and rock density, (gm.cm⁻³). C_i and C_f are the initial and final lithium concentrations in the rock(g.kg⁻¹) and F is the flux of lithium from the system (g.s⁻¹). A total reaction time of 2.9 × 10⁵ years and a fluid residence time of 1.9 × 10³ years can be calculated based on published estimates of the reservoir dimensions and porosity. Approximately 150 fluid reservoir volumes have passed through the system. Clearly from this calculation, the isotopic as well as the ideal geochemical model must be considered an open rather than closed system.

A hydrothermal rate expression, applicable to all silicate minerals (Wood and Walther, 1983) can be rewritten in a Arrhenius expression,

$$k = \frac{1}{N} 10^{\left(\frac{-2900}{T} - 6.85\right)}, \quad (4)$$

where N is the moles of oxygen atoms in the reacting mineral phase and T is temperature (K°).

The assumption is made in the rate calculations that fluid movement in the reservoir is constant over the 1.9 × 10³ years and that it occurs along a linear temperature gradient. The single pass model permits both temperature and time to be described as linear functions of ξ, the reaction variable in the reaction path calculation. Mathematically the mass of a reacted mineral, M, can be written based on the above conditions as,

$$M = R_k \int_{\xi=0}^{\xi=1} 10^{\left(\frac{-2900}{298.15+300\xi}\right)} \delta\xi, \quad (5)$$

where the effective rate constant is defined as

$$R_k = \frac{10^{4.15}}{N} A \quad (6)$$

A summation of the amount of each mineral phase reacted in Figure 3 at $\xi = 1$ equals 18.91 moles of oxygen. The total mineral assemblage has an oxygen content of 1.82 moles of O_2 per mole of rock. The resulting value of reactive surface area, A , integrated over the entire temperature based on Equations 5 and 6 is therefore $6.15 \times 10^2 \text{ cm}^2$ per kg. of rock.

Results

The EQ3NR/EQ6 simulation of the high temperature reservoir successfully reproduces the fluid chemistry and secondary mineral assemblage using only one undefined fitting parameter, the mass of calcium carbonate supplied to the system. Calcite dissolution contributes carbon to the system which increases the P_{CO_2} and calcium which promotes epidote saturation and fixes the P_{O_2} . Plots of P_{CO_2} and P_{O_2} against temperature for variable amounts of reacted calcite are presented in Figure 4. Parameters of pH, P_{CO_2} and P_{O_2} , in addition to other aqueous species, are controlled by complex interactions involving dissolution of primary minerals and precipitation of secondary minerals.

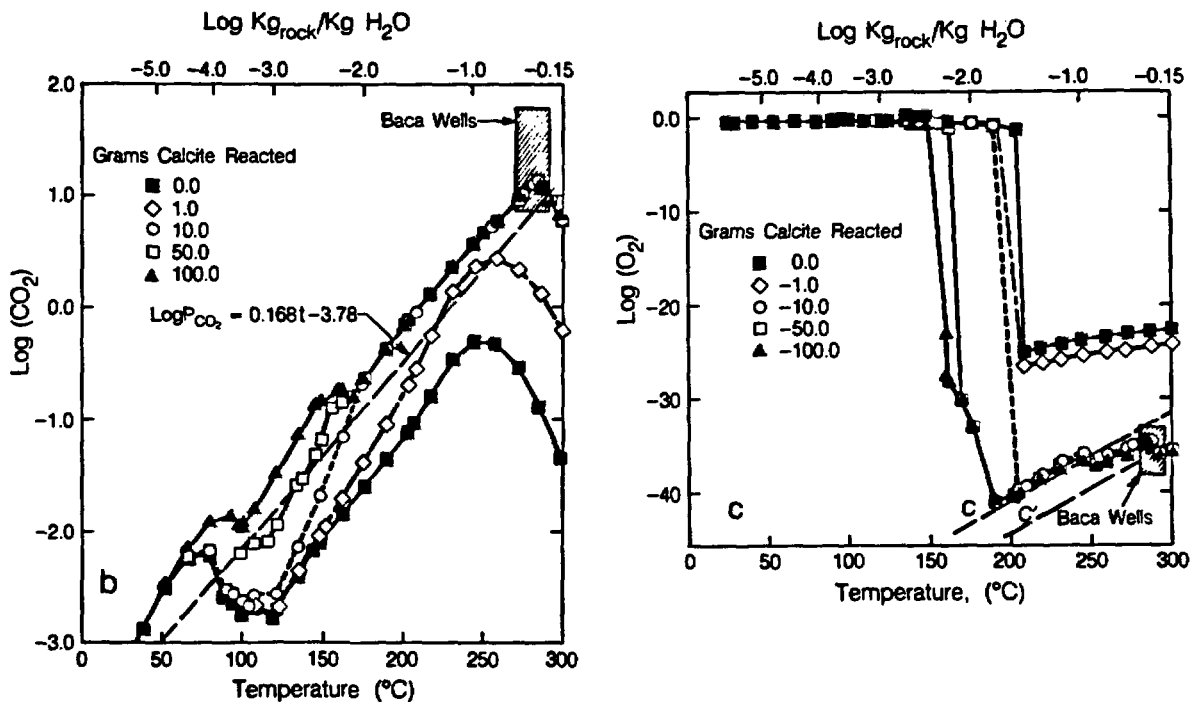
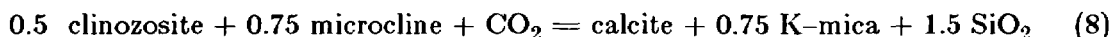


Figure 4. Reaction path P_{CO_2} and P_{O_2} versus temperature for differing masses of reacted calcite. Shaded areas are ranges in Baca Reservoir chemistry. Line B indicates P_{CO_2} control from Ca silicate-calcite equilibria (Equation 7) and; Line C and C', P_{O_2} control from silicate-pyrite buffers (D'Amore and Gianelli, 1984).

The simulated P_{CO_2} (Figure 4) is strongly related to the extent of calcite reaction with the maximum partial pressures becoming univariant with temperature again at a reacted calcite mass of 1×10^{-2} kg or above. This P_{CO_2} -temperature relationship generally follows the approximate fit to K feldspar-illite coexistence represented by the expression (Giggenbach, 1984)

$$\log P_{\text{CO}_2} = .0168T - 3.78 \quad (7)$$

which may be represented by the thermodynamically specific end member components,



Variations in the fit between the reaction path simulation and Equation 8 are related to differing solid solution composition involving clinozosite-epidote and Kmica-illite.

The simulated P_{O_2} of the system (Figure 4) decreases markedly in the temperature range 150°C - 210°C corresponding to the onset of pyrite precipitation. The P_{O_2} also decreases with increasing calcite reaction below a total reacted calcite mass of 1×10^{-2} kg and becomes invariant above 200°C for a calcite mass of 1×10^{-2} kg or greater. The fixed O_2 simulation reproduces reservoir P_{O_2} at comparable temperatures, as calculated from the $\text{H}_2/\text{H}_2\text{O}$ couple, and also falls within the range of a P_{O_2} mineral buffer involving in part pyrite-epidote-chlorite proposed by D'Amore and Gianelli (1984). The lines C and C' in Figure 4 correspond to their buffers assuming respective epidote compositions, $\text{pistalite} = 0.275$ and 0.125 , and with a fixed Fe/Mg chlorite ratio of 0.5.

When the mass of CaCO_3 equals or exceeds 1×10^{-2} kg, the chemical components of the hydrothermal system become equilibrated with a full assemblage of secondary minerals. Under such conditions there are 12 chemical components (C) in the system, Na, K, Ca, Mg, Al, Fe, S, O, C, Si, H, and Cl and 11 stable mineral phases (P), quartz, calcite, pyrite, magnetite, dolomite, diopside, epidote, chlorite, albite, K-feldspar and illite (K-mica). Therefore three independent variables (F) must exist in the system based on the Gibbs phase rule, $P + F = C + 2$. From the data of Helgeson et al. (1978), the change in the free energy of formation of minerals as a function of pressure up to a hundred bars will not significantly influence overall stability. This reduces the number of variables in the equilibrated system to two, temperature and the mobile Cl component, a condition representative of many hydrothermal systems (Arnorsson et. al., 1982).

Chemical and gas parameters generated by the code such as P_{CO_2} and P_{O_2} closely adhere to analytical solutions to phase equilibria developed by previous workers. In rock-dominated, highly equilibrated systems such as the Baca reservoir, a mass action code such as EQ3NR/EQ6 may be expected to reproduce results generated by analytical considerations of equilibria as shown by Giggenbach (1984). The agreement between the two approaches for the Baca reservoir is therefore a validation of the computational methods employed in the code.

References

- Ake, G.D. and Anderson, N. (1974) Numerical Methods. Prentice-Hall Inc. Englewood, N.J., 572 p.
- Arnorsson, S., Gunnlaugsson, E. and Sevavorsson, H. (1982b) The chemistry of geothermal waters in Iceland. II. mineral equilibria and independent variables controlling water compositions. *Geochim. et Cosmochim. Acta* 47, 547-566.

- D'Amore, F. and Gianelli, G. (1984) Mineral assemblages and oxygen and sulphur fugacities in natural water-rock interaction processes. *Geochim. Cosmochim. Acta* 48, 847-857.
- Gardner, J.N., Goff, F., Garcia, S., and Hagan, R. (1986) Stratigraphic relationships and lithologic variations in the Jemez volcanic field, New Mexico. *J. Geophys. Res.* 91, 1763-1978.
- Giggenbach, W.F. (1984) Mass transfer in hydrothermal alteration systems - A conceptual approach. *Geochimica Cosmochimica Acta* 48, 2693-2711.
- Helgeson, H.C. Delany, J.M., Nesbitt, H.W., and Bird, D.K. (1978) Summary and critique of the thermodynamic properties of rock-forming minerals. *Amer. J. Science* 278-A, 1-228.
- Henley, R.W., Truesdell, A.H. and Barton, P.B., Jr. (1984) Fluid-mineral equilibria in hydrothermal systems. *Reviews in Economic Geology*, 1, 268 pp.
- Phillips, F. M., Goff, F., Vuataz, F. Bentley, H. W. Elmore, D. and Gove, H. E. (1984) Chlorine -36 as a tracer in geothermal systems: Example from the Valles Caldera, New Mexico. *Geophys. Res. Lett.* 11, 1227-1230.
- Taylor, H.P. (1977) Water-rock interactions and the origin of H₂O in granitic batholiths. *J. Geol. Soc. (London)* 133, 509-558.
- Truesdell, A.F. and Janik, C. (1980) Reservoir processes and fluid origins in the Baca geothermal system, Valles Caldera, New Mexico. *J. Geophys. Res.* 91, 1817-1834.
- Vuataz, F.D. and Goff, F. (1986) Isotope geochemistry of thermal and nonthermal waters in the Valles Caldera, Jemez Mountains, northern New Mexico. *J. Geophys. Res.* 91, 1835-1854.
- White, A.F. (1986) Chemical and isotopic characteristics of fluids within the Baca Geothermal Reservoir, Valles Caldera, New Mexico, *J. Geophys. Res.* 91, 1855-1866.
- Wolery, T.J. (1979) Calculation of chemical equilibrium between aqueous solution and minerals: The EQ 3/6 software package. Lawrence Livermore Laboratory Dept UCRL-52658, 38pp.
- Wolery, T.J. (1984) EQ3NR, A computer program for geochemical aqueous speciation solubility calculations: users guide and documentation. Lawrence Livermore National Laboratory UCRL-53414. 85p.
- Wood, B.J. and Walther, J.V. (1983) Rates of hydrothermal reactions. *Science* 222, 413-415.

Serpentinization Reaction Pathways: Implications for Modeling Approach

D. R. Janecky
Los Alamos National Laboratory
Los Alamos, NM 87545 USA

Abstract

Experimental seawater-peridotite reaction pathways to form serpentinites at 300°C, 500 bars, can be accurately modeled using the EQ3/6 codes in conjunction with thermodynamic and kinetic data from the literature and unpublished compilations. These models provide both confirmation of experimental interpretations and more detailed insight into hydrothermal reaction processes within the oceanic crust. The accuracy of these models depends on careful evaluation of the aqueous speciation model, use of mineral compositions that closely reproduce compositions in the experiments, and definition of realistic reactive components in terms of composition, thermodynamic data, and reaction rates.

Introduction

For several reasons, oceanic serpentinization processes offer an ideal case for testing and examining hydrothermal water-rock reaction models. First, serpentinites and their precursor peridotites are composed of relatively restricted assemblages of minerals. Second, the processes, precursors, and products of serpentinization have been extensively characterized by field and laboratory studies of mineral assemblages, mineral stability, chemical compositions, reaction pathways, and mineral dissolution kinetics (Janecky and Seyfried, 1986; Murphy, 1985; and references therein). This paper will discuss how examination of hydrothermal seawater-peridotite serpentinization reaction pathways illustrates the constraints and limitations of reaction pathway modeling and the necessity of integrating database evaluation, geology, and experimental results into the modeling process.

Serpentinized peridotites are relatively common rocks found both in oceanic and continental crust. Oceanic ultramafic rocks undergoing serpentinization are composed primarily of olivine, enstatite, and diopside in the variable proportions that form dunites, harzburgites, lherzolites, and aluminous peridotites, and are primarily derived from the mantle (Bonatti and Hamlyn, 1981; Nicolas and Poirier, 1976; and references therein). Serpentine is the dominant alteration phase (primarily lizardite as defined by XRD), but magnetite, talc, hematite, chlorite, tremolite-actinolite, scapolite, truscottite, sepiolite, magnesite, and aragonite are also found in varying amounts (Aumento and Loubat, 1971; Aumento, 1970; Prichard, 1979; Engel and Fisher, 1975; Bonatti *et al.*, 1980; Bonatti and Hamlyn, 1981). Brucite appears to be much less common in oceanic than in continental serpentinites, whereas Ca-bearing silicates (*e.g.*, tremolite-actinolite) appear to be more common, even in alteration products of low-Ca peridotites. Serpentine minerals are Fe-bearing in both oceanic and continental occurrences (Dick, pers. comm.; Dungan, 1979; Wicks and Plant, 1979) and less than 5% magnetite is present (Smith *et al.*, 1982).

Experimental interaction of equigranular peridotites with seawater or "evolved"-seawater solutions at elevated temperatures and pressures has produced mineral assemblages and compositions that are generally similar to those described from oceanic samples above (Janecky and Seyfried, 1986, and references therein). In addition, these experiments have defined solution reaction pathways and relative reaction rates between olivine, enstatite, and diopside.

Seawater initially loses Mg, Ca, and SO_4 , and pH decreases, but SiO_2 and Fe increase. After approximately 1000 hours of experimental reaction, pH increases and Mg, Ca, SiO_2 , Fe, Cl, and CO_2 decrease. This division into two stages of reaction is also found in the mineralogical evolution of the system: the first stage involves olivine plus pyroxenes reacting to form serpentine; in the second stage olivine reacts to serpentine and brucite after the pyroxenes have been consumed. Relative reaction rates between olivine, enstatite, and diopside, determined from these experiments with equigranular starting materials, are approximately 1.0/1.0/0.1 in moles per unit time, or (corrected for relative surface areas) 1.0/3.3/0.7 in moles per unit time per unit surface area.

Methods and Materials

The reaction path models discussed below were calculated using the EQ3/6 code package (Wolery, 1978, 1979, 1983). Parameters for the aqueous solvent and extended Debye-Huckel activity coefficients were calculated by the methodology and thermodynamic data of Helgeson (1969), Helgeson and Kirkham (1974a and b, 1976), Lietzke and Stoughton (1975), and Helgeson *et al.* (1981). Dissociation constants for pertinent aqueous species from 25°C to 350°C were compiled from the literature or taken from other unpublished compilations (Janecky, 1982; Janecky and Seyfried, 1983; Seyfried and Dibble, 1980; Karaka and Barnes, 1973). Mineral hydrolysis constants were calculated using the SUPCRT computer code and thermodynamic data for minerals, aqueous ions, gases, and water (Helgeson *et al.*, 1978; Helgeson and Kirkham, 1974a and b, 1976; Helgeson *et al.*, 1981). Thermodynamic data for sheet silicates not included in Helgeson *et al.* (1978) were taken from the data set estimated by Wolery (1978); data for Mg-hydroxy-sulfate-hydrate (MHS) was taken from Janecky and Seyfried (1983).

Although a universal, verified database for hydrothermal systems would be of tremendous advantage to geochemical modelers, it is necessary to critically examine any such database because of known uncertainties in aqueous activity coefficient models and incomplete and/or ill-defined aqueous dissociation reaction constant data for solution composition, temperature, and pressure. In the case of the database for solution and minerals specified above, its applicability has been examined and partially verified by comparing calculation results with a variety of experimental data, including seawater heating experiments (Janecky and Seyfried, 1983; Bischoff and Seyfried, 1978), serpentinization experiments (Seyfried and Dibble, 1980; Janecky and Seyfried, 1986; Janecky, 1982), and magnetite-hematite experiments (Janecky *et al.*, 1986). Though data for lizardite does not exist in the database, these calculations indicated that chrysotile thermodynamic data could be used in examining the experiments in which lizardite was the primary serpentine formed (Seyfried and Dibble, 1980; Janecky, 1982; Janecky and Seyfried, 1986).

Initial reactants used in the calculations were 546 millimolar Cl^- seawater (Millero, 1974) and harzburgite composed of 75 and 25 wt.% olivine and enstatite, respectively. Olivine and enstatite compositions were those of the minerals used experimentally by Janecky and Seyfried (1986). Individual minerals, rather than bulk harzburgite, were used as reactants because the reaction rates observed experimentally were a function of the dissolution rates specific to each mineral and the amount of mineral present.

Results

Harzburgite reaction with seawater at 300°C, 500 bars, calculated for experimentally defined relative reaction rates, generally matches the results of experimental reaction pathway investigations discussed above (Figure 1). However, the calculations indicate formation of significant amounts of talc not found in experimental products and magnetite in excess of that produced in the experiments. As a consequence, dissolved Fe and f_{O_2} are significantly

lower in the calculated model than in the experiments. A major factor in these discrepancies is the formation of pure Mg-serpentine, in contrast to the formation of ~10 mole % Fe serpentine in the experiments, as illustrated by the reaction:

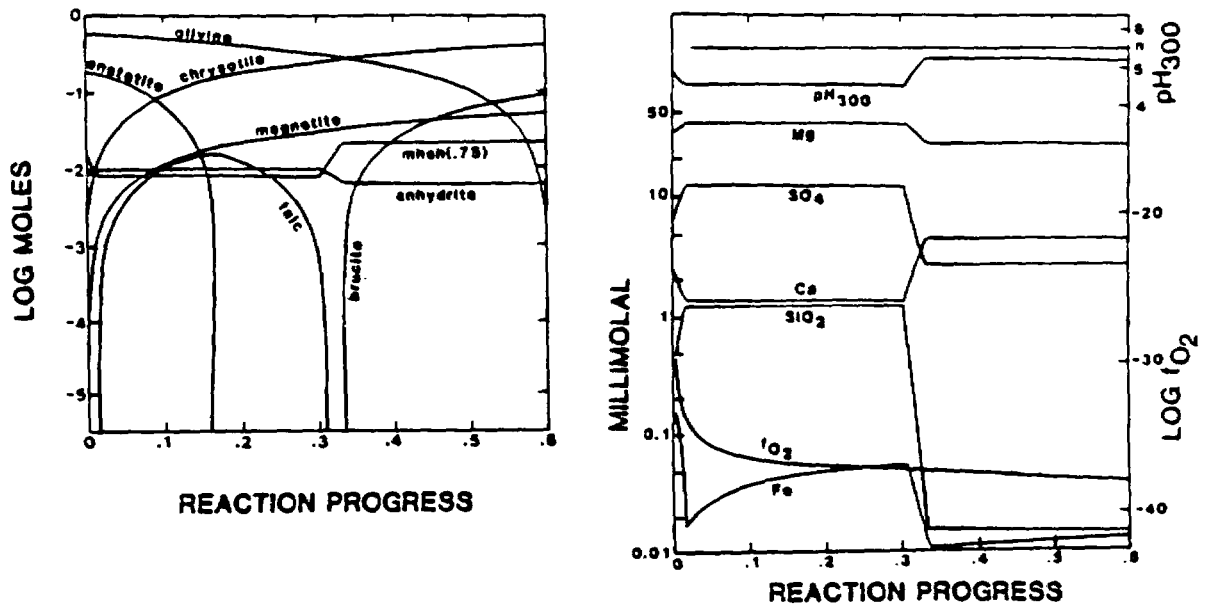
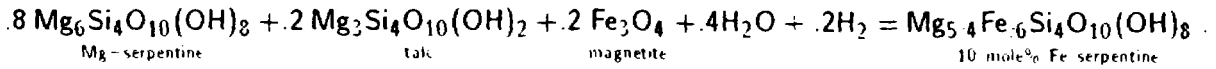


Figure 1. Calculated harzburgite reaction pathway with seawater at 300°C, 500 bars, for a total water-rock mass ratio of 10. Relative reaction rates were set to those determined in experimental studies (Janecky, 1982; Janecky and Seyfried, 1986) and sulfate-sulfide equilibrium was suppressed.

Dissolution constants for an Fe-bearing serpentine, equivalent to that experimentally formed, were calculated using data for chrysotile and greenalite from the database, assuming an ideal solid solution. Calculated reaction pathways using this estimate for a fixed solid solution serpentine are much more consistent with the experimental results (Figure 2). In particular, magnetite amounts and the f_{O_2} pathway in this model closely reproduce those observed experimentally. Fe in solution, during the first stage of reaction, increases by approximately one order of magnitude in this calculation relative to the first, which is closer to experimental results but still approximately one half of the concentrations observed experimentally. One possible explanation for this difference is lack of equilibration between magnetite and solution in the experiments; this explanation is consistent with kinetics of equilibration observed in magnetite-hematite experiments (Janecky *et al.*, 1986).

The second model (Figure 2) also includes calculation of pH-dependent dissolution rates by using transition state theory models (Murphy, 1985, and references therein). Input data to these kinetic models were extrapolated to 300°C, from data extracted from low-temperature

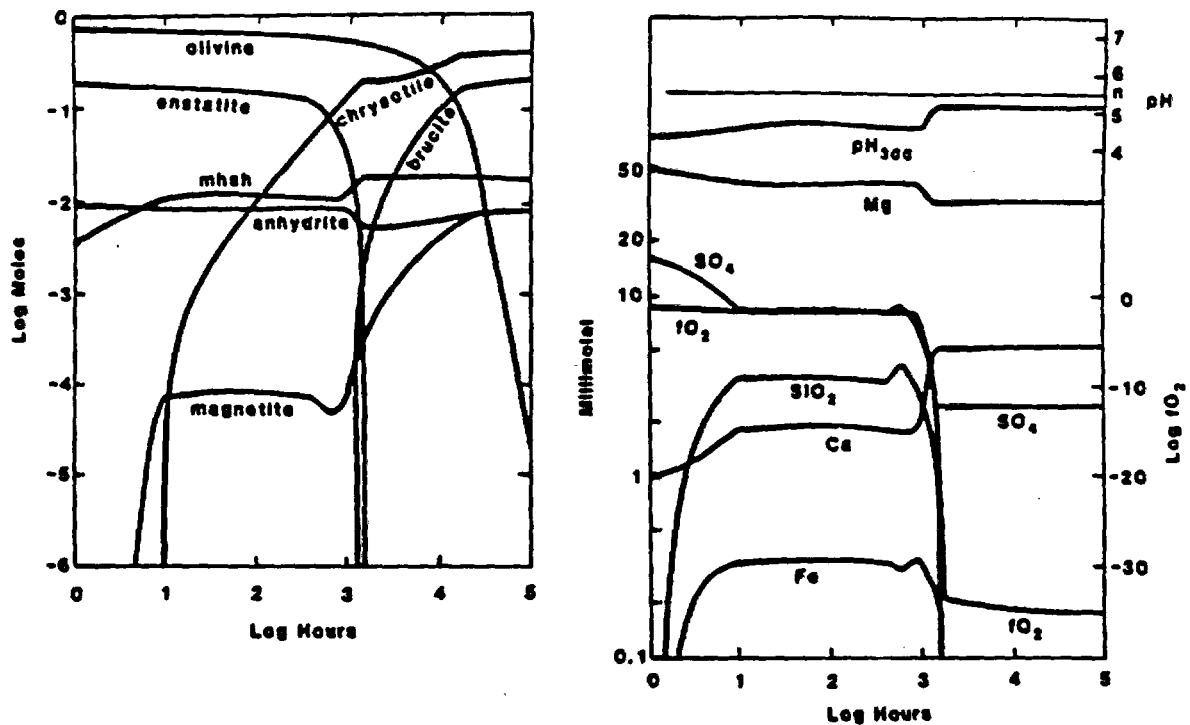


Figure 2. Calculated harzburgite reaction pathway with seawater at 300°C, 500 bars, for a total water-rock mass ratio of 10; the serpentine composition was constrained to be 10 mole % Fe end-member. Reaction rates were calculated using transition-state theory models and data from Murphy (1985) that were extrapolated to conditions of interest.

dissolution experiments (Grandstaff, 1977, 1978, 1980) by Murphy (1985). These data confirm the relative rates for equigranular olivine and enstatite determined from the experimental studies, and they accurately model the timing of enstatite disappearance and consequent chemical and mineral assemblage changes in the experiments. Differences between experimental results and the models in the second stage of reaction (particularly in pH) are probably due to precipitation of Cl^- and incorporation of Fe into brucite during the experiments, both of which are not accounted for in the models.

Conclusions

This modeling effort indicates that accurate results can be obtained when the investigator is cognizant of three major aspects of the modeling process: (1) Does the database provide consistent results for carefully constrained parts or examples of the system of interest? (2) Are reaction components and rates consistent with the system to be modeled? (e.g., is reaction of a bulk rock composition reasonable, or must the rock be subdivided into mineral components?) and (3) Are the mineral compositions calculated by the models consistent with natural and/or experimental systems for at least major elements (and minor elements if they are also included)? The success of the efforts described above in modeling the experimental serpentinization reaction pathway prepares the way for more extensive investigation of serpentinization reactions by allowing a wide variety of variables to be investigated, including variations in grain size between olivine and enstatite and reactions with other possible solutions such as those from adjacent basaltic crust (Janecky, 1982; Janecky, 1986; Janecky and Seyfried, in prep.).

Acknowledgements

This work has benefited from discussion and collaboration with W. Seyfried, H. Dick, T. J. Wolery, W. Murphy, and K. Kimball. Comments and suggestions by C. J. Duffy and J. Heiken substantially improved this manuscript. The research was supported by NSF Grants OCE-7908569 and OCE-820056. Preparation of this paper and continued refinement of these approaches to examining the consequences of water-rock interaction is supported by funding from US DOE Office of Basic Energy Science to Los Alamos National Laboratory.

References

- Aumento, F. (1970) Serpentine mineralogy of ultrabasic intrusions in Canada and on the Mid-Atlantic Ridge. *Geol. Survey Canada Paper* **69-53**.
- Aumento, F. and Loubat, H. (1971) The Mid-Atlantic Ridge near 45°N. XVI. Serpentinized ultramafic intrusions *Can. Jour. Earth Sci.* **8** 631-663.
- Bischoff, J. L. and Seyfried, W. E., Jr. (1978) Hydrothermal chemistry of seawater from 25°C to 350°C. *Am. Jour. Sci.* **278** 838-860.
- Bonatti, E. and Hamlyn, P. R. (1981) Oceanic ultramafic rocks, in *The Sea* **7**, 241-283 (C. Emiliani, ed.) J. Wiley and Sons, New York.
- Bonatti, E., Lawrence, J. R., Hamlyn, P. R., and Breger, D. (1980) Aragonite from deep sea ultramafic rocks. *Geochim. Cosmochim. Acta* **44** 1207-1215.
- Dungan, M. A. (1979) A microprobe study of antigorite and some serpentine pseudomorphs. *Can. Mineral.* **17** 771-784.
- Engel, C. C. and Fisher, R. L. (1975) Granitic to ultramafic rock complexes of the Indian Ocean ridge system, western Indian Ocean. *Geol. Soc. Am. Bull.* **86** 1553-1578.
- Grandstaff, D. E. (1977) Some kinetics of bronzite orthopyroxene dissolution. *Geochim. Cosmochim. Acta* **41** 1097-1103.
- Grandstaff, D. E. (1978) Changes in surface area and morphology and the mechanism of forsterite dissolution. *Geochim. Cosmochim. Acta* **42** 1899-1901.
- Grandstaff, D. E. (1980) The dissolution rate of forsteritic olivine from Hawaiian beach sand. in *Proceedings of the 3rd International Symposium on Water-Rock Interaction* (Edmonton, Canada).
- Helgeson, H. C. (1969) Thermodynamics of hydrothermal systems at elevated temperatures and pressures. *Am. Jour. Sci.* **267** 729-804.
- Helgeson, H. C. and Kirkham, D. H. (1974a) Theoretical prediction of the thermodynamic behavior of aqueous electrolytes at high pressures and temperatures. I. Summary of the thermodynamic/electrostatic properties of the solvent. *Am. Jour. Sci.* **274** 1089-1198.
- Helgeson, H. C. and Kirkham, D. H. (1974b) Theoretical prediction of the thermodynamic behavior of aqueous electrolytes at high pressures and temperatures. II. Debye-Huckel parameters for activity coefficients and relative partial molal properties. *Am. Jour. Sci.* **274** 1199-1261.
- Helgeson, H. C. and Kirkham, D. H. (1976) Theoretical prediction of the thermodynamic behavior of aqueous electrolytes at high pressures and temperatures. III. Equation of state for aqueous species at infinite dilution. *Am. Jour. Sci.* **276** 97-240.
- Helgeson, H. C., Kirkham, D. H., and Flowers, G. C. (1981) Theoretical prediction of the thermodynamic behavior of aqueous electrolytes at high pressures and temperatures. IV. Calculation of activity coefficients, osmotic coefficients, and apparent molal and standard and relative partial molal properties to 600°C and 5 kb. *Am. Jour. Sci.* **281** 1249-1517.
- Helgeson, H. C., Delany, J. M., Nesbitt, H. W., and Bird, D. K. (1978) Summary and critique of the thermodynamic properties of rock-forming minerals. *Am. Jour. Sci.* **278a** 1-229.
- Janecky, D. R. (1982) Serpentinization of peridotite within the oceanic crust: Experimental and theoretical investigations of seawater-peridotite interaction at 200°C and 300°C, 500 bars. PhD. thesis, University of Minnesota. 244p.
- Janecky, D. R. (1986) Peridotite-solution interaction within the oceanic crust: Theoretical investigations. *EOS, Am. Geophys. Union* **67** 392.

- Janecky, D. R. and Seyfried, W. E., Jr. (1983) The solubility of magnesium hydroxide sulfate hydrate in seawater at elevated temperatures and pressures. *Am. J. Sci.* **283** 831-860.
- Janecky, D. R. and Seyfried, W. E., Jr. (1986) Hydrothermal serpentinization of peridotite within the oceanic crust: Experimental investigations of mineralogy and major element chemistry. *Geochim. Cosmochim. Acta* **50** 1357-1378.
- Janecky, D. R., Seyfried, W. E., Jr., and Berndt, M. E. (1986) Fe-O-S redox reactions and kinetics in hydrothermal systems, in *Proceedings, 5th International Symposium on Water-Rock Interaction*.
- Karaka, Y. K. and Barnes, I. B. (1973) SOLMNEQ: Solution-mineral equilibrium computations. *NTIS, U.S. Dept. of Commerce Pb.* **215** 899, 92p.
- Lietzke, M. W. and Stroughton, R. W. (1975) The prediction of osmotic and activity coefficients for electrolyte mixtures at elevated temperatures. *Oak Ridge National Laboratory Rep.* **4999** 16p.
- Millero, F. J. (1974) Seawater as a multicomponent electrolyte solution, in *The Sea* **5**, 3-80 (E.D. Goldberg, ed.) Wiley-Interscience, New York.
- Murphy, W. M. (1985) Thermodynamic and kinetic constraints on reaction rates among minerals and aqueous solutions. PhD. thesis, University of California, Berkeley. 160p.
- Nicolas, A. and Poirier, J. P. (1976) *Crystalline plasticity and solid state flow in metamorphic rocks*. J. Wiley and Sons, 444p.
- Prichard, H. M. (1979) A petrographic study of the process of serpentinization in ophiolites and the ocean crust. *Contrib. Mineral. Petrol.* **68** 231-241.
- Seyfried, W. E., Jr. and Dibble, W. E., Jr. (1980) Seawater-peridotite interaction, an experimental study at 300°C, 500 bars: Implications for the origin of oceanic serpentinites. *Geochim. Cosmochim. Acta* **44** 309-321.
- Smith, G. M., Janecky, D. R., Banerjee, S. K., and Seyfried, W. E., Jr. (1982) Magnetic characteristics of experimental and natural serpentinites. *EOS, Trans. Am. Geophys. Union* **63** 918.
- Wicks, F. J. and Plant, A. G. (1979) Electron-microprobe and x-ray-microbeam studies of serpentine textures. *Can. Mineral.* **17** 785-830.
- Wolery, T. J. (1978) Some chemical aspects of hydrothermal processes at mid-oceanic ridges — a theoretical study I. — Basalt-seawater reaction and chemical cycling between the oceanic crust and the oceans. II. — Calculation of chemical equilibrium between aqueous solutions and minerals. Unpublished PhD. thesis, Northwestern University.
- Wolery, T. J. (1979) Calculation of chemical equilibrium between aqueous solution and minerals: the EQ3/6 software package. Lawrence Livermore National Laboratory **UCRL-52658**.
- Wolery, T. J. (1983) EQ3NR: A computer program for geochemical aqueous speciation-solubility calculations: User's guide and documentation. Lawrence Livermore National Laboratory **UCRL-53414**.

PREDICTED REACTION PATHS DURING THE HYDROTHERMAL ALTERATION OF COLUMBIA RIVER BASALT: A SENSITIVITY ANALYSIS OF VARIABILITY IN THE COMPOSITION OF THE MESOSTASIS

R.C. Arthur*

Rockwell Hanford Operations
Richland, WA 99352 USA

Abstract

Theoretical simulations of hydrothermal reactions of Columbia River Basalts and groundwater, using EQ3/6, show significant differences in the predicted concentrations of aqueous components and in predicted alteration mineralogy depending on small compositional differences in the solid reactants used in the models. This sensitivity is not a simple function of the differences in composition of the reactants. Mass balance considerations show that the variations are due to both the differences in the reactant compositions and the similarity of the predicted amounts of the components precipitated in alteration minerals. When applied to reaction-path models, sensitivity analyses must be bounded by the uncertainties in measured parameters as well as by the uncertainties in the conceptual models of the system.

Introduction

The Basalt Waste Isolation Project (BWIP) is investigating the feasibility of constructing a high-level nuclear waste repository in the Columbia River Basalts of southeastern Washington. Characterizing the expected near-field geochemical environment in the repository is necessary in order to assess the performance of natural and engineered barriers in limiting the release of radionuclides to the accessible environment for periods up to 10,000 years. The BWIP is developing a conceptual model of the expected repository environment by integrating the results from hydrothermal experiments and studies of selected characteristics of natural analogs (e.g., geothermal systems in Icelandic basalts (Ulmer and Grandstaff, 1984)), and through theoretical simulations of basalt/water interactions. Preliminary modeling studies have been conducted to simulate reactions involving basalts from either the Cohasset or Umtanum flows of the Grande Ronde formation and synthetic groundwater at 300 °C.

When dealing with the dissolution of Cohasset or Umtanum basalts there are three reasons to consider the dependence of predicted reaction paths on the composition of the dissolving phase. First, the phases in Umtanum and Cohasset basalts apparently react at different rates. The dominant reactive phase in autoclave experiments appears to be the glassy intersertal mesostasis of the basalts (Allen et al., 1986; Moore et al., 1985). The mesostasis developed from late stage residual fluids evolved from a parent basaltic magma (Long et al., 1984). Consequently, while bulk rock compositions are typical of continental flood basalts, the composition of the mesostasis is more dacitic to rhyolitic (Allen and Strope, 1983). Reaction path models should therefore use the composition of the evolved mesostasis and not a composition based on bulk rock analyses to represent the dominant solid reactant.

The preferential reactivity of the mesostasis leads to a second concern in selecting an accurate composition for the reactive phase in the simulations. That concern is due to the highly variable composition of the mesostasis in Cohasset and Umtanum rocks (Allen and Strope, 1983; Allen et al., 1985). The mesostasis consists of nearly equal amounts of glass and microcrystallites predominantly of plagioclase, pyroxene and titaniferous magnetite (Allen and Strope, 1983). Microprobe analyses of the mesostasis may therefore represent a composite of the glass and microcrystalline phase compositions. While this may account for some of the variability in compositions, Allen and Strope (1983) have shown

* Present address: Battelle, Pacific Northwest Laboratories, PO Box 999, Richland WA., 99352

that the glass composition itself is also variable on a very small scale (microns), and that there may be more than a single type of glass present.

Finally, differences in mesostasis compositions will to some extent lead to differences in predicted reaction paths. Because the thermodynamic stabilities of many of the alteration minerals produced by basalt/water reactions are similar (Arnorsson et al., 1983), the predicted occurrence of one mineral rather than another may depend on small variations in the relative abundances of cationic constituents released to solution as the mesostasis dissolves.

The question addressed in the present study therefore is whether or not the observed variability in the composition of the mesostasis in Cohasset and Umtanum basalts can lead to significant differences in predicted reaction paths.

Model Parameters

The sensitivity of predicted reaction paths on the variability in mesostasis compositions was determined by conducting a set of simulations of rock/water hydrothermal reactions which differed only by the composition chosen for the mesostasis. The five analyses of the mesostasis from Cohasset and Umtanum basalts considered are shown in Table 1. The data in the table are normalized arbitrarily to 20 moles oxygen/mole mesostasis. Samples are from the entablature unit of the Umtanum flow (RUE-1 and RUE-2), the entablature unit of the Cohasset flow (RCE-1), and the colonnade units of the Umtanum and Cohasset flows (RUC-1 and RCC-1, respectively).

Table 1. Mesostasis compositions (moles/mole mesostasis).

	RUE-1 ¹	RUE-2 ²	RCE-1 ³	RUC-1 ³	RCC-1 ³
Si	7.34	7.17	7.53	8.14	8.26
Ti	0.14	0.13	0.09	0.06	0.06
Al	1.89	1.72	1.91	1.66	1.64
Fe	0.76	1.03	0.52	0.14	0.18
Mg	0.09	0.10	0.09	—	—
Ca	0.46	0.49	0.38	0.06	0.08
Na	1.05	1.62	0.94	0.88	0.60
K	0.39	0.40	0.50	0.94	0.84
P	0.07	0.06	0.06	0.02	—
Mn	—	0.02	0.04	—	—

1 -- Based on analysis reported in Allen and Strope (1983)

2 -- Based on analysis reported in Noonan et al. (1981)

3 -- Based on analysis reported in Allen et al. (1985)

Other than the differences in mesostasis compositions, all run parameters were the same in the simulations. Each run modeled the irreversible, incongruent dissolution of 100 grams of mesostasis in 1 kg of solution at 300 °C. The only restriction placed on reaction products was that all silica polymorphs other than cristobalite were not allowed to precipitate. This restriction placed a limit on maximum aqueous silica concentrations in the simulations.

The initial solution composition used in all of the simulations was taken as the starting solution composition in one experiment in which Umtanum entablature was reacted at 300 °C and 30 MPa (run BR-8 in Moore et al., 1985). The initial redox state of the solution was set in the simulations by assigning an oxygen fugacity of 0.21 bars (air saturation).

The simulations were carried out using the 3230 version of EQ3/6 (Wolery 1983;1984). In each case the initial solution was charge balanced at 25 °C (by adjusting the concentration of Na⁺) using EQ3. Then the solution was charge balanced at 300 °C by adjusting H⁺ concentrations in order to fix the high-temperature pH. This solution was used as the initial solution in the reaction-path runs. Before the first increment of mesostasis dissolution, EQ6 equilibrated the aqueous phase by precipitating small amounts of minerals with which the initial solution was supersaturated at 300 °C. This procedure ensured that the mesostasis reacted with an identical high-temperature aqueous phase in each simulation. The following assumptions were employed in all of the simulations: 1) equilibrium among the aqueous solution and alteration minerals is maintained in the closed system during the irreversible dissolution of the mesostasis, 2) no solid-solution minerals precipitate, and 3) release of components from the mesostasis takes place stoichiometrically.

Results of the Simulations

The simulated solution compositions are shown in Figure 1, where it can be seen that significant variations occur in the concentrations of Na, K, Ca, and Al, and in pH and redox conditions (log fO₂). Very little variation in Si concentrations exists, largely because its concentration becomes fixed in all of the simulations by cristobalite solubility.

The trends exhibited in Figure 1 for Na, K, Al, Ca and pH fall into two distinct groups. One group (RUE-2 and RUC-1) is characterized by increasing pH, Na and K, and decreasing Al and Ca. The second group (RUE-1, RCE-1 and RCC-1) shows generally opposite trends: pH and Na decrease continuously, K decreases after an initial rise (coincident with group 1 samples), and Ca and Al generally increase following initial declines (common to all of the samples).

The differences in the trends between these groups are not simply related to differences in the composition of the mesostasis. For example, although sample RUE-2 is the most Na rich mesostasis in the simulations, the other group 1 sample, RUC-1, is one of the most Na deficient. Similarly, RUC-1 is the most K rich member of the set but RUE-2 is nearly the most K deficient. It appears therefore that the groups cannot generally be interpreted *a priori* based on the relative enrichment of the components in the mesostasis. An important exception, however, is that the steep drop in Log fO₂ can be correlated reasonably well with the concentrations of ferrous iron in the mesostasis.

The two general trends in the aqueous component concentrations also cannot be simply related to differences in alteration mineralogy. For example, Figure 2 shows the abundance of alteration minerals for a range of reaction progress coincident with the onset of differences in aqueous concentrations for RUE-1 (group 1) and RUE-2 (group 2). The alteration minerals and their abundances are very similar in the two simulations. Important differences are present, however, including the disappearance of epidote in RUE-2 and its persistence in RUE-1, and the substitution of Ca-saponite for Na-saponite in RUE-1. Although these differences may affect the aqueous concentrations of Ca, similar controls on other components are not evident. For example, Na control by alteration mineralogy is not obvious because for both runs nearly the same amounts of identical Na-bearing minerals precipitate. The behavior of the only K-bearing mineral in Figure 2, phlogopite, is also very similar in both runs.

These results indicate that: 1) predicted reaction paths can be very sensitive to the measured, relatively narrow, range of mesostasis compositions used in the models, and 2) the sensitivity cannot be interpreted simply on the basis of the differences in the compositions of the mesostases. To account for these results an evaluation of the causes of sensitivity in reaction path models is necessary and this is considered in the next section.

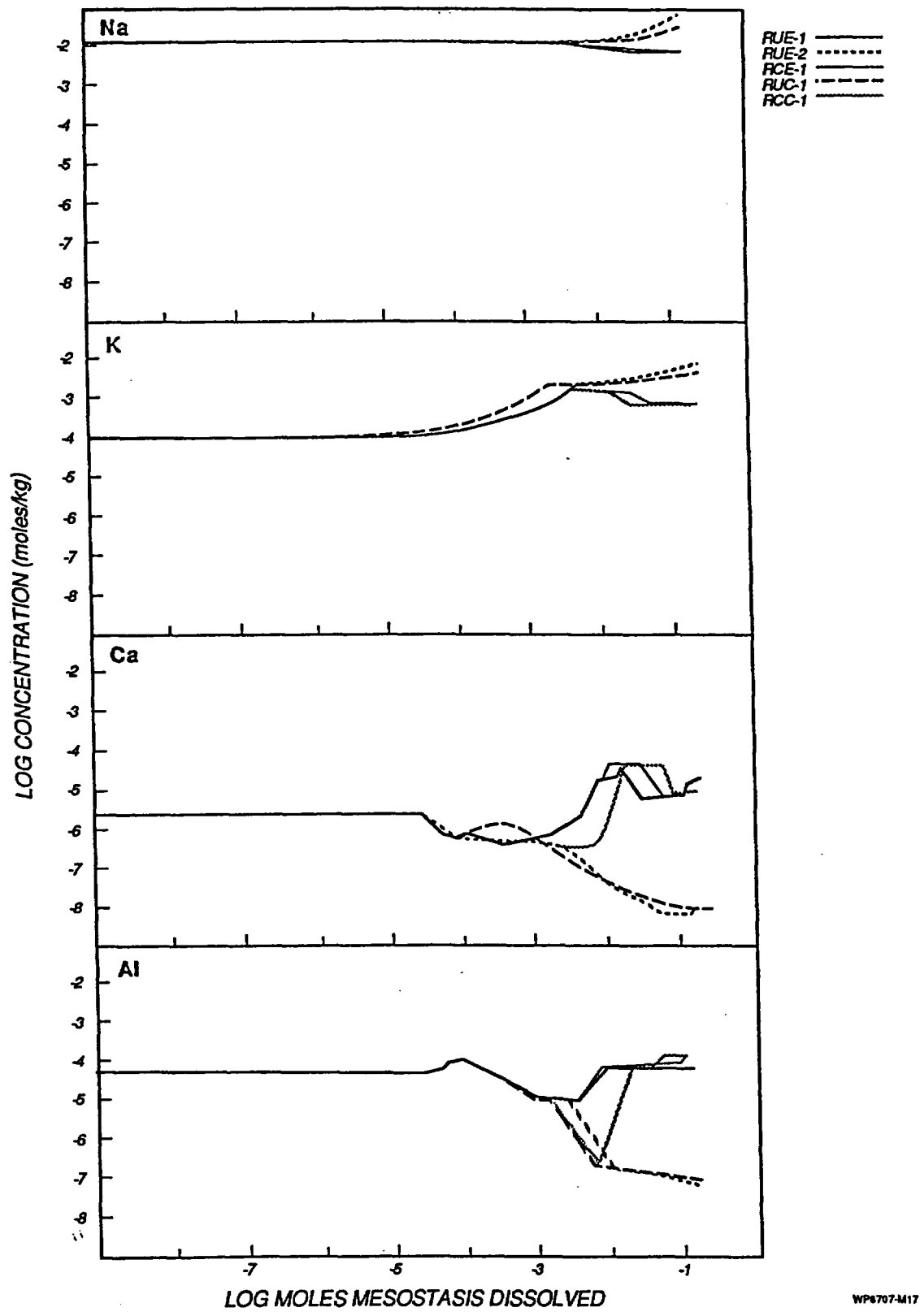


Figure 1. Aqueous Component Reaction Paths

WP6707-M17

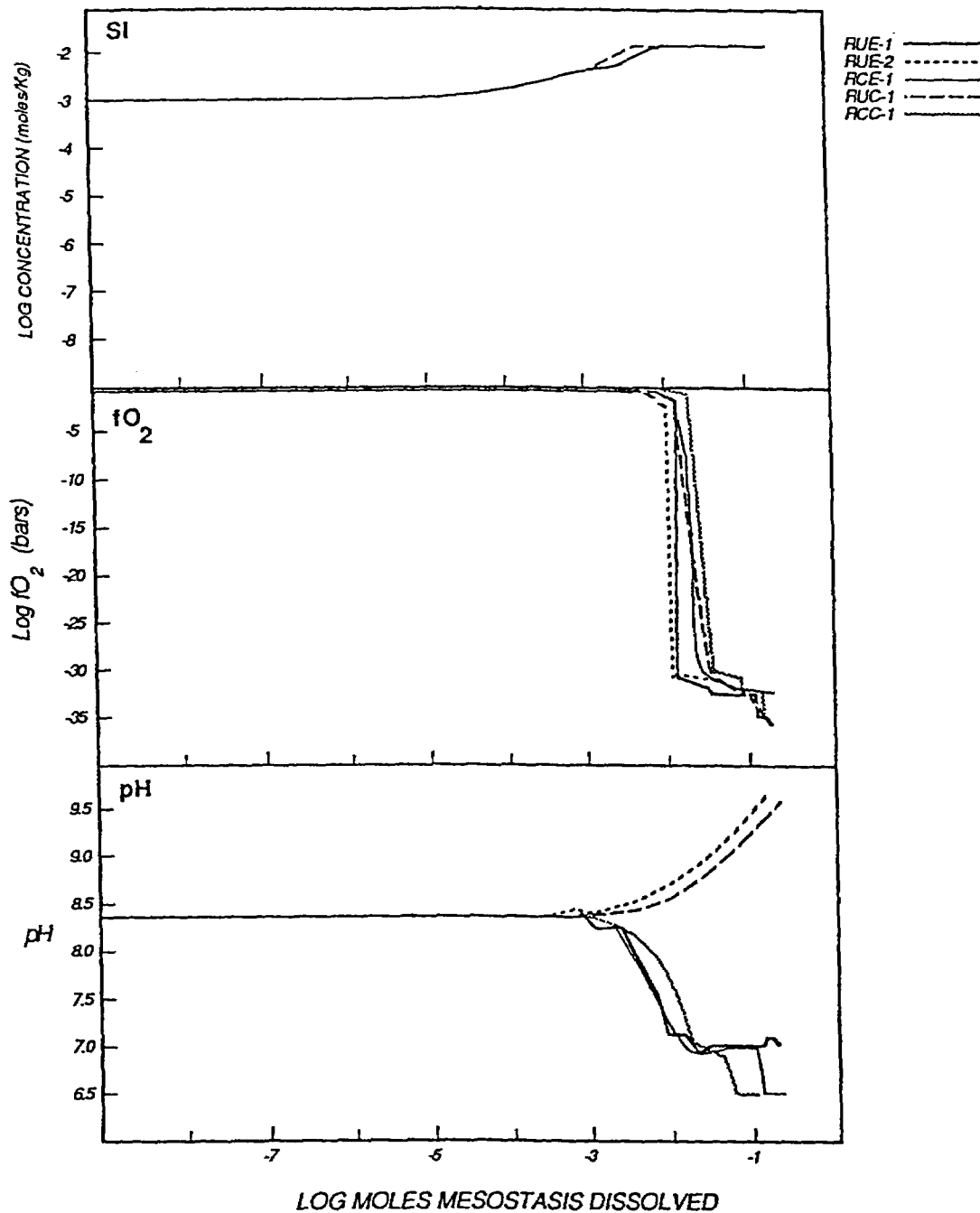


Figure 1. Aqueous Component Reaction Paths (Continued)

Sensitivity in Reaction Path Models

Reaction paths in closed systems are constrained in part by a mass balance for each component, i , of the system (Helgeson, 1968), where, in the current model, i may exist in the mesostasis, alteration minerals and aqueous solution. Therefore, at any stage of reaction progress:

$$v_{i,\text{meso}} m_{\text{meso}} + \sum v_{i,j} m_j + \sum v_{i,k} m_k = m_{i,\text{tot}}$$

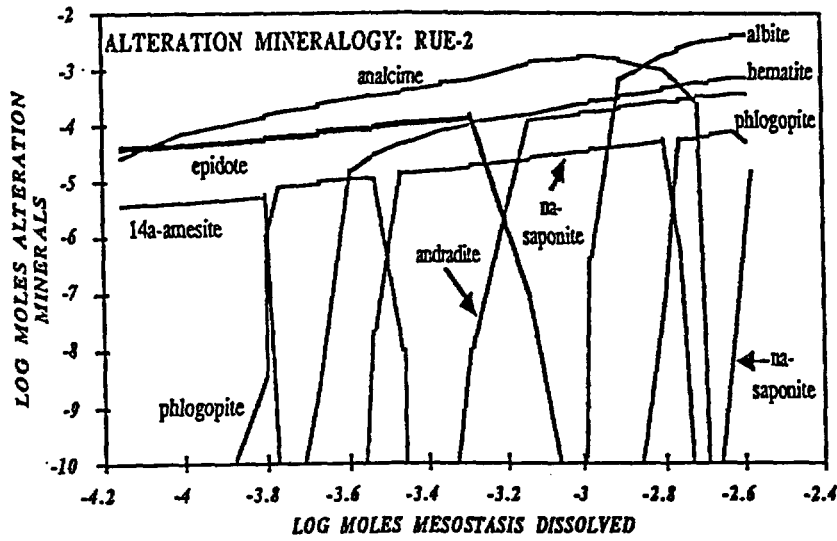
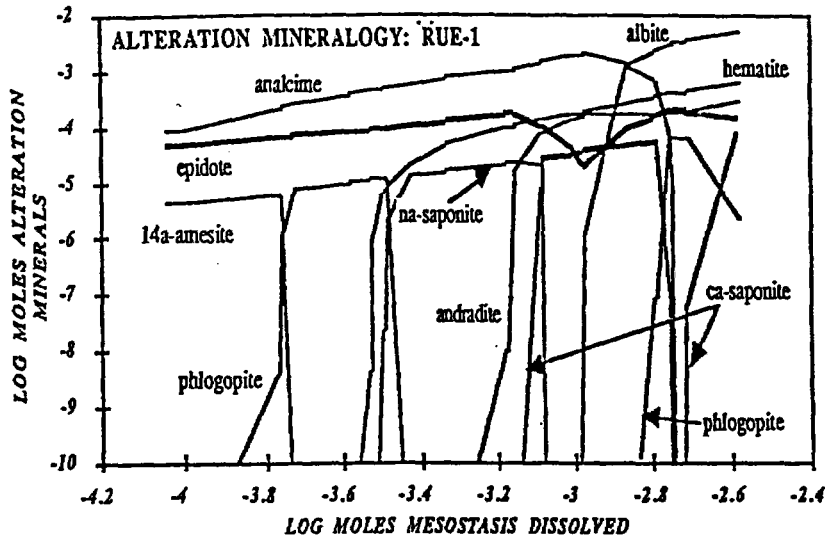


Figure 2. Comparison of predicted alteration mineralogy between runs RUE-1 and RUE-2.

where $v_{i,meso}$, $v_{i,j}$, and $v_{i,k}$ are the number of moles of the monatomic component, i , in one mole of mesostasis (meso), the j th alteration mineral and the k th aqueous species. The parameter m is the number of moles of the subscripted solid or aqueous entity (in the system with 1 kg of water), and the sums in equation (1) are for all j minerals or k aqueous species. The total number of moles of i in the system, $m_{i,tot}$, is independent of reaction progress.

For an increment of mesostasis dissolution, dm_{meso} , equation (1) becomes

$$-v_{i,meso} + \sum v_{i,j} \frac{dm_j}{dm_{meso}} + \sum v_{i,k} \frac{dm_k}{dm_{meso}} = 0 \quad (2)$$

where the derivatives are negative for dissolution of a solid, or for decreasing aqueous species

concentrations. The terms in equation (2) can be related to the results of the simulations discussed earlier. The coefficients in Table 1 are equal to $v_{i,meso}$ for each of the components in the table. The term, $\sum v_{i,k} dm_k/dm_{meso}$, is reflected in Figure 1 for the components Na, K, Ca, Al and O_2 . The term, $\sum v_{i,j} dm_j/dm_{meso}$, for i-bearing minerals can be obtained from data such as shown in Figure 2.

The sensitivity of the predicted reaction paths on mesostasis compositions can be interpreted in terms of the component mass balance equation. Equation (2) indicates that the divergence of slopes for any two reaction paths in Figure 1 (as determined from the third term in the equation) can result only if the net rate of i precipitated in alteration minerals in two reaction paths (the second term in equation (2)) is similar and is bracketed by the values of $v_{i,meso}$ used in the runs. This means that divergence sensitivity depends not only on the differences in composition of the mesostasis chosen for the runs but also on the similarity of the predicted reaction paths, insofar as the paths predict similar amounts of the component precipitated in alteration minerals. Divergence will not result, despite a significant difference in reactant compositions, if the resulting reaction paths are also sufficiently dissimilar.

To illustrate these relationships, consider the Na data for runs RUE-1, RUE-2 and RUC-1. The Na content of RUE-2 mesostasis is greater than in RUE-1 and this leads to the divergence in Na concentrations shown in Figure 1, because the amount of Na precipitated in secondary minerals is very similar (see Figure 2). On the other hand the Na content of RUC-1 is even less than RUE-1, yet its Na path virtually parallels that of RUE-2. This is because the reaction path for RUC-1 involves the precipitation of more phlogopite and (later) K-feldspar because of the high K content of RUC-1 mesostasis. Precipitation of K-bearing minerals decreases the amount of other components, like Al, available for the precipitation of Na-bearing phases such as albite. As a result, the amount of Na precipitated in alteration minerals is less than the amount of Na dissolved from the mesostasis which leads to an increasing aqueous Na concentration in the fluid. This key dissimilarity in the predicted reaction paths compensates for the differences in reactant compositions between samples RUE-2 and RUC-1 so that the trends in aqueous Na concentrations evolve very similarly.

The sensitivity of the aqueous component data in Figure 1 can thus be interpreted relative to the first two terms in the mass balance equation. These two terms differ in one very important respect. The first term in equation (2) is independent of any assumptions used to define the conceptual model of the system (i.e., it is derived from measurement). The derivative in the second term of the equation, however, can be very dependent on the assumed conditions in the model. This is because the precipitation of alteration minerals is governed fundamentally by mass-action relationships, and assumptions (e.g., equilibrium, solid-solution formation, quality of the thermodynamic data) must usually be made before these relationships can be employed in mass-transfer models. In the present study, these assumptions have been specified in the section describing model parameters. Because of the implicit dependence of the second term in the mass balance equation on model assumptions, the sensitivity analysis in this study is only directly applicable to the adopted conceptual model.

Conclusions

Sensitivity analyses can be applied to reaction-path models of water/rock reactions, and component mass balance equations provide a useful basis for interpreting the causes of the sensitivity. The present study has shown that significant differences in reaction paths can arise from small differences in the composition of the starting solid reactants. A complete analysis of sensitivity, however, must be bounded by both the uncertainty in reactant compositions as well as by the assumptions (i.e., the uncertainties) in the conceptual models of the system.

Acknowledgments

S.A. Rawson provided the entablature data in Table 1 and provided many useful discussions of mesostasis compositions, mineralogy and textures.

References

- Allen, C.C. and Strope, M.B. (1983) Microcharacterization of basalt— Considerations for a nuclear waste repository. Microbeam Analysis - 1983, 51-54, San Francisco Press, San Francisco.
- Allen, C.C., Kasper, R.B., Lane, D.L., Johnston, R.G., and Rawson, S.A. (1986) Experimental approaches to determining the extent of equilibrium in a basaltic hydrothermal system. *in* Burkholder, H.C. (ed.), High-Level Nuclear Waste Disposal, 371-380, Battelle Press, Richland, WA.
- Allen, C.C., Johnston, R.G., and Strope, M.B. (1985) Characterization of reference umtanum and cohassett basalt. SD-BWI-DP-053, Rockwell Hanford Operations, Richland, WA, 47p.
- Arnorsson, S., Gunnlaugsson, E., and Svavarsson, H. (1983) The chemistry of geothermal waters in Iceland. II. Mineral equilibria and independent variables controlling water compositions. *Geochim. et Cosmochim. Acta.* **47**, 547-566.
- Helgeson, H.C. (1968) Evaluation of irreversible reactions in geochemical processes involving minerals and aqueous solutions - I. Thermodynamic relations. *Geochim. et Cosmochim. Acta.* **32**, 853-877.
- Long, P.E., Landon, R.D., Cross, R.W., Fairchild, K.R., and Chamness, M.A. (1984) Geology of candidate repository horizons. *in* Long, P.E., (ed.), Repository Horizon Identification Report, SD-BWI-TY-001 DRAFT, vol. 1, Rockwell Hanford Operations, Richland, WA.
- Moore, E.L., Ulmer, G.C., and Grandstaff, D.E. (1985) Hydrothermal interactions of Columbia Plateau basalt from the umtanum flow (Washington, U.S.A.) with its coexisting groundwater. *Chem. Geol.* **49**, 53-71.
- Noonan, A.F., Fredriksson, K. and Nelen, K. (1981) Phase chemistry of the umtanum basalt, a reference repository host in the columbia plateau. *in* Moore, J.G., (ed.), Scientific Basis for Nuclear Waste Management, **3**, 51-58, Plenum Press, N.Y.
- Ulmer, G.C. and Grandstaff, D.E. (1984) Icelandic basaltic geothermal field: A natural analog for nuclear waste isolation in basalt. SD-BWI-TI-257, Rockwell Hanford Operations, Richland, Wa, 41p.
- Wolery, T.J. (1983) EQ3NR, a computer program for geochemical aqueous speciation-solubility calculations, user's guide and documentation. Lawrence Livermore Laboratory (UCRL-53414). 191p.
- Wolery, T.J. (1984). EQ6, a computer program for reaction-path modelling of aqueous geochemical systems, user's guide and documentation. Lawrence Livermore Laboratory (in press).

Sedimentary and Low Temperature Environments

CHEMICAL EQUILIBRIUM IN MINERAL FORMATION AND DIAGENESIS IN THE CARBONATE EVAPORITE SYSTEM: AN ASSESSMENT OF CHEMICAL MODEL APPLICATION TO SITE PERFORMANCE

John H. Weare, Nancy Møller,
Jerry Greenberg, and Andrew Felmy
Department of Chemistry B-014 UCSD
La Jolla, CA 92093 USA

Recently there has been considerable interest in predicting the long-range geochemical behavior of nuclear waste repository sites via thermodynamic modeling. The success of such an approach relies on the availability of highly accurate and general chemical models. While aqueous solution models of the required generality are available, their accuracy for the most part has not been tested against laboratory data. The limited testing that has been done (e.g., Kerrisk (1981); Harvie and Weare (HW) (1980)) has shown that chemical model calculations may differ significantly from experimental values, particularly above dilute concentration ($I > .1m$). This testing underscored the necessity of carefully validating geochemical models for application to complex natural settings.

The recent work of Harvie, Møller, and Weare (HMW) (1984) has shown that it is possible to develop geochemical models which are highly reliable from dilute to high concentration if sufficient attention is paid to phenomenology, parameterization and model validation. The HMW solubility modeling approach is based on the aqueous electrolyte equations of Pitzer (1973). HMW showed that models of highly complex systems (Na-K-H-Mg-Ca-Cl-OH-HSO₄-SO₄-HCO₃-CO₃-H₂O-CO₂(g)) can be parameterized entirely from data in relatively simple binary and ternary systems. In the HMW approach, the accuracy of the final model parameterization is routinely tested by extensive comparison to laboratory solubility data in these and more complicated systems. The agreement with the latter represents the reliability of model predictions since these data were not used in the model parameterization. Validation of model predictive capabilities also includes comparison to field data. These 25°C solubility models have been successfully applied to a variety of natural settings (e.g., Harvie, Weare, Hardie and Eugster (1980), Brantley, Crerar, Møller, and Weare (1984)).

The applicability of the solubility models of Weare and coworkers will be significantly broadened by including variable temperature. Recently, Møller (in preparation) has constructed a variable temperature model which accurately calculates solubilities in the Na-Ca-Cl-SO₄-H₂O system from 25°C to 250°C and from zero to high concentration ($I \sim 18m$). Fig. (1) compares this model's calculated (solid line) anhydrite solubilities in aqueous NaCl solutions with the experimental data at 200°C. Also included in this figure are the solubilities predicted by EQ3/6. Results for other solutions (e.g., CaSO₄-Na₂SO₄-H₂O) and for other temperatures are

similar. The EQ3/6 results (shown by the dashed line on the figure) were calculated using the B-dot equation of Helgeson (1969) and the EQ3NR code of Wolery (1983). New versions of EQ3/6 will include an option to use the 25°C HMW model (Wolery, personal communication). While the number of parameters in the HMW and variable temperature models is large, it is roughly the same number as used in the less accurate chemical models based on ion pairing (HW (1980)). The solubility models of Weare and coworkers include ion pair species explicitly in the specific interaction formalism of Pitzer only when there is clear evidence of association (e.g., $H + SO_4 = HSO_4$). When ion pairs are included, it is generally necessary to accurately account for changes in the activity of the associated species in order to obtain reliable predictions at high concentration.

The 25°C HMW model and the variable temperature model include species for which sufficient data are available for detailed parameterization. When little data exist for a system, parameterization of any geochemical model must rely on approximations based on chemically similar systems. Extensively validated models of well-characterized systems for which an adequate database is available are important for such approximations. The success of such an approach using the Pitzer formalism is illustrated by the models of the $BaSO_4$ - $NaCl$ - H_2O system at 25°C (Rogers (1981)) and at 100°C to 250°C (Møller, in preparation) using parameters based on the $CaSO_4$ system.

The HMW model has now been extended to treat the chemically very complicated borate system (Felmy and Weare (FW), to be published *Geochim. Cosmochim. Acta.*). This system involves complex borate polymerization reactions as well as acid-base reactions. Solubility predictions of this model (solid lines) are compared to laboratory solubility data in Fig. (2).

The borate model was developed to study borate deposition in natural environments. Borate minerals are very soluble and therefore are products of highly evaporated waters. An important example of borate deposits occurs in Searles Lake (southeastern California). The economic importance of the formation waters from this system has led to their being frequently sampled. A field validation of the FW model is shown in Table (1) which gives the normalized saturation indices for the minerals known to be in the formation. The normalized S.I. in FW is equal to the logarithm of the saturation ratios ($SR = \prod \text{activity (ion)}/K_{sp}(\text{mineral})$) divided by the number of ions in each solid. In every case, the calculated S.I. values are within .03 pK units of the equilibrium value of 0. A more extensive discussion of these results is given in FW. This comparison to a complex natural setting serves as a stringent test of the accuracy of the model. It also shows that, within the accuracy of the model, the formation water is in equilibrium with the mineral formation.

The borate model was also used to simulate the formation of the Searles Lake mineral deposit. In this simulation, the initial composition of the water was taken to be that of Owens River, which is the principal source of the Searles Lake water. Owens River water was evaporated to dryness at 25°C using the equilibrium algorithm of Harvie, Greenberg and Weare (to be published, *Geochim. Cosmochim. Acta.*). The results of this simulation are discussed in detail in FW. In order to correctly predict

Table 1: Normalized mineral saturation indices for interstitial brines in the Searles Lake upper salt^a calculated by the model of Felmy and Weare.

Mineral	S.I.
Aphthitalite	-.0210 ^b
Borax	.0145
Burkeite	.0104
Halite	.0115
Thenardite	.0015
Trona	.0077

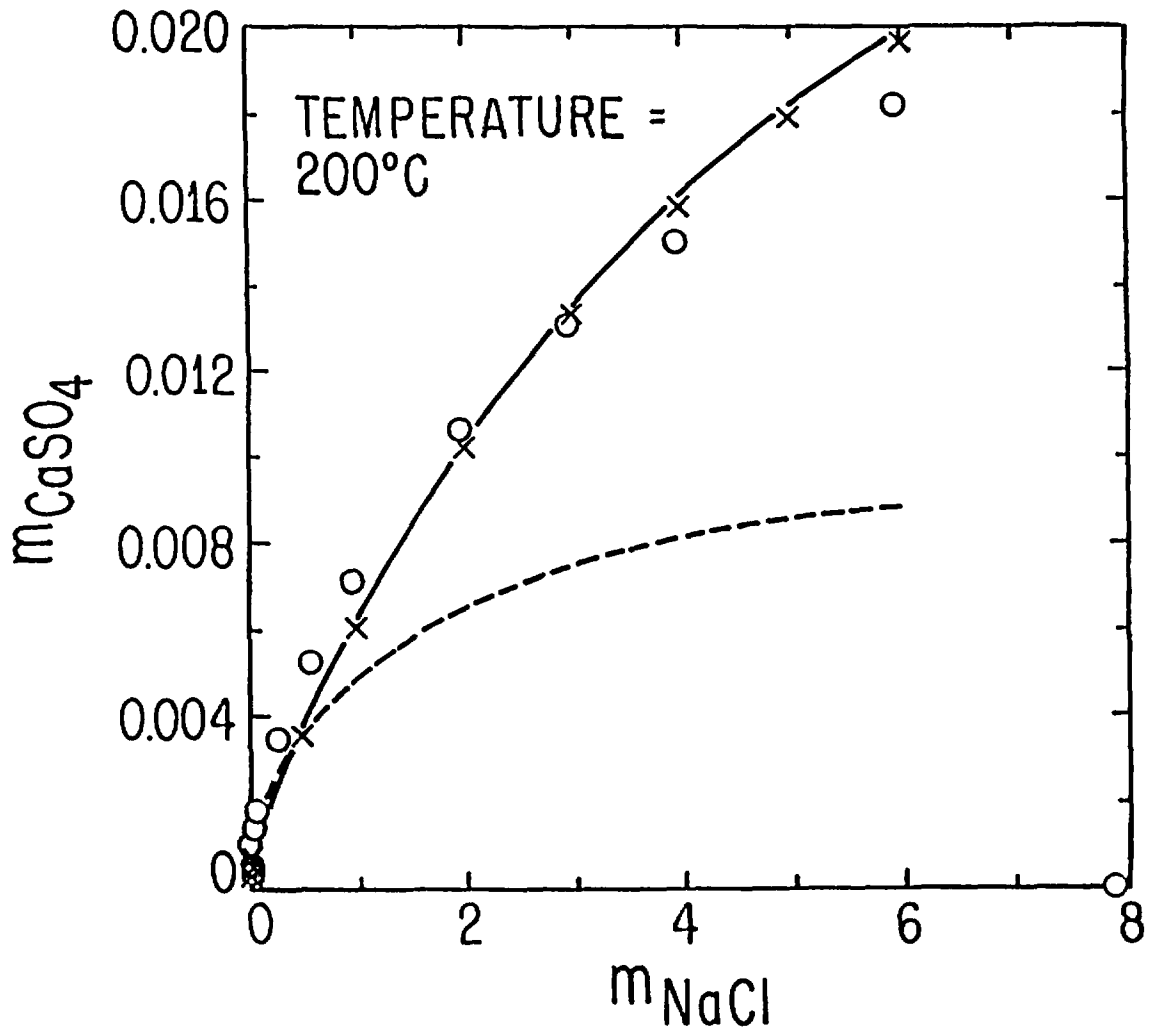
the observed mineral formation, two important restrictions had to be placed on the evaporation pathway. First, in order to allow the formation of trona, a mineral which comprised 37% of the volume of the formation, backreactions forming pirssonite between the upper salt and the calcium carbonate-rich parting mud had to be prevented. Second, in order to keep the magnesium in the brine high enough to eventually precipitate northupite, a mineral which is present in the upper salt, dolomite precipitation had to be prevented in the early stages of evaporation.

Our applications of well-defined chemical models to field settings have several important implications for applying models to natural systems in general. First, we have shown that *detailed models of systems with very complex chemistry can be developed which are accurate to high concentration*. Second, the Searles Lake application showed that *the model not only could correctly predict the geochemistry of a complex natural system but also that the mineral formation is in equilibrium with the formation water*. Third, (and perhaps the most important for assessing the feasibility of using models to reliably predict geochemical processes on a long-time scale) *certain geochemical controls (e.g., late dolomitization and limited communication between units in the formation) were necessary to bring the model into good agreement with the chemistry of the real setting*. These controls affected only the interpretation of field processes and in no way affected the parameterization or validation of the model. In the application to the Searles Lake borate deposit, these controls led to important information about possible geochemical processes involved in the formation of evaporative mineral deposits in lake beds. Prior to modeling the system, there was no *a priori* way to make these assumptions. This result has important implications when the application of less well-defined models to poorly defined settings is considered. In such situations, it may not be possible to separate effects due to model inaccuracies from the various unknown geochemical controls operating in the natural setting.

a. Data taken from Smith (1976)

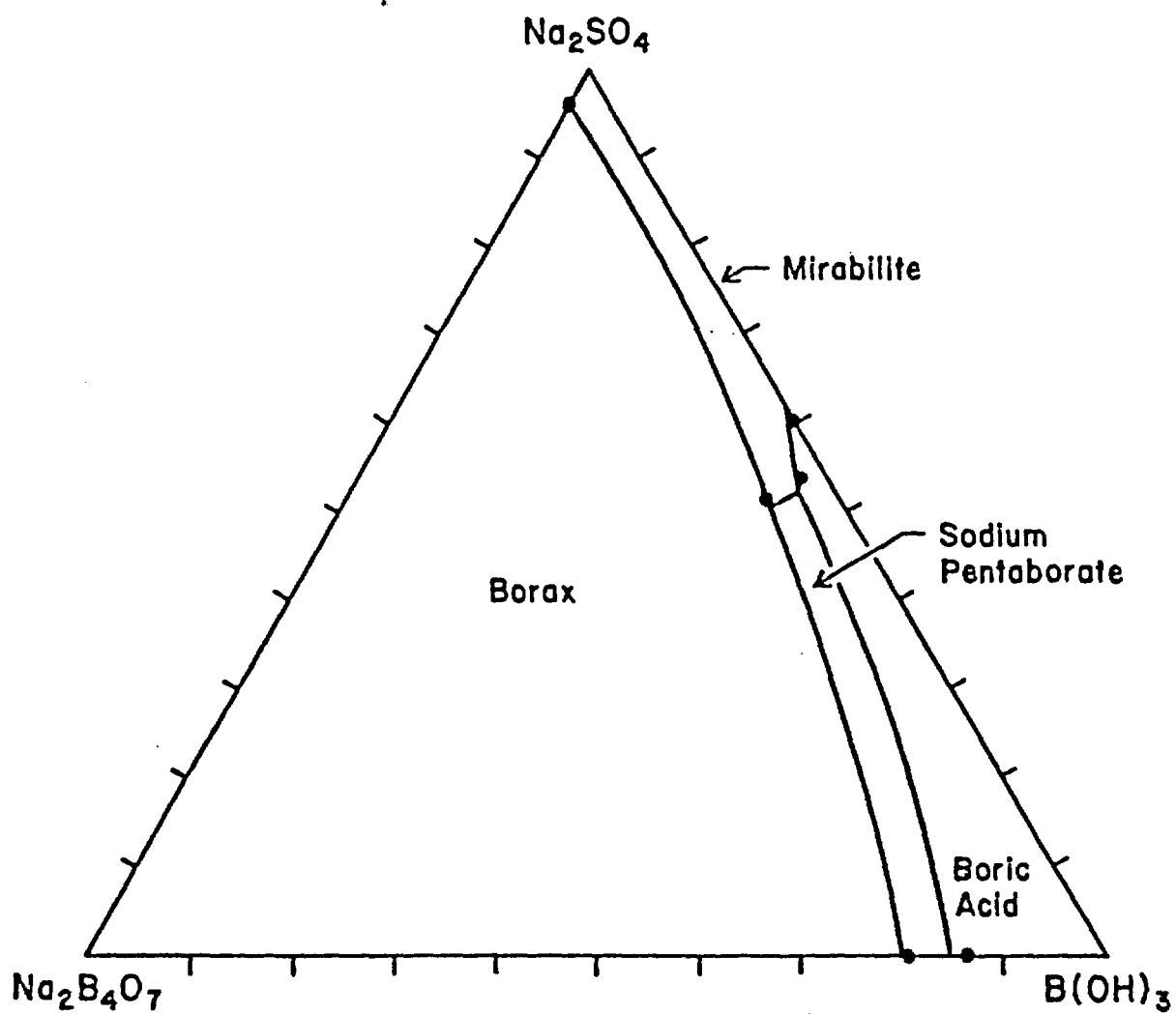
b. Uses Gale's water measurements (see Felmy-Weare). Using Smith's water measurements a higher S.I. is obtained.

Figure 1



A comparison of anhydrite solubility in aqueous NaCl solutions at 200°C calculated by the variable temperature Na-Ca-Cl-SO₄-H₂O model (solid line) of Møller (in preparation) with the experimental data of Blount and Dickson (1969) and Marshall, Slusher, and Jones (1964). Solubilities predicted by EQ3/6 (see text) are given by the dashed line.

Figure 2



Jänecke projection for the system $\text{Na}_2\text{B}_4\text{O}_7\text{-B(OH)}_3\text{-Na}_2\text{SO}_4$ at 23.5°C calculated (solid lines) by the model of Felmy and Weare (to be published, *Geochim. Cosmochim. Acta.*). The closed circles represent the experimental data of Teeple (1929).

ACKNOWLEDGEMENTS:

This work has been supported by funds from the Department of Energy: DOE DE-AC-85SF-15522 and the National Science Foundation: NSF OCE 85-07902.

REFERENCES

- BLOUNT C.W. and DICKSON F.W. (1969) The solubility of anhydrite (CaSO_4) in $\text{NaCl-H}_2\text{O}$ from 100 to 450°C and 1 to 1000 bars. *Geochim. Cosmochim. Acta* 33, 227-245.
- BRANTLEY S.L., CRERAR D.A., MØLLER N.E. and WEARE J.H. (1984) Geochemistry of a modern marine evaporite: Bocana de Virrila, Peru. *Jour. Sed. Petrol.* 54, 447-462.
- HARVIE C.E., MØLLER N. and WEARE J.H. (1984) The prediction of mineral solubilities in natural waters: The Na-K-Mg-Ca-H-Cl-SO₄-OH-HCO₃-CO₃-CO₂-H₂O system to high ionic strengths at 25°C. *Geochim. Cosmochim. Acta* 48, 723-751.
- HARVIE C.E. and WEARE J.H. (1980) The prediction of mineral solubilities in natural waters: The Na-K-Mg-Ca-Cl-SO₄-H₂O system from zero to high concentration at 25°C. *Geochim. Cosmochim. Acta* 44, 981-997.
- HARVIE C.E., WEARE J.H., HARDIE L.A. and EUGSTER H.P. (1980) Evaporation of seawater: calculated mineral sequences. *Science* 208, 498-500.
- HELGESON H.C. (1969) Thermodynamics of hydrothermal systems at elevated temperatures and pressures. *Am. J. Sci.* 267, 729-804.
- KERRISK J.F. (1981) Chemical equilibrium calculations for aqueous geothermal brines. Los Alamos, N.M. Science Lab. Report LA-8851-MS.
- MARSHALL W.L., SLUSHER R. and JONES E.V. (1964) Solubility and thermodynamic relationships for CaSO_4 in $\text{NaCl-H}_2\text{O}$ solutions from 40°C to 200°C, 0 to 4 molal NaCl. *J. Chem. Eng. Data* 9, 187-191.
- PITZER K.S. (1973) Thermodynamics of electrolytes. I: Theoretical basis and general equations. *J. Phys. Chem.* 77, 268-277.
- ROGERS P.S.Z. (1981) Thermodynamics of geothermal fluids. Ph.D. Dissertation, U.C. Berkeley, Berkeley, Ca.
- SMITH, G.I. (1976) Origin of lithium and other components in the Searles Lake evaporites California, In: Lithium Resources and Requirements by the Year 2000. J.D. Vine, ed: U.S. Geological Survey Prof. Paper 1005, p.92-103
- TEEPLE, J.E. (1929) The industrial development of Searles Lake brines with equilibrium data. In *American Chemical Society Monograph Series*, The Chemical Catalog Company, Inc.
- WOLERY T.J. (1983) EQ3NR A computer program for geochemical aqueous speciation-solubility calculations: user's guide and documentation. Lawrence Livermore Lab. Report UCRL-53414.

MODELLING MASS TRANSFER REACTION RATES: CALCITE PRECIPITATION AND CO₂ OUTGASSING IN A KARST STREAM

Janet S. Herman and Michelle M. Lorah
Department of Environmental Sciences
University of Virginia
Charlottesville, VA 22903

Abstract

While theoretical and experimental studies are widely reported in the geochemical kinetics literature, field studies are relatively few in number. In this study, the evolution of water chemistry along a well-defined flow-path was quantified by modelling the mixing of two discrete waters and mass transfer reactions between sampling points using WATEQF and PHREEQE and observed chemical compositions. The reaction time between sampling locations was estimated from measurements of stream discharge and geometry. The major reactions considered were CO₂ outgassing and calcite precipitation from ground and surface waters in a limestone terrane. The kinetics of calcite dissolution and precipitation have been especially well-studied, and the reaction rates obtained from the combination of the mass transfer modelling and hydrologic measurements of this study could be compared with the rates predicted from a laboratory-derived rate law. The agreement in rates was generally within an order of magnitude and routinely within a factor of 2 or 3. Least agreement between measured and predicted rates was obtained for sections of flow-path where relatively little change in bulk chemical composition occurred, which were the sections with the greatest mass transfer modelling error. For the travertine-depositing stream of Warm River Cave and Falling Spring Creek, VA, the coupling of equilibrium speciation and mass transfer geochemical models with simple field measurements in a hydrologically well-defined system allowed successful field-based quantification of reaction rates.

Introduction

The processes of CO₂ exchange and mixing of different carbonate waters exert a major control on the thermodynamic stability of calcite in solution. The CO₂ content in carbonate groundwaters can reach values much above normal atmospheric CO₂, and when this groundwater emerges at or near the earth's surface, CO₂ outgasses. This exchange of CO₂ between solution and atmosphere is the dominant process causing supersaturation with respect to calcite in many carbonate waters. Several field studies have shown that the combination of a high supply rate of dissolved CO₂ to spring-fed streams and agitation of the water at cascades allows a great amount of CO₂ outgassing to occur (Dandurand et al., 1982), but no previous study has quantified

the mass transfer and the rate of removal of CO_2 .

Ultimately, calcite will precipitate from the increasingly supersaturated solution. But calcite does not precipitate immediately as supersaturation is reached. A certain critical degree of supersaturation must be achieved for significant precipitation to occur, and it can be as much as 10 times the equilibrium calcite solubility value. High degrees of supersaturation with respect to calcite have been maintained in solutions in both field and laboratory studies without noticeable calcite precipitation taking place.

Mixing of one water with another solution that differs in chemical composition will also cause a shift in the saturation state of the water with respect to calcite. Because calcite solubility is a non-linear function of variables such as ion activity, PCO_2 , ionic strength, and temperature, mixing of two carbonate waters produces complex non-linear effects. Mixing is believed to be a common process in subsurface waters, however, geochemical field evidence of the results of mixing is difficult to obtain.

Thermodynamic, or equilibrium, models can be used to determine whether or not a solution will tend to evolve CO_2 or to precipitate calcite. Kinetic information is required, however, to determine the rates at which these reactions occur. Many laboratory studies of calcite dissolution and precipitation kinetics have been conducted. Several different rate laws have been published, but the Plummer et al. (1978) empirical model is the only one that attempts to describe both dissolution and precipitation rates at all solution pH and PCO_2 values. Although the Plummer et al. rate law has been tested and generally supported by laboratory kinetic studies, the rate equation has not been tested in a field situation.

Very few researchers have quantified calcite dissolution or precipitation rates in field studies. The purpose of the present research is to conduct a field investigation of CO_2 outgassing, calcite precipitation or dissolution, and mixing of two carbonate waters. The effect of these processes on the chemical evolution of a travertine-depositing stream is assessed (Herman and Lorah, 1986). Rates of CO_2 outgassing and calcite precipitation are quantified by mass transfer calculations and are compared to rates predicted with a laboratory-derived rate law.

Methods

The study area is located inside Warm River Cave and along Falling Spring Creek, Virginia (Herman and Loarh, 1986). The spring issuing in Warm River Cave, like other thermal springs in the region, is fed by deeply-circulated meteoric water that was heated under a normal geothermal gradient. The thermal water circulates through a thick sequence of Cambrian and Ordovician

limestones and dolomites. The warm spring inside Warm River Cave exceeds 38°C. This spring water flows through the cave as a warm stream and converges with a cold stream derived from shallow groundwater. The mixed stream ultimately resurges on the surface as Falling Spring, issuing from the breakdown pile that closes off Warm River Cave and forming Falling Spring Creek. Approximately 0.8 km downstream from Falling Spring, the stream breaches a small sandstone ridge and flows over a 20-m vertical waterfall. The cliff is covered in travertine and more travertine deposits are evident in the streambed immediately above and below the waterfall.

Ten field trips to collect water samples were completed between April, 1984, and June, 1985. Cave water samples were collected on three of those trips. Twelve sampling sites were established along a 5.2-km stretch of Falling Spring Creek. Seven collection sites inside Warm River Cave were located along the accessible parts of the warm, cold, and mixed streams. Temperature, pH, conductivity, and discharge were determined in the field. Complete major cation and anion analyses were performed on filtered samples in the laboratory.

The data analysis included (1) defining the saturation state of the waters with respect to calcite and CO₂, (2) determining mass transfers of calcite and CO₂ along the flow path, and (3) calculating the rates of calcite precipitation and CO₂ outgassing. Aqueous speciation, theoretical PCO₂, and the saturation state of each solution sample was determined using WATEQF (Plummer et al., 1976) and the chemical concentration data and field pH and temperature. Data were input to WATEQF with the program WATIN (Moses and Herman, 1986).

PHREEQE (Parkhurst et al., 1980) was used to determine mass transfers. Given an observed initial water composition and thermodynamic constraints for a set of plausible reactants and products, the model calculates the amounts of minerals or gases that would have to be added or lost from the solution to meet the thermodynamic constraints. Calcite and CO₂ are the most plausible reactants or products controlling the water chemistry in this system. The SI_C and PCO₂ values obtained from WATEQF were used as the thermodynamic constraints in PHREEQE. To calculate the mass transfer (mol kg⁻¹ H₂O) between two successive points along the flow-path, the observed chemical composition of the upstream site is input to PHREEQE and required to equilibrate with the SI_C and PCO₂ of the downstream site. The net amount of calcite that had to be precipitated or dissolved and the net amount of CO₂ that had to be added or lost from the water between the two sampling sites to produce the composition of the final water is calculated.

The mixing of warm and cold streams inside Warm River Cave can also be simulated with PHREEQE. Mass balance was applied to the conservative constituent fluoride to define the fraction of each end-member water in the resulting mixture. That mixing

fraction was applied to all other constituents in the warm and cold stream to estimate what their total concentrations would be. By comparing the predicted conservative mixture with the observed chemical composition of the mixed stream, mass transfers that occur during the mixing process are determined.

Rates ($\text{mol kg}^{-1} \text{H}_2\text{O s}^{-1}$) of calcite precipitation or dissolution and CO_2 outgassing were calculated using the mass transfers between two sites divided by estimates of reaction time. The stream velocity was calculated from discharge and cross-sectional area measurements. Reaction time was computed from distance between sampling sites divided by velocity.

A laboratory-derived equation for calcite dissolution and precipitation was also used to calculate rates (Plummer *et al.*, 1978). The net rate of calcite dissolution, R ($\text{mol cm}^{-2} \text{s}^{-1}$), is the sum of three forward reaction rates and a backward reaction rate

$$R = k_1 a_{\text{H}^+} + k_2 a_{\text{H}_2\text{CO}_3^*} + k_3 a_{\text{H}_2\text{O}} - k_4 a_{\text{Ca}^{2+}} a_{\text{HCO}_3^-}$$

The activities of dissolved species are obtained from the WATEQF output. An estimated surface area for the streambed and the volume of water flowing between two sampling locations were used to convert the calculated calcite precipitation rates to the same units as the mass transfer rates.

Results

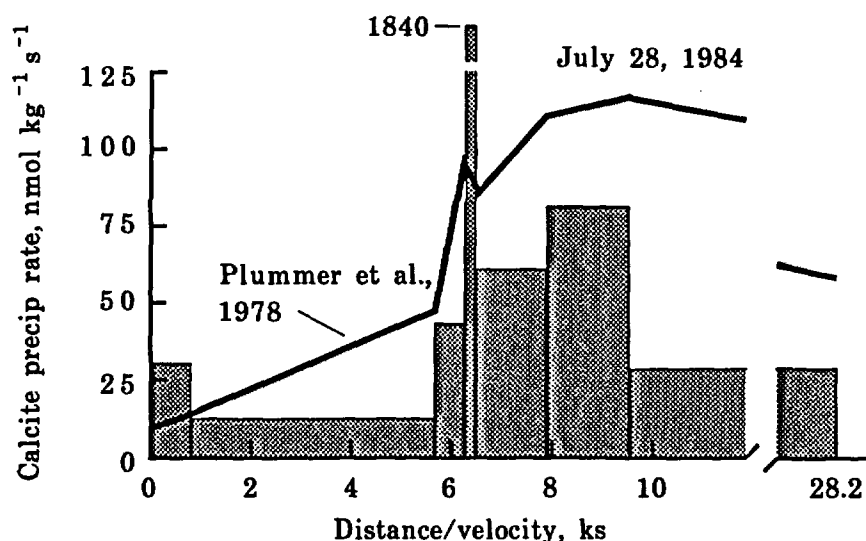
Ca^{2+} and HCO_3^- dominate the chemical character of the water at every point in this system. In the cave, the warm relatively concentrated water mixed with the dilute cold water to define the composition of the mixed stream. Ca^{2+} and HCO_3^- concentrations decrease along the flow-path. The largest decreases occur in the cave at the junction of the warm and cold streams and on the surface at the falls and just downstream of the falls.

The cave and surface waters are almost always supersaturated with respect to CO_2 and calcite. Calculated PCO_2 values decreased downstream, especially just above and at the waterfalls, but they remained above normal atmospheric values for the entire 6-km flow-path. Associated with the loss of CO_2 is an increase in pH. SI_c increased along the warm stream and then dropped at the mixed stream. During low-flow conditions of summer and fall, the entire length of the surface stream was supersaturated. In the high-flow conditions of spring and winter, the springs were undersaturated, but the water was supersaturated by the time it reached the crest of the falls.

The mass transfer calculations show that calcite precipitation and CO_2 outgassing characterized the chemical changes in the cave and surface waters. During the high-flow

conditions of winter, some calcite dissolution was calculated for early segments of the flow-path. Net calcite precipitation occurred throughout the year, but the total amount precipitated during the summer and fall was roughly twice that formed in the winter and spring months.

The rate results obtained by the two different methods agreed within an order of magnitude. Both methods gave the same trends, with low rates above the falls and higher rates at and downstream from the falls. At the falls, however, the mass transfer results showed a one or two order of magnitude increase while the rate equation predicted a much smaller increase in rate. During the few instances of calcite dissolution being predicted by the mass transfer calculations near the springs, the rate law predicted precipitation.



Discussion

The thermal spring water has an extremely high CO_2 content. Outgassing causes the PCO_2 of the water to drop significantly. The greatest decrease in HCO_3^- concentration in the cave occurs at the junction of the streams. The cold shallow groundwater dilutes the warm water, but calculations show that CO_2 continues to outgas during the mixing of the two waters.

An important source of error in the mass transfer and rate calculations for the cave stream is the poorly-defined influx of cold groundwater to the warm stream. The estimates of CO_2 outgassing and calcite precipitation from mass transfer calculations reflect the inability to define discrete inputs of groundwater to the stream that caused dilution. The greatest variability in predicted reactions occurred in December when the dilution by shallow groundwater was greatest.

On the surface, the water continues to outgas, and the pH increases. After a smooth, straight segment of stream where outgassing rates are low, the rates increase at the riffles near the top of the falls. At the falls, outgassing proceeds at a rate 10 to 30 times greater than upstream. Rates decrease again downstream of the falls where the concentration gradient from solution to atmosphere is lower, the temperature is lower, and the stream is once again following a relatively smooth path.

The thermal spring water is initially near equilibrium with respect to calcite. Along its flow-path, SI_C increases as the solution loses CO_2 . Rimstone dams are observed in the warm stream, and they are a sink for calcium and bicarbonate. The cold groundwater has much lower concentrations, and it was undersaturated with respect to calcite during high flow conditions. Diffuse input of such water would lead to calculation of calcite precipitation with PHREEQE, an error due to the poor definition of the flow system. At the obvious junction of the saturated warm stream and the undersaturated cold stream, an even more undersaturated mixture is formed.

The surface stream loses CO_2 , pH increases, and calcite precipitates. All these reactions are more dramatic than for the cave stream because the lower PCO_2 of the open atmosphere and the greater turbulence in the stream cause more CO_2 to outgas. Although the stream water may be supersaturated, calcite precipitation is inhibited until the crest of the falls. Mass transfer calculations for the segments of stream between the springs and the falls show almost no calcite precipitation while the SI_C increases. Near the crest of the falls, a rapid increase in the SI_C occurs in response to the higher outgassing rate. Just above the falls the water reaches approximately 10 times supersaturation with respect to calcite and significant precipitation begins. A large decrease in Ca^{2+} and HCO_3^- concentrations where there is no source of dilution indicates that significant calcite precipitation begins at the falls, with rates increasing two orders of magnitude over the rates immediately upstream. It is at the base of the falls that calcite is seen to form fresh white crusts on everything. Calcite precipitation continues along the rest of the 4-km flow-path below the falls, but the rates are lower. By the last sampling site, SI_C finally decreases, but the solution is still supersaturated with respect to calcite. Seasonally, the amount of calcite precipitated in the surface stream is tied to the mixing of the two waters inside the cave. During low-flow conditions the concentrated thermal water is not as diluted with shallow groundwater, and higher SI_C values are reached, greater rates of precipitation are observed, and larger mass of calcite is deposited.

Calcite precipitation rates were determined from the mass transfers of calcite simulated with PHREEQE and from calculations with Plummer et al.'s rate law. The rates obtained with PHREEQE are affected by errors in the simulated mass

transfers and in the hydrologic data used to obtain the reaction times. Both the chemical composition of the initial water and the SI_C of the final water are needed to model mass transfer of calcite; therefore inaccurate chemical analyses and pH and temperature measurements could cause error in predicted rates. One indication that the calculations were successful is that the final water composition predicted by PHREEQE to match the thermodynamic constraints of SI_C and PCO_2 matches the analyzed final water chemistry nearly exactly. Some PHREEQE results are clearly suspect, though, because they indicate calcite dissolution into a supersaturated water. These contradictory results were only seen over stretches of stream where the Ca^{2+} concentration remained the same or changed very little. Because only very small changes in Ca^{2+} concentrations were being simulated by PHREEQE, relatively small errors in the chemical analyses or convergence errors in the model iterations would have been noticeable. Errors in reaction time could clearly lead to errors in rate estimates. Errors could arise from poor discharge measurements or from the incorrect assumption of uniform velocity along the entire stream on each sampling date. Since the same estimates of reaction time were applied to both rate calculations, that error is not a factor in the comparison.

While laboratory precipitation studies have given support to the rate expression of Plummer et al. over a wide range of solution conditions, no field studies have previously reported the use of this rate law. The range of solution conditions and rates of calcite precipitation calculated for Falling Spring Creek agree with experimental values (Reddy et al., 1981). For the present study, the mass transfer rate results are compared to the rate equation predictions. These two methods of determining rates differ greatly. One approach derives from an experimental study of the kinetics of dissolution and precipitation reactions; the other approach applies mass balance calculations to observed chemical data for a natural water system (Plummer and Back, 1980). Yet the results agree remarkably well. The largest difference is seen at the waterfall where the rate law always gave much lower rates. The agreement in rates at the falls is within a factor of 10 to 50. The rate law results gave the maximum rate just below the falls. For all other segments of the stream than the falls, rates agreed within a factor of 1 to 10.

Problems in estimating the surface area of the stream could explain some of the disagreement between the rates. The Plummer et al. expression gives reaction rates in terms of surface area, while PHREEQE results are in terms of volume of water. The results from Plummer et al.'s expression were multiplied by the surface area over which the chemical reactions could be occurring in Falling Spring Creek. The reactive surface area of a streambed is impossible to characterize accurately. A uniform rectangular shape was assumed. Although this description of the streambed is clearly wrong, all other simple geometric shapes led to an estimate of area on the same order of

magnitude. At the waterfalls the streambed deviates more from the geometric simplification than at any other site. Because the large irregularly shaped deposits of travertine would provide numerous nucleation sites for fresh calcite, the surface area might have been underestimated, leading to an underestimate of the rate law results.

Conclusions

Using a laboratory-derived rate law (Plummer et al., 1978), calcite precipitation rates could be predicted within an order of magnitude of the mass transfer rates along Falling Spring Creek. Errors in surface area estimation at the falls led to a poor comparison of the two types of rates there. Imprecise definition of diffuse input of groundwater to the cave stream caused those mass transfer rates to be unreliable. Overall, however, the agreement between field-determined rates and the predictions of the rate law agreed very well - within an order of magnitude. The comparisons between the PHREEQE results and the rate law calculations do not prove the validity of the rate expression, but considering the vastly different theoretical bases of the two methods, the agreement between the reaction rates is good enough to give encouragement that the rate law may be used outside of the laboratory.

References

- DANDURAND J.L., GOUT R., HOEFS J., MENSCHER G., SCHOTT J., and USDOWSKI E. (1982) Kinetically controlled variations of major components and carbon isotopes in a calcite-precipitating spring. *Chem. Geol.* 36, 299-315.
- HERMAN J.H. and LORAH M.M. (1986) CO₂ Outgassing and Calcite Precipitation in Falling Spring Creek, Virginia. *Chem. Geol.* In press.
- MOSES C.O. and HERMAN J.S. (1986) WATIN - A computer program for generating input files for WATEQF. *Ground Water* 24, 83-89.
- PARKHURST D.L., THORSTENSON D.C., and PLUMMER L.N. (1980) PHREEQE - A computer program for geochemical calculations. *U.S. Geol. Surv., Water-Resour. Invest.* 80-96.
- PLUMMER L.N., JONES B.F., and TRUEDELL A.H. (1976) WATEQF - A FORTRAN IV version of WATEQ, a computer program for calculating chemical equilibria of natural waters. *U.S. Geol. Surv., Water-Resour. Invest.* 76-13.
- PLUMMER L.N., WIGLEY T.M.L., and PARKHURST D.L. (1978) The kinetics of calcite dissolution in CO₂-water systems at 5° to 60°C and 0.0 to 1.0 atm CO₂. *Amer. Jour. Sci.* 278, 179-216.
- PLUMMER L.N. and BACK W. (1980) The mass balance approach: application to interpreting the chemical evolution of hydrologic systems. *Amer. Jour. Sci.* 280, 130-142.
- REDDY M.M., PLUMMER L.N., and BUSENBERG E. (1981) Crystal growth of calcite from calcium carbonate solutions at constant PCO₂ and 25°C: A test of a calcite dissolution model. *Geochim. Cosmochim. Acta* 45, 1281-1289.

PREDICTING MINERAL DISSOLUTION AND PRECIPITATION DURING BURIAL:
SYNTHETIC DIAGENETIC SEQUENCES

Carol J. Bruton
Lawrence Livermore National Laboratory
P.O. Box 808
Livermore, CA 94550 USA

Abstract

Diagenetic changes with depth, reflecting the influence of source terrane, depositional environment and burial history, can be simulated using the EQ3/6 geochemical model of fluid-rock interaction. Synthetic diagenetic sequences are constructed by simulating reaction between rocks and pore fluids during burial and tracking mineral precipitation and dissolution events that occur as the rock and fluid attempt to come to equilibrium with each other.

Four representative rock compositions, including a quartzose sandstone, two quartzofeldspathic sandstones and a volcanic sandstone, were chosen to simulate the control of source terrane on diagenesis. Using EQ3/6, the rocks were reacted with representative river and sea water to study the influence of fresh water and marine depositional environments, respectively, on diagenesis. The rock-fluid system was assumed to be closed. A burial rate of 0.07 mm/yr along a geothermal profile with a gradient of 30°C/km, which was chosen to simulate present-day conditions in the Texas Gulf Coast, was modeled. Rates of mineral dissolution were calculated in three different manners for comparison: 1) linear arbitrary kinetics; 2) zeroth order kinetics; and 3) transition state theory assuming pH-independent rates. Subsequent fluid-rock reactions, including mineral precipitation, were assumed to be reversible and to occur instantaneously.

Simulation results indicate that the sequence of diagenetic events for reaction between a given rock and fluid is largely independent of the rate law used to describe mineral dissolution. Synthetic diagenetic sequences also agree reasonably well with observed diagenetic reactions in natural systems. Calculation of the absolute timing of diagenetic events, however, appears to depend on reactive surface area, precipitation kinetics, and other rate-limiting phenomena. Precipitation kinetics and potential rate-limiting phenomena must be provided for prior to effective application of kinetic models to the study of diagenetic processes.

Introduction

Diagenetic changes with depth, reflecting the influence of source terrane, depositional environment and burial history, can be simulated using geochemical models of fluid-rock interaction. The synthetic diagenetic sequences that are constructed in this manner are analogous to paragenetic sequences determined through petrologic study. They are calculated as a function of

rock type, fluid composition, temperature, and relative rates of fluid flow and mineral dissolution to simulate burial diagenesis in a wide variety of geologic settings. The timing of diagenetic events can be determined if rates of mineral dissolution are coupled to burial history.

Synthetic diagenetic sequences can be used to predict diagenetic changes with depth, determine controls of mineral dissolution and precipitation, and evaluate the consequences and relative importance of changes in source terrane, depositional environment and burial history on diagenesis. The purpose of this paper is to show that: 1) synthetic diagenetic sequences agree reasonably well with diagenetic sequences determined by petrographic observation; and 2) that the absolute timing of diagenetic events appears to depend not only on the magnitude of mineral surface area, but also on precipitation kinetics and rate-controlling phenomena which have not yet been identified clearly.

Synthetic Diagenetic Sequences

Synthetic diagenetic sequences are constructed by simulating reaction between rocks and pore fluids during burial with the EQ3/6 computer software package of Wolery (1978). Four representative rock compositions, including a quartzose sandstone, two quartzofeldspathic sandstones with varying amounts of K-feldspar and plagioclase, and a volcanic sandstone, were chosen to simulate the control of source terrane on diagenesis. The rocks were reacted in separate simulations with dilute river water and sea water to study the influence of fresh water and marine depositional environments, respectively, on diagenesis. Reaction of quartzose sandstone with river water will be described in this paper.

Simulations yield the sequence and types of mineral precipitation and dissolution events that occur when the rock and fluid attempt to come to equilibrium with each other during the increases in temperature associated with burial. The rock-fluid system was assumed to be closed.

Simulation Input

The mineralogic composition of the quartzose sandstone used as an example in this study is listed in Table 1. The composition of the sandstone, an ortho-quartzite from Pettijohn (1975), is dominated by quartz, with minor amounts of kaolinite, microcline, albite, anorthite, calcite, magnetite and a Mg-chlorite represented by 14Å-clinochlore. Equal amounts of albite and anorthite proxy for the end member components of an ideal plagioclase solid solution with the composition An_{50} . Note that the presence of kaolinite and calcite suggests that the quartzose sandstone has been subjected to surface weathering. The composition of the dilute river water used in the simulations and listed in Table 2 was taken from Livingstone (1963). An Al concentration of 1 ppb and a pH of 7 were assumed. A burial history consisting of uniform subsidence at a rate of 0.07 mm/year along a geothermal profile with a gradient of 30°C/km (1.65°F/100 ft), which corresponds to a constant heating rate of 1.8°C/million years, was modeled. These conditions were chosen to approximate present day conditions in the Lower Tertiary

Table 1. Mineralogic composition of type quartzose sandstone (from Pettijohn, 1975).

<u>Mineral</u>	<u>Vol %</u>
Quartz	93.3
Kaolinite	0.8
Microcline	1.3
Albite	0.9
Anorthite	0.9
Calcite	2.4
14 Å-clinocllore	0.1
Magnetite	0.3

Table 2. Composition of type river water (from Livingstone, 1963).

<u>Species</u>	<u>mg/l</u>
Na	6.3
K	2.3
Ca	15.0
Mg	4.1
Al	0.001
SiO ₂	13.1
Cl	7.8
SO ₄	11.2
HCO ₃	58.4
pH	7.0
T.D.S.	118

Wilcox Group and Frio and Vicksburg Formations along the Texas Gulf Coast.

Rates of mineral dissolution were described using three methods for comparison: 1) linear rates of mineral dissolution that are not explicit with respect to time (i.e. arbitrary kinetics) but are proportional to the volume fraction of the mineral in the rock; 2) zeroth order kinetics; and 3) transition state theory assuming pH-independent rates of dissolution. Method 1 was used to illustrate a possible modeling approach when no estimates of rates of mineral dissolution are available. Rate constants from Walther and Wood (1986), which are applicable to high temperature reactions, were assumed to suffice at low temperatures in method 2. Rates of mineral dissolution are then calculated assuming that rates do not slow as equilibrium is approached. Method 3, in contrast to method 2, takes explicit account of the control of solution composition and the decrease of rates of dissolution close to equilibrium. Method 3 is, therefore, the most realistic of the three approaches, despite the fact that pH-independent rates were assumed. Intra-aqueous reactions and secondary mineral precipitation and dissolution were assumed to occur reversibly and instantaneously.

Rate constants used in transition state rate laws were taken variously from Knauss and Wolery (1986; albite), correlation plots of Walther and Wood (1986; kaolinite, 14Å-clinocllore, magnetite), Rimstidt and Barnes (1980; quartz) and Delany, Puigdomenech and Wolery (1985; calcite). Rate constants for microcline and anorthite were assumed to equal those of albite. Temperature dependencies of the rate constant were estimated from correlation plots of Walther and Wood (1986) if not given in the above references.

Rates of mineral dissolution were used to calculate synthetic diagenetic sequences as a function of time, temperature and surface area. Time and temperature were linked by assuming a constant heating rate of 1.8°C/million years. Rates of dissolution vary, however, as a function of the surface area available for reaction. The surface area of each mineral was assumed to equal the total surface area of the rock multiplied by the volume percentage of the mineral in the rock. Total surface area was assumed to remain constant during burial.

Generalized Synthetic Diagenetic Sequences

Simulation results indicate that the sequence of diagenetic events for reaction between a given rock and fluid is largely independent of the rate law used to describe mineral dissolution. The generalized diagenetic sequence for reaction of quartzose sandstone with river water is, therefore, first described independently of time. The synthetic sequence is then compared with petrologic descriptions of natural diagenetic sequences.

Diagenetic events predicted to occur during burial of quartzose sandstone and river water are shown in Figure 1. The depth of burial, and thus temperature, increase from left to right along the abscissa. The bars represent the stability range of each mineral. The beginning of the bar signifies the start of mineral precipitation, and the addition of the mineral to the stable diagenetic assemblage. The end of the bar indicates complete dissolution of the mineral, and its deletion from the stable phase assemblage.

Hematite, pyrite, smectite and quartz are the first phases to precipitate during burial. Hematite and pyrite represent early sinks for Fe. Smectite precipitates throughout burial, and continually changes in composition from a Ca-nontronite to Ca-saponite and finally to Ca-beidellite. Tardy-Garrels estimation techniques are used to derive thermodynamic data for smectites in the EQ3/6 data base (Wolery, 1978). Quartz overgrowth formation is favored throughout burial. The carbonates dolomite and calcite precipitate next. Note that two generations of dolomite cement are formed, even though the simulation was made in a closed system. The formation of multiple generations of minerals or zoning does not, therefore, necessarily imply fluid flushing in an open system. Carbonates are followed by the clays muscovite and kaolinite. Muscovite, in these computations, can be considered as a proxy for an illite with a layer charge of -1.

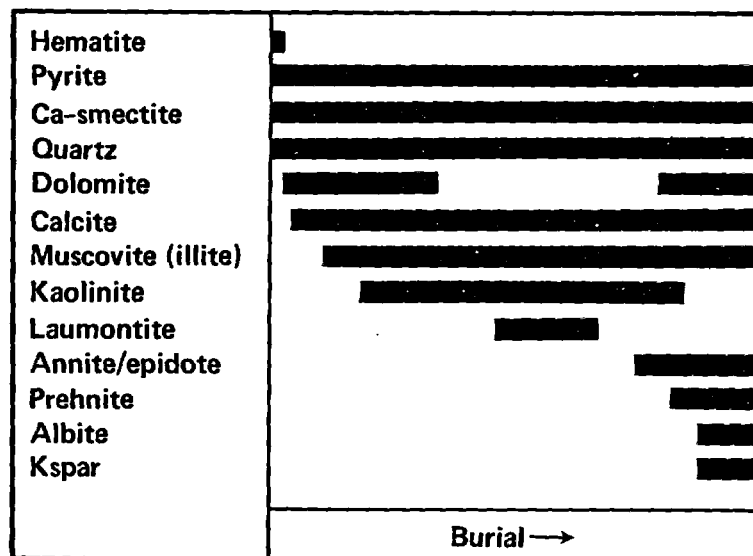


Figure 1. Generalized synthetic diagenetic sequence for reaction between quartzose sandstone and river water.

The precipitation of laumontite signals entry into the zeolite metamorphic facies. Annite or epidote forms as a late sink for Fe, depending on temperature. Prehnite precipitation is followed by albitization and the formation of K-feldspar overgrowths.

A chronological sequence of diagenetic events in sandstones deposited in fresh to brackish environments as determined through petrographic observation and compiled by McBride (1983) is shown in Table 3. Hematite forms an early Fe-sink, and is followed by a variety of clays, including chlorite, illite/smectite and kaolinite, which are analogous to smectite in the simulation. Early K-feldspar and albite overgrowths were not formed in the simulations. Precipitation of quartz is followed by carbonates in both the simulated and observed sequences. A dissolution event ascribed to hydrocarbon migration was not reproduced in the simulations. The simulations were carried out assuming a closed system in which no fluid flow occurs. Dolomite dissolution occurred in the closed system model, nonetheless. Kaolinite is observed to precede illite and Fe-carbonate in nature. Kaolinite coexists with illite and carbonate in the burial simulation. The zeolite in McBride's sequence is represented by laumontite in the simulation.

Preliminary results suggest that synthetic diagenetic sequences predict general diagenetic trends reasonably well, even though the simulations were carried out in a closed system. Natural systems are considered to be open, and formation fluids evolve to saline brines at depth. The simulations, in contrast, are carried out in a closed system in which the fluid is constrained to remain relatively dilute. Nonetheless, the synthetic diagenetic sequences correspond well with observed diagenetic sequences.

Timing of Diagenetic Events

Absolute timing of diagenetic events was calculated using zeroth order kinetics and transition state theory for comparison and contrast. The total surface area of the rock was calculated by assuming spherical grains and 30% porosity. A rock composed of spherical grains of 1 mm diameter and with 30% porosity has a total surface area of 10^{5-15} cm²/kg fluid. The

Table 3. Chronologic sequence of diagenetic events in sandstones deposited in non-marine environments deduced through petrographic study (after McBride, 1983).

- hematite
- chlorite
- illite/smectite
- kaolinite
- K-feldspar-albite
- quartz
- calcite
- dolomite
- dissolution/HC migration
- kaolinite
- illite
- Fe-carbonate
- zeolite

surface area of each mineral was calculated by multiplying the total surface area of the rock by the volume fraction of the mineral in the rock.

The synthetic diagenetic sequence as a function of time and temperature for reaction between quartzose sandstone and river water assuming a reactive surface area of $10^{5.15}$ cm²/kg fluid and zeroth order kinetics is shown in Figure 2. A diagenetic sequence similar to the one shown in Figure 1 is present in Figure 2, but is formed in a very short period of time. The entire diagenetic sequence up to prehnite precipitation forms within 1 million years as the temperature increases from 10 to 12°C, and the rock is buried to a depth of 70 m. Isotopic measurements, in contrast, suggest that kaolinite, for example, often precipitates between 50 and 100°C, and albite may not precipitate until temperatures reach 100 to 150°C.

Helgeson, Murphy and Aagaard (1984) suggest that reactive or effective surface area, which is in part controlled by the outcrop of surface active sites such as dislocations, is two orders of magnitude less than total surface area. Reduction of the surface area by five orders of magnitude, to $10^{0.15}$ cm²/kg fluid, was required to yield a more reasonable match to the natural data as shown in Figure 3. Kaolinite starts to precipitate at 40°C, and laumontite begins to precipitate after 35 my at 80°C. However, albitization does not occur in the simulation even after 100 my, in contrast to its presence in Texas Gulf Coast reservoirs less than 50 my old.

The temperature dependence of mineral equilibration, in °C, is shown in Figure 4 as a function of the logarithm of the surface area of the rock, expressed in cm²/kg fluid, given a porosity of 30%. The time of equilibration, in millions of years, is given for reference along the top of the x axis.

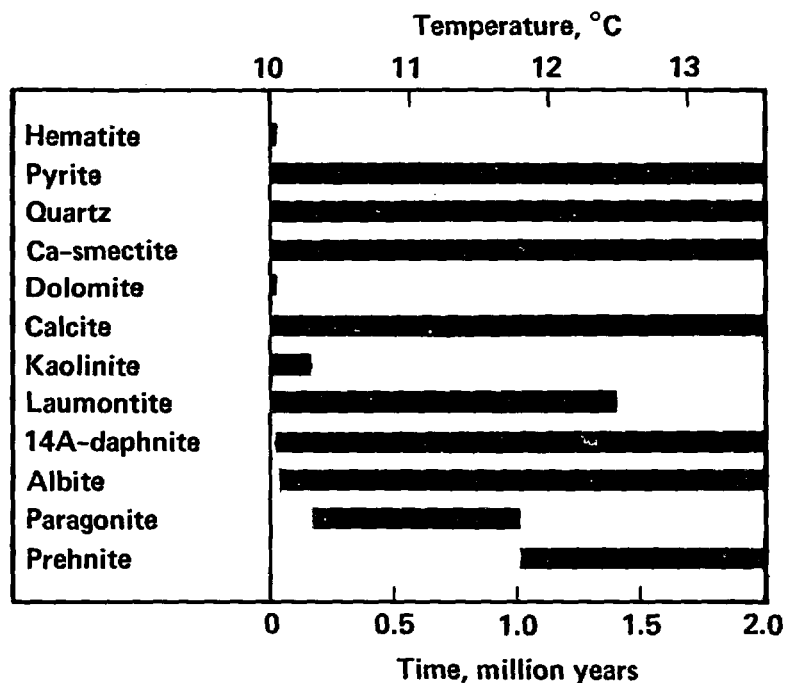


Figure 2. Synthetic diagenetic sequence for reaction between quartzose sandstone and river water assuming zeroth order kinetics and a surface area of $10^{5.15}$ cm²/kg fluid.

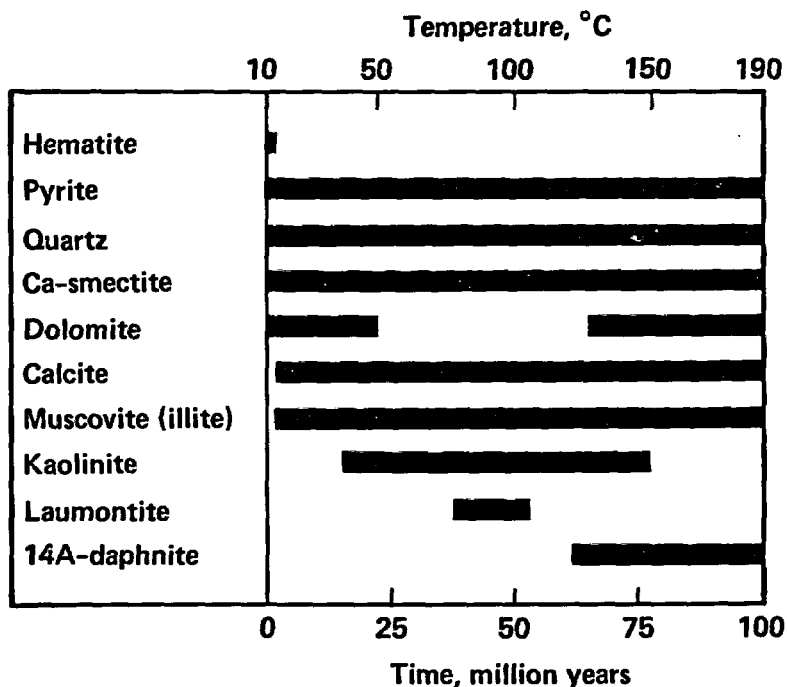


Figure 3. Synthetic diagenetic sequence for reaction between quartzose sandstone and river water assuming zeroth order kinetics and a surface area of $10^{0.15}$ cm^2/kg fluid.

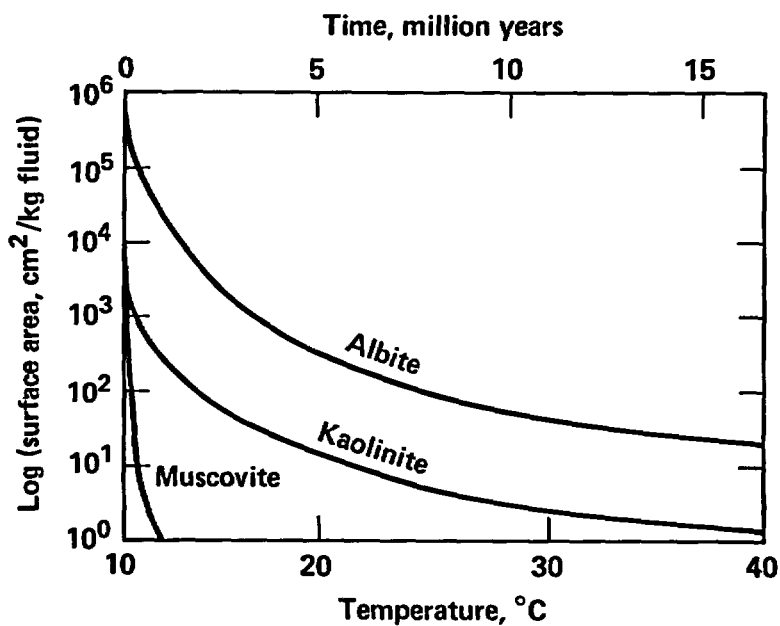


Figure 4. Temperature and timing of mineral equilibration as a function of the logarithm of surface area (in cm^2/kg) for reaction of quartzose sandstone with river water assuming zeroth order kinetics.

Assuming that total surface area equals effective surface area, albite precipitation occurs at less than 11°C in a sandstone with 1 mm grains and a surface area of $10^{5.15}$ cm^2/kg fluid. Significant reductions in effective surface area are required to generate albitization at 100°C , as is commonly reported in natural sequences.

Synthetic diagenetic sequences for reaction between quartzose sandstone and river water calculated using transition state theory are shown in Figures 5 and 6 assuming surface areas of $10^{5.15}$ and $10^{3.15}$ cm^2/kg fluid, respectively. Note the same strong dependence of the timing of diagenetic events on the choice of surface area as observed using a zeroth order rate law.

The above calculations suggest that either effective surface areas are many orders of magnitude smaller than total surface area, or phenomena in

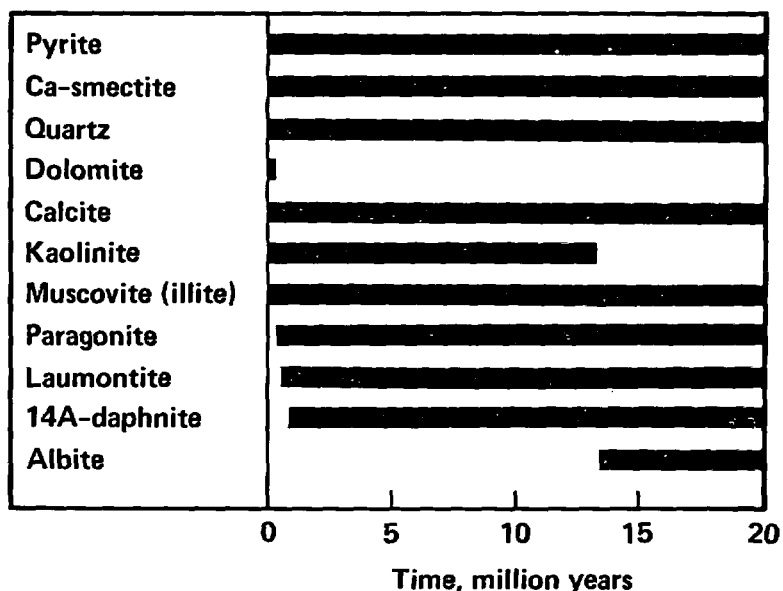


Figure 5. Synthetic diagenetic sequence for reaction between quartzose sandstone and river water assuming transition state theory reaction kinetics and a surface area of $10^{5.15}$ cm^2/kg fluid.

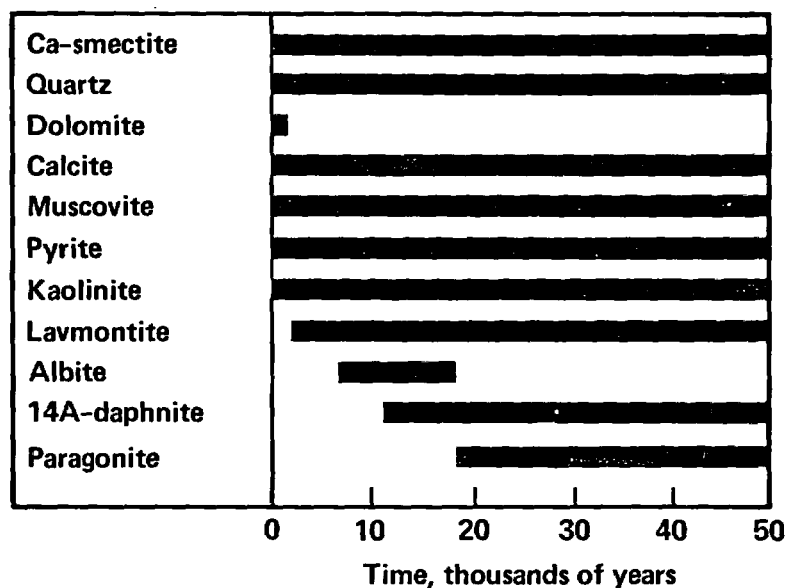


Figure 6. Synthetic diagenetic sequence for reaction between quartzose sandstone and river water assuming transition state theory reaction kinetics and a surface area of $10^{3.15}$ cm^2/kg fluid.

addition to the density of reactive surface sites affect rates of mineral dissolution. Precipitation kinetics, in particular, must be considered as a prime factor in the timing of diagenetic events. Phenomena whose effects may have been implicitly included in the surface area term when matching observation with simulation results include poisoning of mineral surfaces by aqueous species, and armoring effects of pore-lining mineral precipitates. Effective application of kinetic models to the study of diagenetic processes requires explicit provision for precipitation kinetics and other potential rate-controlling phenomena.

Conclusion

Synthetic diagenetic sequences correspond reasonably well with observed diagenetic sequences in natural systems. The interactions of various rock types and fluid compositions during burial can therefore be synthesized to produce alteration sequences that serve as a general guide to diagenetic changes with depth as a function of source terrane, depositional environment and burial history. The sequence of diagenetic events for reaction between a given rock and fluid is largely independent of the rate law used to describe mineral dissolution. Calculation of the absolute timing of diagenetic events, however, appears to depend not only on estimates of the reactive surface area of minerals but also on other rate-controlling phenomena.

References

- DELANY, J. M., PUIGDOMENECH, I., and WOLERY, T. J. (1986) Precipitation Kinetics Option for the EQ6 Geochemical Reaction Path Code, Lawrence Livermore National Laboratory, UCRL-53642.
- HELGESON, H. C., MURPHY, W. M., and AAGAARD, P. (1984) Thermodynamic and kinetic constraints on reaction rates among minerals and aqueous solutions. II. Rate constants, effective surface area, and the hydrolysis of feldspar. *Geochim. et Cosmochim. Acta*, **48**, p. 2405-2432.
- KNAUSS, K. G., and WOLERY, T. J. (1986) Dependence of albite dissolution kinetics on pH and time at 25°C and 70°C. *Geochim. et Cosmochim. Acta*, **50**, p. 2481-2498.
- LIVINGSTONE, D. A. (1963) *Chemical Composition of Rivers and Lakes*. U.S. Geol. Survey Paper, 440G.
- MCBRIDE, E. F. (1983) *Sandstone Diagenesis: Principles useful in exploration*. New Orleans Geological Society Short Course, Nov. 17, 1983.
- PETTIJOHN, F. J. (1975) Sedimentary Rocks. Harper and Row.
- RIMSTIDT, J. D., and BARNES, H. L. (1980) The kinetics of silica-water reactions. *Geochim. et Cosmochim. Acta*, **44**, p. 1683-1699.
- WALTHER, J. V., and WOOD, B. J. (1986) Mineral-fluid reaction rates. Fluid-Rock Interactions during Metamorphism. Springer-Verlag.
- WOLERY, T. J. (1978) Some aspects of hydrothermal processes at mid-oceanic ridges- a theoretical study. I. Basalt-sea water reaction and chemical cycling between the oceanic crust and the oceans. II. Calculation of chemical equilibrium between aqueous solutions and minerals. Ph.D. thesis, Northwestern Univ., Evanston, Ill.

MODELLING INTERACTION OF DEEP GROUNDWATERS WITH BENTONITE¹

Hans Wanner

OECD Nuclear Energy Agency, NEA Data Bank
91191 Gif-sur-Yvette Cedex, France

ABSTRACT

Based on available experimental data on the interaction of sodium bentonite and groundwater, a model has been developed which represents means of extrapolation from laboratory data to the conditions in compacted bentonite. The basic reactions between sodium bentonite and groundwater are described by an ion-exchange model for sodium, potassium, magnesium and calcium. The model assumes equilibrium with calcite and quartz. All calculations are carried out for two types of granitic groundwater: the Swiss Reference Groundwater ($I = 0.24 M$) and the Standard Swedish Groundwater ($I = 0.0044 M$). It is calculated that the pore water of compacted sodium bentonite will have a pH of 9.7 and a carbonate activity of $8 \cdot 10^{-4} M$ in the Swiss case, and $\text{pH} \approx 10.2$ and $\{\text{CO}_3^{2-}\} = 8 \cdot 10^{-3} M$ in the Swedish case.

The long-term situation, which is important for nuclear waste disposal, is modelled by the assumption that the near-field of a radioactive waste repository behaves like a mixing tank. In this way, an attempt is made to account for the continuous water exchange between the near-field and the host rock. It is calculated that sodium bentonite will be slowly converted to calcium bentonite. The time period for this transformation is estimated to be in the order of 10^6 years, depending on the groundwater flow and composition and the dimensions of the repository.

INTRODUCTION

The understanding of the chemical processes occurring between bentonite and groundwater is very important for the safety assessments of final repositories for nuclear waste, because the extent of radionuclide release from a high-level waste repository to the geosphere depends strongly on the solubility of these nuclides in the available groundwater. Deep repositories are preferably envisaged to be backfilled with bentonite due to its considerable swelling capacity and low permeability. Hence, the solubility limits of the radionuclides in the bentonite pore water can be taken as upper limits for the radionuclide release from a repository into the geosphere. Based on available experimental data, this work describes a thermodynamic model which can be used to estimate the chemical composition of the pore water in compacted sodium bentonite. The modelled pore water composition can serve as a basis for the calculation of radionuclide speciation and solubility limits in the near-field of a deep repository (WANNER 1986).

¹This work has been carried out at the Swiss Federal Institute for Reactor Research (EIR) in collaboration with the National Cooperative for the Storage of Radioactive Wastes (NAGRA).

THE BENTONITE MODEL

Among the very few experiments performed to date to study the consequences of bentonite reaction with groundwater, only one deals with the gradual change of the chemical composition of groundwater when brought into contact with bentonite (SNELLMAN 1984). The results of a replication of this experiment (SNELLMAN 1985) are listed in *Table 1*, showing

- no evidence that an equilibrium state is reached between the groundwater and the bentonite after 90 days.
- an increase of the sodium concentration in the liquid phase, accompanied by a decrease of the concentrations of calcium, magnesium and potassium.
- a marked increase of the alkalinity.
- a significant rise in pH during the first 7 days of contact followed by a surprising decrease during the subsequent time period, probably due to inadequate sampling (dissolution of CO₂ from the air).
- the concentration of silicic acid remains more or less unchanged.

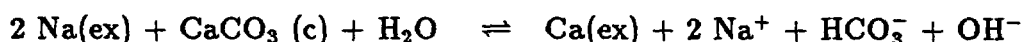
Table 1: Interaction experiments between 1500 cm³ of synthetic Standard Swedish Groundwater and 40 g of sodium bentonite MX-80 (SNELLMAN 1984 and 1985).

Component (charges omitted)	Initial concentration [mol/l]	Concentration [mol/l] after contact with bentonite		
		7 days	30 days	90 days
Al	-	-	-	4.5 E-6
Na	2.26 E-3	5.35 E-3	8.52 E-3	1.01 E-2
K	1.0 E-4	7.7 E-5	5.6 E-5	4.6 E-5
Mg	1.9 E-4	1.2 E-4	1.4 E-5	1.9 E-5
Ca	4.64 E-4	2.84 E-4	3.17 E-5	4.57 E-5
Fe	-	-	-	4. E-7
NH ₃	3. E-7	2.9 E-5	6. E-7	-
SiO ₂	1.39 E-4	* 2.01 E-4	1.6 E-4	1.80 E-4
Cl	1.48 E-3	1.62 E-3	1.8 E-3	1.88 E-3
F	-	1.4 E-5	2.2 E-5	3.0 E-5
NO ₃	3. E-7	2. E-7	1.8 E-6	-
NO ₂ **	7. E-8	2. E-7	1.5 E-6	1. E-7
PO ₄	2.1 E-6	-	1.5 E-6	8.3 E-6
HCO ₃	1.80 E-3	1.63 E-3	3.31 E-3	6.78 E-3
CO ₃	-	7.90 E-4	7.50 E-4	5.67 E-4
SO ₄	1.0 E-4	5.99 E-4	6.09 E-4	1.52 E-4
pH	8.12	9.58	* 9.26	9.09
Alkalinity [eq/l]	1.94 E-3	3.24 E-3	5.20 E-3	7.93 E-3
Eh [mV]	-	-	-	-200 to -300

* Large differences in replicate samples

** Nitrite is not taken into consideration in the bentonite model.

Assuming ion-diffusion reactions between the liquid in the packed bentonite powder and the bulk solution to be the rate determining processes (neglecting the possible occurrence of mineral transformation) and therefore the species in the analysed samples to be in thermodynamic equilibrium with each other, allows the use of the code MINEQL/EIR (SCHWEINGRUBER 1982 and 1984) to check the consistency of the experimental analyses. The results are shown in *Table 2a* and reveal that the charge balance is not satisfactory for the 7-days and especially the 30-days analysis, which indicates some experimental inadequacy. Further, the bentonite solutions are found to be oversaturated with respect to calcite. Since the turbid samples had not been filtered before analysis (SNELLMAN 1985), it is possible that part of the turbidity consisted of precipitated calcium carbonate. Therefore, the speciation calculations are repeated, allowing calcium carbonate to precipitate as calcite. In this way, the total concentration of calcium, which is an important parameter for the development of the bentonite model discussed below, can be corrected for the amount of calcite precipitate. The results of these evaluations are listed in *Table 2b*. From these experimental results, the main reactions between sodium bentonite and groundwater can be described in the following way: Sodium ions in the bentonite exchange for calcium ions from the groundwater, which leads to a considerable decrease of the calcium concentration in the aqueous solution. The subsequent dissolution of carbonates from the sodium bentonite (limited by the solubility product of calcite) is the reason for the increase of the alkalinity (see *Table 1*) and of pH:



It is important to realize that a model of the chemical composition of pore water in compacted bentonite involves more than interpretation of laboratory data and qualitative extrapolation to the possible situation in a deep repository. Qualitative extrapolations are very difficult, especially if the dominating processes are ion-exchange reactions affecting key parameters such as the carbonate activity which is indirectly influenced by the calcium activity through the saturation equilibrium of calcite. The whole system is thus very sensitive to the proportion of calcium reacting with the bentonite and, since ion-exchange reactions are concerned, is very sensitive to the clay/water ratio. In the experiments performed to date, the clay/water ratio lies between 0.02 and 0.2, whereas in compacted and water-saturated bentonite the ratio is around 5, *i.e.*, one to two orders of magnitude higher. The chemical composition of the water in compacted sodium bentonite could therefore considerably deviate from that measured in the laboratory.

Model Assumptions

The model developed here, which can be applied to predict the pore water chemical composition in compacted sodium bentonite, involves a number of assumptions:

- It is assumed that thermodynamic models can be applied to describe the chemical processes occurring in water-saturated, compacted sodium bentonite.
- Sodium, potassium, magnesium and calcium are assumed to be the only ions participating in ion-exchange reactions between the sodium bentonite and the aqueous phase. The ion-exchange processes modelled are based on complex formation equilibria involving ion-exchange sites (represented as Z^-) of the montmorillonite and

Table 2: Specification of the water analyses listed in Table 1 by means of the code MINEQL/EIR, assuming thermodynamic equilibrium between the dissolved species.

	Initial	7 days	30 days	90 days
a) <u>No precipitation assumed:</u>				
Charge balance (%) *	+2.0	+3.7	+9.6	+1.4
pH calculated	8.15	9.66	9.45	9.02
log p(CO ₂)	-3.09	-4.63	-4.14	-3.41
log SI ** of calcite	-0.03	1.06	0.14	0.20
log SI ** of dolomite	-0.17	2.09	0.26	0.34
log SI ** of quartz	0.10	0.03	0.01	0.15
Ionic strength [mol/l]	0.0044	0.0073	0.0094	0.0108
b) <u>Calcite Precipitation:</u>				
Charge balance (%) *	2.0	3.9	9.6	1.4
pH calculated	8.15	9.53	9.44	9.01
log p(CO ₂)	-3.09	-4.51	-4.14	-3.40
CaCO ₃ precipitated [mol/l]	-	2.53 E-4	8.41 E-6	1.60 E-5
Calc. calcium conc. [mol/l]	4.64 E-4	3.09 E-5	2.33 E-5	2.97 E-5
log SI ** of dolomite	-0.17	0.92	0.12	0.14
log SI ** of quartz	0.10	0.09	0.01	0.16
Ionic strength [mol/l]	0.0044	0.0066	0.0094	0.0108

* Percentage difference between the total positive and the total negative charge, referred to the total positive charge.

** SI = saturation index. SI is defined as the quotient of the ion activity product of the potentially dissolved free components of the solid, and the solubility product, K_{so}, of the solid. SI > 1 (log SI > 0) represents oversaturation.

$$SI(\text{Calcite}) = \frac{\{Ca^{2+}\} \cdot \{CO_3^{2-}\}}{K_{so}(\text{CaCO}_3)}$$

the cations mentioned, as shown in the picture below. The ion-exchange sites are theoretically treated as simple ligands dissolved in the pore water. All sites are considered equivalent, carrying one negative charge and being capable of coordinating sodium, potassium, magnesium and calcium only. The energetics of the coordination reactions are described by equilibrium constants derived from the corrected analytical data of groundwater having been in contact with sodium bentonite for 90 days at a temperature of 25°C (Tables 1 and 2b), and from data on the exchangeable cations of sodium bentonite MX-80. From these data absolute values of the formation constants cannot be extracted, but they are chosen so high ($\log K(1) = 20.0$, by definition) that virtually no uncoordinated sites, Z^- , exist. The derivation of these constants is described in detail elsewhere (WANNER 1986). The estimated constants are listed in Table 3.

- The pore water in compacted sodium bentonite is assumed to be saturated with respect to calcite and quartz. This assumption is not unreasonable as long as enough carbonates are available in the bentonite, since most groundwaters are found to be in equilibrium with these two minerals.
- Long-time extrapolations (which are of interest for safety analyses of nuclear waste repositories) are modelled for the dimensions of a potential Swiss high-level waste repository (NAGRA 1985). In the Swiss case, the main components of the near-field are the glass waste-matrix, a thick steel canister horizontally stored in a drift, and a backfill of highly compacted bentonite. The long-term behaviour is modelled considering the near-field as a box or mixing tank. The groundwater which flows past the repository is modelled to mix with the near-field water and to leave the repository area with an altered composition resulting from the equilibrium with sodium bentonite. In this way, account is taken for the leaching of the bentonite.

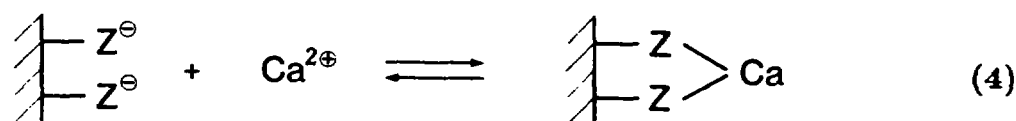
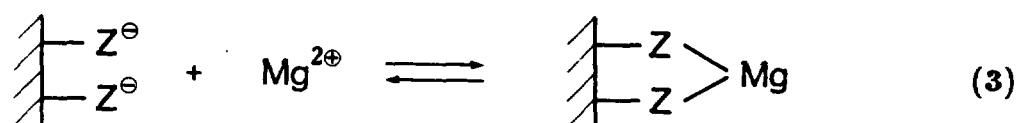
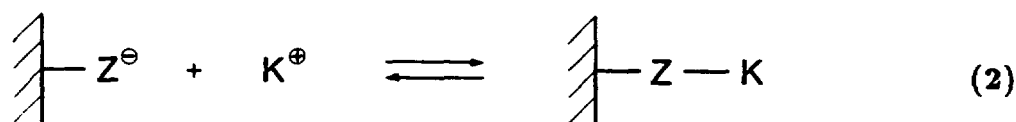
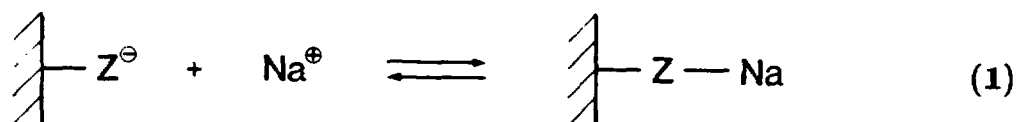


Table 9: Equilibrium constants calculated for the 4 fundamental reactions involved in the ion-exchange processes considered: (1), (2), (3) and (4), and those derived for the ion-exchange reactions.

(1)	Z^-	+	Na^+	\rightleftharpoons	ZNa	;	$\log K(1)$	=	20.0 (by def.)
(2)	Z^-	+	K^+	\rightleftharpoons	ZK	;	$\log K(2)$	=	20.4
(3)	2 Z^-	+	Mg^{2+}	\rightleftharpoons	Z_2Mg	;	$\log K(3)$	=	41.7
(4)	2 Z^-	+	Ca^{2+}	\rightleftharpoons	Z_2Ca	;	$\log K(4)$	=	42.4
(5)	ZNa	+	K^+	\rightleftharpoons	ZK	+	Na^+	;	$\log K(5)$ = 0.4
(6)	2 ZNa	+	Mg^{2+}	\rightleftharpoons	Z_2Mg	+	2 Na^+	;	$\log K(6)$ = 1.7
(7)	2 ZNa	+	Ca^{2+}	\rightleftharpoons	Z_2Ca	+	2 Na^+	;	$\log K(7)$ = 2.4
(8)	2 ZK	+	Mg^{2+}	\rightleftharpoons	Z_2Mg	+	2 K^+	;	$\log K(8)$ = 0.9
(9)	2 ZK	+	Ca^{2+}	\rightleftharpoons	Z_2Ca	+	2 K^+	;	$\log K(9)$ = 1.6
(10)	Z_2Mg	+	Ca^{2+}	\rightleftharpoons	Z_2Ca	+	Mg^{2+}	;	$\log K(10)$ = 0.7

The Extrapolation Model

Two different types of groundwater are used for the application of the bentonite model. The Swiss Reference Groundwater is a deep-crystalline groundwater sampled in the granitic basement of northern Switzerland, at a depth of 1326 meters below the surface. The water is characterized by a relatively high degree of mineralization ($I = 0.24 M$) and a calcium concentration of 21.7 mM (WANNER 1986). The Standard Swedish Groundwater is a poorly mineralized granitic groundwater with $I = 0.0044 M$. Its composition is listed in *Table 1*.

The extrapolation from the experimental conditions to those in compacted sodium bentonite, is modelled as a titration experiment, where the water is titrated with bentonite (represented by Z) by increasing $[Z]_{tot}$ from $10^{-4} M$ to $10 M$. As counter-ions to Z^- , the cations Na^+ , K^+ , Mg^{2+} and Ca^{2+} are introduced according to their proportional contribution to the ion-exchange capacity of sodium bentonite (see WANNER 1986). The changes of some parameters during the extrapolation process are presented in *Figure 1* for both types of groundwater. The dotted vertical intersection at $[Z]_{tot} = 3.35 M$ gives the chemical composition of the pore water in saturated, compacted sodium bentonite. Although the pore water compositions given by these vertical intersections are similar for both types of groundwater, the buffering effect of the highly mineralized Swiss Reference Groundwater is obvious. Contrary to the Standard Swedish Groundwater, no major changes in the water composition would be expected if the experiment by Snellman (SNELLMAN 1984 and 1985, where $[Z]_{tot} = 1.95 \cdot 10^{-2} M$) were carried out with Swiss Reference Groundwater. The assumption of calcite and quartz saturation leads to a total dissolution of $7.5 \cdot 10^{-3} mol CaCO_3$ and $9.3 \cdot 10^{-4} mol SiO_2$ per litre of Swiss Reference Groundwater, or $3.5 \cdot 10^{-2} mol CaCO_3$ and $6.9 \cdot 10^{-3} mol SiO_2$ per litre of Standard Swedish Groundwater for $[Z]_{tot} = 3.35 M$.

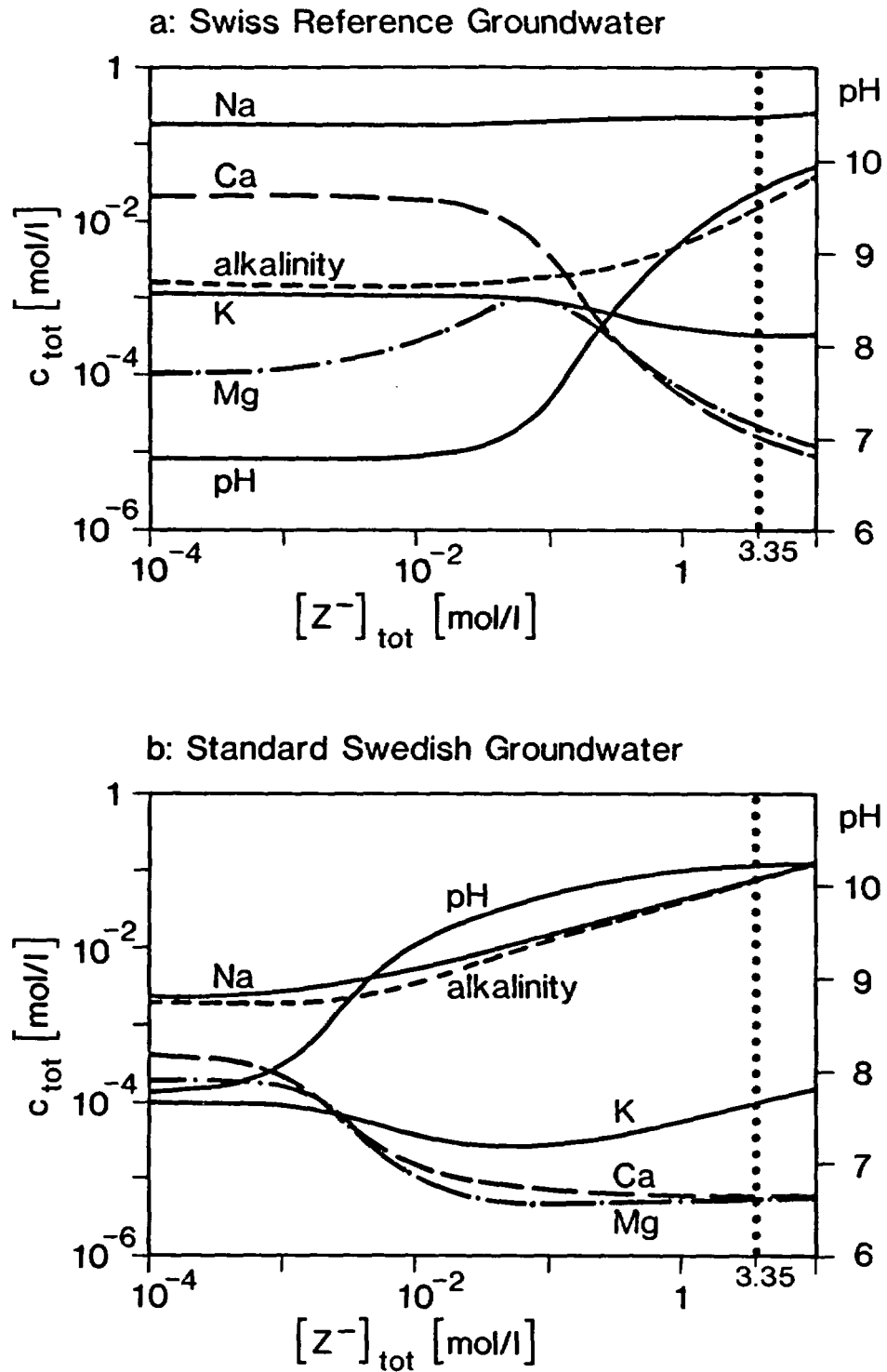


Figure 1: Modelled change in the composition of Swiss Reference Groundwater (a) and Standard Swedish Groundwater (b) when brought into contact with an increasing quantity of sodium bentonite (represented by the total concentration of ion-exchange sites, Z^-). Alkalinity is expressed in eq/l . The dotted vertical line represents the predicted conditions in water saturated compacted sodium bentonite.

The Mixing Tank Model

In a final nuclear waste repository, the compositions of the bentonite backfill and the bentonite pore water will not remain constant, but will slowly change with time because diffusion of ions between the near-field and the host rock will take place. As it is important to know more about these long-time alterations, a very simple model is applied in order to yield information on trends of variation in the composition of the bentonite pore water in the very far future. The following calculations are based on the assumption that the near-field behaves like a mixing tank: Within a certain time period, the total volume of the equilibrated bentonite pore water is replaced by fresh groundwater, which then contacts the new distribution of exchangeable ions in the bentonite. Again, the equilibrium state is calculated. This water exchange procedure is repeated a number of times (N) for both types of groundwater. The total number of available ion-exchange sites, Z^- , in the bentonite is assumed to remain constant. Taking the dimensions of a potential Swiss high-level waste repository (NAGRA 1985) and assuming a constant annual water flow of 0.71 ℓ past each canister (containing 52.8 m^3 bentonite, see WANNER 1986), the time period for one water exchange cycle ($N=1$) is estimated to be roughly 30,000 years. The results of these calculations are presented in *Figures 2* and *3*. In the case of Standard Swedish Groundwater, the available carbonates in the bentonite (initially 1.4%, calculated as $CaCO_3$) will be dissolved after about 35 water exchange cycles, which causes the pH to drop to that of the initial groundwater ($pH \approx 8$). At this point, the pore water will be only poorly buffered with respect to pH , and ion-exchange reactions involving H^+ will become important. In the case of Swiss Reference Groundwater, less than one sixth of the carbonate pool will be dissolved by this mechanism and be carried away. The pH of the near-field water will have returned to that of the host rock water after 60 to 70 water exchange cycles, indicating exhaustion of the ion-exchange capacity relative to the groundwater chemical composition. *Figure 3* shows that the sodium bentonite will convert to calcium bentonite during this water exchange process.

CONCLUSIONS

The model presented here should be considered as a first attempt to quantitatively describe the most important short- and long-term chemical processes expected between groundwater and compacted sodium bentonite in a deep repository. Refinement and extension of the model seems sensible only if an extended and consistent experimental data set on the bentonite-groundwater interaction is available. Although uncertainties in the chosen parameters, such as ion-exchange constants, are estimated to have no principal influence on the model predictions, it would be helpful to know more about the ranges of uncertainty and to reduce them as far as possible. The performance of a number of experiments under completely anaerobic conditions with systematic parameter variations is suggested, *e.g.*, variation of temperature, alteration of the bentonite-mass-to-water-volume ratio, and the use of a number of distinctly different groundwaters. Further developments should also try to model the slow effects of clay mineral alteration.

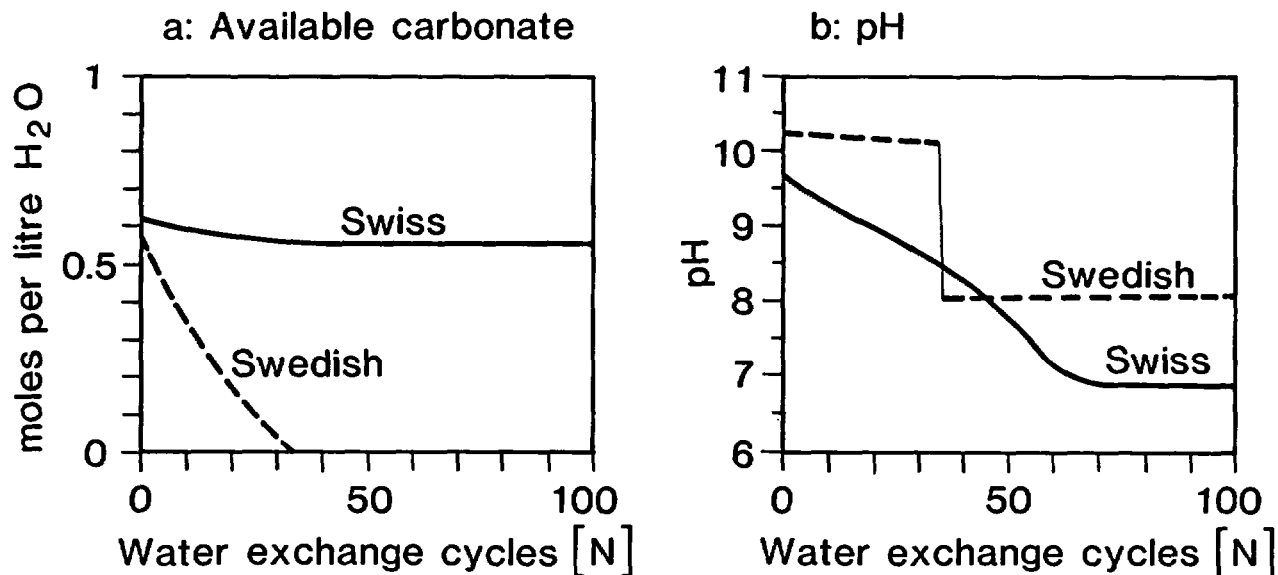


Figure 2: Long-term change in the carbonate reservoir (calculated as calcium carbonate available for 1 litre of water) present in sodium bentonite (a), as well as in the pH of the near-field pore water (b), calculated by application of the mixing tank model to the Swiss Reference Groundwater and to the Standard Swedish Groundwater (dashed).

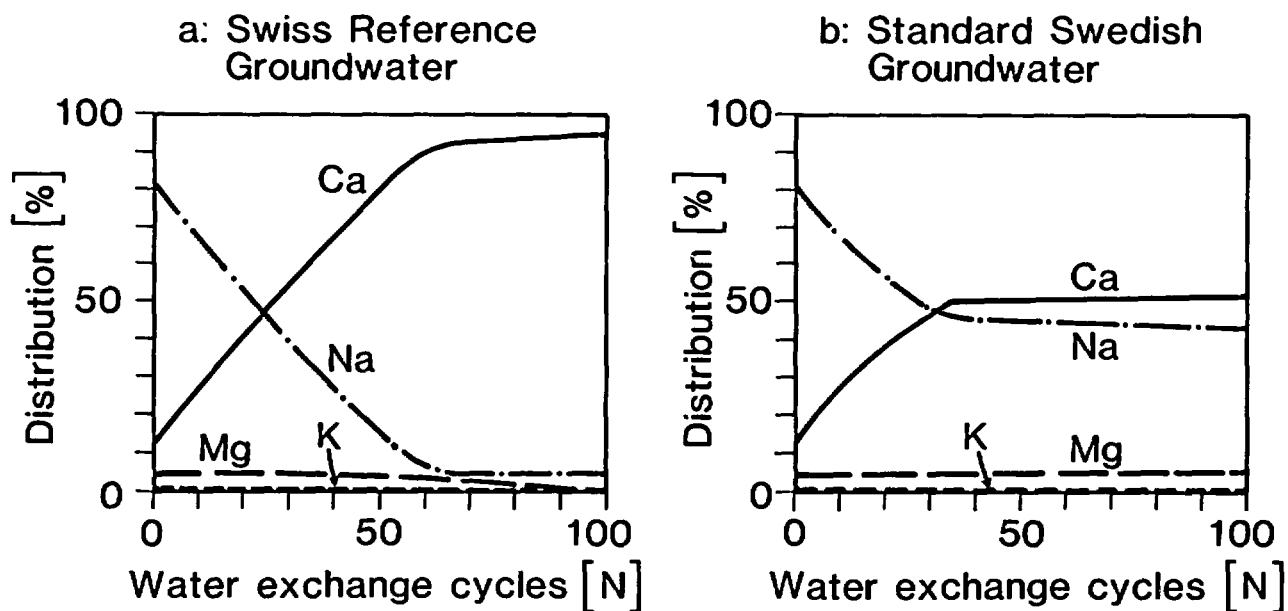


Figure 3: Alteration of the percentage distribution of exchange cations in sodium bentonite as a function of exchange cycles by Swiss Reference Groundwater (a) and Standard Swedish Groundwater (b).

REFERENCES

NAGRA (1985), *Nuclear Waste Management in Switzerland: Feasibility Study and Safety Analyses*, Project Gewähr 1985, NAGRA NGB 85-09.

SCHWEINGRUBER M. (1982), *User's Guide for Extended MINEQL (EIR version) — Standard Subroutine/Data Library Package*, EIR Internal Report TM-45-82-38.

SCHWEINGRUBER M. (1984), *Revision 1 of: User's Guide for Extended MINEQL (EIR version) — Standard Subroutine/Data Library Package*, EIR Internal Report TM-45-84-39.

SNELLMAN M. (1984), *Chemical Conditions in a Repository for Spent Fuel*, Report YJT-84-08, 98p.

SNELLMAN M. (1985), private communication.

WANNER H. (1986), *Modelling Interaction of Deep Groundwaters with Bentonite and Radionuclide Speciation*, EIR Report No. 589 and NAGRA NTB 86-21, 103p.

EVALUATION OF AN EQUILIBRIUM SPECIATION MODEL
FOR THE ACID AQUEOUS IRON SULFATE SYSTEM AT 25°C

Susan L. Stipp,
Environmental Engineering, Stanford University
Stanford, Calif., 94305

Abstract

A series of solutions with known concentrations of Fe(II), Fe(III), and SO_4 were prepared to cover the chemical composition and pH range commonly encountered in acid mine waters: $10^{-5} < \text{Fe}_T < 10^{-2} \text{ m}$, $10^{-3} < \text{SO}_4 \text{ T} < 10^{-1} \text{ m}$, $1 < \text{pH} < 4$ and ionic strength $< 0.35 \text{ m}$. An ion speciation model was designed to calculate the concentrations of all species from the total concentrations of solute and H^+ (derived from pH) and the thermodynamic constants. From the species concentrations it was possible to calculate pe and the charge balance error. This provided two independent parameters with which to test the consistency of the model.

The model was found to be effective in predicting laboratory results for all waters. Slight discrepancies result from error in pH electrode measurements and from model parameter uncertainties such as activity coefficient estimations and equilibrium constants. Conditioning and calibration of the pH electrode in a buffer of similar concentration to the unknown proves necessary for measuring solutions with $\text{pH} < 2.0$. The model results are most sensitive to the method of calculating single-ion activity coefficients. Use of the Truesdell-Jones equation yields the closest agreement for measured and predicted pe. Model predictions are less sensitive to equilibrium constant uncertainties for the various iron, hydroxide, sulfate and bisulfate pairs. Of these, the uncertainty in the dissociation constant for FeSO_4^+ has the greatest effect.

Introduction

Waters in contact with non-carbonate, pyrite-bearing rocks typically have low pH, high concentrations of iron and sulfate and are capable of mobilizing toxic concentrations of heavy metals and radionuclides. Safe management of coal, base metal, and uranium mining and milling sites is facilitated by an ability to simulate and predict the chemical evolution of the ground and surface waters in these environments. NORDSTROM et al (1979) found that mineral solubility predictions in acid effluent may be limited by the uncertainty in ion activity coefficients at lower pH, and by a lack of thermodynamic data for iron-bisulfate ion pairs, rendering speciation tenuous for waters with $\text{pH} < 2.5$. The purpose of this paper is to test the predictive ability of an equilibrium speciation model for iron-sulfate waters with pH between 1 and 4.

Model Development

The equilibrium speciation model makes use of measured pH and known solution concentrations for input into mass balance equations, along with mass action expressions for acid/base and ion-ion association reactions. A literature review was conducted to determine the uncertainty in the equilibrium constants. The details are presented in STIPP (1983) and the species incorporated in the model are listed in Table 1, along with their respective constants and the uncertainty associated with each.

When pH is moderately low and Fe(III) concentration is high, Fe(OH)^{2+} and Fe(OH)_2^+ are major species. If sulfate is also present, ferric hydroxide complexes with SO_4^{2-} probably form. No data is reported for these species, but comparison of pK values for similar complexes indicates that constants for Fe(OH)SO_4^0 and $\text{Fe(OH)}_2\text{SO}_4^-$ would be about 2.3 and 0.8, respectively. In waters with pH < 2, constants for FeHSO_4^+ and FeHSO_4^{2+} have been measured but with considerable uncertainty. Constants for these four species were included in the model, one at a time, in order to test their effect on speciation. Pairing of ClO_4^- with iron was found to have a negligible effect on speciation when tested with pK=0.9 for dissociation of FeClO_4^+ (BEUKENKAMP and HERRINGTON, 1960) and pK=1.15, for FeClO_4^{2+} (SMITH and MARTELL, 1976).

The computational procedure applies an iterative approach in which each single-ion activity coefficient (γ) is estimated and subsequently refined until convergence is attained. Three different equations for estimating γ , Debye-Hückel, Davies, (STUMM and MORGAN, 1981) and TRUESDELL-JONES (1974) were used. The Debye-Huckel equation is:

$$\log \gamma_i = \frac{-Az_i^2 \sqrt{I}}{1 + Ba_i \sqrt{I}} \quad (1)$$

where I represents ionic strength; z_i , the charge on species i; a_i , the parameter of closest approach (KIELLAND, 1937; RUTLER, 1964) and A and B are parameters dependent on temperature and pressure (HELGESON and KIRKHAM, 1974). The Davies equation is:

$$\log \gamma_i = \frac{-Az_i^2 \sqrt{I}}{1 + \sqrt{I}} + 0.3 I \quad (2)$$

and the Truesdell-Jones equation is:

$$\log \gamma_i = \frac{-Az_i^2 \sqrt{I}}{1 + Ba_i \sqrt{I}} + 0.3 I \quad (3)$$

The dissociation constants for all reactions and the total concentrations of all dissolved constituents are specified in the speciation model, so pH may be independently calculated. However, by using measured pH, pe may be predicted from the $\text{Fe}^{3+}/\text{Fe}^{2+}$ ratio with the Nernst equation.

Table 1. Statistics from speciation model testing. pK's are all for dissociation reactions, i.e., $\text{Fe(OH)SO}_4^0 \rightleftharpoons \text{Fe(OH)}^{2+} + \text{SO}_4^{2-}$

Test for effect of:				r^2	β	α	$\sigma_f(\%)$
pH Measurement Error (calculations made using listed pK's and T-J model for γ)							
i	Liquid Junction Potential (LJP) corrections made for pH and Eh measurements.			0.94	0.97	0.45	0.74
ii	LJP corrections omitted.			0.95	0.96	0.41	1.32
iii	-0.1 adjustment made to pH < 1.7 to partially compensate for electrode memory effect *			0.94	0.98	0.29	0.37
Model for γ Estimation (calculations made using pH corrected for LJP and listed pK's)							
Ref							
i	Truesdell-Jones	17		0.94	0.97	0.45	0.74
ii	Davies	16		0.94	0.82	2.15	1.75
iii	Debye-Hückel	16		0.93	0.88	1.45	2.09
Uncertainty in Equilibrium Constants (with pH corrected for LJP and T-J for γ)							
Species	Ref**	pK	Adjustment				
H ₂ O	15	13.997	-0.003	0.94	0.97	0.45	0.74
HSO ₄ ⁻	15	1.99	-0.02	0.94	0.97	0.49	0.70
KSO ₄ ⁻	12	0.85	-0.02	0.94	0.97	0.48	0.74
Fe(OH) ²⁺	1,15	11.81	-0.02	0.94	0.97	0.43	0.74
Fe(OH) ₂ ⁺	1,15	22.3	-0.1	0.94	0.97	0.43	0.74
FeSO ₄ ⁰	15	2.2	-0.1	0.94	1.0	0.09	0.49
FeSO ₄ ⁺	15	4.04	-0.1	0.94	0.94	0.87	1.49
			+0.1	0.94	1.0	0.00	0.00
Fe(SO ₄) ₂ ⁻	15	5.38	-1.0	0.93	0.90	1.34	1.18
			-0.1	0.94	0.95	0.67	0.84
FeHSO ₄ ⁺	7	0	+1.08	0.95	0.96	0.53	0.20
			+1.5	0.94	0.97	0.48	2.83
FeHSO ₄ ²⁺	7	0	+2.47	0.95	0.97	0.36	0.69
			+1.5	0.94	0.97	0.44	0.57
Fe(OH)SO ₄ ⁰	estimate	0	+2.3	0.94	0.98	0.28	0.73
Fe(OH) ₂ SO ₄ ⁻	estimate	0	+0.8	0.94	0.97	0.45	0.74

* maximum charge balance error improved from $\pm 40\%$ to $\pm 5\%$ with this change.

** for more thorough literature review see Stipp, 1983.

Comparison of measured with predicted pe provides one check for testing reliability, and the calculated charge balance yields another. Speciation was influenced by the choice for γ estimation, by uncertainties in the equilibrium constants, and by errors in pH measurement. To study the effect of each source of uncertainty, the deviation factor was determined,

$$\sigma_f = \frac{\sum (pe_c - pe_m)^2}{DF} \times 100 \quad (4)$$

where DF represents the degrees of freedom for the population. If correlation between predicted and measured pe values is ideal, $\sigma_f = 0\%$.

Experimental Method

The solutions for this study were prepared with total iron concentration ranging from 10^{-5} m (0.56 ppm) to 10^{-2} m (558 ppm) with Fe(III)/Fe(II) equal to 1. The pH ranged from 1 to an upper limit determined by $Fe(OH)_3(s)$ saturation. Sulfate concentration varied from 10^{-3} m (96 ppm) to 10^{-1} m (9600 ppm). Although acid mine drainage waters have been found to contain more than 17,000 ppm total iron, three times as much sulfate and pH as low as 0.55 (DUBROVSKY, 1985; NORDSTROM, 1977 and 1985), most waters from mine sites fall in the above concentration range. A more detailed description of the experimental procedure is presented in STIPP (1983).

The pH and Eh electrodes, buffers and test solutions were maintained at $25^\circ C (\pm 0.1^\circ)$ in a water bath. The Orion-Ross combination glass electrode was calibrated before and after each series of measurements with the 4.01 NBS buffer and a standardized 2.095 pH H_2SO_4 solution and checked with 1.68 pH tetroxalate and 1.00 pH HCl + KCl buffers. The Markson 1202 platinum Eh electrode was polished periodically with very fine emery paper to remove surface alteration products (WHITFIELD, 1971) and was calibrated in ZoBell solution (NORDSTROM, 1977). All measurements were corrected for drift of potential with time, and for liquid junction potentials using the Henderson equation (PLUMMER and BUSENBERG (1982)). Reproducibility for pH measurements was ± 0.02 pH units and for Eh, was better than ± 0.025 pe units (± 1.48 mV) except for samples where iron concentration was $\leq 10^{-5}$ m.

Results

The full data set is presented in STIPP (1983). Figure 1 shows all data for predicted pe plotted as a function of measured pe. The pe calculations were made with Truesdell-Jones γ estimates and the equilibrium constants listed in Table 1. For ideal correlation, the line of best fit would have a coefficient of determination (r^2) and slope (β) of 1.0, and a y-intercept (α) and deviation factor (σ_f) of 0%. For the actual data, r^2 was 0.94 for a population size (n) of 130 points; $\beta=0.97$ was not significantly different than 1.0 at the 95% confidence limit; α was 0.45; σ_f was 0.74%. The significant correlation of the data and the closeness of the line of best fit to the ideal line demonstrate the effectiveness of the conventional model in describing speciation in acid mine waters.

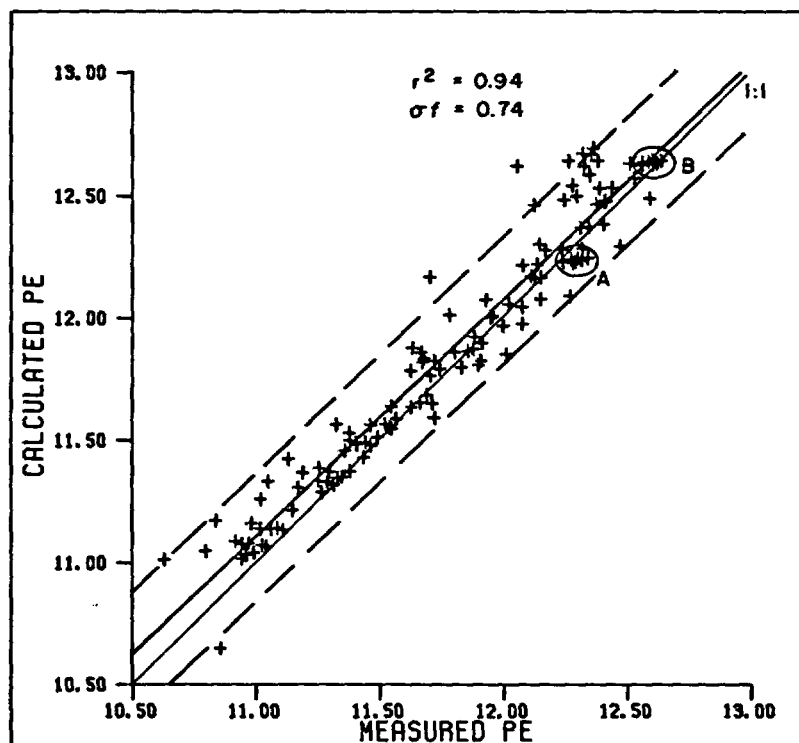


Figure 1. Plot of pe predicted by the speciation model versus measured pe for all data. Single-ion activity coefficients were determined with the Truesdell-Jones equation. The line of best fit for this data is not significantly different than the 1:1 line. The 95% confidence limits are shown by dashed lines (± 0.27 pe units or 16 mV). The points marked A and B represent solutions containing only iron and perchloric acid, no sulfate.

Discussion

Although the model predicts pe without significant deviation at the 95% confidence limit, systematic differences in the data do exist. The degree of discrepancy varies, depending on the pH and the composition of the test solution. These differences are attributed to the following sources:

- 1) uncertainties in electrode measurement,
- 2) the method for estimation of single-ion activity coefficients, and
- 3) the uncertainties in equilibrium constants and/or the existence of ion pairs not accounted for in the speciation model. The relative effects of these sources of uncertainty are evaluated and discussed in the following paragraphs.

Electrode Response. The uncertainty in the electrode measurements was evaluated by an analysis of pH measurement error and by a test of the importance of the liquid junction potential correction for both pH and Eh electrodes. The charge balance error showed an increase in anion excess with decreasing pH and an imbalance of as much as 40% in solutions with pH below 1.0. The input concentrations of all major constituents except H^+

were known with less than 2% uncertainty. The H^+ concentrations, however, were derived from measured pH. The logarithmic nature of pH and the dominance of H^+ as a cation in acid solutions result in magnification of the uncertainties derived from errors in the γ_{H^+} estimate and the pH electrode readings. Estimated γ_{H^+} varies, depending on the model selected. Large negative charge imbalances were calculated for solutions with pH < 1.5 by all models, so error in γ_{H^+} estimation could be only part of the cause for the large apparent H^+ deficit.

For this study, the pH electrode was stored in 4.01 pH NBS buffer. Measurements were reproducible (± 0.02 pH units) but where pH was less than 1.7, slight and prolonged downward drift of potential was observed. Additional experiments were performed in pure H_2SO_4 ranging in concentration from 0.05 to 5 M to test electrode performance with different methods of conditioning and calibration. Measurements made with an electrode that was conditioned in the 1.0 pH buffer for several hours, then calibrated with 4.01 and 1.00 buffers, were remarkably stable. They reflected no memory effect when compared with pH calculated by speciation programs using both Pitzer and Truesdell-Jones models for γ estimation. Readings for the $Fe-SO_4-H_2O$ test solutions with pH < 1.7 were adjusted by -0.1 pH units; the maximum charge balance was reduced to $\pm 5\%$ and predicted pe was much closer to the experimental data (Table 1). It is recommended that electrodes for use in solutions where pH < 2 , be conditioned for several hours before use and calibrated with a buffer of acid similar in composition and pH to the solution to be measured.

Liquid junction potential corrections (less than 0.03 pe or pH units of 2 mV) are within the reproducibility of the readings. Although correction with this systematic error significantly improved the correlation for experimental data, it need not be considered in routine field measurements.

Activity Coefficients. Single-ion activity coefficients form one set of speciation model parameters. Substantially different γ 's result, depending on which estimation method is chosen. For example, at $I = 0.05$ m, the γ 's for the di- and trivalent species vary by 15 and 50%, respectively. At the maximum ionic strength of the study solutions ($I = 0.36$ m), γ 's vary by as much as 20% for the monovalent species, and by 92% for Fe^{3+} . This contributes significantly to the uncertainty of the model results for $I > 0.05$ m (Table 1).

Estimations made with the Debye-Hückel equation do not include a correction for the ion interaction effect, so γ uncertainty increases with ionic strength. As a result, the predicted pe for solutions with high sulfate, high iron, or low pH are consistently higher than the measurements. With Davies model estimations, predicted pe was significantly different than measured pe at the 95% confidence limit. Comparison of the statistics for the three models suggests that for this system, γ estimations are substantially improved by the inclusion of both the hydrated size parameter (a_1) and the ion interaction term (0.3I) with the Truesdell-Jones equation.

Equilibrium Constants. Speciation was tested for sensitivity to the uncertainty in each of the equilibrium constants. The statistics are tabulated in Table 1. The $Fe-H_2O$ system has been investigated more fully

than the one containing SO_4 and there is less uncertainty in the data. The uncertainty effect is further minimized by the low relative concentration of iron hydroxide species in acid, high sulfate waters. Large pK uncertainty does not necessarily result in larger differences in predicted concentrations. FeSO_4^+ is often an abundant species in acid mine and tailings water; a small change of 0.1 to the pK resulted in a shift of σ_f for the test solutions from 0.74 to 1.49%, whereas the much larger adjustment of 1.0 to the pK for $\text{Fe}(\text{SO}_4)_2^-$ resulted in a change in σ_f from 0.74 to 1.18%. The model results were tested for the effect of inclusion of the uncertain pK's for $\text{Fe}(\text{OH})\text{SO}_4^0$, $\text{Fe}(\text{OH})_2\text{SO}_4^-$, FeHSO_4^+ and FeHSO_4^{2+} . Predicted concentrations were not significantly affected by the constants for the ferric hydroxide-sulfate complexes. Inclusion of constants for the iron-bisulfate pairs slightly improved the relationship between measured and predicted pe.

Conclusions

Equilibria in the aqueous acid iron-sulfate system at 25°C can reliably be predicted using a speciation program which incorporates presently accepted equilibrium constants. If the pH and solute concentrations are known, the model is effective in predicting pe within ± 0.26 pe units (± 15 mV) at the 95% confidence level, over the typical range of composition for acid mine and tailings water. Uncertainties in the predictions result from error associated with pH electrode measurements and from uncertainty in the two main sets of model parameters: single-ion activity coefficients and the equilibrium constants.

For solutions where pH is less than 1.7, large charge imbalance is caused by error in calculated H^+ concentration. This imbalance partly results from uncertainty in γ_{H^+} estimates, but mostly is a function of the technique adopted for conditioning and calibrating the pH electrode. The model predictions are slightly sensitive to the correction for the liquid junction potential for all measurements with the Eh and pH electrodes. Speciation is most sensitive to uncertainties in the estimates for activity coefficients. Of the three methods used, the Truesdell-Jones equation produced the least difference between measured and predicted pe values. The model results are not sensitive to changes in pK for any of the iron-hydroxide complexes. They are sensitive to uncertainties in equilibrium constants for iron-sulfate pairs, particularly FeSO_4^+ . Predictions are affected by inclusion in the model of approximated constants for FeHSO_4^+ and FeHSO_4^{2+} .

In summary, the equilibrium speciation model for the aqueous acid iron-sulfate system, as outlined in this paper, is satisfactory for predicting species concentrations at ionic strengths less than 0.4 m in the pH range of 1 to 4. To insure accurate predictions using the model in application to real field data where $\text{pH} < 2.0$, care must be taken to condition and calibrate the pH electrode in a buffer of similar acid concentration to the unknown. Aside from difficulty in pH measurement below 2.0, the greatest source of uncertainty in model predictions lies with the method of calculating single-ion activity coefficients. Uncertainties in the equilibrium constants of the species involved appear to be of secondary importance.

Acknowledgements

I wish to thank ERIC J. REARDON for guidance and support and D. KIRK NORDSTROM for discussion and encouragement. Financial support was provided by the Natural Sciences and Engineering Research Council of Canada at the University of Waterloo, Ontario.

References

1. BAES C.F. JR. and MESMER R. E. (1976) The Hydrolysis of Cations. Wiley.
2. BEUKENKAMP J. and HERRINGTON K.D. (1960) Ion-exchange investigation of the nature of iron (II) in sulfuric and perchloric acid. *J. Amer. Chem. Soc.* 82, 3022-3025.
3. BUTLER J.N. (1964) Ionic Equilibrium. Addison Wesley.
4. DUBROVSKY N. (1985) Ph.D. Thesis, University of Waterloo.
5. HELGESON H.C. and KIRKHAM D.R. (1974) Theoretical prediction of the thermodynamic behavior of aqueous electrolytes at high pressures and temperatures: Part II. *Amer. J. Sci.* 274, 1199-1261.
6. KIELLAND J. (1937) Individual activity coefficients of ions in aqueous solutions. *J. Am. Chem. Soc.* 59, 1675-1678.
7. MATTIGOD S.V. and SPOSITO G. (1977) Estimated association constants for some complexes of trace metals with inorganic ligands. *Soil Science Soc. of Amer. J.* 41, 1092-1097.
8. NORDSTROM D.K. (1977) Thermochemical redox equilibria of ZoBell's solution. *Geochim. Cosmochim. A.* 41, 1835-1941.
9. NORDSTROM D.K., JENNE E.A. and BALL J.W. (1979) Redox equilibria of iron in acid mine waters. In: *Chemical Modeling in Aqueous Systems*. JENNE E.A. (ed), ACS Symposium Series 93, 51-79
10. NORDSTROM, D.K. (1985) The formation of acid mine waters: A review. In: *BONNER A.J. (ed). Proceedings of the Hazardous Materials Management Conference/West, Long Beach, Calif. Dec. 3-5, 1985*, 453-457.
11. PLUMMER, L.N. and BUSENBERG E. (1982) The solubilities of calcite, aragonite and vaterite in CO₂-H₂O solutions between 0 and 90°C, and an evaluation of the aqueous model for the system CaCO₃-CO₂-H₂O. *Geochim. Cosmochim. A.* 46, 1011-1040.
12. REARDON E.J. (1975) Dissociation constants of some monovalent sulfate ion pairs at 25°C from stoichiometric activity coefficients. *J. Phys. Chem.* 79, 422-425.
13. ROBINSON R.A. and STOKES R.H. (1970) Electrolyte Solutions. Butterworths.
14. SAPIESZKO R.S., PATEL R.C. and MATIJEVIC E. (1977) Ferric hydrous oxide sols: 2. Thermodynamics of aqueous hydroxo- and sulfato ferric complexes. *J. Phys. Chem.* 81, 1061-1068.
15. SMITH, R.M. and MARTELL A.E. (1976) Critical Stability Constants. Plenum.
16. STIPP S.L. (1983) Evaluation of an equilibrium speciation model for the aqueous iron-sulfate system at 25°C. MSc Thesis, University of Waterloo.
17. STUMM W. and MORGAN J.J. (1981) Aquatic Chemistry, Wiley.
18. TRUESDELL A.H. and JONES B.F. (1974) WATEQ, A computer program for calculating chemical equilibria of natural waters. *J. Res. USGS* 2, 233-248.
19. WHITFIELD M. (1971) Ion Selective Electrodes for the Analysis of Natural Waters. Aust. Mar. Sci. Assoc., Handbook 2, Sydney.

THERMODYNAMIC AND KINETIC MODELING OF GLASS LEACHING IN A WASTE PACKAGE ENVIRONMENT

B. Grambow
Hahn-Meitner-Institut Berlin,
Glienicke Str.100, 1000 Berlin 39, FRG

Abstract

Modeling of the aqueous dissolution of nuclear waste forms is a necessary step for extrapolating short term laboratory results to the long-term performance in a repository. For nuclear waste borosilicate glasses a dissolution model (GLASSOL [1,2]) is proposed, which combines thermodynamic reaction path calculations (PHREEQE code [3]) with kinetic constraints. The model was developed in the frame of the JSS-project (joint Japanese, Swedish, Swiss Project) to allow interpretation of leach data from a radioactive glass delivered from COGEMA ("JSS-A" glass) [4]. Experimental conditions include leach tests in static and flowing solutions, variations of temperature, pH and S/V (sample surface area-to-solution volume ratio) and the presence of various waste package components (i.e. bentonite or steel corrosion products). The ongoing validation of the model is performed by a description of all major experimental results and by its application to natural analogue systems [2, 5, 6]. This paper gives an overview of the key ideas in the model, and, for some experimental conditions, the results of computer simulations are compared with laboratory data.

Mechanism of glass corrosion

The release of glass constituents is controlled either by matrix dissolution, by solubility, or by sorption processes. Selective extraction of alkali ions from the glass matrix plays only a minor role in the overall mass balance of the reaction [7]. During reaction, surface layers of sparingly soluble glass constituents are formed. Solid reaction products include both crystalline and amorphous products. The actual reaction occurs at the interface (reaction zone thickness $<0.1 \mu\text{m}$) between the pristine glass and the surface layer.

At high dilution (i.e. high flow rates) and in the absence of low permeable surface layers matrix corrosion proceeds with constant rate ("forward rate k_+ "). If dissolved silica accumulates in solution (static or slow flow rate leach tests), the rate decreases substantially due to saturation effects. The glass phase will never be in equilibrium with the bulk solution, but at saturation condensation of surface silanol groups stabilizes the glass [1]. A residual affinity of reaction remains at silica saturation and the reaction proceeds at a slow rate until the glass has completely reacted in the long term. In the presence of low permeable surface layers a gradient of silicic acid may be established and the rate of reaction may slow down faster than predicted from solution concentration alone [8].

Both the initial rate and the saturation concentration of total silica depend on the solution pH, which usually changes with reaction progress. By

means of changing pH and silica concentration, waste package components can influence the release of radionuclides. For example, in the presence of cast iron corrosion products, silica is removed from solution by sorption onto the Fe-corrosion product and the dissolution rate of the glass is increased [9].

Rate Equation

A general rate equation is proposed [1] based on equilibrium and irreversible thermodynamics and on transition state theory. In its simplest form, this equation may be given as

$$r_m = k_+ * (1 - a_{si}/a_{sat}) \quad (1)$$

where r_m is the dissolution rate, k_+ is the rate constant for the forward reaction, a_{si} is the actual activity of ortho silicic acid in solution and a_{sat} is the corresponding activity at saturation. The values of k_+ and a_{sat} can be derived from the experimental data [5]. Alternatively, within a factor of three of uncertainty, k_+ can be calculated from the free energy of reaction dG_R [1] using the equation:

$$k_+ = X * \exp(-dG_R/RT) * \exp(-E_A/RT) \quad (2)$$

where x is a proportionality constant and E_A is the activation energy (ca. 50-120 kJ/mol). The free energy dG depends both on glass composition and on pH. Calculation of dG is based on a solid solution model for the glass phase [10,11]. The final rate of reaction ($r_m=r_{fin}$) is achieved, when a_{si} is close to saturation. The final affinity of reaction keeps a certain small difference between a_{si} and a_{sat} .

The transport of silicic acid through the surface layer are described by Eq. 3 [2] (where the rate of transport is assumed to be equal to the rate of dissolution):

$$r_m = k_+ * (1 - a_{si,s}/a_{sat}) = D/L (a_{si,s} - a_{si,b}) + r_{fin} \quad (3)$$

Eq. 1 is included into Eq. 3, but it no longer refers to bulk values (subscript b) of ortho silicic acid but to its activity at the surface (subscript s). The diffusion coefficient for silicic acid is D , and L is the thickness of the growing surface layer, r_{fin} , the final rate of reaction describes the dissolution process at saturated conditions, when there is no diffusion gradient for silicic acid.

Solving Eq. 3 first for $a_{si,s}$ and then for r_m yields a rate equation, which is applicable to the glass/water reaction both with and without transport control:

$$r_m = k_+ * ((D*(a_{sat} - a_{si,b})/L + r_{fin}) / (D*a_{sat}/L + k_+)) \quad (4)$$

The term $D*a_{sat}/L$ is the maximum transport rate for a given layer thickness L , i.e. the transport rate when the solution concentration is zero and the surface concentration is at saturation. If this transport rate is much higher than the forward rate of reaction, then Eq. 4 equals Eq. 1 (rate

control by surface reaction). If the maximum transport rate is much lower than k_+ , then under certain conditions, the rate may decrease with the square root of time.

Computer Code "GLASSOL"

Based on Eq. 4 the code GLASSOL was developed. The effects of S/V, flow rate, temperature, time, solution chemistry, and of waste package components (bentonite and iron corrosion products) are considered.

The constants k_+ , a_{sat} , D and r_{fin} were derived from the experimental results [2]. For leaching JSS-A glass at 90°C, the constants are included in Table 1. The saturation concentration for silicic acid a_{sat} is replaced by the stability constant K_{SiO_2} for the reaction $SiO_2 + 2H_2O \rightleftharpoons H_4SiO_4$ ($K_{SiO_2} = a_{sat}$ for $a_{H_2O} = 1$).

Table 1: Constants for JSS-A glass modeling with GLASSOL at 90°C

k_+	1.5	$g/(m^2 \cdot d)$
r_{fin}	0.0025	$g/(m^2 \cdot d)$
D	10^{-9}	cm^2/sec
$\log K_{SiO_2}$	-2.934	

The variables L and $a_{s,b}$ depend on the reaction progress ξ . The dependence of $a_{s,b}$ on ξ is calculated with the geochemical code PHREEQE, because secondary reactions may be considered, such as hydrolysis of silicic acid, precipitation of silicates, dissolution of bentonite backfill or sorption on iron hydroxide, etc.

The PHREEQE code simulates the stepwise addition of glass to solution. The calculations yield the distribution of glass constituents among solution and solid alteration products. The solid reaction products constitute a replacement surface layer on the glass. There are various options to modify a reaction path by considering additional reactions with waste package components, such as bentonite or steel corrosion products.

The GLASSOL code uses the output from PHREEQE as input to calculate the resulting activity of silicic acid and Eq. 4 to calculate the time interval between two steps in the PHREEQE model and the total time of experiment. From Eq. 1 and 4, the activity of silicic acid at the glass surface is calculated. The corresponding surface pH and surface solution composition is derived from the PHREEQE reaction path model.

The effect of flow rate F (volumetric units), has been included in the GLASSOL code using Eq. 5:

$$dC_G/dt = S/V * r_m - F/V * C_G \quad (5)$$

where C_G is the amount of glass reacted, in units of concentration [mg/L].

Application of the model

For the reaction of JSS-A glass with deionized water the results from the PHREEQE reaction path calculations are shown in Fig. 1. The solution concentrations are normalized to the glass composition and are plotted versus the amount of glass reacted per unit volume of solution.

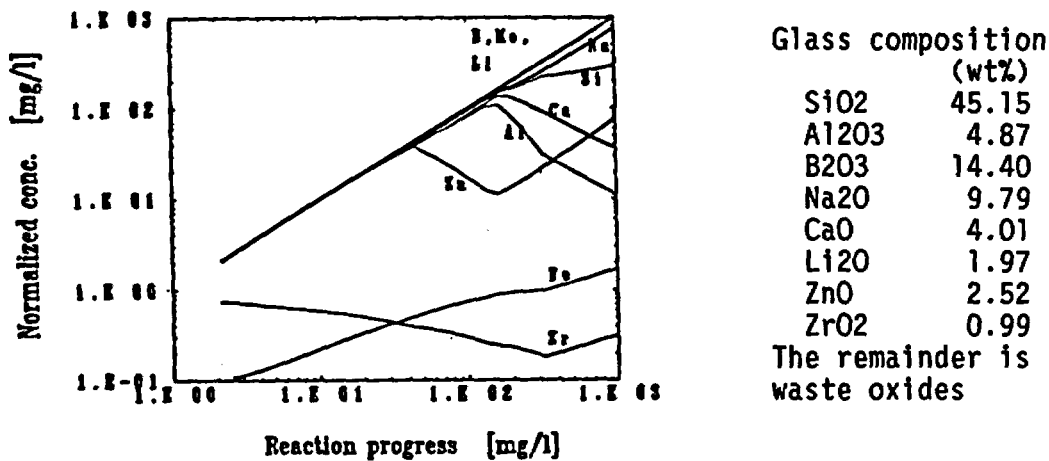


Fig. 1. Reaction path model for JSS-A glass and glass composition.

Fig. 2a and b show two quite different examples for the time dependence of leaching as calculated from the same reaction path (Fig.1). In Fig. 2a, the experimental results from static leaching are compared with the calculated curves for various glass constituents, and Fig. 2b shows for a dynamic leach test the calculated and observed boron releases. The only difference is the GLASSOL input parameters between the two plots is the flow rate, e.g. 0 ml/d and 2.9 ml/d.

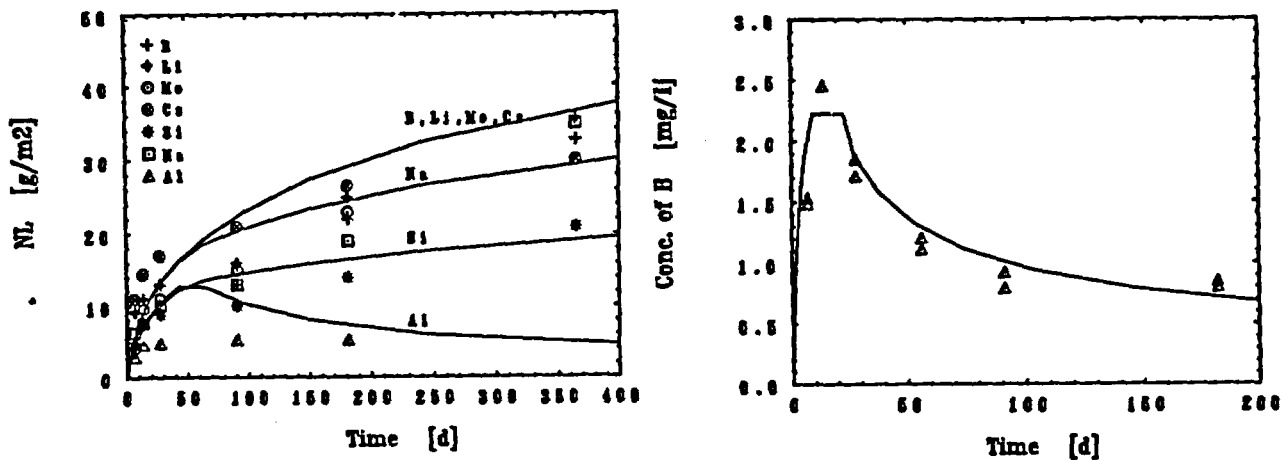


Fig. 2. Time dependence of JSS-A glass dissolution at 90°C calculated using GLASSOL for a) static test (10 m⁻¹) and b) dynamic test (2.9 ml/d)

The agreement between the calculated and observed values verifies the proposed dissolution mechanism. In the flow test, the decrease in solution concentration and reaction rate results from slow transport of silicic acid in the growing surface layer. In the surface layer, the silica concentration increased with growing layer thickness and, hence, the reaction rate decreases. In bulk solution the content of silicic acid decreases due to the decreasing rate.

Model for Glass Dissolution in the Presence of Bentonite

Fig. 3 shows schematically the reactions in the overall glass/bentonite/water system.

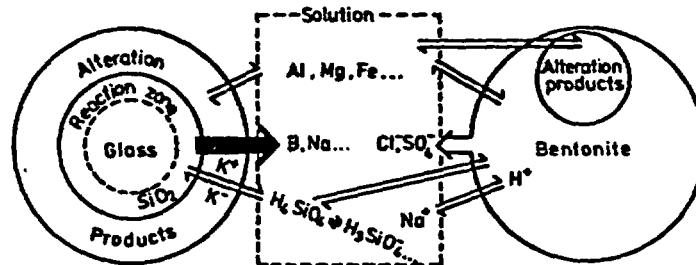


Fig. 3: Scheme of the glass/bentonite/water model

The bentonite/water model describes the effect of bentonite on solution chemistry using equilibrium thermodynamics. The active component of bentonite is montmorillonite, the formula, which for this study, is [11]:



It is assumed that the solution is in equilibrium with montmorillonite. Solubility and ion exchange equilibria are considered in the PHREEQE reaction path model. The formal description for ion exchange is used from the model of Wanner [11]:



$$K_M = a_{\text{MZ}_n} / (a_{\text{Z}^-}^n * a_{\text{M}^{\text{n}+}})$$

The exchange sites are denoted as Z⁻. In addition to the metal ions (M= Na⁺, Ca²⁺, K⁺, Mg²⁺) in Wanner's model, the present model also uses H⁺ for exchange.

As in the simple glass/water system, the reaction path for glass dissolution is calculated depends on the precipitation of alteration products. The dependence of the silicic acid concentration on reaction progress is used by GLASSOL to compute the time dependence of the reaction.

For the corrosion of JSS-A glass in the presence of 1 g of bentonite in 40 ml solution with a S/V = 10 m⁻¹ at a temperature of 90°C. Fig. 4a shows the comparison of calculated and experimental results and Fig. 4b shows the calculated effect of the bentonite water ratio on glass corrosion.

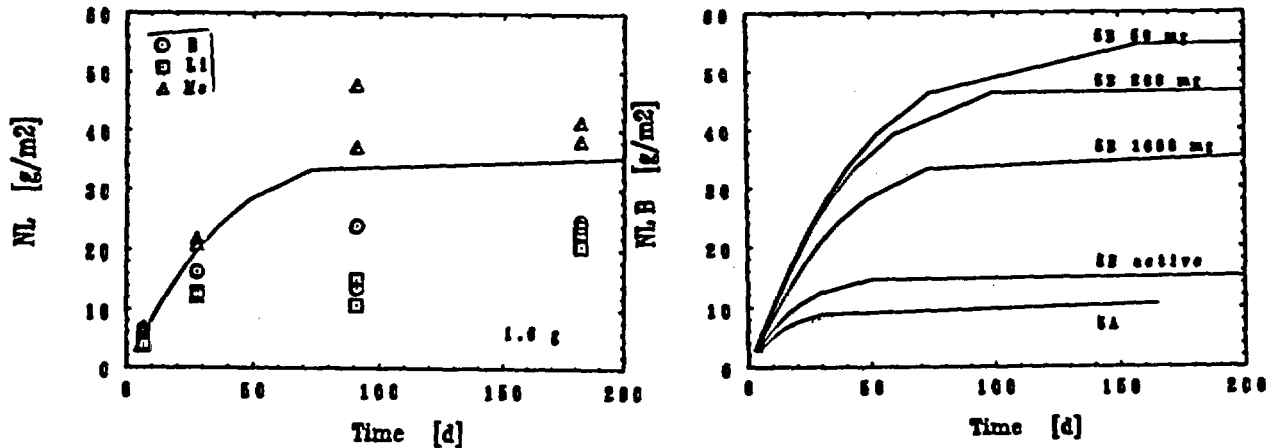


Fig. 4: Glass corrosion in presence of bentonite at 90°C -
 a) comparison of experimental results with the computer simulations (40 ml solution, 1 g bentonite, S/V = 10 m⁻¹)
 b) dependence of glass corrosion on the amount of bentonite present

There is reasonable agreement between observed and calculated results. This is also true for most experiments performed at other bentonite/water ratios. The decrease of glass corrosion with increasing amount of bentonite is due to the decrease in solution pH which decreases the silica solubility. The decrease in solution pH with increasing amount of bentonite is confirmed experimentally [13].

Final Remarks

The kinetic parameters of the model provide a means to evaluate nuclear waste forms. The constants are also meaningful in other areas of research. For example, the value of the diffusion coefficient for silicic acid in the surface layer is similar to diffusion coefficients in clay.

The agreement of model and experiment increases the confidence level for short-term predictions. Long-term predictions require detailed understanding of the factors which influence the final affinity of reaction. Nevertheless, the application of the model to natural analogue systems [6] is promising for future reliable long-term predictions.

References

- 1 GRAMBOW, B. (1985) "A General Rate Equation for Nuclear Waste Glass Corrosion." In *Scientific Basis for Nuclear Waste Management VIII*, eds. C. M. Jantzen, J. A. Stone, R. C. Ewing, North-Holland, New York, pp. 15-24
- 2 GRAMBOW, B., HERMANSSON, H. P., BJOERNER, I. K., CHRISTENSEN, H., WERME, L. (1986) "Reaction of Nuclear Waste Glass with Slowly Flowing Solutions", paper presented at the 88th Annual Meeting of the American Ceramic Society, Inc., Chicago, Ill., USA April 27 - May 1
- 3 PARKHURST, D. L., THORSTENSEN, D. C., PLUMMER, L. N. (1984) *Water-Resources Investigations 80-96*, U.S. Geological Survey, Reston, Virginia, USA, (1980) extension to run precipitation controlled reactions by P. Offermann, Hahn-Meitner-Institute, Berlin, FRG (1983), updated with the MINTEQ data base by W. Howden and K. Kruppka, Pacific Northwest Laboratories, Richland, Washington, USA
- 4 "JSS-Project Phase I (1984) : A Summary of Work Performed at Studsvik Energiteknik AB and at Swiss Federal Institute for Reactor Research (EIR)." JSS-Project Technical Report 83-03, SKB, Stockholm, Sweden
- 5 GRAMBOW, B., HERMANSSON, H. P., BJOERNER, I. K., WERME, L. (1986) "Glass/Water Reaction with and without Bentonite Present - Experiment and Model" In *Scientific Basis for Nuclear Waste Management*, ed. L. Werme, North-Holland, New York, in press
- 6 GRAMBOW, B., JERCINOVIC, M. J., EWING, R. C., BYERS, C. D. (1985) "Weathered Basalt Glass: A Natural Analogue for the Effect of Reaction Progress on Nuclear Waste Glass Alteration", Mat. Res. Soc. Symp. Proc., Vol. 50, pp. 263-272, Materials Research Society
- 7 MENDEL, J. E., et al. (1984) Final Report of the Defense High-Level Waste Leaching Mechanism Program, PNL-5157, Richland, WA 99352
- 8 WALLACE, R. M. and WICKS, G. G. (1983) "Leaching Chemistry of Defense Borosilicate Glass." In *Scientific Basis for Nuclear Waste Management*, Vol. VI, D. G. Brookins, ed., North-Holland, New York, pp. 23-28
- 9 MCVAY, G. L. and BUCKWALTER, C. Q. (1983) "Effect of Iron on Waste-Glass Leaching" J. Am. Cer. Soc., Vol. 66, No. 3, pp. 170-174
- 10 PLODINEC, M. J., JANTZEN C. M., and WICKS, G. G. (1982) A Thermodynamic Approach to Prediction of the Stability of Proposed Radwaste Glasses. DP-MS-82-66, Savannah River Laboratory, Savannah, Georgia
- 11 VONMOOS, M. M. and KAHR, G. (1983) Technischer Bericht 83-12, Nagra, Baden, Switzerland
- 12 WANNER, H. (1986) "Modelling Radionuclide Speciation and Solubility Limits in the Near-Field of a Deep Repository." In *Scientific Basis for Nuclear Waste Management IX*, ed. L. Werme, North-Holland, New York, in press

- 13 LANZA, F. and RONSECCO, C. (1982) "Influence of a Backfilling Material on Borosilicate Glass Leaching." In Scientific Basis for Nuclear Waste Management V, ed. W. Lutze, North-Holland, New York, pp. 173-180

COMPUTER MODELING OF THE AQUEOUS GEOCHEMISTRY OF THE ARCHEAN HYDROSPHERE AND THE FORMATION OF BANDED IRON FORMATIONS*

*William E. Glassley, Kenneth J. Jackson, and William L. Bourcier
Lawrence Livermore National Laboratory
Livermore, CA 94550*

INTRODUCTION

Constraints on the composition of the hydrosphere during the Archean and early Proterozoic have been difficult to establish because of the lack of an unmetamorphosed sedimentary record. However, it may be possible to significantly restrict the range of possible values for the redox state and concentrations for some of the major components of the Archean hydrosphere by combining key observations from banded iron formations, evaporites, fluid inclusions, and paleosols. Recent developments in the capabilities of geochemical modeling codes have made it possible to accurately model such complex systems. Preliminary modeling efforts have concentrated on the geochemistry of the formation of Archean banded iron formations and their implications for the composition of the Archean hydrosphere.

From the earliest Archean to the early Proterozoic, banded iron formations are a common and persistent lithology in the sedimentary record. These rock units, although diverse in their petrologic detail, consistently preserve several similar mineralogic features that include the prevalence of iron oxide phases (hematite and magnetite), alternating silica-rich and iron oxide-rich layers, the presence of a siderite or ankerite carbonate phase, and the association of minor amounts of iron-rich clay phases (James, 1966; Holland, 1984). Additional geologic evidence suggests that banded iron formations of the Algoman type, common in the Archean, were deposited in shallow basins, in close proximity to volcanic centers (Gross, 1980).

MODELING APPROACH

Our approach has been to model the chemical interaction between an acidic, volcanically derived fluid with a hypothetical Archean ocean water in order to determine whether mixing these solutions will result in precipitation of an iron-rich chemical sediment. The EQ3/6 geochemical modeling codes (Wolery, 1979, 1983) were used to perform the simulation. The first step (Figure 1a) was to constrain the composition of the Archean ocean as follows: The CO₂ fugacity was assumed to be fixed at 10^{-2.7}

* This work was performed under the auspices of the U.S. Department of Energy by Lawrence Livermore National Laboratory under contract No. W-7405-Eng-48.

bars by equilibrium among the aqueous solution and siderite, hematite, and magnetite, which is a common assemblage in banded iron formations. Likewise, the oxygen fugacity was assumed to be fixed by the presence of hematite and magnetite at 10^{-72} bars. The initial silica activity was set at amorphous silica saturation, and major cation abundances and pH were set equal to those of modern seawater (Figure 2). Chloride was fixed by adjusting the concentration to achieve charge balance. EQ6 was used to precipitate all supersaturated phases, which comprised dolomite, magnesite and talc. The resulting composition is similar to modern ocean water in sodium, potassium, and chloride concentrations as shown in Figure 2. Calcium and magnesium concentrations are reduced somewhat due to equilibrium precipitation of dolomite and talc, and the pH drops from 8.1 to 7.5. Because of the low oxidation state ferrous iron is predominant relative to ferric iron, and the total iron concentration in solutions is relatively high (about 10 ppm). Modern oceans contain dissolved iron concentrations that vary by a factor of two to four orders of magnitude smaller. Aluminum activity is fixed by assuming equilibrium with smectite. In summary, we have taken modern sea water, reduced the oxidation state to correspond to the hematite+magnetite buffer, saturated it with respect to the iron oxides, and precipitated all supersaturated phases in order to estimate the composition of Archean ocean water.

In addition, we have assumed that the salinity of the Archean ocean was roughly similar to that of modern oceans. Recent data on the salinities of fluid inclusions in 3.4 billion year old barites from a massive sulfide-type mineral deposit in the Pilbarra block of western Australia support this assumption (Bourcier et al., 1984). Although most of the fluid inclusions preserved in these barites have been affected by a lower-greenschist facies metamorphism, there is a population of presumably primary inclusions having consistent phase relations that give freezing temperatures of -2.5 to -3.0°C . These data indicate an NaCl equivalent salinity of 4.5 wt. percent. This value is similar to fluid inclusion salinities measured in Phanerozoic massive sulfide deposits. The increase in salinity above that of seawater (3.5 wt. percent) is most likely due to water-rock interactions in the hydrothermal systems that gave rise to the deposits. The similarity in the salinities of the ancient fluid inclusions to those of derived seawater trapped in fluid inclusions in modern equivalents of Archean submarine geothermal systems strongly suggests a salinity of Archean oceans similar to that of the present oceans.

Step 2 involved a determination of the composition of the volcanically derived acidic water that was reacted with the ocean water (Figure 2b). It was determined by using EQ6 to react water, komatiite, and arbitrary amounts of acidic volcanic components (e.g., HCl or HNO_3). In this case, we have reacted komatiite with an HCl solution and allowed the reaction path to proceed from an initial pH of 7.0 to a pH of 3.5. This resulted in a reduced, acidic solution rich in magnesium and iron. Silica, aluminum, and calcium activities were limited to values in equilibrium with the product phases

Step #1: Initial constraints for seawater composition

- CO₂ fugacity set by mineral assemblage siderite+magnetite+hematite buffer.
- O₂ fugacity and total Iron set by hematite+magnetite buffer.
- SiO₂ set by amorphous silica saturation.
- Major element concentrations of seawater from modern seawater.
- Chloride concentration from charge balance.
- Precipitate all supersaturated phases.

Step #2: Generation of acid iron-rich water

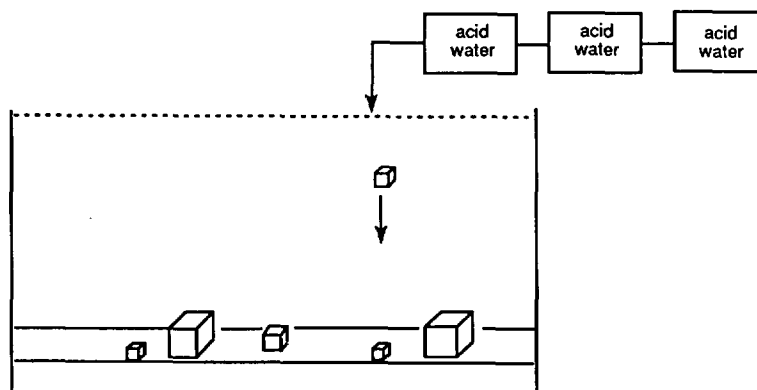
Initial compositional constraints

- React komatiite with acidic solution (HCl).
- Precipitate out all supersaturated phases.

Results

- Oxygen fugacity fixed by Fe⁺⁺/Fe⁺⁺⁺ ratio of komatiite
- Reaction stopped arbitrarily at pH of 3.5.
- Total Mg and total Fe of .001 molal

Step #3: Mix river basin into ocean basin



Titrate aliquots of acidic iron-rich water into basin, allow the reaction to proceed, and record changes in fluid and gas compositions.

Figure 1. Sequence of steps used to generate seawater and acid iron-rich fluid mixing model for origin of banded iron formations.

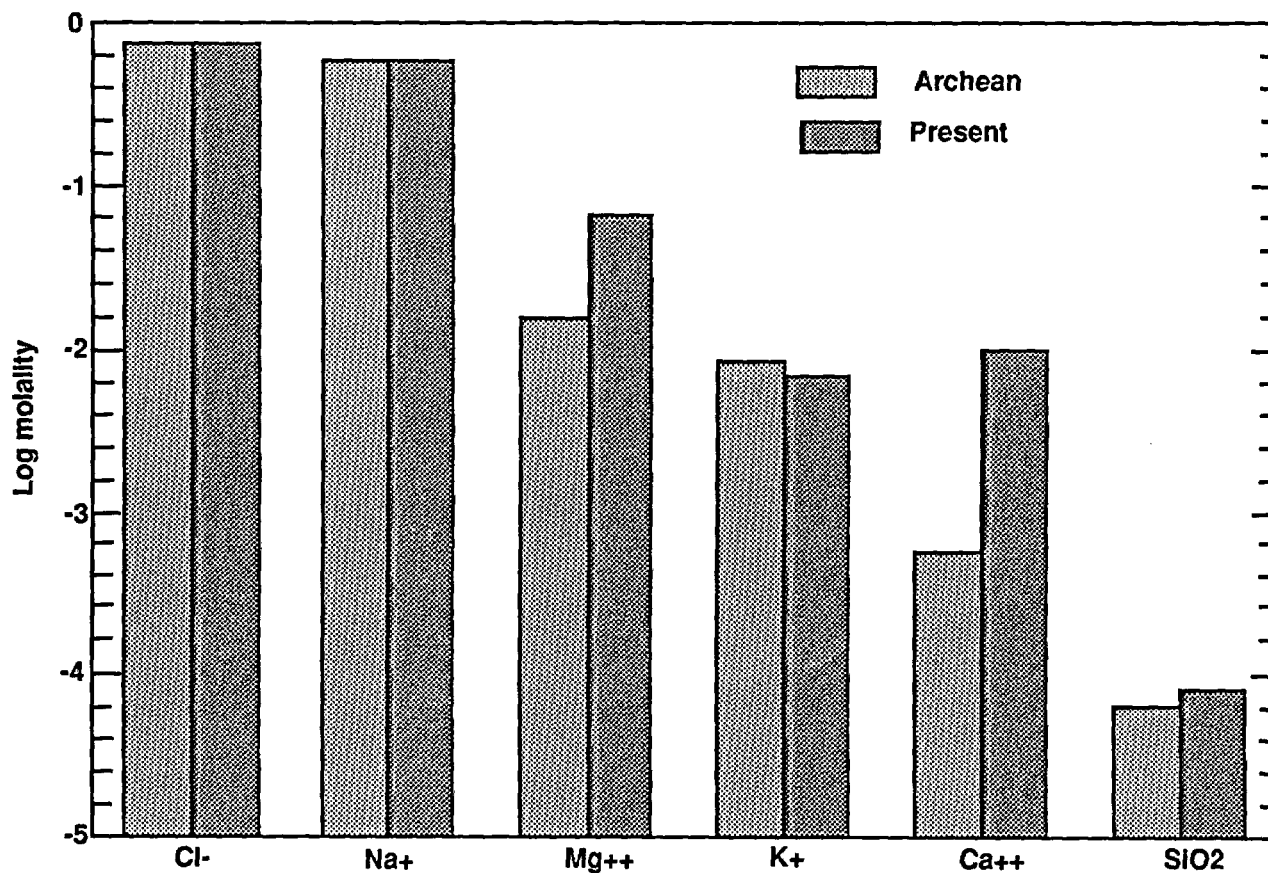


Figure 2. Histogram comparing hypothetical Archean and present-day ocean compositions. The iron concentration (not shown) of Archean seawater is assumed to be 10 ppm, two to four orders of magnitude higher than in the present oceans.

smectite, chlorite, and kaolinite, that precipitated during the reaction process. The solution was highly reduced because of the low ferrous/ferric ratio of the komatiite with which it was reacted.

Using EQ6, the acidic solution was reacted with a reservoir of simulated Archean ocean water and the system was allowed to equilibrate through the precipitation and dissolution of product phases (Figure 2c). This model was used to simulate the processes that might occur as a result of the addition of hydrothermal fluids or river waters to an ocean basin.

RESULTS

Initial modeling results indicated that mixing the two hypothetical solutions discussed above produced no product phase other than a magnesium-rich smectite clay. This was because the pH dropped rapidly as a function of reaction progress. In order to prevent the pH from dropping too rapidly and diverging from the iron-oxide and iron aluminosilicate stability fields, it was necessary to maintain the system in equilibrium with a pH buffering mineral phase. By assuming that the system remained in equilibrium with a carbonate phase (such as calcite or siderite), the mineralogy typical of banded iron formations was predicted by the modeling runs. Geologically, this is a reasonable assumption that is equivalent to allowing some dissolution of carbonate phases present on the seafloor during the initial stages of influx of acid water into the ocean basin.

The minerals calculated to precipitate and dissolve in the reaction path modeling are shown in Figure 3. Reaction progress, plotted on the x axis indicates the log of the number of milliliter of acid water added to one kilogram of the ocean water. The y axis gives the log of the number of moles of product phases that EQ6 predicted would form. The first phase precipitated was hematite, followed by cronstedite (an iron-rich hydroxy-silicate), dolomite, magnesite, and saponite (a sodium smectite component). As more of the reduced acidic fluid is added, the oxidation state of the system, initially at the hematite+magnetite boundary, drifts downward and ends up in the magnetite field. This causes the early formed hematite to redissolve and be replaced by magnetite in the mineralogic sequence. Biotite and siderite appear as reaction products late in the reaction. The sequence of mineral products predicted to be stable include assemblages of hematite plus magnetite, and magnetite plus siderite. Hematite and siderite are not predicted to coexist in the model, and this mineral pair is seldom seen to coexist on a fine scale in nature.

Rerunning the same model using the solid solution option (Bourcier, 1985) in the most recent version of EQ3/6 produced similar results. The main difference was that the phases dolomite, magnesite and siderite were replaced by an ankeritic carbonate solid solution composed mainly of the iron and magnesium components. The carbonate solid solution composition fell in the range of measured ankerites in Algoman-type banded iron formations in western Australia (Klein and Gole, 1981).

It should be noted that the sequence of precipitate minerals predicted to form was relatively insensitive to the pH chosen for the acidic fluid. Similar results were obtained with the acidic component having an initial pH of 4.5 although smaller amounts of each of the iron minerals were produced.

Even at advanced stages of this reaction, only a small amount of the acid solution had been added. At a reaction progress equivalent to adding one gram of acid water to one

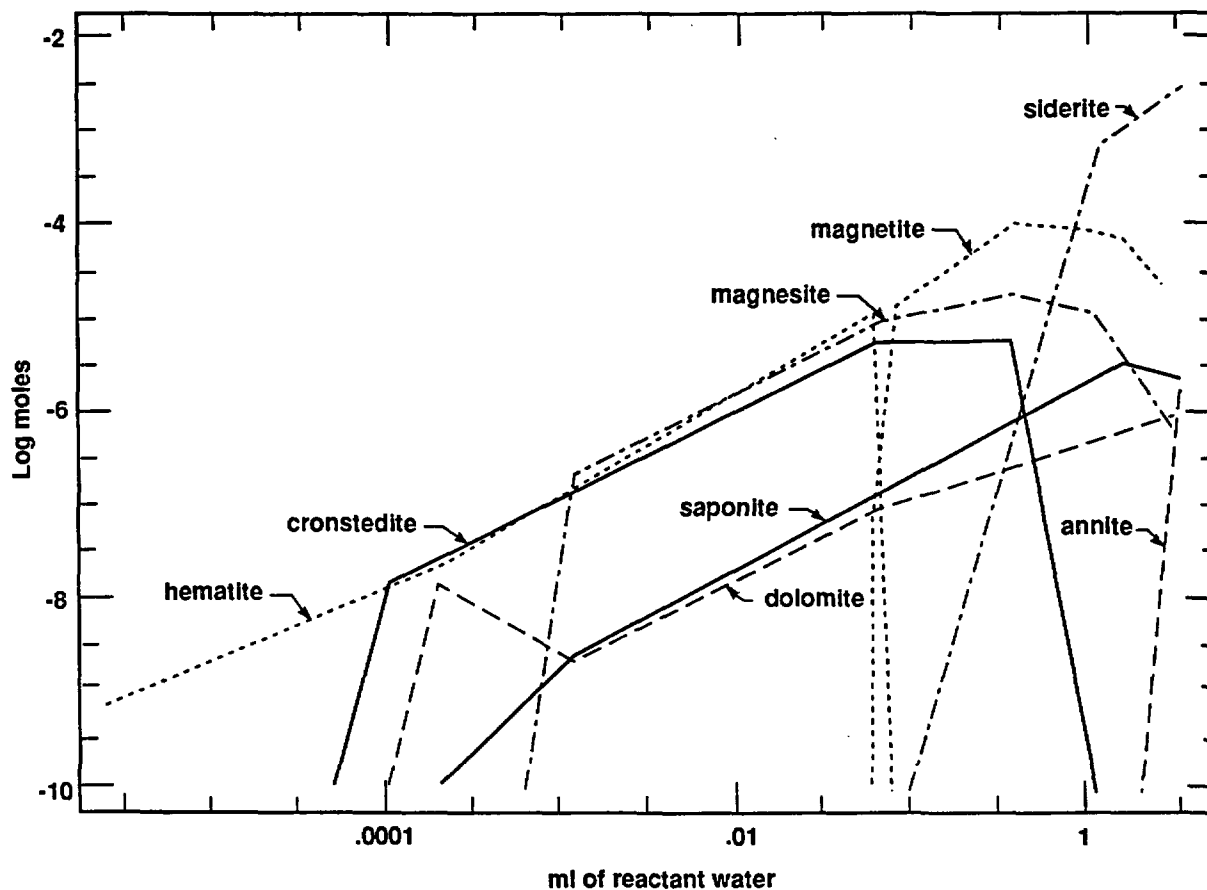


Figure 3. Sequence and amounts of mineral precipitates that form as a consequence of mixing 1 kilogram of Archean seawater with the reactant acidic iron-rich fluid using EQ6.

kilogram of ocean water, approximately 10^{-4} moles of magnetite was precipitated from the mixture. This would correspond to about 0.05 mm of iron-rich chemical sediment precipitating from a water column 100 meters deep. In addition, although rather severe changes took place in the sequence of mineral precipitants, only minor changes in major element concentrations and pH were evident. For example, the pH of the mixture dropped by only 0.1 pH units during the reaction, and magnesium, calcium, and bicarbonate activities were essentially unchanged.

These results can explain the major iron-rich accumulation of banded iron formations. The mechanism for producing the microbanding of iron and silica-rich layering often observed in banded iron formations has not yet been established. A possible mechanism for producing the microbanding that has been proposed is that of seasonal tem-

perature changes affecting iron and silica solubilities in so as to cause alternating deposition of iron and silica-rich layers. Initial results indicate that this mechanism is consistent with calculations of the solubility of iron in equilibrium with the assemblage hematite plus magnetite plus siderite in our hypothetical Archean ocean water. However, more modeling work is necessary to determine whether these temperature dependencies hold for the metastable precipitates such as amorphous iron hydroxides that likely control iron concentrations during precipitation in natural waters.

CONCLUSION

In conclusion, the results of our EQ3/6 modeling effort suggest that inorganic chemical processes can result in the precipitation of phases that closely mimic the mineralogy of the iron-rich portions of banded iron formations. Mixing of ocean water with an acidic fluid that has been equilibrated with a basalt or komatiite results in a pH change and subsequent precipitation of iron-rich chemical sediment. A more neutral fluid cannot dissolve a high enough concentration of iron to contribute significantly to the formation of iron-rich sediments.

The generation of acid waters responsible for banded iron formation may result either from terrestrial volcanic input into runoff or active seafloor vents in the banded iron formation basin. These mechanisms require no change in the oxygen fugacity of the local hydrosphere, and do not require biological activity.

Future efforts will be directed at more critically evaluating the predictions of our model, the sensitivity of model results to input constraints, and comparison of modeling results to detailed field observations.

REFERENCES

- Bourcier, W. L. (1985) Improvements in the Solid Solution Modeling Capabilities of the EQ3/6 Geochemical Code. UCID-20587, Lawrence Livermore National Laboratory, Livermore, CA.
- Bourcier, W. L., E.K. Gibson, Jr., and R. K. Kotra (1984) Characterization and gas analysis of fluid inclusions in barites from the Warrawoona Group, Northwestern Australia. In *Lunar and Planetary Science XV*, p. 82-83.
- Gross, G. A. (1980) A classification of iron formations based on depositional environments. *Canadian Min.* 18, p. 215-222.
- Holland, H.D. (1984) *The Chemical Evolution of the Atmosphere and Oceans*. Princeton University Press, Princeton, New Jersey.
- James, H. L. (1966) Chemistry of the iron-rich sedimentary rocks. In *Data of Geochemistry*, 6th ed., edited by M. Fleischer, chap. W. U.S. Geol. Surv. Prof. Paper 440-W. Washington, D.C.: U.S. Govt. Printing Office.

Klein, C., and M. J. Gole (1981) Mineralogy and petrology of parts of the Marra Mamba Iron Formation, Hamersley Basin, Western Australia. *Am. Mineralogist* **66**, p. 507-525.

Wolery, T. J. (1979) *Calculation of Chemical Equilibrium between Aqueous Solutions and Minerals: The EQ3/6 Software Package*, UCRL-52658, Lawrence Livermore National Laboratory, Livermore, CA.

Wolery, T. J. (1983) *EQ3NR A computer program for geochemical aqueous speciation-solubility calculations: User's guide and documentation*. UCRL-53414, Lawrence Livermore National Laboratory, Livermore, CA.

Database Development

THE NEA THERMOCHEMICAL DATA BASE

Hans Wanner
OECD Nuclear Energy Agency, NEA Data Bank
91191 Gif-sur-Yvette Cedex, France

ABSTRACT

The OECD Nuclear Energy Agency (NEA) has undertaken the development of a CODATA-compatible chemical thermodynamic data base for a number of elements of interest to various areas of nuclear technology, especially to radioactive waste management research areas such as the safety analysis of nuclear waste repositories. The development of this data base involves not only a compilation of all relevant published thermodynamic data, but also a detailed critical review and, finally, the selection of a "best data set" which will be recommended. Each review is being performed by a group of four to five internationally acknowledged experts in chemical thermodynamics. Each expert team has at least one member who is CODATA liaison, to assure compatibility with the CODATA tables. The first 10 elements to be reviewed are: Uranium, neptunium, plutonium, americium, technetium, cesium, strontium, radium, iodine and lead. The thermodynamic data being compiled and reviewed for each species include:

$\Delta_f G^0$	the standard Gibbs free energy of formation	(kJ·mol ⁻¹)
$\Delta_f H^0$	the standard enthalpy of formation	(kJ·mol ⁻¹)
S^0	the standard entropy of formation	(J·mol ⁻¹ ·K ⁻¹)
C_p	the standard heat capacity (at constant pressure)	(J·mol ⁻¹ ·K ⁻¹)

together with uncertainties and, if available, the temperature functions. Emphasis is placed on data for 298.15 K, 10⁵ Pa and zero ionic strength.

In addition, an interface program is being developed which makes it possible to extract specific data from the thermodynamic data base and to convert them into a form in which they are readable by geochemical modelling codes, such as PHREEQE, MINEQL and EQS/6, all of which are widely used geochemical reaction path computer codes. The data could also be made available in a form compatible with other computer codes if there is any demand from users.

INTRODUCTION

The development of an international chemical thermodynamic data base is a recent activity of the NEA Data Bank carried out jointly with the Division of Radiation Protection and Waste Management of NEA. It was initiated to account for the increasing need of such data for modelling purposes in safety analyses for nuclear waste repositories (MULLER 1985). Although a number of thermodynamic data compilations and reviews have been published in recent years, none of them can be used as a complete source data table to study the behaviour of radioelements in the environment. Some are of a general nature, not giving a comprehensive review of the data, whereas others—like the CODATA tables—

contain critically evaluated thermodynamic data, though not including elements which are of particular interest for nuclear waste management purposes. Consequently, most modelling groups supporting the performance assessment of radioactive waste disposal, have developed their own data base from the scientific literature. However, the geochemical modellers in different countries may not have the specialized experience in this field to distinguish between good and bad data appearing in the literature. Hence, these individual data bases often differ considerably from each other, especially in the data of the actinides. It is thus not surprising that radionuclide speciation and maximum solubilities calculated by different groups, with different geochemical computer codes and data, but for similar conditions, often turn out to differ by orders of magnitude. It has been recognized that the reason for these discrepancies are not the different codes but the different data bases. The needs for a comprehensive, internally consistent and internationally recognized chemical thermodynamic data base meeting the requirements of the modellers in nuclear fields have thus been acknowledged by a number of technical groups within the NEA Member countries. It is in response to this need that the NEA has undertaken its thermochemical data base development.

STRUCTURE OF THE DATA BASE SYSTEM

A schematic presentation of NEA's chemical thermodynamic data base development system is given in *Figure 1*. The development of the data base includes the compilation of all published thermodynamic data, a critical review of them, and the selection and publication of recommended data. Another important part of the data base system is the retrieval of data requested by users in different countries, as well as the conversion of them into forms compatible with the input formats of geochemical modelling codes, such as PHREEQE, MINEQL and EQ3/6. The heart of the system, the Thermodynamic Data Base (TDB), consists of a number of records, as shown in *Figure 2*. The DATA record comprises for each species fundamental thermodynamic data at 298.15 K and $10^5 Pa$:

- $\Delta_f G^0$ the standard Gibbs free energy of formation
- $\Delta_f H^0$ the standard enthalpy of formation
- S^0 the standard entropy of formation
- C_p the standard heat capacity (at constant pressure)

All data are compiled in SI units. As the parameters in this set vary as a function of temperature, provision has been made to include the compilation of empirical temperature functions of $\Delta_f G$, $\Delta_f H$, S and C_p data, as well as the temperature ranges over which they are valid. The ELEMENTS record contains all 104 elements of the periodic table, whereas the FORMULAE record contains the chemical formulas of each species compiled in the data base. The FORMEL record contains the elements and chemical formulas and acts as a link between the ELEMENTS and the FORMULAE record. The temperature coefficients are stored in the records G-COEF, H-COEF, S-COEF and C-COEF. The formulas are entered consistent with basic Hill notation to avoid ambiguity arising from the fact that both superscripts and subscripts have to be placed on the same line as the symbols of the elements. The formula is the actual entry point for data retrieval. A special sub-program allows to decode formulas, so that formation constants for species can be readily calculated for any components or master species.

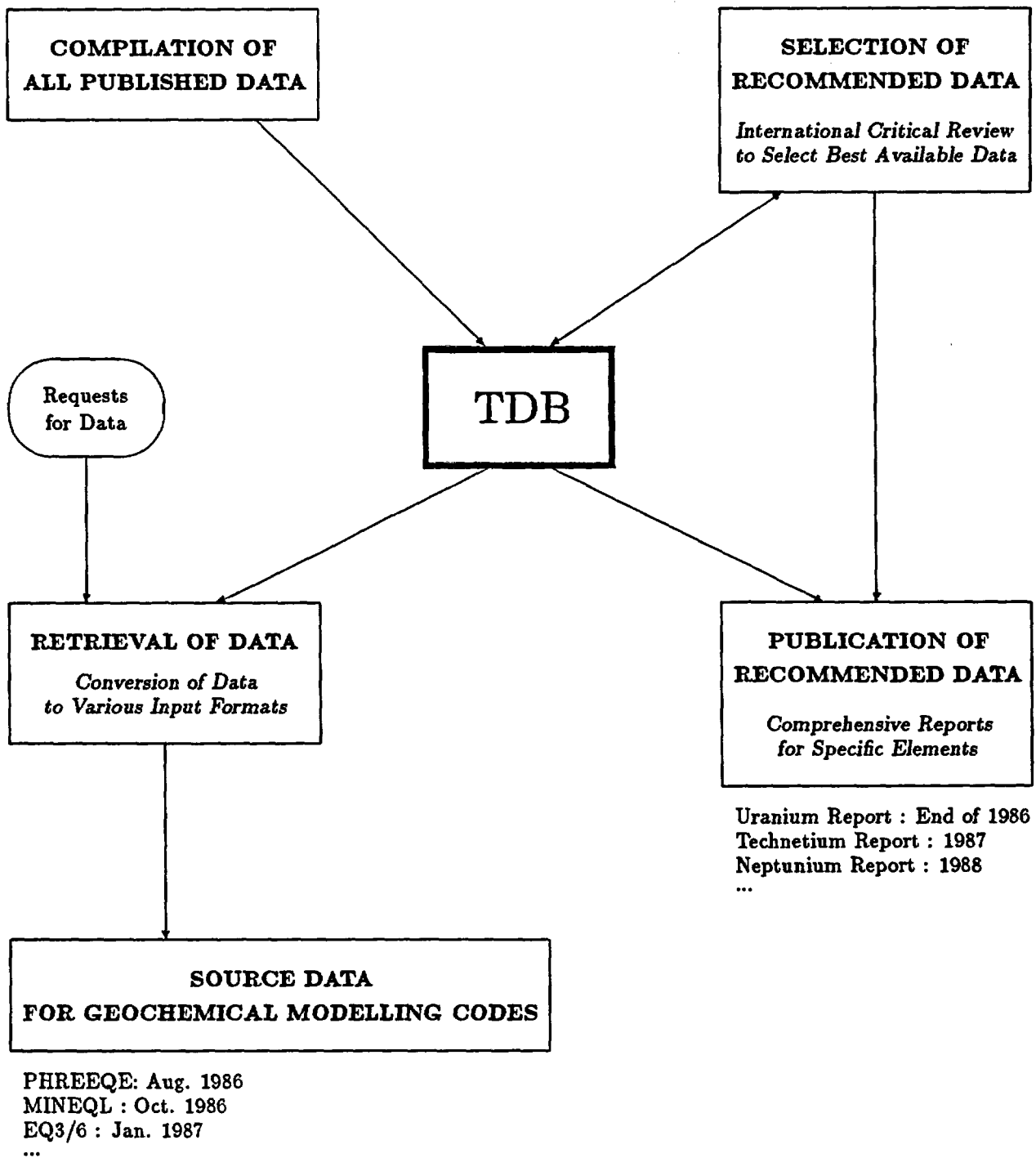


Figure 1: Structure of the NEA Thermochemical Data Base System

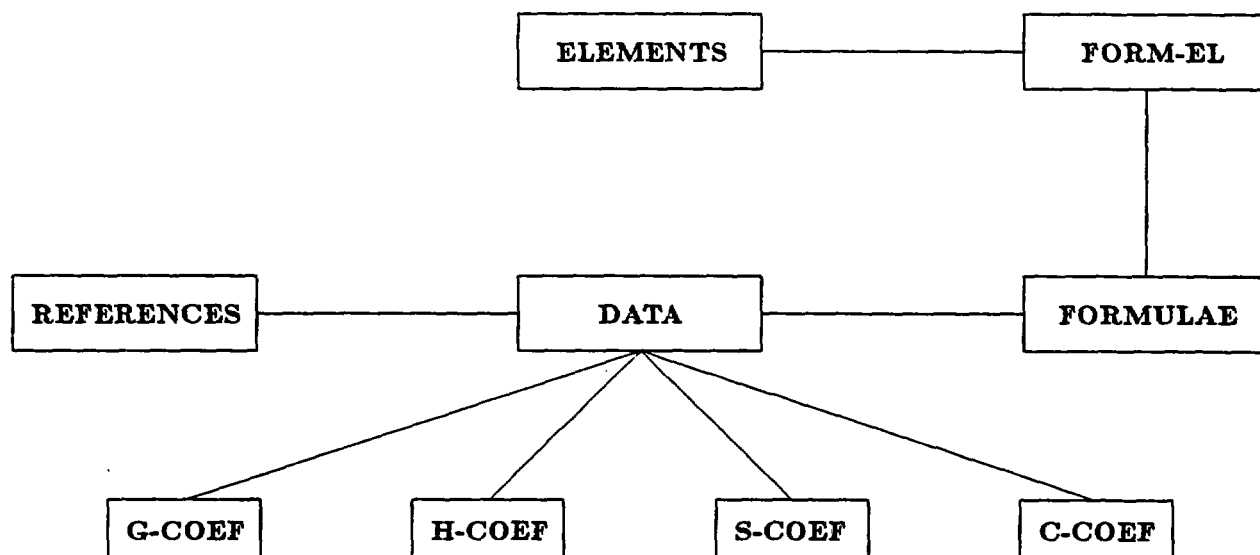


Figure 2: The Thermochemical Data Base Schema

CRITICAL INTERNATIONAL REVIEW OF THERMODYNAMIC DATA

Generally, all thermodynamic data published in the open literature are compiled by NEA. However, preference is given to data for 298.15 K and $10^5 Pa$ as well as unit activity (*i.e.*, zero intersolute interactions, $I=0 M$) in the reviewing process. The selection of best available data is done by a specialist team for each element considered. Data selections already made by other reviewer groups, *e.g.*, the CODATA and IAEA thermodynamic data tables (CODATA 1978 and IAEA), are accepted as selected data in the NEA Thermochemical Data Base. NEA specialist teams have been established for the following elements:

uranium
 neptunium
 plutonium
 americium
 technetium
 cesium¹
 strontium¹
 radium
 iodine¹
 lead¹

¹The expert team for this element is only partly established.

Each team consists of four to five internationally recognized experts in chemical thermodynamics. One member of each team is selected in consultation with the CODATA Task Group on Chemical Thermodynamic Tables and has the special responsibility to assure that the review is performed consistent with CODATA procedures and recommendations. The critical reviewing work of each team is coordinated by the NEA Secretariat. A detailed description of the critical reviewing procedure is given elsewhere (MULLER 1985). The resulting selected data set for each element considered, including uncertainties as well as data found and not selected, will be published by the NEA under the authorship of the specialist teams. These reports will also contain detailed discussions of the scientific rationale used in the reviewing procedure. The first review report, the uranium volume, is planned before the end of 1986. The uranium publication will be followed by one on technetium, and then by a neptunium volume.

DATA RETRIEVAL

The retrieval of compiled data and selected auxiliary data is an important routine procedure in the critical review of thermodynamic data. On the other hand, the users of thermodynamic data, *e.g.*, the geochemical modellers, mostly do not use the fundamental Gibbs energy data for each species they consider in their calculations, but rather the formation constants from components or master species. Most geochemical computer codes actually require formation constants, *log K values*, as source data, rather than Gibbs energies, ΔG^0 . For this reason, an interface program has been developed which allows to extract thermodynamic data from the TDB and to convert them into a format in which they can be directly used as source data for the code PHREEQE. The master species can be freely chosen by the requester of data, and the retrieved data can be sent on magnetic tape. A similar version of this interface program is under development for the code MINEQL, and a version for EQ3/6 is planned. Modellers requesting thermodynamic data from the NEA are advised to specify the elements or particular species for which data are desired, as well as the master species of the element.

REFERENCES

- CODATA (1978), *Recommended Key Values for Thermodynamics 1977*, Committee on Data for Science and Technology (CODATA) Bulletin 28, Paris: International Council for Scientific Unions, 16p.
- IAEA, *The Chemical Thermodynamics of Actinide Elements and Compounds*, (OETTING F.L., ed.) 14 Parts, International Atomic Energy Agency, Vienna, in press.
- MULLER A.B. (1985), *International Chemical Thermodynamic Data Base for Nuclear Applications*, Radio. Waste Manage. Nucl. Fuel Cycle 6(2), 131-141.

EQ3/6 DATA BASE - ONGOING DEVELOPMENT

AT

LAWRENCE LIVERMORE NATIONAL LABORATORY

Joan M. Delany

Earth Sciences Department
Lawrence Livermore National Laboratory
Livermore, CA 94550

Abstract

The EQ3/6 Data Base has been revised and enhanced to meet the maintenance needs of a large continuously evolving data base. Within the last year a new data-base structure has been developed to manage the manipulation, basic data entry, import/export, retrieval and display features. The data management approach includes visual simplicity, on-line documentation, information management and controls to limit user error, ensure data protection and proper documentation of thermodynamic values and their sources.

Introduction

The goal of this project is to develop a software product responsive to the Scientific and Engineering Software QA Procedure of the Nevada Nuclear Waste Storage Investigations Project. (Wolery, 1988)

The new data-base structure is composed of a master data maintenance program (MDAP) that has been developed specifically to accept, reorganize and report thermodynamic data in the EQ3/6 format. This code is menu driven and includes both dynamic and typed command strategies. Support functions such as automatic updating and data reporting capabilities are also available. MDAP runs attached to a newly created master data file, MDAR. MDAR was designed and constructed to be a data holding bank and records file that can meet the needs of all software quality assurance requirements that are expected to be imposed on the EQ3/6 Task.

Data evaluation has begun on a single element basis for existing values. Recently completed revisions of thermodynamic data for many aqueous and solid species of Am, U, and Pu has demonstrated the need for an EQ3/6 experimental data-base activity. (For example see Kerrisk and Silva, 1988). As a result, a laboratory program has been started at LLNL to make necessary experimental measurements and to correct gaps and/or conflicts in the master data file. This activity commenced during the last half of FY86, and is planned over a 5-year period.

Data Base Structure

The upcoming release of the EQ3/6 Software Package (version 3245) will contain several pre-processor codes and data files. A schematic of the data base codes and data files shown in Figure 1. The master or MCRT Thermodynamic Data File exists in both direct access (MDAR) and sequential (MDAS) format. All data maintenance is done by MDAP, a data maintenance code. MDAR also runs attached to MCRT, a data pre-processor code that has been part of the EQ3/6 software package since its inception. Extensive modifications and restructuring have been done to bring MCRT into active status with the new master data file format. MCRT output files are now also completely compatible with DATA0 format. DATA0, is the EQ3/6 main thermodynamic data file. A new pre-processor code, DARP, is used to manipulate and maintain the DATA0 file. DARP is a companion code to MDAP and runs in a similar menu-driven environment. MCRT is now designed to process all DATA0 species in a single run, and DARP can upload this output to the DATA0 file also with a single command. The pre-processor codes are described in more detail below. (Also see Wolery et al., 1988).

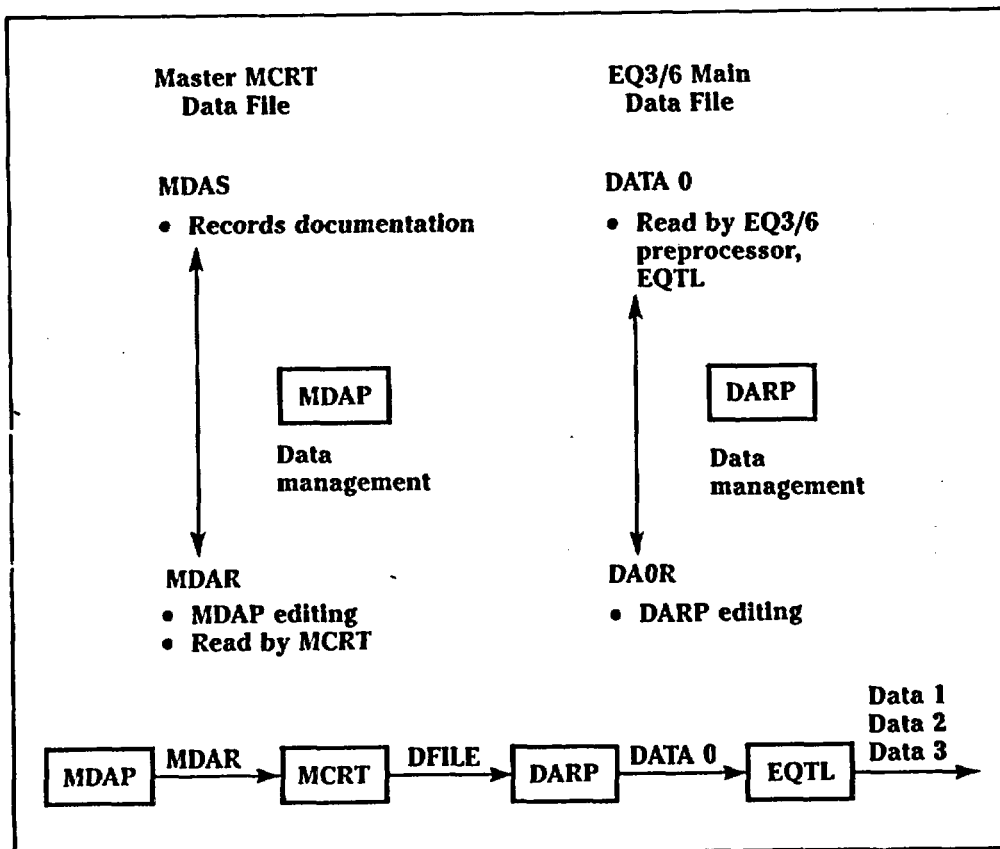


Figure 1. Architecture of the EQ3/6 Data Base.

MDAP is a menu-driven data management code. The program boots to a main menu of self-explanatory choices that include import, retrieval, replace, and display options to maintain the archival data base of thermodynamic data. Each menu option displays a submenu of additional options. User interface for data entry and revision has been reduced to editing individual MDAR species blocks. The need for multiple files to be opened and edited has been eliminated. All data import and export functions accept ASCII files. The MCRT code has been restructured and currently runs attached to the master data file. The current default provision is to run all species except those explicitly designated by an internal flag in each species block.

MCRT is a thermodynamic code that is run attached to the master data file, MDAR. It is used to identify active species and calculate logK values as a function of temperature. DFILE output can be directly inserted into DATAO through the DARP replace option. The MCRT file structure has been changed, MDELEM and REAC have been eliminated as individual files. The REAC file has been interspersed into MDAR. All DATAO reactions are now located within the appropriate species block. MDELEM has been incorporated into MDAR as a single elements block. All element data can be updated in MDAR and replaced into the header portion of DATAO through MCRT DFILE output.

A second data maintenance program, DARP, has been developed to allow the user to search, view and update the thermodynamic data file, DATAO. This menu-driven code was written as a companion code to MDAR, but, yet it does not contain many of the enhanced support functions available in MDAR. DARP runs attached to the thermodynamic data file in direct access format, DAOR. Output from the MCRT code in DFILE format can be used as a replace file to update the entire DATAO file. Structural changes made to the thermodynamic data file, DATAO and the subsequent EQ3/6 data files, DATA1, DATA2, and DATA3, have been relatively minor.

Work in Progress

- A customized data entry form is being constructed. This capability will supersede standard ASCII file format and local editing procedures currently used for adding new species to MDAR. The interactive format will provide the user with default values, typed command strategy, and calculated fields where appropriate. This procedure will help eliminate data-editing errors and protect accurate data input.
- Data protection mechanisms are being developed to provide the necessary security for a multi-user data base. Certain core subsets will be protected. All data-base users will be assigned valid passwords. The password utility will provide user interface on three levels; (1) species data and references can be displayed or

extracted, (2) experienced users can modify thermodynamic values and add or suppress species from the master data file, (3) reserved for the data base administrator, to revise the structure of the data base and control access to security and password utilities.

- All CODATA recommended key values are being adopted. (CODATA, 1978) This change will coincide with a conversion to SI units. This data set will protected as a key subset. In early 1987, the EQ3/6 Data Base will be fully CODATA compatible.
- A conversion to SI units will be made for the entire EQ3/6 software package. A utility option will be available in MDAR to allow the user to generate a copy of the master data file thermochemical calories for literature comparisons.
- Thermodynamic data for Np solids and aqueous species are being reviewed and incorporated into MDAR. Major emphasis is being given to species that may be significant in geochemical applications of radioactive waste disposal.
- The rock-forming minerals data set is under review for revision. The existing thermodynamic data includes the SUPCRT data base for rock-forming minerals (Helgesen et al., 1978). Current plans are to (1) update all minerals for which new experimental data has been reported; (2) expand the heat-capacity fit equation to five parameters.

Laboratory Experiments

The goal of the EQ3/6 Data Base Program is the thermodynamic characterization of a complete set of solution species and solid phases. Measurements will be made as a function of temperature, ionic and oxidation state as required. Our initial review of the thermodynamic data for Am, U, and Pu has led to the following proposed research FY86-88. (Silva and Delany, 1986)

Americium Laboratory Measurements

This work is being done as a joint effort with Lawrence Berkeley Laboratory. The free energy of the solubility reactions of amorphous and crystalline $\text{Am}(\text{OH})_3$ will be determined. Also under investigation is the nature and characterization of the solid phase that forms in solutions with pH values greater than 9. We are investigating the carbonate complexation of Am^{+++} to verify the existence of bicarbonate and hydroxycarbonate complexes. If possible, formation constants will be also obtained.

Laser-Induced Pulsed Photo-Acoustic Spectroscopy

A pulsed photo-acoustic (PA) spectroscopy system using a Nd-YAG pumped dye laser and associated computer-control instrumentation is being developed to

investigate the capabilities and sensitivity limitations for characterizing waste radionuclide species in aqueous solutions. A completed system would allow detection of concentrations in the submicromolar region.

Plutonium Laboratory Measurements

The initial phase of this work involves determining the hydrolysis and carbonate complex formation constants for PuO_2^+ . Synthesis, characterization and solubility product constants will also be determined for $\text{PuO}_2(\text{OH})_2(\text{s})$ and $\text{PuO}_2(\text{OH})(\text{am})$ under this activity.

Uranium Laboratory Measurements

Synthesis, characterization and the determination of the free energies for the solubility reactions of soddyite, uranophane, na-boltwoodite, Ca-haiweeite and schoepite are underway. Solubility measurements are to begin in early FY87.

Calorimetric Measurements

This work is being done as a sub-contract to ANL. Facilities are available to yield complete thermodynamic properties of material from 0 to 1500 K. Individual techniques include: low-temperature calorimetry, enthalpy of solution or reaction calorimetry, fluorine- and oxygen-bomb calorimetry and high-temperature drop calorimetry. Mineral samples of soddyite, uranophane, and clinoptilolite will be measured.

References

- WOLERY, T.J. (1988) EQ3/6 - Status and Future Development. Proceedings from the workshop on Geochemical Modeling; September 14-17, 1986, Fallen Leaf Lake, CA (this volume).
- KERRISK, J.F. and SILVA, R.J. (1987) A Consistent Set of Thermodynamic Constants for Americium(III) Species with Hydroxyl and Carbonate. Proceedings from the workshop on Geochemical Modeling; September 14-17, 1986, Fallen Leaf Lake, CA (this volume).
- JACKSON, K.J., WOLERY, T.J., BOURCIER, W.L., DELANY, J.M., MOORE, R.M., CLINNICK, M.L., and LUNDEEN, S.R., (1988) MCRT User's Guide and Documentation. UCRL report (in preparation). Lawrence Livermore National Laboratory, Livermore, CA.
- CODATA Task Group on Key Values for Thermodynamics (1978) Recommended Key Values for Thermodynamics, 1977, J. Chem. Thermo. 10, 903-906.
- HELGESON, H.C., DELANY, J.M., NESBITT, H.W., and BIRD, D.K., (1978) "Summary & Critique of the Thermodynamic Properties of Rock Forming Minerals," Amer. J. Sci., 278-a, p. 229.
- SILVA, R. and DELANY, J.M. (1986) "The Chemical Behavior of Waste Radionuclides Under Ground Water Conditions" Annual Report of Nuclear Chemistry Division, UCAR-10062-86, p.3-21.

A CONSISTENT SET OF THERMODYNAMIC CONSTANTS FOR AMERICIUM (III) SPECIES WITH HYDROXYL AND CARBONATE*

Jerry F. Kerrisk and Robert J. Silva
Los Alamos National Laboratory, Los Alamos, NM 87545 USA
Lawrence Livermore National Laboratory, Livermore, CA 94550 USA

Abstract

A consistent set of thermodynamic constants for aqueous species and compounds of Am(III) with hydroxyl and carbonate ligands has been developed. The procedure used to develop these constants involved establishing a value for one formation constant at a time in a sequential order, starting with the hydrolysis products and hydroxide solids, and then proceeding to carbonate species. The EQ3NR chemical-equilibrium model was used to test the constants developed. These constants are consistent with most of the experimental data that form their basis; however, considerable uncertainty still exists in some aspects of the Am(III) data.

Introduction

Americium is one of the major contributors to the radioactivity of high-level waste that will eventually be stored in geologic repositories. Under natural conditions, only one oxidation state of americium should exist, Am(III). To model the transport of americium in water, information is needed about aqueous species and solids of Am(III) that exist under repository conditions. Although numerous experimental studies have been done that contribute information about aqueous species and solids of americium, these data must be interpreted within a theoretical framework to assure that the data are internally consistent and to allow predictions under conditions that differ from the experiments. Thermodynamics provides the best framework for these data, as long as it is applicable, that is under equilibrium conditions.

This paper describes the development of a consistent set of thermodynamic constants for the formation of Am(III) complexes and solids with hydroxyl and carbonate ions. These anions are important because they form strong complexes with Am(III) and are present in most natural waters. Existing experimental data were used for this analysis. Because of disagreements among the results of some experiments, a set of thermodynamic constants that was consistent with all of the experimental data could not be developed.

Existing Experimental Data

Experimental data that form the basis for the constants developed here include distribution coefficients between organic and aqueous phases as a function of pH and carbonate content, potentiometric measurements as a function of pH, and solubility measurements as a function of pH and carbonate content.

*This work was supported by the Nevada Nuclear Waste Storage Investigation Project.

Experiments designed to determine hydrolysis constants are generally done in a neutral (noncomplexing) electrolyte to limit complex formation to hydrolysis products only. Two measurements of the distribution of Am(III) between organic and aqueous phases were used here. Lundqvist (1982) measured distribution coefficients in a perchlorate medium ($\mu = 1$ M) at pH 4 to 9 (μ is ionic strength and M is concentration in molar units). Caceci and Choppin (1983) measured distribution coefficients in a chloride medium ($\mu = 0.7$ M) at pH 5.9 and 8.1 as a function of oxalate content and determined the first hydrolysis constant from data for oxalate complexes using competing reactions. Another measurement of Am(III) distribution between organic and aqueous phases (Desire et al. 1969) was considered, but not included in the analysis. Data from two potentiometric titrations were also used. Nair et al. (1982) titrated Am(III) in perchlorate ($\mu = 1$ M) from pH 4 to 7. Edelstein et al. (1983) titrated two chemical analogs of Am(III) [Cm(III) and Nd(III)] in a chloride medium ($\mu = 0.1$ M). Hydrolysis constants and solubility-product constants can also be determined from solubility measurements. Four sets of solubility data for Am(III) in neutral electrolytes were considered. They include the measurements of Silva (1982) in perchlorate ($\mu = 0.1$ M) at pH 7 to 9.5; Rai et al. (1983) in chloride ($\mu = \sim 0.01$) at pH 7 to 13; Bernkopf and Kim (1984) in perchlorate ($\mu = 0.1$ to 0.3) at pH 6.5 to 13; and Nitsche and Edelstein (1985) in perchlorate ($\mu = 0.1$ M) at pH 7. Data for crystalline $\text{Am}(\text{OH})_3(\text{c})$ and amorphous $\text{Am}(\text{OH})_3(\text{am})$ hydroxide solids were reported. Significant differences among these results are apparent in a number of cases; choices made for this analysis are discussed in the following section.

Four sets of experimental data were used to determine constants for carbonate species with Am(III). Lundqvist (1982) measured Am(III) distribution between organic and aqueous phases in perchlorate ($\mu = 1$ M) at pH 4 to 7.5 under 0.1 and 1 atm CO_2 pressure. Bidoglio (1982) measured distribution coefficients in perchlorate ($\mu = 0.2$ M) at pH 8 to 9 and fixed total carbonate concentrations (1 to 6 mM); equilibrium CO_2 pressures were calculated to be 0.0001 to 0.001 atm. Silva and Nitsche (1983) measured the solubility of Am(III) in a carbonate solution under 0.008 atm CO_2 pressure at pH 6 ($\mu = 0.1$ M in perchlorate) and identified $\text{AmOHCO}_3(\text{c})$ as the solid. Bernkopf and Kim (1984) measured Am(III) solubility in carbonate solutions controlled by a CO_2 pressure of 0.00032 atm ($\mu = 0.1$ to 0.3 M in perchlorate) at pH 6 to 10.

Procedure

A variety of procedures can be used to determine one or more formation constants from a set of experimental data (Rossotti and Rossotti 1961). In the situation described here, where a large variety of data from different kinds of experiments was used, the procedure of employing a least-squares method or some equivalent technique to determine all the constants of a model in a single step did not seem practical. Instead, we tried to determine formation constants for one species at a time, in each case using only the experimental data that are sensitive to that species and previously determined formation constants. The EQ3NR chemical equilibrium model (Wolery 1983) was used to calculate experimentally observable parameters such as the distribution of Am(III) between organic and aqueous phases or the solubility of Am(III) under conditions applicable to the various experiments; these calculated values were compared with experimental data as a means of testing the formation constants.

The process started with the first hydrolysis constant of Am(III), which can be determined in a neutral electrolyte in a pH range where other hydrolysis products are not present in significant quantities. The formation constant for AmOH^{2+} was taken as the average of values reported by Lundqvist (1982), Caceci and Choppin (1983), Nair et al. (1982), and Edelstein et al. (1983), corrected to $\mu = 0$. The resulting logK is 7.41 (see Table I). EQ3NR calculations of the distribution experiments were done by defining fictitious species to simulate Am(III) in an organic phase and by estimating a logK for these species from the experimental distribution coefficients. Calculations of Am(III) distribution and average ligand number (for the potentiometric titrations) showed good agreement with the data of Lundqvist (1982) and Caceci and Choppin (1983), but underpredicted the average ligand number of Nair et al. (1982) over the pH range of 4 to 8.

Next, the availability of solubility data for $\text{Am(OH)}_3(\text{c})$ and $\text{Am(OH)}_3(\text{am})$ at pH 7 allowed solubility product constants for these solids to be determined in a pH range in which the first hydrolysis constant is the only important complex. Using the measured solubilities of Silva (1982) for $\text{Am(OH)}_3(\text{c})$ at pH 7, and of Rai et al. (1983) and Nitsche and Edelstein (1985) for $\text{Am(OH)}_3(\text{am})$ at pH 7, values of $\log K(\mu = 0)$ for the formation of these solids were calculated to be 26.60 and 25.10, respectively (see Table I).

Solubility data for $\text{Am(OH)}_3(\text{c})$ and $\text{Am(OH)}_3(\text{am})$ show that the solubility becomes constant for sufficiently high pH (see Fig. 1). This indicates that Am(OH)_3° is an important aqueous species but that Am(OH)_4^- is not present in significant amounts because formation of Am(OH)_4^- would increase solubility at high pH. Solubility data at high pH for either solid could be used to determine the formation constant of Am(OH)_3° , which is the only aqueous species present in significant quantity in the pH range where the solubility is constant; we used the solubility of $\text{Am(OH)}_3(\text{c})$ at pH 9.5 (Silva 1982) to determine logK for formation of Am(OH)_3° as 18.20 at $\mu = 0$ (see Table I).

TABLE I
FORMATION CONSTANTS OF Am(III) SPECIES AT ZERO IONIC STRENGTH

Reaction	logK
$\text{Am}^{3+} + \text{OH}^- = \text{AmOH}^{2+}$	7.41
$\text{Am}^{3+} + 2\text{OH}^- = \text{Am(OH)}_2^+$	≤ 12.00
$\text{Am}^{3+} + 3\text{OH}^- = \text{Am(OH)}_3^\circ$	18.20
$\text{Am}^{3+} + 3\text{OH}^- = \text{Am(OH)}_3(\text{c})$	26.60
$\text{Am}^{3+} + 3\text{OH}^- = \text{Am(OH)}_3(\text{am})$	25.10
$\text{Am}^{3+} + \text{CO}_3^{2-} = \text{AmCO}_3^+$	8.26
$\text{Am}^{3+} + 2\text{CO}_3^{2-} = \text{Am(CO}_3)_2^-$	13.30
$\text{Am}^{3+} + 3\text{CO}_3^{2-} = \text{Am(CO}_3)_3^{3-}$	14.95
$\text{Am}^{3+} + \text{OH}^- + \text{CO}_3^{2-} = \text{AmOHCO}_3(\text{c})$	22.60

The formation constant for the second hydrolysis product, $\text{Am}(\text{OH})_2^+$, was determined by comparing the calculated solubilities with measurements taken by Rai et al. (1983) and Silva (1982) in the pH range of 8 to 9. This gave a value of $\log K$ for the formation of $\text{Am}(\text{OH})_2^+$ as ≤ 12.00 at $\mu = 0$ (see Table I).

Figure 1 shows the calculated solubility of $\text{Am}(\text{OH})_3(\text{c})$ and $\text{Am}(\text{OH})_3(\text{am})$ based on these constants (using EQ3NR) compared with experimental data. The data of Rai et al. (1983) are for amorphous material at low pH and crystalline at higher pH. Below pH 9.5, generally good agreement exists among the experiment comparisons, other than Bernkopf and Kim (1984), and between calculated and observed solubilities. Above pH 9.5, the calculated curve for crystalline material is about two orders of magnitude above that for the data from Rai et al. (1983). The data of Bernkopf and Kim (1984) are for amorphous material but have a lower solubility than either the crystalline or amorphous solids of other experiments. These data were not used in this analysis because they disagree with the generally consistent data of other experimenters and because the solid phase used in their work was not identified. Figure 2 shows a plot of the distribution of aqueous species in a neutral electrolyte calculated using the data in Table I.

After formation constants for Am(III) species in a neutral electrolyte were established, species with carbonate were considered next. The species AmCO_3^+ and $\text{Am}(\text{CO}_3)_2^-$ were considered first because they were identified by

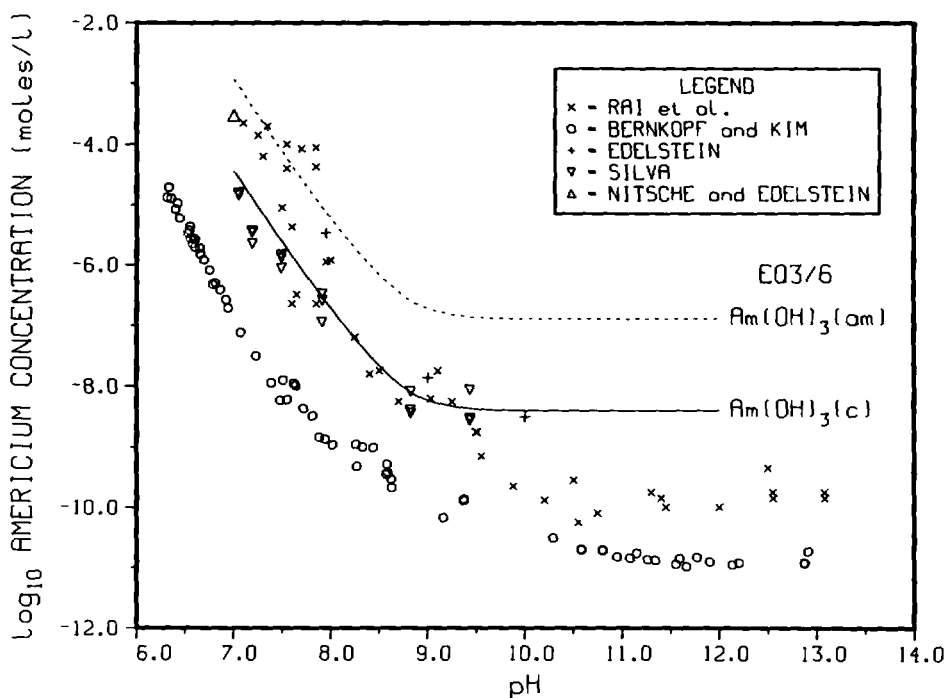


Fig. 1. Am(III) solubility in a neutral electrolyte at 25°C.

Lundqvist (1982) as being present under the conditions of his experiments; $\text{Am}(\text{CO}_3)_2^-$ was also identified by Bidoglio (1982) as the most important carbonate complex in his experiments. These species have also been identified for trivalent rare earths (Ferri et al. 1983; Lundqvist 1982). The value of $\log K$ for the formation of AmCO_3^+ was taken from Lundqvist (1982) and corrected to $\mu = 0$, giving a corrected value of 8.26; the value for $\text{Am}(\text{CO}_3)_2^-$ was taken as an average of the values reported by Lundqvist (1982) and Bidoglio (1982), corrected to $\mu = 0$, to give 13.30 (see Table I). Comparisons of experimental data with the calculated (with EQ3NR) distribution of Am(III) between organic and aqueous phases under the conditions of these two experiments gave generally good agreement using only these two carbonate species; it was not necessary to include the bicarbonate or hydroxy-carbonate complexes postulated by Bidoglio (1982) and by Bernkopf and Kim (1984).

These two Am(III)-carbonate complexes and the solubility data of Silva and Nitsche (1983) at pH 6 were used to calculate $\log K$ for $\text{AmOHCO}_3(\text{c})$ at $\mu = 0$, giving a value of 22.60 (see Table I). Because these measurements were made at only one pH, the one used to determine the formation constant, further comparisons between calculated and measured data could not be made. However, the solubility measurements of Bernkopf and Kim (1984) in carbonate solution also involved $\text{AmOHCO}_3(\text{c})$. EQ3NR calculations of the solubility of $\text{AmOHCO}_3(\text{c})$ under the conditions of the Bernkopf and Kim (1984) experiment compared well with measurements up to about pH 8; above that pH however, the calculated solubility dropped below the measured data. By analogy with rare-earth carbonates, the presence of $\text{Am}(\text{CO}_3)_3^{3-}$ was postulated (Ferri et al. 1983), and a value of $\log K$ of 14.95 for formation of this species at

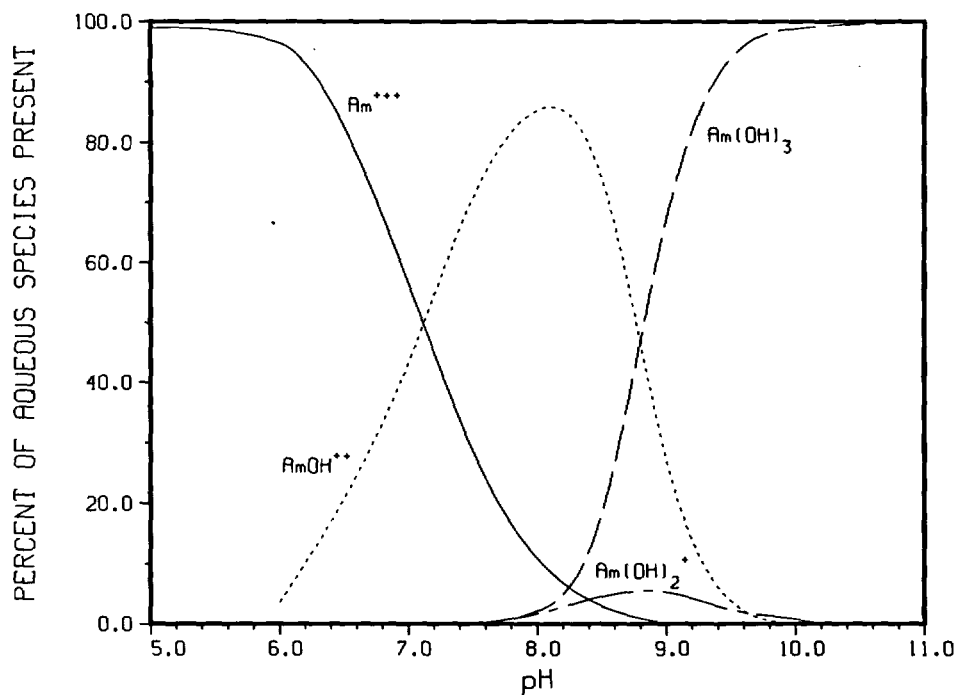


Fig. 2. Am(III) speciation in a neutral electrolyte at 25°C.

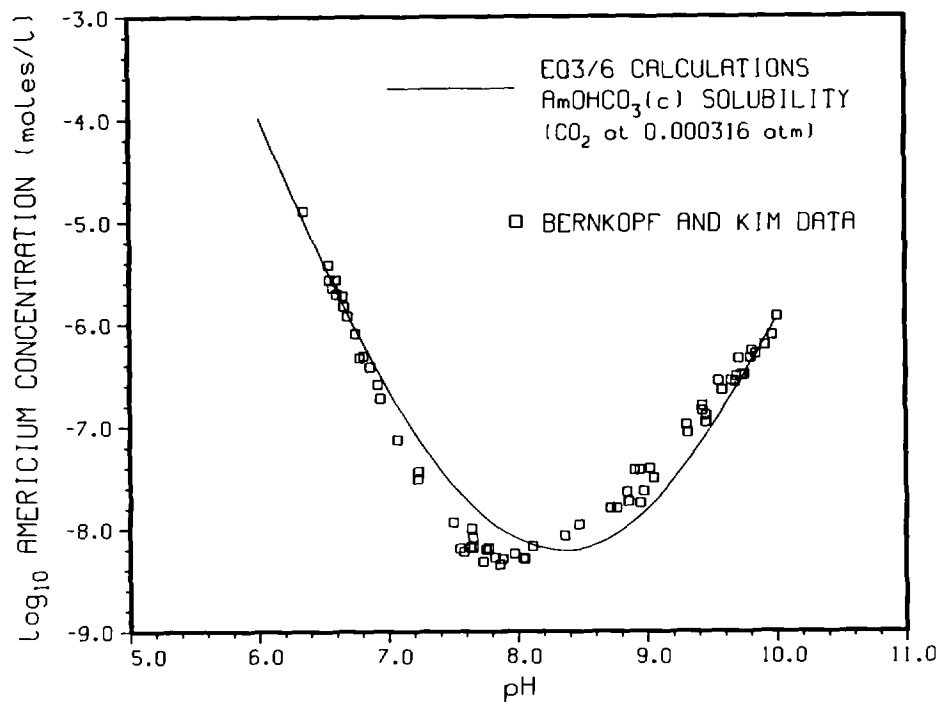


Fig. 3. Am(III) solubility in a carbonate solution with 0.000316 atm CO_2 pressure.

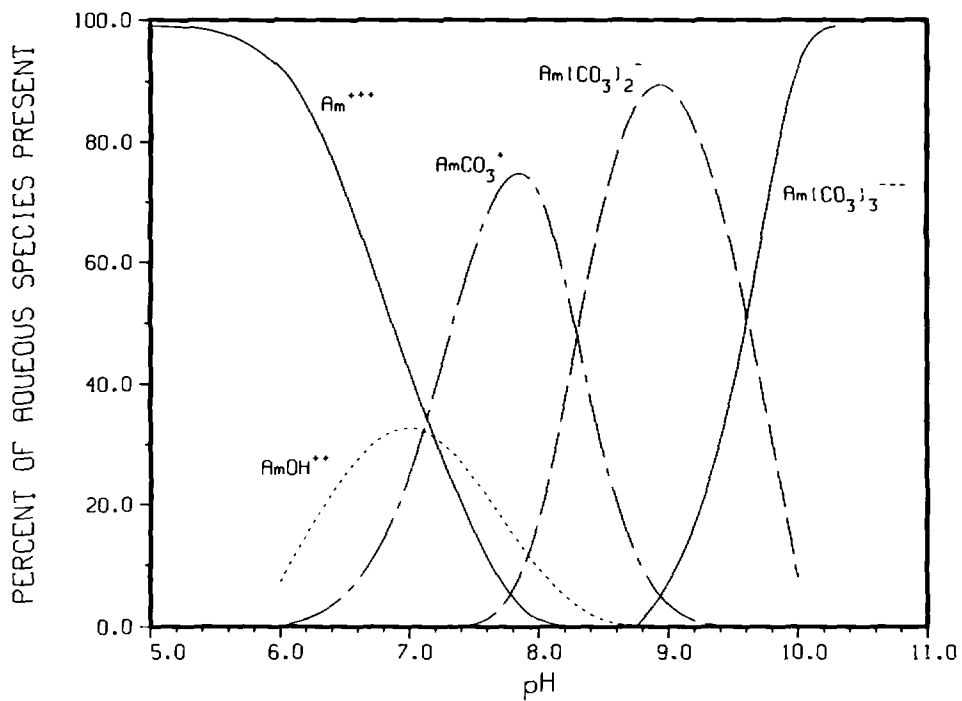


Fig. 4. Am(III) speciation in a carbonate solution with 0.000316 atm CO_2 pressure.

$\mu = 0$ was determined (see Table I). Use of this species along with the other two carbonate complexes gave generally good agreement between the calculated solubility and the measured data of Bernkopf and Kim (1984) (see Fig. 3). Figure 4 shows a distribution of species under the conditions of the Bernkopf and Kim (1984) solubility experiments; it differs significantly from that proposed by Bernkopf and Kim (1984). Only one hydrolysis product, AmOH^{2+} , is present in significant quantities; the importance of this species would be reduced at higher carbonate contents (higher equilibrium CO_2 pressures).

Problem Areas

Considerable uncertainty still exists in some aspects of Am(III) chemistry under natural conditions. One of the major areas of uncertainty is caused by disagreement among various experimenters about the identity of aqueous species present under the conditions of their experiments. Kerrisk (1984) pointed out that Lundqvist (1982) should have seen evidence of some of the Am(III) carbonate species reported by Bidoglio (1982); and likewise, Bidoglio (1982) should have seen some of the species reported by Lundqvist (1982). This situation occurs because the species used in these models have not been identified by some technique such as spectroscopy, but are inferred from the data. This situation will not be remedied until higher-sensitivity instruments, such as a photoacoustic spectrometer, are used to identify aqueous species.

A second problem area results from the disagreement among the various experiments about the solubility of Am(III) in a neutral electrolyte. Disagreements exist over the entire pH range (7 to 13) of the measurements (see Fig. 1). Part or all of these disagreements may have been caused by the different solid species controlling solubility in these experiments. Bernkopf and Kim (1984) did not report any identification of their solid: only a preparation technique. Silva (1982) identified his starting material as $\text{Am}(\text{OH})_3(\text{c})$ using x-ray data, but only visually compared the final solid to the starting material. Rai et al. (1983) saw evidence of an amorphous solid (probably $\text{Am}(\text{OH})_3(\text{am})$) at low pH and $\text{Am}(\text{OH})_3(\text{c})$ at high pH in the final material. Plots of the solubility data as a function of pH, taken from the experiments of Bernkopf and Kim (1984) and of Rai et al. (1983), show a break around pH 8.5 to 9.5, with a drop to lower solubilities at higher pH; this may be a signal of a change in the identity of the solid controlling solubility. This problem requires additional experimental work, giving strong emphasis to the identification of the solid phase or phases that control solubility under these conditions.

A final problem affecting the results reported here is the ionic-strength corrections to measured $\log K$ values. Many of the experiments discussed here were done at $\mu = 1$ M; others ranged from $\mu = 0.7$ down to $\mu < 0.1$. Thermodynamic models such as EQ3NR use $\log K$ values at $\mu = 0$ and provide their own ionic-strength corrections. Experimentally derived activity coefficients were used to correct the measured values of $\log K$ to $\mu = 0$ (Robinson and Stokes 1959; Pitzer and Peiper 1980; Khoo et al. 1981; and Peiper and Pitzer 1982). Because of the high charge on Am^{3+} , activity coefficients of about 0.02 apply for this species at $\mu = 1$ M. In comparing these activity coefficients with the values calculated by EQ3NR, the EQ3NR activity coefficients were found to be significantly different in a number of cases. For the EQ3NR

calculations discussed here, values of the β parameter used in the activity-coefficient calculation (Wolery 1983) were modified so that the calculated activity coefficients were comparable to experimentally derived values. This involved changing β as follows: from 8.0 Å to 5.0 Å for Am^{3+} , from 9.0 Å to 5.0 Å for H^+ , from 4.5 Å to 3.5 Å for CO_3^{2-} , from 4.5 Å to 4.0 Å for HCO_3^- , and from 3.0 Å to 4.0 Å for Cl^- . This type of correction, which is needed to adjust data measured over a range of ionic strengths to some common value, adds additional uncertainty to the results.

References

- BERNKOPF, M. F. and J. I. KIM (1984) Hydrolysereaktionen und Karbonatkomplexierung von Dreiwertigem Americium im Natürlichen Aquatischen System. Institut für Radiochemie der Technischen Universität report RCM-02884, München; see also KIM, J. I., M. BERNKOPF, C. LIERSE, and F. KOPPOLD (1983a) Hydrolysis Reactions of Am(III) and Pu(VI) Ions in Near Neutral Solutions. Paper presented at the 185th American Chemical Society Meeting, Seattle, Wa., March, 1983, paper No. 91.
- BIDOGLIO, G. (1982) Characterization of Am(III) Complexes with Bicarbonate and Carbonate Ions at Groundwater Concentration Levels. *Radiochemical and Radioanalytical Letters*, 53, 45-60; see also BIDOGLIO, G., A. DEPLANO, and A. CHATT (1983) Studies on Speciation of Americium, Technecium, and Neptunium in Simulated Vitrified-Waste Leachates. In *Scientific Basis for Nuclear Waste Management*, Materials Research Society Symposium Proceedings, Vol. 15, G. Brookins, (ed.), North Holland Publishing Co., Inc., pp. 373-382.
- CACECI, M. and G. R. CHOPPIN (1983) The Determination of the First Hydrolysis Constant of Eu(III) and Am(III). *Radiochimica Acta*, 33, 101-104.
- DESIRE, B., M. HUSSONNIOS, and R. GUILLAUMONT (1969) Determination de la première constante d'hydrolyse de l'americium, du curium, du berkelium et du californium," *C. R. Acad. Sc. Paris*, 269, 448-451.
- EDELSTEIN, N., J. BUCHER, R. SILVA, and H. NITSCHKE (1983) Thermodynamic Properties of Chemical Species in Nuclear Waste. Lawrence Berkeley Laboratory report LBL-14325.
- FERRI, D., I. GRENTHE, F. HIETANEN, and F. SALVATORE (1983) Studies on Metal Carbonate Equilibria. 5. The Cerium(III) Carbonate Complexes in Aqueous Perchlorate Media. *Acta Chemica Scand.*, A37, 359-365.
- KERRISK, J. F. (1984) Americium Thermodynamic Data for the EQ3/6 Database. Los Alamos National Laboratory report LA-10040-MS.
- KHOO, H. K., T. K. LIM, and C. Y. CHAN (1981) Activity Coefficients in Aqueous Mixtures of Hydrochloric Acid and Lanthanum Chloride at 25°C. *Jour. Solution Chem.*, 10, 683-691.
- LUNDQVIST, R. (1982) Hydrophilic Complexes of the Actinides. I. Carbonates of Trivalent Americium and Europium. *Acta Chemica Scand.*, 36, 741-750.
- NAIR, G. M., K. CHANDER, and J. K. JOSHI (1982) Hydrolysis Constants of Plutonium(III) and Americium(III). *Radiochimica Acta*, 30, 37-40.
- NITSCHKE, H. and N. M. EDELSTEIN (1985) Solubilities and Speciation of Selected Transuranium Ions. A Comparison of a Non-Complexing Solution with a Groundwater from the Nevada Tuff Site. *Radiochimica Acta*, 39, 23-33.
- PEIPER, J. C. and K. S. PITZER (1982) Thermodynamics of Aqueous Carbonate Solutions Including Mixtures of Sodium Carbonate, Bicarbonate, and Chloride. *Jour. Chem. Thermodynamics*, 14, 613-638.
- PITZER, K. S. and J. C. PEIPER (1980) Activity Coefficients of Aqueous NaHCO_3 . *Jour. Phys. Chem.*, 84, 2396-2398.

- RAI, D., R. G. STRICKERT, D. A. MOORE, and J. L. RYAN (1983) Am(III) Hydrolysis Constants and Solubility of Am(III) Hydroxide. *Radiochemica Acta*, 33, 201-206.
- ROBINSON, R. A. and R. H. STOKES (1959) Electrolytic Solutions, Academic Press.
- ROSSOTTI, F. J. and H. ROSSOTTI (1961) The Determination of Stability Constants, McGraw-Hill Book Co.
- SILVA, R. J. (1982) The Solubilities of Crystalline Neodymium and Americium Trihydroxides. Lawrence Berkeley Laboratory report LBL-15055.
- SILVA, R. J. and H. NITSCHKE (1983) Thermodynamic Properties of Chemical Species of Waste Radionuclides. In NRC Nuclear Waste Geochemistry '83, U. S. Nuclear Regulatory Commission report NUREG/CP-0052, pp. 70-93.
- WOLERY T. (1983) EQ3NR, A Computer Program for Geochemical Aqueous Speciation-Solubility Calculations: User's Guide and Documentation. Lawrence Livermore National Laboratory report UCRL-53414.

Software for the Computation and Graphical Display
of
Intensive Variable Phase Diagrams

E.H. Perkins

Alberta Research Council, Oil Sands Research Department,
PO Box 8330, Postal Station F,
Edmonton, Alberta, Canada. T6H 5X2

R. Berman and T.H. Brown

Department of Geological Sciences, UBC
Vancouver, B.C., Canada. V6T 2B4

Abstract

The use of intensive variable diagrams to portray the stability relationships of minerals, aqueous species and gases is one of the most critical tools available to evaluate the stability of natural assemblages. With the increasing accuracy and size of thermodynamic databases for minerals, gases and aqueous species, and the continually increasing speed and power of modern computers, it is now possible to interactively and quickly calculate diagrams relating all possible stability relationships for a given system.

PT-SYSTEM and its derivatives (TX-SYSTEM, PX-SYSTEM, TFO2-SYSTEM, PA-SYSTEM, TA-SYSTEM and AA-SYSTEM) allow the calculation of phase diagrams as functions of pressure versus temperature, temperature versus fluid composition, pressure versus fluid composition, temperature versus oxygen fugacity, pressure versus activity of a specified component, temperature versus activity of a specified component, and activity versus activity of two different components. By default, only the stable diagram is calculated and is present in tabular form and as a plot. All curves are labelled with the correct assemblage on each side of the curve.

The programs are versatile with many different run time options, including: projection from a given phase or assemblage; limiting the calculation of curves to those which contain a given phase or assemblage; inclusion of meta-stable equilibria, and the use of various solid solution models for solids and equations of state for gases. It includes equations for disorder, polymorphic transitions as well as extended heat capacity functions and volumetric equations of state for solids.

The first versions of the programs were written in 1977, and they have been continually tested, debugged, and upgraded since that time. Currently available in ANSI standard FORTRAN 77, these programs are running at over 30 sites on a range of machines, including a Cray, almost all of the IBM and CDC mainframes, all VAX's,

several different Primes and HPs, and various minicomputers, including IBM pc's and their clones.

Introduction

Intensive variable phase diagrams have been among the most useful tools available to geologists in evaluating the stability relationships of minerals, aqueous species and gases. They allow the pressure, temperature and compositional constraints of the formation of mineral assemblages to be assessed. They are essential in evaluating the consistency of thermodynamic data and extremely useful in planning further experimental work. With the increasing availability of large thermodynamic data bases, the increased power of computers, it is now feasible to calculate and confidently use these diagrams.

PT-SYSTEM is one of a group of related programs which allow the calculation of intensive phase diagrams, using almost any two intensive variables as axis variables. These programs are user friendly and designed to run interactively with a minimum of necessary input. The thermodynamic data is read from a file which can be easily read and modified by any text editor. The output from the programs is given in both tabular and graphic formats.

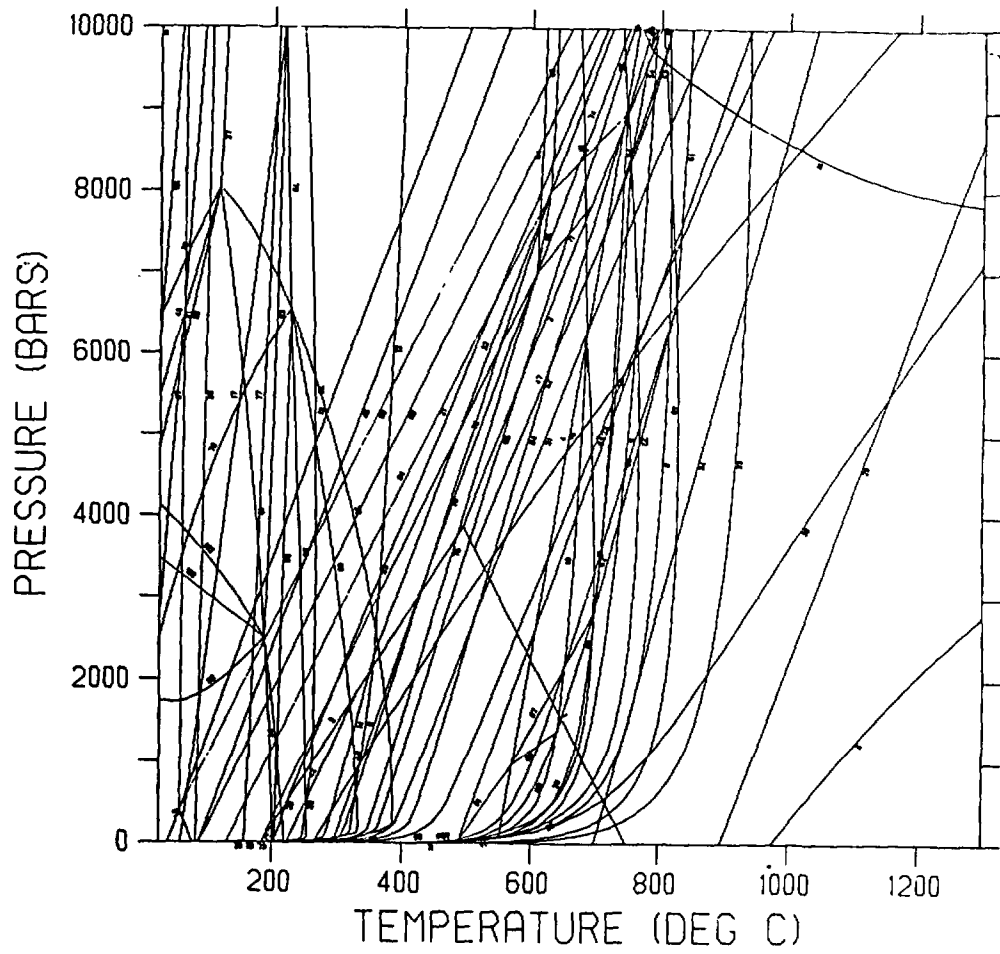
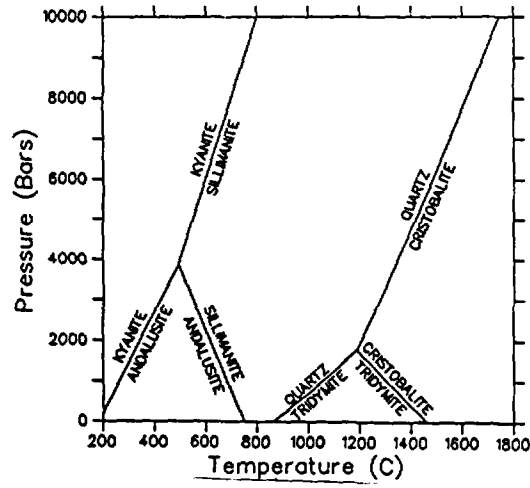
Whenever possible, the philosophy behind these programs has been to allow the user to specify, use and test different thermodynamic data sets for the phases and species, and different equations of state for the gases, and then to compare the results. It is this process which builds confidence in the programs, the dataset and any predictions/evaluations made.

Examples of computed intensive variable diagrams.

In the following figures, we have used the thermodynamic data base for minerals of Berman, Brown and Greenwood (1985), and either the Haar equation of state for water (Haar, Gallagher, Kell, 1984) or a Redlich-Kwong (Kerrick and Jacobs, 1981) formulations for water-carbon dioxide mixtures. All diagrams were plotted on a laser printer. Because of the limited size available for diagrams, only "simple" diagrams with few curves have been shown. Diagrams with thousands of stable reactions have been calculated but it is difficult to show these.

Figure one is a pressure temperature diagram for perhaps the simplest geological system: $SiO_2 - Al_2O_3$. The diagram has sufficiently few reactions that there is room for the complete mineral name to be used in labeling the curve. At the users option, abbreviations of the names could be used.

Figures One and Two



Figures Three, Four and Five

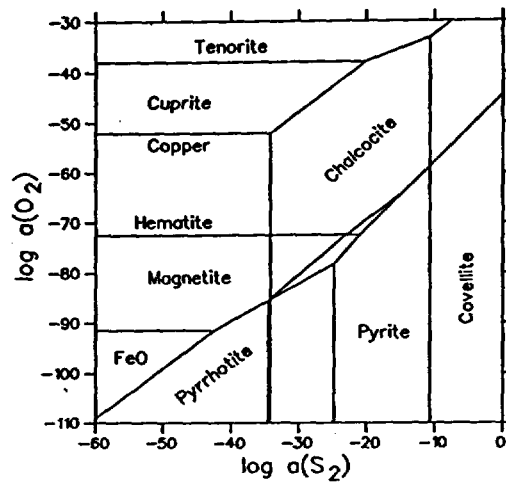
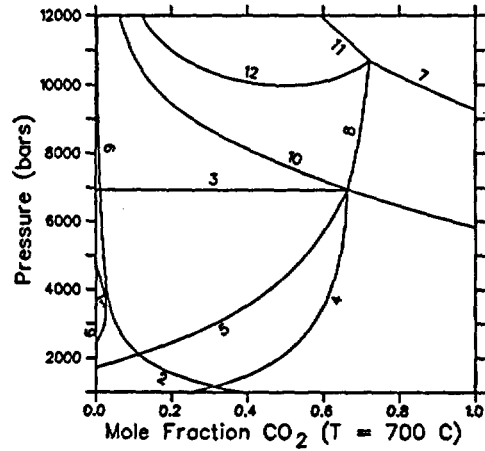
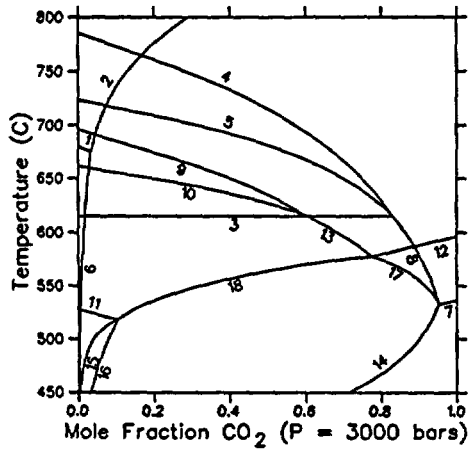


Figure two is a more complicated P-T diagram, including a fluid phase, which would appear cluttered and unreadable if the names were used. Here, the user has specified that the curves be numbered. The program prints a separate table with these reaction numbers and the corresponding reaction labels. The number is always plotted on the product side of the equilibria. The Haar equation of state for water was used, phases used were a subset of the system Mg-Ca-AL-Si-O-H.

Figure three is an example of a temperature versus mole fraction ($H_2O - CO_2$) diagram, calculated at three kilobars, using the Redlich-Kwong equation of state for

water, carbon dioxide and their mixtures from Kerrick and Jacobs (1981). The curves have been numbered rather than labelled for clarity.

Figure four is a pressure versus mole fraction water-carbon dioxide diagram, calculated with the same phases as figure three. The temperature is 700 degrees on this diagram

Figure five is an example of an activity versus activity diagram for the iron-copper-oxygen-sulphur system. This diagram has been modified using a graphic editor, leaving the chalcopyrite field unlabelled for clarity.

Many other diagrams with different axis variables can be calculated, the limits exist only in the mind of the user and in the availability of the appropriate thermodynamic data.

Calculation Strategy

All of the programs follow the same basic strategy for the calculation of phase diagrams. These may be summarized as follows:

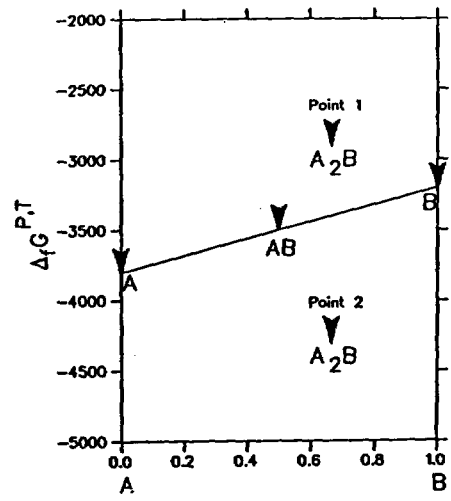
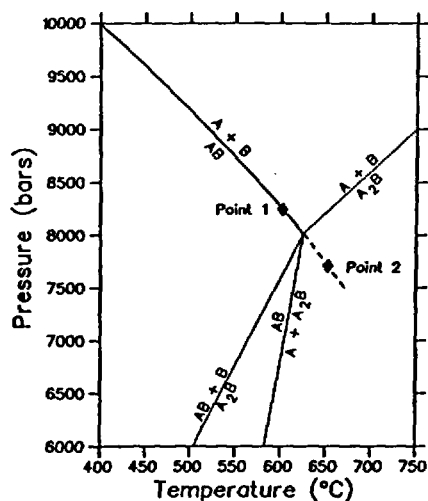
Steps performed once

- User selects P-T-X-A range of diagram, chemical system, and various options.
- Program reads thermodynamic database.
- User selects phases to be included and their activity (optional).
- Program generates coefficients of all possible reactions among the selected phases.

Repeated for each reaction

- Evaluate if curve is present on diagram. If not, remove all curves containing meta-stable assemblage from the list of remaining curves, then get next curve. If present, continue.
- Compute locus of points on equilibrium curve.
- Check stability of each computed point. See details below.
- Write stable points of curve to a file.
- Plot on screen or in file (optional: generally not used on mainframes, but generally used in micros).

Figures Six and Seven



- If all curves have been evaluated, close files, exit.

Post-processing

- Print summary file (optional as it is often big).
- View/edit completed phase diagram, with option of making copies on various output devices.

Figures six and seven illustrate the most critical steps in the calculation procedure, determining the stability of points on the equilibrium curves. Stability level is calculated by comparing the position of the component chemical potential plane with the chemical potential of every other phase in the system. For example, in figure six at point 1, the chemical potential of phase A_2B is above that defined by the stable univariant A-B-assemblage. At point 2, the situation is reversed, indicating that this univariant assemblage is metastable. The exact location of the 4-phase invariant point is located by interval halving between stable and metastable points on the univariant reaction.

The strong point of the strategy summarized above is that it ensures that all stable equilibria in a selected system of phases will be located. Its main shortcoming lies in the inefficiency of having to compute most of the equilibria in order to find the stable ones.

We are currently exploring an alternate strategy that utilizes the information regarding the full phase assemblage at invariant points to generate only stable reactions.

In addition to increasing speed by not calculating the positions of any metastable equilibria, this procedure also offers the advantage of not having to first compute the coefficients of all possible reactions, a time-consuming task for systems with more than several thousand possible reactions. Although various schemes can be used to quickly find the first stable reaction, we have not yet developed an adequate technique for finding reactions that are not connected to the stable net.

Program details

The programs are written in FORTRAN 77 and need a full ANSI standard compiler. The programs have currently been tested on almost every IBM, CDC and DEC mainframe, as well as MICRO-VAX's, various of the larger HP computers, several PRIME computers and a CRAY 1S. To the best of the authors knowledge, all mainframes support a full standard FORTRAN 77 compiler although it may not be present at specific sites. There are several minor differences between the various compilers, these generally reflect file naming/opening/rewinding/closing conventions. Areas of the code which might need to be changed are flagged and alternative versions are given.

The software can be run on microcomputers---it has been successfully compiled and run on IBM-XTs, IBM-ATs, and various of the clones. If the programs are not modified, at least 500 KB, the 8087 math chip and either the IBM professional fortran 77 compiler or the Lahey F77L compiler are required. Various other pc compilers are currently being investigated. The MICRO-SOFT FORTRAN 77 compiler is an ANSI substandard FORTRAN 77 compiler and can not be used without major modifications to these programs.

The program has a considerable number of defaults. These range from the default answers for the questions, the size of labels on the plots and the amount of information written to the interactive unit. These are designed to be easily modified by the user to provide a "custom" version of the programs.

Copies of the mainframe versions of the programs can be obtained from the senior author, versions suitable for minicomputer use can be obtained from the second author. Documentation, a database, and examples are provided with the programs.

References

- Berman, R.G., Brown, T.H., and Greenwood, H.J. (1985) An internally-consistent thermodynamic data base for minerals in the system $\text{Na}_2\text{O}-\text{K}_2\text{O}-\text{CaO}-\text{MgO}-\text{FeO}-\text{Fe}_2\text{O}_3-\text{Al}_2\text{O}_3-\text{SiO}_2-\text{TiO}_2-\text{H}_2-\text{CO}_2$: Atomic Energy of Canada Technical Report TR-377, 70p.
- Haar, L., Gallagher, J.S. and Kell, G.S. (1984) NBS/NRC steam Tables. McGraw-Hill.

Kerrick, D.M. and Jacobs, G.K. (1981) A modified Redlich-Kwong equation for H₂O, CO₂ and H₂O-CO₂ mixtures at elevated pressures and temperatures: *American Journal of Science*, 281, p 735-767.

CHLORITE SOLUBILITY BETWEEN 200°C AND 350°C: AN EXPERIMENTAL AND THEORETICAL MODELING STUDY

Edward C. Thornton, William E. Seyfried, Jr., and Jeffrey Seewald
Dept. of Geology and Geophysics, University of Minnesota, Minneapolis, MN 55455

INTRODUCTION

Computer modeling of rock/water interaction processes can contribute greatly to our understanding of mineral alteration and mass transport in hydrothermal systems. These models, however, may be applied in a quantitative manner only if we have accurate thermodynamic data for the solubilities of common rock-forming minerals. Currently, solubilities of many minerals can only be approximated owing to a lack of experimental data at the appropriate conditions. We present here recently acquired solubility data for chlorite and illustrate how it may be integrated into a computer model for rock/water interaction.

PROCEDURES

The experiment reported here was conducted in flexible cell hydrothermal equipment for a period of 11 months. A mineral assemblage consisting of Mg-chlorite, kaolinite, gibbsite, magnetite, and hematite was employed to buffer the fluid chemistry with respect to aluminum, silica, and oxygen fugacity; all dissolved components were measured in the fluid samples obtained during the experiment, however, to test the reliability of these buffers and to provide information for assessing the approach of the system to equilibrium conditions. These minerals were reacted with seawater at an initial water/rock mass ratio of 5. The experiment was conducted at 200, 250, 300, and 350°C at 500 bars to investigate the role of temperature in the alteration process. Temperature was subsequently decreased in a similar manner to evaluate reversibility of the system.

SOLVEQ, a computer program developed by Reed (1982), was utilized to assess aqueous speciation and ionic activities at experimental conditions from the fluids analyses. This information permitted calculation of mineral solubilities for comparison with estimates provided by SUPCRT (Helgeson *et al.*, 1978). Alteration of fluid chemistry during rock/water interaction was compared with that predicted by the EQ3/6 software package (Wolery, 1979) as a means of assessing the impact of mineral solubility changes on the theoretical reaction path model.

RESULTS

Petrographic and x-ray diffraction examination of reactants and products indicated no major changes in the mineral assemblage other than the transformation of gibbsite to boehmite, alteration of a portion of the magnetite to hematite, and the formation of a minor amount of smectite. The chlorite phase (essentially a pure clinocllore) was not significantly altered during the experiment. Kaolinite was present in the products, though its abundance decreased relative to the reactants.

Changes in fluid chemistry included an increase in silica concentration to near quartz saturation levels with dissolved aluminum in the range of 0.005 to 0.01 millimoles/kg (Table 1). Also observed was the development of moderately acid conditions and decrease of dissolved magnesium in response to precipitation of chlorite. Dissolved iron concentrations subsequently rose in response to the acid state of the fluid. Minor chloride depletions were observed early in the experiment in response to the dehydration of gibbsite to boehmite. This

Table 1. Concentrations for dissolved components (millimoles/kg) and pH for chlorite solubility experiment.

Temperature	Time (hrs)	Al	SiO ₂	Mg	pH(25°C)
seawater, 25°C	--	<.002	<.01	53.4	7.9
200°C	22.0	0.005	1.91	45.5	5.00
	116.5	0.004	2.20	44.2	4.26
	213.0	0.006	2.26	43.6	4.15
	479.0	--	2.23	43.2	4.15
	1126.5	0.008	2.33	42.8	4.06
250°C	44.5	0.007	5.23	43.8	2.85
	212.5	0.010	5.44	42.2	2.81
	761.0	0.004	5.88	42.0	2.73
300°C	23.5	0.007	11.1	38.4	2.28
	170.0	0.005	11.6	38.3	2.22
	456.0	0.006	11.9	37.1	2.21
	1152.0	0.006	11.8	35.0	2.15
350°C	22.0	0.008	19.9	27.0	1.98
	165.5	0.009	18.7	24.1	1.97
	453.5	0.007	18.8	22.3	1.97
300°C	934.0	0.007	18.6	20.2	1.96
	332.5	0.007	13.9	30.0	2.09
	837.0	0.007	13.9	30.0	2.14
250°C	382.0	0.003	8.55	34.0	2.25
	959.0	0.007	8.35	34.1	2.30
	1727.0	0.005	8.20	34.0	2.30
200°C	380.5	<.002	4.41	37.3	2.69
	1101.0	<.002	4.33	36.3	2.73

transformation appears to have gone to completion during the 250°C heating stage of the experiment.

DISCUSSION

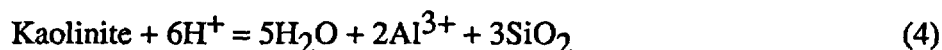
The mineral assemblage Mg-chlorite/boehmite/kaolinite buffers the activities of the ions Al³⁺ and SiO₂ and the ratio of Mg²⁺ activity to H⁺ activity at a given pressure and temperature by the following reactions:



Ionic activities may be calculated by using the mineral solubility data from SUPCRT or computed directly using EQ3/6. Alternatively, activities may be computed for the experimental fluid chemistry using SOLVEQ and then utilized to compute mineral solubilities. Comparison of the experimental data and theoretical models may thus be employed to assess the impact of mineral solubilities on rock/water interaction. This approach may be illustrated by

considering the fluid data collected at 300°C from the experiment. Reversibility was well demonstrated at this temperature and appears to provide reliable data on boehmite-clinochlore solubility.

Examination of the fluid data indicates that dissolved Al concentrations were significantly lower than predicted by solubility data for boehmite (reaction 1) from the SUPCRT code. This, in turn, results in lower values for aqueous SiO₂ in the theoretical model relative to the experimental data owing to kaolinite dissolution:



This is illustrated by the activity diagram shown in Figure 1. Recent boehmite solubility data provided by Kuyunko *et al.* (1983) agrees very well with that observed in the experiment and hence was incorporated into the SUPCRT and EQ3/6 data bases. This resulted in a model that agreed reasonably well with the experiment from the standpoint of dissolved Al concentrations. The SiO₂ concentrations predicted on the basis of reaction 2, however, then exceed quartz saturation and render kaolinite unstable. The experimental SiO₂ concentrations appear to reflect equilibrium with quartz and, indeed, do correspond very well with quartz solubility data after correction for salinity effects (Fournier, 1983).

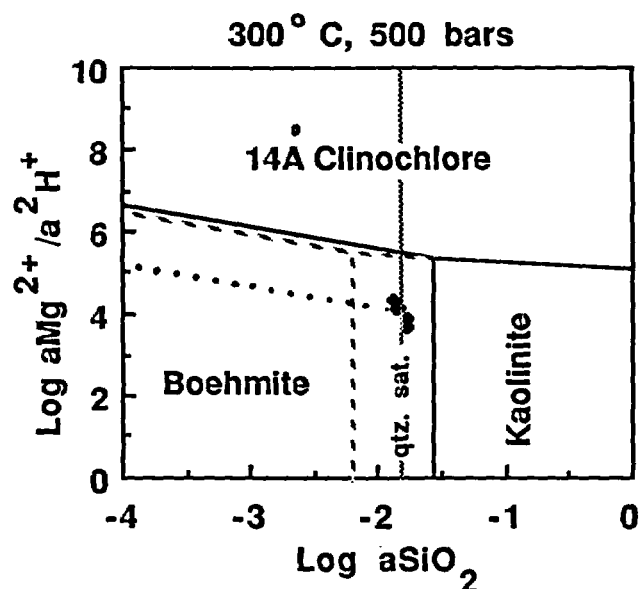
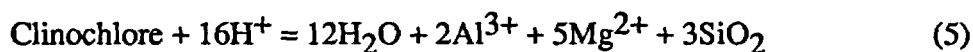


Figure 1. Activity diagram for the system HCl-MgO-SiO₂-(Al₂O₃) showing phase relationships using original SUPCRT data (dashed lines) and revised boundaries incorporating the solubility data for boehmite of Kuyunko *et al.* (1983) (solid lines). Solid symbols demonstrate reversible approach to equilibrium of experimental fluid chemistry from higher and lower temperatures thus constraining the position of the inferred invariant point and boehmite-clinochlore phase boundary (dotted line).

Examination of the fluid data also revealed that the Mg content of the fluids and the *in situ* pH were considerably lower than predicted from estimated clinochlore solubility data provided by SUPCRT. This is illustrated in Figure 1, where it can be seen that the clinochlore stability field constructed from the experimental data is considerably larger than the theoretical stability field. The position of the univariant boundary between clinochlore and boehmite deduced from the experimental data provides a basis for calculating the solubility of clinochlore at 300°C and 500 bars, where clinochlore solubility is expressed in terms of the hydrolysis reaction:



The activity of Al³⁺ for this reaction is constrained by boehmite solubility (reactions 1 and 3).

This approach was utilized over the entire temperature range investigated during the experiment to establish the variation of chlorite solubility with temperature. This is illustrated in Figure 2 where the experimental values of log K for reaction 5 are shown and are compared to those values calculated by SUPCRT at 500 bars. It is apparent from this study that the solubility of clinochlore is considerably lower than the theoretical value.

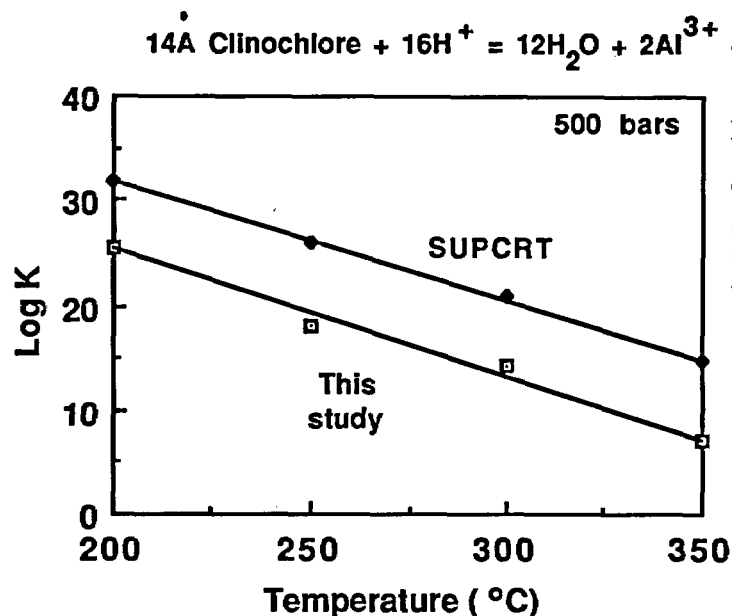


Figure 2. Variation of clinochlore solubility as a function of temperature. This study indicates clinochlore is less soluble under hydrothermal conditions than predicted by the current thermodynamic data present in SUPCRT (Helgeson et al , 1978).

CONCLUSIONS

The experimental data presented here indicates that the solubility of boehmite is lower than predicted by SUPCRT; our results are in agreement with those of Kuyunko *et al.* (1983) and thus clearly indicate a need for updating the SUPCRT data base for this phase. Incorporation of the revised boehmite solubility data into EQ3/6 indicates that kaolinite may not be stable at 300°C owing to conversion to quartz. Clinochlore solubility calculated from this study is considerably lower than that predicted by SUPCRT in the temperature range of 200°C to 350°C at 500 bars.

Further experimental studies should be conducted to evaluate aluminosilicate solubilities under hydrothermal conditions. Incorporation of this data into SUPCRT and the EQ3/6 data base may be readily performed as it becomes available. This approach is essential to accurate modeling of mass transport of chemical components during rock/water interaction and will ultimately increase our understanding of hydrothermal alteration processes in a variety of geological environments.

REFERENCES

- Fournier, R.O. (1983) A method of calculating quartz solubilities in aqueous sodium chloride solutions. *Geochem. Cosmochim Acta* 47, 579-586.
- Helgeson, H.C., Delany, J.M., Nesbitt, N.H. and Bird, D.K. (1978) Summary and critique of thermodynamic properties of rock-forming minerals. *Amer. J. Sci.* 278-A, 229p.

- Kuyunko, N.S., Malinin, S.D. and Khodakovskiy, I.L. (1983) An experimental study of aluminum ion hydrolysis at 150, 200, and 250°C. Geokhimiya 3, 419-428. [in Russian].
- Reed, M.H. (1982) Calculation of multicomponent chemical equilibria and reaction processes in systems involving minerals, gases, and an aqueous phase. Geochim. Cosmochim. Acta 46, 513-528.
- Wolery, T.H. (1979) Calculation of chemical equilibrium between aqueous solution and minerals: the EQ3/6 software package. Lawrence Livermore Laboratory Report UCRL-52658, 41p.

Appendices

Appendix A. Agenda

Monday, September 15

- Morning Session** **Geochemical Model Development**
Session Chairman: *William McKenzie*
- 8:40 a.m. EQ3/6 - Status and Future Development - *Tom Wolery*
- 9:05 a.m. Reduced Basis Method for Calculating Heterogeneous Geochemical Equilibria in Multicomponent Reaction Paths - *Craig Bethke*
- 9:35 a.m. A Theoretical Basis for the Coupling of Chemical Reactions to Open System Processes - *Ernie Perkins*
- 10:20 a.m. Calculations of Geochemical Mass Transfer as a Function of Temperature and Time - *William Murphy*
- 10:50 a.m. Comparison of Reaction Path and Interacting Continua Models of Mass Transfer in Geochemical Systems - *Peter Lichtner*
- 11:20 a.m. Comparison of Measured and Predicted Solubilities of Aluminosilicates in Aqueous Solution - *John Apps*
- 11:50 a.m. Surface Complexes in Geochemical Processes - *James Leckie*
- Evening Session** **Ore Deposits**
Session Chairman: *Ken Jackson*
- 7:30 p.m. Chlorite Solubility Between 200 and 350°C - An Experimental and Theoretical Modeling Study - *Edward Thornton, Jeffrey Seewald, and William E. Seyfried, Jr.*
- 8:00 p.m. Boiling of Geothermal Waters: Base and Precious Metal Precipitation, Arsenic and Antimony Speciation and the Role of Metal Transport in Gas Phase - *Nicholas Spycher and M. H. Reed*
- 8:30 p.m. Chemical Evolution of Oil-Field Brines and the Formation of Sediment-Hosted Cu-Pb-Zn Sulfide - *Dimitri A. Sverjensky*
- 9:00 p.m. Clay-Carbonate Reactions in Oil Sand Reservoirs During Steam Flooding - *William Gunter and G. W. Bird*

Tuesday, September 16

- Morning Session** **Nuclear Waste Disposal**
Session Chairman: *Virginia Oversby*
- 8:30 a.m. Application of Equilibrium Computations to the Geochemical Interpretation of the Deep Granitic Groundwaters at the Stripa Research Site, Sweden - *D. Kirk Nordstrom*

- 9:00 a.m. Modeling Interaction of Deep Groundwaters with Bentonite -
Hans Wanner
- 9:30 a.m. Reaction-Path Modeling of Interaction Between Basalt and Groundwater
in the Columbia Plateau, Washington - *Cleve Solomon*
- 10:15 a.m. A Consistent Set of Thermodynamic Constants for Americium III Species
with Hydroxyl and Carbonate - *Jerry Kerrisk and Bob Silva*
- 10:45 a.m. Thermodynamic and Kinetic Modeling of Glass Leaching in a Waste
Package Environment - *Bernd Grambow*
- 11:15 a.m. Hydrothermal Alteration of the Auriat Granite (Creuse, France):
Comparison of Experimental Observations and Modeling with EQ3/6 -
J. C. Petit and J. C. Parneix
- 11:45 a.m. Compatibility of Observed Mineralogy in Borehole Cores, Palo Duro
Basin, Texas, with Coexisting Brines, as Computed by EQ3/6 - *Paul Cloke*

Poster Session

- The NEA Thermochemical Data Base - *Hans Wanner*
- Variations of K_D Due to Changes in Solution Chemistry - *James Leckie*
- EQ3/6 Data Base - On-going Development at Lawrence Livermore
National Laboratory - *Joan M. Delany*
- Improvements in the Solid Solution Modeling Capabilities of EQ3/6 -
William L. Bourcier
- Models for Activity Coefficients in Brines - *Ken Jackson and Tom Wolery*
- Computer Modeling of the Aqueous Geochemistry of the Archean
Hydrosphere and the Formation of BIF - *William Glassley, Ken Jackson,
and William L. Bourcier*
- Progressive Mineral Alteration and Oxygen Isotope Depletions in the
Lake City Hydrothermal System (23 Ma), Colorado - *Peter Larson*
- Predicted Reaction Paths During the Hydrothermal Alteration of
Columbia River Basalts: Sensitivity Analysis of Variability in the
Composition Mesostasis - *Randy Arthur*
- Preliminary Chemical Modeling of Epithermal Processes at Creede,
Colorado: The Role of Fluid Mixing as an Ore Deposition Mechanism -
Geoffrey Plumlee and D. O. Hayba
- Software for the Computation and Graphical Display of Intensive
Variable Phase Diagrams - *Ernie Perkins, T. H. Brown, and R. G. Berman*
- Mineral and Stable Isotope Evidence for Regional Fluid Flow and
Rock-Water Interaction in the San Jovan Basin, New Mexico -
Gene Whitney and Roy Northrop

Evening Session Hydrothermal Systems
Session Chairman: *Bill Glassley*

- 7:30 p.m. Application of EQ3/6 to Modeling the Chemical Evolution in Hydrothermal Systems: An Example at the Valles Caldeira, N.M. - *Art White and N. Chuma*
- 8:00 p.m. Chemical Equilibrium and Isotopic Models of Mid-Ocean Ridge Hot Springs - *Teresa S. Bowers*
- 8:30 p.m. Serpentinization Reaction Pathway: Implications for Modeling Approach - *Dave Janecky*

Wednesday, September 17

Morning Session Sedimentary Basins/Groundwater
Session Chairman: *Roger Aines*

- 8:30 a.m. Paleohydrologic Analysis of Geopressures and Meteoric Infiltration in the Gulf Coast Basin - *Wendy Harrison and Craig Bethke*
- 9:00 a.m. Predicting Mineral Dissolution and Precipitation During Burial: Synthetic Diagenetic Sequences - *Carol J. Bruton*
- 10:00 a.m. Modeling Mass Transfer Reaction Rates: Calcite Precipitation and CO₂ Outgassing in a Karst Stream - *Janet Herman*
- 10:30 a.m. Geochemical Modeling of Water-Rock Interactions in High Island Oil Field, Offshore Texas - *Yousif Kharaka and J. D. Cocker*
- 11:00 a.m. Evaluation of an Equilibrium Speciation Model for the Aqueous Low pH Iron-Sulfate System at 25°C - *Susan Stipp*
- 11:30 a.m. Chemical Equilibrium in Mineral Formation and Diagenesis in the Carbonate Evaporite System - *John Weare, Nancy Moller, Jerry Greenberg, and Andrew Felmy*

Appendix B. List of Attendees

Hugh Abercrombie, University of Calgary
Pradeep Aggarwal, U. S. Geological Survey
Roger Aines, Lawrence Livermore National Laboratory
Charlie Alpers, University of Michigan
John A. Apps, Lawrence Berkeley Laboratory
Randy Arthur, Rockwell Hanford Operations
Mark D. Barton, University of California, Los Angeles
Craig Bethke, University of Illinois
Dennis Bird, Stanford University
Mark S. Bloom, Monash University
John Karl Bohlke, Argonne National Laboratory
William Bourcier, Lawrence Livermore National Laboratory
Teresa S. Bowers, Massachusetts Institute of Technology
John Bradbury, U. S. Nuclear Regulatory Commission
Carol Bruton, Lawrence Livermore National Laboratory
Leonel Vaca Castellon, Instituto Costarricense de Electricidad
Paul L. Cloke, Battelle Memorial Institute
Harrison Crecraft, UNOCAL Geothermal
Allan Crowe, University of Alberta
Kenneth Czyscinski, Roy F. Weston Inc.
Joan Delany, Lawrence Livermore National Laboratory
Andrew Dickson, University of California, San Diego
Fiona M. Doyle, University of California, Berkeley
Kenneth Eggert, Lawrence Livermore National Laboratory
Donald O. Emerson, Lawrence Livermore National Laboratory
Robert Erikson, Battelle Pacific Northwest Laboratory
R. Stephen Fisher, University of Texas at Austin
Mormino Gabriele, AGIP - S. p. A.
Alan Gaines, National Science Foundation
Barbara Gallinatti, UNOCAL Geothermal
William Glassley, Lawrence Livermore National Laboratory
Bernd Grambow, Hahn-Meitner-Institut Berlin GmbH.
William Gunter, Alberta Research Council
Linda Hansen, Lawrence Livermore National Laboratory

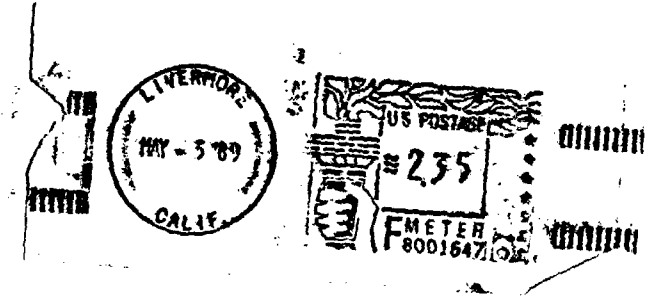
Wendy J. Harrison, Exxon Production Research Co.
Dan Hayba, U. S. Geological Survey
Janet Herman, University of Virginia
C. J. Hostetler, Battelle Pacific Northwest Laboratories
Dwight Hoxie, U. S. Geological Survey
Ken Jackson, Lawrence Livermore National Laboratory
Dave Janecky, Los Alamos National Laboratory
Hamlin Jennings, National Bureau of Standards
Anne Jordan, U. S. Geological Survey
Walt Kelly, U. S. Nuclear Regulatory Commission
Jerry F. Kerrisk, Los Alamos National Laboratory
Yousif Kharaka, U. S. Geological Survey
Deborah Kiraly, Lawrence Livermore National Laboratory
Kevin Knauss, Lawrence Livermore National Laboratory
Brian Koenig, Union Geothermal Division
Linda Kovach, U. S. Nuclear Regulatory Commission
Paul H. Krumrine, PQ Copr.
Ken Krupka, Battelle Pacific Northwest Laboratory
John Y. T. Kwong, B. C. Ministry of Energy, Mines, and Petroleum Resources
Donald Langmuir, Colorado School of Mines
Peter B. Larson, Washington State University
James O. Leckie, Stanford University
Peter Lichtner, University of California, Berkeley
Donald E. Livingston, U. S. Department of Energy
David T. Long, Michigan State University
Bertero Luigi, AGIP S. p. A.
Paul Lundgard, UNOCAL
Rigel Lustwerk, Pennsylvania State University
John J. Mahoney, Battelle Pacific Northwest Laboratory
Steven R. Mattson, Science Applications International Corporation
Arend Meijer, Los Alamos National Laboratory
Indu D. Meshri, Amoco Production Company
Jonathon Meyers, IT Corporation
Kathleen A. Mihm, U. S. Department of Energy
Anthony B. Muller, Science Applications International Corporation
Gregory Murphy, Lawrence Livermore National Laboratory

William M. Murphy, Rockwell Hanford Operations
Ross McCartney, Geoscience Ltd.
William McKenzie, Lawrence Livermore National Laboratory
D. Kirk Nordstrom, U. S. Geological Survey
H. Roy Northrop, U. S. Geological Survey
Helen Nuckolls, Woodward Clyde Consultants
Virginia Oversby, Lawrence Livermore National Laboratory
Roberto Pabalan, University of California, Berkeley
Edward S. Patera, Jr., U. S. Department of Energy
Steve Paulson, U. S. Bureau of Mines
Ernie H. Perkins, Alberta Research Council
Andrew Peterson, Sandia National Laboratories
Jean-Claude Petit, Commissariat a l'Energie Atomique
Geoffrey Plumlee, U. S. Geological Survey
Heather Ponader, Stanford University
Larry Ramspott, Lawrence Livermore National Laboratory
Richard E. Rice, Butler University
Nicholas M. Rose, Stanford University
Patricia Salter, Rockwell Hanford Operations
Jeffrey Seewald, University of Minnesota
Henry Shaw, Lawrence Livermore National Laboratory
Robert J. Silva, Lawrence Livermore National Laboratory
Robert W. Smith, Rockwell Hanford Operations
G. Cleve Solomon, Rockwell Hanford Operations
Sheldon E. Sommer, Mobil
Nicholas Spycher, University of Oregon
Susan Stipp, Stanford University
Denis M. Strachan, Battelle Pacific Northwest Laboratory
Dimitri Sverjensky, The John Hopkins University
Edward C. Thornton, University of Minnesota
Brian E. Viani, Lawrence Livermore National Laboratory
Karen L. Von Damm, Oak Ridge National Laboratory
Jana M. Walker, Amoco Production Co.
Hans Wanner, NEA Data Bank
John H. Weare, University of California, San Diego
David Weill, Aluminum Company of America

Arthur F. White, Lawrence Berkeley Laboratory
Gene Whitney, U. S. Geological Survey
Alan Williams, University of California, Riverside
Timothy Wilson, Michigan State University
Thomas J. Wolery, Lawrence Livermore National Laboratory
Ray W. Wuolo, EWA, Inc.
Albert Yang, U. S. Geological Survey
George Zandt, Lawrence Livermore National Laboratory

Technical Information Department • Lawrence Livermore National Laboratory • University of California • Livermore, California 94551

Nonprofit Org.
U.S. Postage
PAID
Livermore, Ca.
Permit No. 154



P. T. Prestholt
NRC Site Representative
1050 East Flamingo Road, Suite 319
Las Vegas, NV 89119

FOURTH CLASS SPECIAL